Cell Journal (Yakhteh)

Guide for Authors

Aims and Scope: The "Cell Journal (Yakhteh)" is a peer review and monthly English publication of Royan Institute of Iran. The aim of the journal is to disseminate information by publishing the most recent scientific research studies based on medical and developmental biology including cell therapy and regenerative medicine, stem cell biology reproductive medicine, medical genetics, immunology, oncology, clinical biochemistry, neuroscience, and tissue engineering. **Cell J**, has been certified by the Ministry of Culture and Islamic Guidance since 1999 and accredited as a scientific and research journal by HBI (Health and Biomedical Information) Journal Accreditation Commission since 2000 which is an open access journal. **This journal holds the membership of the Committee on Publication Ethics (COPE).**

1. Types of articles

The articles in the field of Cellular and Molecular can be considered for publications in **Cell J.** These articles are as below:

A. Original articles

Original articles are scientific reports of the original research studies. The article consists of English Abstract (structured), Introduction, Materials and Methods, Results, Discussion, Conclusion, Acknowledgements, Author's Contributions, and References **(Up to 40).**

B. Review articles

Review articles are the articles written by well experienced authors and those who have excellence in the related fields. The corresponding author of the review article must be one of the authors of at least three published articles appearing in the references. The review article consists of English Abstract (unstructured), Introduction, Conclusion, Author's Contributions, and References **(Up to 90).**

C. Systematic Reviews

Systematic reviews are a type of literature review that collect and critically analyzes multiple research studies or papers. The Systematic reviews consist of English Abstract (unstructured), Introduction, Materials and Methods, Results, Discussion, Conclusion, Acknowledgements, Author's Contributions, and References **(Up to 90).**

D. Short communications

Short communications are articles containing new findings. Submissions should be brief reports of ongoing researches. The short communication consists of English Abstract (unstructured), the body of the manuscript (should not hold heading or subheading), Acknowledgements, Author's Contributions, and References **(Up to 30).**

E. Case reports

Case reports are short discussions of a case or case series with unique features not previously described which make an important teaching point or scientific observation. They may describe novel techniques or use equipment, or new information on diseases of importance. It consists of English Abstracts (Unstructured), Introduction, Case Report, Discussion, Acknowledgements, Author's Contributions, and References **(Up to 30).**

F. Commentary

Commentaries are short articles containing a contemporary issue that is relevant to the journal's scope and also expressing a personal opinion or a new perspective about existing research on a particular topic. The Commentary consists of English Abstract (unstructured), the body of the manuscript (should not hold heading or subheading), Acknowledgements, Author's Contributions, and References **(Up to 30).**

G. Editorial

Editorials are articles should be written in relevant and new data of journals' filed by either the editor in chief or the editorial board.

H. Imaging in biology

Images in biology should focus on a single case with an interesting illustration such as a photograph, histological specimen or investigation. Color images are welcomed. The text should be brief and informative.

I. Letter to the editors

Letter to the editors are in response to previously published **Cell J** articles, and may also include interesting cases that do not meet the requirement of being truly exceptional, as well as other brief technical or clinical notes of general interest.

J. Debate

Debates are articles which show a discussion of the positive and negative view of the author concerning all aspect of the issue relevant to scientific research.

2. Submission process

It is recommended to see the guidelines for reporting different kinds of manuscripts. This guide explains how to prepare the manuscript for submission. Before submitting, we suggest authors to familiarize themselves with **Cell J** format and content by reading the journal via the website (www.celljournal.com). The corresponding author ensures that all authors are included in the author list and agree with its order, and they must be aware of the manuscript submission.

A. Author contributions statements

It is essential for authors to include a statement of responsibility in the manuscript that specifies all the authors' contributions. This participation must include: Conceptualization, Methodology, Software, Validation, Formal analysis, Investigation, Resources, Data Curation, Writing - Original Draft, Writing - Review & Editing, Visualization, Supervision, Project administration, and Funding acquisition. Authors who do not meet the above criteria should be acknowledged in the Acknowledgments section.

B. Cover letter and copyright

Each manuscript should be accompanied by a cover letter, signed by all authors specifying the following statement: "The manuscript has been seen and approved by all authors and is not under active consideration for publication. It has neither been accepted for publication nor published in another journal fully or partially (except in abstract form). **Also, no manuscript would be accepted in case it has been pre-printed or submitted to other websites.** I hereby assign the copyright of the enclosed manuscript to **Cell J.**" The corresponding author must confirm the proof of the manuscript before online publishing. It is needed to suggest three peer reviewers in the field of their manuscript.

C. Manuscript preparation

Authors whose first language is not English encouraged to consult a native English speaker in order to confirm his manuscripts to American or British (not a mixture) English usage and grammar. It is necessary to mention that we will check the plagiarism of your manuscript by iThenticate Software. The manuscript should be prepared in accordance with the "International Committee of Medical Journal Editors (ICMJE)". Please send your manuscript in two formats word and PDF (including: title, name of all the authors with their degree, abstract, full text, references, tables and figures) and also send tables and figures separately in the site. The abstract and text pages should have consecutive line numbers in the left margin beginning with the title page and continuing through the last page of the written text. Each abbreviation must be defined in the abstract and text when they are mentioned for the first time. Avoid using abbreviation in the title. Please use the international and standard abbreviations and symbols

It should be added that an essential step toward the integration and linking of scientific information reported in published literature is using standardized nomenclature in all fields of science and medicine. Species names must be italicized (*e.g., Homo sapiens*) and also the full genus and species written out in full, both in the title of the manuscript and at the first mention of an organism in a paper.

It is necessary to mention that genes, mutations, genotypes, and alleles must be indicated in italics. Please use the recommended name by consulting the appropriate genetic nomenclature database, e.g., HUGO for human genes. In another words; if it is a human gene, you must write all the letters in capital and italic (*e.g., OCT4, c-MYC*). If not, only write the first letter in capital and italic (*e.g., Oct4, c-Myc*). **In addition, protein designations are the same as the gene symbol but are not italicized.**

Of note, Cell J will only consider publishing genetic association study papers that are novel and statistically robust. Authors are advised to adhere to the recommendations outlined in the STREGA statement (http://www.strega-statement.org). The following criteria must be met for all submissions:

1. Hardy-Weinberg Equilibrium (HWE) calculations must be carried out and reported along with the P-values if applicable [see Namipashaki et al. 2015 (Cell J, Vol 17, N 2, Pages: 187-192) for a discussion].

2. Linkage disequilibrium (LD) structure between SNPs (if multiple SNPs are reported) must be presented.

3. Appropriate multiple testing correction (if multiple independent SNPs are reported) must be included.

Submissions that fail to meet the above criteria will be rejected before being sent out for review.

Each of the following manuscript components should begin in the following sequence:

Authors' names and order of them must be carefully considered (full name(s), highest awarded academic degree(s), email(s), and institutional affiliation(s) of all the authors in English. Also, you must send mobile number and full postal address of the corresponding author).

Changes to Authorship such as addition, deletion or rearrangement of author names must be made only before the manuscript has been accepted in the case of approving by the journal editor. In this case, the corresponding author must explain the reason of changing and confirm them (which has been signed by all authors of the manuscript). If the manuscript has already been published in an online issue, an erratum is needed. Please contact us via info@celljournal.org in case of any changes (corrections, retractions, erratum, etc.).

Title is providing the full title of the research (do not use abbreviations in title).

Running title is providing a maximum of 7 words (no more than 50 characters).

Abstract must include Objective, Materials and Methods, Results, and Conclusion (no more than 300 words).

Keywords, three to five, must be supplied by the authors at the foot of the abstract chosen from the Medical Subject Heading (MeSH). Therefore; they must be specific and relevant to the paper.

The following components should be identified after the abstract:

Introduction: The Introduction should provide a brief background to the subject of the paper, explain the importance of the study, and state a precise study question or purpose.
Materials and Methods: It includes the exact methods or observations of experiments. If an apparatus is used, its manufacturer's name and address should be stipulated in parenthesis. If the method is established, give reference but if the method is new, give enough information so that another author can perform it. If a drug is used, its generic name, dose, and route of administration must be given. Standard units of measurements and chemical symbols of elements do not need to be defined.

Statistical analysis: Type of study and statistical methods should be mentioned and specified by any general computer program used.

Ethical considerations*:* Please state that informed consent was obtained from all human adult participants and from the parents or legal guardians of minors and include the name of the appropriate institutional review board that approved the project. It is necessary to indicate in the text that the maintenance and care of experimental animals complies with National Institutes of Health guidelines for the humane use of laboratory animals, or those of your Institute or agency.

Clinical trial registration: All of the Clinical Trials performing in Iran must be registered in Iranian Registry of Clinical Trials (www.irct.ir). The clinical trials performed abroad, could be considered for publication if they register in a registration site approved by WHO or www.clinicaltrials.gov. If you are reporting phase II or phase III randomized controlled trials, you must refer to the CONSORT Statement for recommendations to facilitate the complete and transparent reporting of trial findings. Reports that do not conform to the CONSORT guidelines may need to be revised before peer-reviewing.

Results: They must be presented in the form of text, tables, and figures. Take care that the text does not repeat data that are presented in tables and/or figures. Only emphasize and summarize the essential features of the main results. Tables and figures must be numbered consecutively as appeared in the text and should be organized in separate pages at the end of the manuscript while their location should be mentioned in the main text.

Tables and figures: If the result of your manuscript is too short, it is better to use the text instead of tables & figures. Tables should have a short descriptive heading above them and also any footnotes. Figure's caption should contain a brief title for the whole figure and continue with a short explanation of each part and also the symbols used (no more than 100 words). All figures must be prepared based on cell journal's guideline in color (no more than 6 Figures and Tables) and also in TIF format with 300 DPI resolution.

Of Note: Please put the tables & figures of the result in the results section not any other section of the manuscript.

Supplementary materials would be published on the online version of the journal. This material is important to the understanding and interpretation of the report and should not repeat material within the print article. The amount of supplementary material should be limited. Supplementary material should be original and not previously published and will undergo editorial and peer review with the main manuscript. Also, they must be cited in the manuscript text in parentheses, in a similar way as when citing a figure or a table. Provide a caption for each supplementary material submitted.

Discussion: It should emphasize the present findings and the variations or similarities with other researches done by other researchers. The detailed results should not be repeated in the discussion again. It must emphasize the new and important aspects of the study.

Conclusion: It emphasizes the new and important aspects of the study. All conclusions are justified by the results of the study.

Acknowledgements: This part includes a statement thanking those who contributed substantially with work relevant to the study but does not have authorship criteria. It includes those who provided technical help, writing assistance and name of departments that provided only general support. You must mention financial support in the study. Otherwise; write this sentence "There is no financial support in this study".

Conflict of interest: Any conflict of interest (financial or otherwise) and sources of financial support must be listed in the Acknowledgements. It includes providers of supplies and services from a commercial organization. Any commercial affiliation must be disclosed, regardless of providing the funding or not.

Of Note: If you have already any patent related to the subject of your manuscript, or you are going to apply for such a patent, it must be mentioned in this part.

References: The references must be written based on the Vancouver style. Thus the references are cited numerically in the text and listed in the bibliography by the order of their appearance. The titles of journals must be abbreviated according to the style used in the list of Journals Indexed in PubMed. Write surname and initials of all authors when there are six or less. In the case of seven or more authors, the names of the first six authors followed by "et al." must be listed. You can download Endnote file for Journal references style: endnote file

The reference of information must be based on the following order:

Article:

Surname(s) and first letter of name &middle name(s) of author(s) .Manuscript title. Journal title (abbr).publication date (year); Volume & Issue: Page number.

Example: Manicardi GC, Bianchi PG, Pantano S, Azzoni P, Bizzaro D, Bianchi U, et al. Presence of endogenous nicks in DNA of ejaculated human spermatozoa and its relationship to chromomycin A3 accessibility. Biol Reprod. 1995; 52(4): 864-867.

Book:

Surname(s) and first letter of name & middle name(s) of author(s).Book title. Edition. Publication place: publisher name; publication date (year); Page number.

Example: Edelman CL, Mandle CL. Health promotion throughout the lifespan. 2nd ed. ST Louis: Mosby; 1998; 145-163.

Chapter of book:

Surname(s) and first letter of name & middle name(s) of author(s).Chapter title. In: Surname(s) and first letter of name & middle name(s) of editor(s), editors. Book title. Edition. Publication place: publisher name; publication date (year); Page number.

Example: Phillips SJ, Whisnant JP. Hypertension and stroke. In: Laragh JH, Brenner BM, editors. Hypertension: pathophysiology, diagnosis, and management. 2nd ed. New York: Raven Press; 1995; 465-478.

Abstract book:

Example: Amini rad O.The antioxidant effect of pomegranate juice on sperm parameters and fertility potential in mice. Cell J. 2008;10 Suppl 1:38.

Thesis:

Name of author. Thesis title. Degree. City name. University. Publication date (year).

Example: Eftekhari Yazdi P. Comparison of fragment removal and co-culture with Vero cell monolayers on development of human fragmented embryos. Presented for the Ph.D., Tehran. Tarbiyat Modarres University. 2004.

Internet references

Article:

Example: Jahanshahi A, Mirnajafi-Zadeh J, Javan M, Mohammad-Zadeh M, Rohani M. Effect of low-frequency stimulation on adenosineA1 and A2A receptors gene expression in dentate gyrus of perforant path kindled rats. Cell J. 2008; 10 (2): 87-92. Available from: http://www.celljournal.org. (20 Oct 2008).

Book:

Example: Anderson SC, Poulsen KB. Anderson's electronic atlas of hematology.[CD-ROM]. Philadelphia: Lippincott Williams & Wilkins; 2002.

D. Proofs are sent by email as PDF files and should be checked and returned within 72 hours of receipt. It is the authors' responsibility to check that all the text and data as contained in the page proofs are correct and suitable for publication. **We are requested to pay particular attention to author's names and affiliations as it is essential that these details be accurate when the article is published.**

E. Pay for publication: Publishing an article in **Cell J** requires Article Processing Charges (APC) that will be billed to the submitting author following the acceptance of an article for publication. For more information please see www.celljournal.org.

F. Ethics of scientific publication: Manuscripts that have been published elsewhere with the same intellectual material will refer to duplicate publication. If authors have used their own previously published work or work that is currently under review, as the basis for a submitted manuscript, they are required to cite the previous work and indicate how their submitted

manuscript offers novel contributions beyond those of the previous work. Research and publication misconduct is considered a serious breach of ethics.

The Journal systematically employs iThenticate, plagiarism detection and prevention software designed to ensure the originality of written work before publication. Plagiarism of text from a previously published manuscript by the same or another author is a serious publication offence. Some parts of text may be used, only where the source of the quoted material is clearly acknowledged.

3. General information

A. You can send your manuscript via online submission system which is available on our website. If the manuscript is not prepared according to the format of **Cell J**, it will be returned to authors.

B. The order of article appearance in the Journal is not demonstrating the scientific characters of the authors.

C. Cell J has authority to accept or reject the manuscript.

D. Corresponding authors should send the manuscripts via the Online Manuscript Submission System. All submissions will be evaluated by the associated editor in order to check scope and novelty. If the manuscript suits the journal criteria, the associated editor would select the single-blind peer-reviewers. The reviewers of the manuscript must not share information about the review with anyone without permission of the editors and authors. If three reviewers pass their judgments on the manuscript, it will be presented to the associated editor of **Cell J**. In the case of having a favorable judgment on the manuscript, reviewers' comments will be presented to the corresponding author (the identification of the reviewers will not be revealed). After receiving the revision, the associated editor would choose the final reviewer among the previous ones. The final decision will be taken by editor-in-chief based on the final reviewer's comments. The review process takes between 2 to 4 months in **Cell J**. The executive member of journal will contact the corresponding author directly within 3-4 weeks by email. If authors do not receive any reply from journal office after the specified time, they can contact the journal office. Finally, the executive manager will respond promptly to authors' request.

After receiving the acceptance letter, the abstract of the paper would be published electronically. The paper will be in a queue to be published in one Cell J. At last, the corresponding author should verify a proof copy of the paper in order to be published.

The Final Checklist

The authors must ensure that before submitting the manuscript for publication, they have to consider the following parts:

1. The first page of manuscript should contain title, name of the author/coauthors, their academic qualifications, designation & institutions they are affiliated with, mailing address for future correspondence, email address, phone, and fax number.

2. Text of manuscript and References prepared as stated in the "guide for authors" section.

3. Tables should be on a separate page. Figures must be sent in color and also in JPEG (Jpg) format.

4. Cover Letter should be uploaded with the signature of all authors.

5. An ethical committee letter should be inserted at the end of the cover letter.

The Editor-in-Chief: Ahmad Hosseini, Ph.D.

Cell Journal *(Yakhteh)*

P.O. Box: 16635-148, Iran

Tel/Fax: + 98-21-22510895

Emails: info@celljournal.org

journals@celljournal.org

Dr. Saeed Kazemi Ashtiani

IN THE NAME OF GOD

Gone But not Forgotten

In the memory of the late Director of Royan Institute, Founder of Stem Cells Research in Iran and Chairman of ***Cell Journal*** *(Yakhteh)*. May he rest in peace.

PUBLISHED & SPONSORED BY:
Publication of Royan Institute (ACECR)

Indexed in:
1. Thomson Reuters (ISI)
2. PubMed
3. PubMed Central (PMC)
4. National Library Medicine (NLM)
5. Biosis Preview
6. Index Medicus for the Eastern Mediterranean Region (IMEMR)
7. Regional Information Center for Sciences and Technology (RICeST)
8. Index Copernicus International
9. Cambridge Scientific Abstract (CSA)
10. EMBASE
11. Scopus
12. Cinahl Database
13. Google Scholar
14. Chemical Abstract Service (CAS)
15. Proquest
16. Directory of Open Access Journals (DOAJ)
17. Open Academic Journals Index (OAJI)
18. Directory of Research Journals Indexing (DRJI)
19. Scientific Information Database (SID)
20. Iranmedex
21. Islamic World Science Citation Center (ISC)
22. Magiran
23. Science Library Index
24. Biological Abstracts
25. Essential Science Indicators
26. EuroPub

ACECR

Editorial Office Address (Dr. Ahmad Hosseini):
Royan Institute, P.O.Box: 16635-148,
Tehran, Iran
Tel & Fax: (+9821)22510895
Website: www.celljournal.org
Emails: info@celljournal.org
journals@celljournal.org

Printing Company:
Naghshe e Johar Co.
No. 103, Fajr alley, Tehranpars Street,
Tehran, Iran.

CONTENTS

Systematic Review

Original Articles

Short Communication

Cell J
Cell Journal (Yakhteh)
Homepage: https://www.celljournal.org/
Systematic Review
Vol 25, No 9, September 2023, Pages: 591-602

Potential Utilisation of Secretome from Ascorbic Acid-Supplemented Stem Cells in Combating Skin Aging: Systematic Review of A Novel Idea

Komang Ardi Wahyuningsih, M.D.[1, 2*], Wimpie I Pangkahila, M.D., Ph.D.[1], I Wayan Weta, M.D., Ph.D.[1], I Gde Raka Widiana, M.D., Ph.D.[1], Ida Ayu Ika Wahyuniari, M.D., Ph.D.[1]

1. Doctoral Program, Faculty of Medicine, Universitas Udayana, Denpasar, Indonesia
2. Histology Department, School of Medicine and Health Sciences, Atma Jaya Catholic University of Indonesia, Jakarta, Indonesia

Abstract

The secretome of stem cells consists of a spectrum of bioactive factors secreted by stem cells grown in culture media-cytokines, chemokines, and growth factors in addition to extracellular vesicles (exosomes and microvesicles). Ease of handling and storage of secretomes along with their bioactivity towards processes in skin aging and customizability makes them an appealing prospective therapy for skin aging. This systematic review aims to investigate the potential usage of ascorbic acid (AA)-supplemented stem cell secretomes (SCS) in managing skin aging. We extracted articles from three databases: PubMed, Scopus, and Cochrane. This review includes *in vitro, in vivo*, and clinical studies published in English that discuss the correlation of AA-supplemented-SCS with skin aging. We identified 1111 articles from database and non-database sources from which nine studies met the inclusion criteria. However, the study results were less specific due to the limited amount of available research that specifically assessed the effects of AA-supplemented SCS in skin aging. Although further studies are necessary, the AA modification of SCS is a promising potential for improving skin health.

Keywords: Ascorbic Acid, Secretome, Skin Aging, Stem Cells

Citation: Wahyuningsih KA, Pangkahila WI, Weta IW, Widiana IGR, Wahyuniari IAI. Potential utilisation of secretome from ascorbic acid-supplemented stem cells in combating skin aging: systematic review of a novel idea. Cell J. 2023; 25(9): 591-602. doi: 10.22074/CELLJ.2023.1995999.1253

Introduction

Stem cells are a group of cells characterised by their versatility; they can differentiate into a variety of cell lineages. Thus, they have a significant role in the facilitation of tissue repair. The stem cell "secretome" refers to the collective spectrum of bioactive factors secreted by stem cells grown in culture media, and it is responsible for the cellular actions of stem cells. The secretome includes soluble proteins such as cytokines, chemokines, and growth factors in addition to extracellular vesicles such as exosomes and microvesicles (1). While both secretomes and stem cells confer regenerative and anti-inflammatory properties, secretomes have several advantages in comparison to cell-based therapies, such as ease of manufacturing, handling, and storage. They also have less immunogenicity (2, 3). This, together with the precise tackling of mechanisms by which skin aging occurs, such as oxidative stress, DNA damage, chronic inflammation, microRNA dysregulation, and cellular senescence, makes secretome an appealing prospective therapy for cutaneous aging (4, 5). Previous studies have demonstrated anti-aging activities from the secretomes of mesenchymal stem cells (MSCs) sourced from adipose (6) and cell-free blood cell secretome (7). Other studies reported the use of secretome from human Wharton's jelly for antiviral activity (8) and from bone marrow MSCs for neuroprotective effects in a rat model of Parkinson's disease (9).

One well-documented feature of secretomes is the ability to modify their compositions and this benefit grants secretomes the flexibility to adjust themselves to specific treatment goals (2). Ascorbic acid (AA) supplementation is proposed to suppress stem cell senescence via its antioxidant property and promote the proliferation rate of MSCs, which ultimately leads to a more effective preparation (10). Furthermore, AA has the potential to optimise secretomes. A preclinical study of human adipose-derived MSCs (hADMSCs) demonstrated supplementation of basal media with AA increased type I collagen mRNA expression. Type I collagen is a structural protein with major implications in skin aging (11).

Although there are published studies about the utilisation of secretomes in dermatology, fewer studies have used AA to modulate the secretome of stem cells in skin aging. This systematic review aims to explore the impact of AA supplementation on stem cell secretomes (SCS) in terms of skin aging.

Received: 12/March/2023, Revised: 10/June/2023, Accepted: 24/June/2023
*Corresponding Address: Doctoral Program, Faculty of Medicine, Universitas Udayana, Denpasar, Indonesia
Email: komang.wahyuningsih@atmajaya.ac.id

Royan Institute
Cell Journal (Yakhteh)

Materials and Methods

This systematic review was conducted according to the Preferred Reporting Items for Systematic Review and Meta-Analysis (PRISMA) (12). The protocol for this review was registered as Open Science Framework Registries ID: 8s9n7 (13).

Search strategy

The search was conducted on 20 September 2022 for articles that pertained to the secretome of stem cells grown in AA-supplemented media. The following keywords were used during the search: (secretome) AND ((vitamin c) OR (ascorbic acid) OR (ascorbate). Table S1 (See Supplementary Online Information at www.celljournal.org) lists detailed keywords used for each database. Because the term "skin aging" did not produce any results in all of the databases, we expanded the search query by omitting this term. The five investigators (KAW, WP, IWW, IGRW, IAIW) independently searched for studies in the PubMed, Scopus, and Cochrane databases. Any discrepancies were discussed together, and the decisions were recorded in a Google Sheets spreadsheet program.

Study eligibility criteria

This review included *in vitro*, *in vivo*, and clinical studies. Studies that included secretomes of stem cells that correlated with the process of skin aging were included. Review articles, studies published in languages other than English, studies that did not mention the AA concentration used, and studies that did not study the specifically study the effect of AA supplementation were excluded.

Data extraction

A predetermined outcome sheet was used to include the following data to be extracted: i. Author and year of publication, ii. Stem cell line used, iii. Growth media, iv. Concentration of AA supplemented, v. Other compounds present in the media, vi. Incubation period, and vii. Secretome-associated outcome. Four researchers (WP, IWW, IGRW, AIAW) extracted the data and the fifth researcher (KAW) verified the accuracy of the extracted data. Any disputes were resolved by discussion between the reviewers.

Results

Search selection and characteristics

Figure 1 details the flow of the literature search. We identified 1111 records from the databases and six from non-database sources. We eliminated four duplicates and 514 studies were marked as ineligible by the spreadsheet program. Thus, 593 titles and their abstracts were screened; ultimately, 55 studies were retrieved and assessed. After application of the exclusion criteria, we included nine studies in this review (11, 14-21).

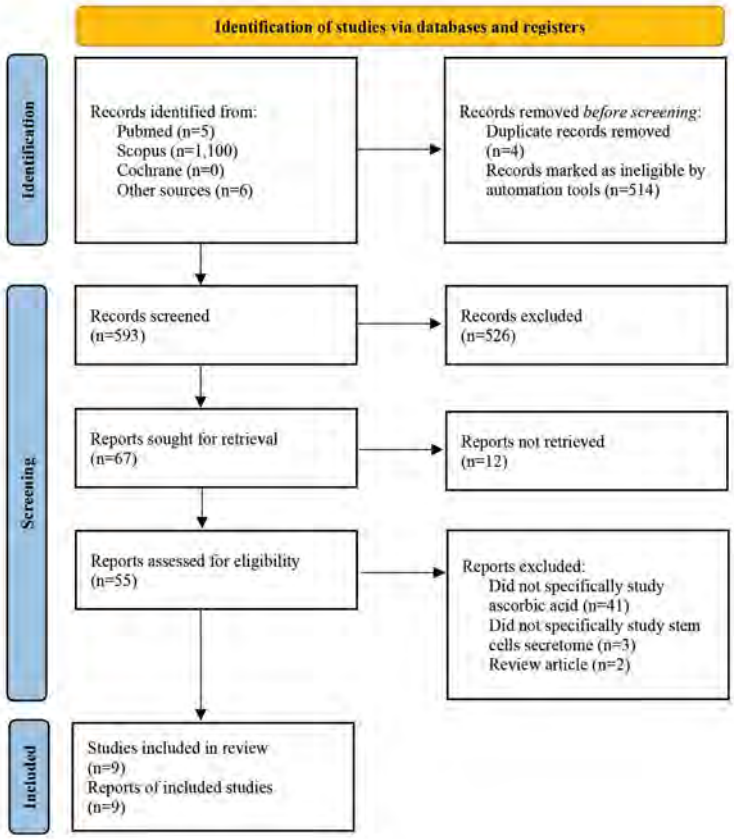

Fig.1: Details the flow of literature search based on the Preferred Reporting Items for Systematic Review and Meta-analysis (PRISMA) criteria.

Table 1: Study characteristics of the included studies

Author (reference) (Year) Citation*	Stem cell		Induction of differentiation					Post-culture or post-induction treatment
	Lineage	Growth media	Duration	Target type	Media	Ascorbic Acid concentration	Induction period	
Wei et al. (14)(2012) Citations: 263	Human periodontal ligament stem cells (hPDLSCs) and minipig-PDLSCs	a-MEM (Gibco) with other compounds at 37°C in 5% CO_2	Not mentioned	N/A	N/A	N/A	N/A	PDLSCs was treated with various doses of AA: 0, 5, 10, 20 and 50 µg/mL
Lui et al. (15)(2016) Citations: 79	Sprague-Dawley rat tendon-derived stem cells	Low glucose DMEM (Gibco) with other compounds	Not mentioned	Tenogenic	Complete culture medium (Invitrogen) at 37°C and 5% CO_2	N/A	14 days	Addition of CTGF and 25 µmol/L AA during induction
Diomede et al. (16) (2019) Citations: 3	Human gingival mesenchymal stem cells	MSCGM-CD; changed every 2 days	2 weeks	Undifferentiated Osteogenic	Undifferentiated MSCGM-CD, MSCGM-CD + AA Osteogenic Osteogenic differentiation medium (Lonza)	Undifferentiated MSCGM-CD: 0 µg/mL MSCGM-CD +AA: 60 µg/mL, 90 µg/mL Osteogenic Not mentioned	21 days	None
Diomede et al. (17) (2019) Citations: 34	Human dental pulp stem cells	MSCGM-CD at 37°C and 5% CO_2	Not mentioned	Osteogenic Adipogenic	Osteogenic Osteogenic culture media kit (Lonza) Adipogenic Adipogenic medium kit (Lonza)	Osteogenic Not mentioned Adipogenic None	Osteogenic 21 days Adipogenic 28 days	HEMA: 2 mM AA: 50 µg/mL Cells grouped to: (1) Control (2) HEMA only (3) AA only(4) HEMA + AA All are treated for 24 hours
Wahyuningsih et al. (11) (2020) Citations: 6	Post-thawed human adipose-derived stem cells	Expanded with in-house media Subsequently cryopreserved thawed, and cultured in either DMEM, DMFA or DMFA + AA	Not mentioned	N/A	N/A	N/A	N/A	Cells grouped to: (1) DMEM (2) DMFA + 0 AA (3) DMFA + 50 µg/mL AA (4) DMFA + 100 µg/mL AA
Bhandi et al. (18) (2021) Citations: 15	Stem cells from human exfoliated deciduous tooth	FBS (Gibco) at 37°C and 5% CO_2 Maintained in DMEM (Invitrogen) with other compounds at 37°C, 5% CO_2. Culture medium replenished 2x weekly	Initial incubation is 24 hours	Adipogenic Osteogenic Chondrogenic	Adipogenic Adipogenic Media (Sigma-Aldrich) Osteogenic Osteogenic Induction Medium (Sigma-Aldrich) Chondrogenic Chondrogenic Induction Medium (Sigma-Aldrich)	Adipogenic None Osteogenic 50 µM Chondrogenic 50 µg/mL	Adipogenic 21 days Osteogenic 21 days Chondrogenic 28 days	Each target type was grouped to: (1) 10 µM AA group (2) No AA added

Table 1: Continued

Author (reference) (Year) Citation*	Stem cell			Induction of differentiation				Post-culture or post-induction treatment
	Lineage	Growth media	Duration	Target type	Media	Ascorbic Acid concentration	Induction period	
Marconi et al. (19) (2021) Citations: 28	Human periodontal ligament stem cells	MSCGM-CD at 37°C and 5% CO_2; changed every 2 days	2 weeks	Adipogenic Osteogenic	Adipogenic MSCBM-CD with other compounds Osteogenic MSCBM-CD with other compounds	Adipogenic None Osteogenic 50 mmol/L	Adipogenic 28 days Osteogenic 21 days	LPS-G: 5 µg/mL AA: 50 µg/mL Cells grouped to: (1) hPDLSCs vs (2) hPDLSCs + LPS-G vs (3) hPDLSCs + AA vs (4) hPDLSCs + LPS-G + AA
Pizzicannella et al. (20) (2021) Citations: 6	Human gingiva-derived mesenchymal stem cells (hGMSCs) and endothelial-hGMSCs	MSCGM-CD at 37 °C and 5% CO_2; changed every 2 days	2 weeks	hGMSCs Adipogenic, osteogenic e-hGMSC Endothelial	Adipogenic MSCBM-CD with other compounds Osteogenic MSCBM-CD with other compounds Endothelial Endothelial growth medium (Lonza) composed of various compounds	Adipogenic None Osteogenic 50 mmol/L Endothelial Not mentioned	Adipogenic 28 days Osteogenic 21 days Endothelial 10 days	LPS-G: 5 µg/mL AA: 50 µg/mL Cells grouped to: (1) hGMSCs vs (2) hGMSCs + LPS-G vs (3) hGMSCs + AA vs (4) hGMSCs + LPS-G + AA (1) e-hGMSCs vs (2) e-hGMSCs + LPS-G vs (3) e-hGMSCs + AA vs (4) e-hGMSCs + LPS-G + AA
Pranskunas et al. (21) (2021) Citations: 4	Rabbit periosteum-derived mesenchymal stem cells	DMEM with other compounds at 37°C and 5% CO_2	Not mentioned	Undifferentiated Osteogenic	Undifferentiated DMEM with other compounds Osteogenic osteogenic-inducing media (in-house)	Undifferentiated None Osteogenic 25 µg/mL	24 days	None

*; As of 2 June 2023, α-MEM; Alpha-modified Eagle's medium, FBS; Fetal bovine serum, AA; Ascorbic acid, MSCGM-CD; Chemically-defined mesenchymal stem cell growth medium (Lonza, Switzerland), DMEM; Dulbecco's Modified Eagle's Medium (Gibco, USA), DMFA; DMEM+10% fetal bovine serum + antibiotic-antimycotic, HEMA; 2-hydroxyethylmethacrylate. LPS-G; P, gingivalis lipopolysaccharide, and ROS; Reactive oxygen species.

The studies included were published from 2012-2021. All were either conducted *in vitro* or *in vivo*, and the cell lineages varied from periodontal stem cells to tendon-derived stem cells from human or animal sources. The studies had different protocols and target type of cell differentiation, such as osteogenic or adipogenic cells. Some studies did not perform induction for cell differentiation. The studies also varied by AA concentration and timing of supplementation (during induction, after culture, or after induction). Table 1 provides details of the study characteristics.

Study outcomes

Table 2 lists the summary of the outcomes of each included study. Increased telomerase activity, higher expressions of structural protein such as collagen, modulation of anti-inflammatory and proinflammatory cytokines, regulation of NF-κB, and influences on other proteins were the various secretome-associated outcomes from AA supplementation of stem cells. Lower amounts of reactive oxygen species (ROS) were also observed in studies that included ROS levels as a study outcome.

Table 2: Outcome of included studies

Author (reference) (Year)	Outcome
Wei et al. (14) (2012)	Increased telomerase activity Higher expression of COL I, fibronectin and β1 integrin mRNAs
Lui et al. (15) (2016)	Improved tendon healing Better collagen arrangement (tightly packed fibrils) due to increased tendon-related mRNA expression (COL1A1)
Diomede et al. (16) (2019)	Increased upregulation of COL1A1 mRNA in Osteogenic Differentiation Medium (Lonza) and in AA 90 µg/mL medium compared to control
Diomede et al. (17) (2020)	AA significantly downregulated NF-κB in HEMA treated cells AA significantly decreased mean ROS production in HEMA treated cells
Wahyuningsih et al. (11) (2020)	Supplementation of AA increased type 1 collagen expression compared to control. No significant difference in collagen expression between 50 and 100 µg/mL AA group.
Bhandi et al. (18) (2021)	Increased secretion of: VEGF, SCF, IGF-1, HGF, bFGF, Ang-1 and EGF Increased secretion of anti-inflammatory cytokines: NO, IDO, PGE-2, IL-10, IL-6 Decreased secretion of inflammatory cytokines: CCL2, TGF-b1
Marconi et al. (19) (2021)	hGMSCs+LPS-G group: increased levels of NF-κB, MyD88, p300, and ROS hGMSCS+LPS-G+AA group: attenuated levels of NF-κB, MyD88, p300, and ROS
Pizzicannella et al. (20) (2021)	hGMSCs+LPS-G group: increased p300 and ROS; decreased DNMT1 hGMSCs+LPS-G+AA group: physiological expression of p300 and DNMT1; reduced ROS
Pranskunas et al. (21) (2021)	Supplementation of AA in osteogenic group resulted in: - Promotion of collagen alpha-1(I) chain, AE binding protein 1, and stanniocalcin-1 - Suppression of fibrillin-2 and cathepsin K Proteins expressed in both groups include collagen alpha-2(I) chain, alpha-1(XII) chain, and fibrillin-1

AA; Ascorbic acid, HEMA; 2-hydroxyethylmethacrylate, and ROS; Reactive oxygen species.

Discussion

Stem cells and secretomes

Stem cells are cells that self-renew and have the capability to differentiate into other cell lineages to repair tissue damage. Hence, they are extensively used in regenerative medicine. Stem cells can be procured from various sources and classified as either embryonic or somatic. Somatic stem cells are commonly used in research and medicine, and they include MSCs and hematopoietic stem cells (1). Somatic stem cells are commonly sourced from perinatal or postnatal sources; they can be procured from the placenta, amniotic fluid, bone marrow, fat, blood, skin, and other sources (1, 22). The most frequently used stem cells in clinical trials are MSCs as they are easily sourced from various adult tissues. The aforementioned capacity to differentiate and heal injured tissues are attributed to secretomes, a collection of substances released by stem cells that can mediate cell-to-cell communication as well as modulate immunity and regeneration (2). Some texts may also refer to secretomes as "conditioned medium" (5).

The secretome of a stem cell is composed of various substances. For instance, the secretome of mesenchymal cells may include peptides that have anti-microbial and immunomodulatory activities such as interleukin (IL)-1β, IL-6, IL-10, and TGF-β; growth factors such as vascular endothelial growth factor, fibroblast growth factor-2, platelet-derived growth factor, and epidermal growth factor that are responsible for stimulating angiogenesis and growth of other tissues; extracellular matrix (ECM) proteins such as matrix metalloproteinases (MMPs), elastin, and collagen that promote ECM production and remodelling; and other compounds enclosed in exosomes such as miRNAs, lipids, and noncoding RNAs that may regulate inflammatory pathways (2, 23, 24). The

therapeutic potentials of MSC secretomes have been studied in models of cutaneous wound healing, psoriasis, and muscle injuries. Its anti-photoaging, antioxidative, and hair growth properties have been reported (5, 23-25).

Mechanism of skin aging

Skin aging is described as a gradual process where the skin's appearance changes due to intrinsic and extrinsic aging from environmental damage (26). Some of the more prominent signs of aging are dyspigmentation, sagging, and telangiectasia. However, wrinkling is a key sign of aging in many validated and non-validated aging scales (27). Wrinkles mainly occur when there is a decrease in the production of collagen, which helps anchor the dermal-epidermal junction (11). Histological studies of aging skins have shown progressive reduction of dermis vasculature, thinning of collagen fibres, and lysis and thickening of the fibres in the deep dermis. Elastic fibres in the skin are mainly composed of elastin, and they also tend to diminish. They are also non-functioning, amorphous, curled, thickened, and fragmented. These pathological changes in elastic skin fibre are characteristic of photoaging and termed "solar elastosis" (28, 29).

The multifaceted process of skin aging is thought to involve various mechanisms such as oxidative stress, changes in genetic material, and others. These processes could occur intrinsically as a result of genetic factors and natural processes such as structural and functional changes in the components of the ECM. However, it could also occur extrinsically with environmental factors such as ultraviolet (UV) light and various free radical exposure (4, 30).

Reactive oxygen species and oxidative stress

Oxidative stress is a phenomenon that could occur in the body's cells and tissues when there is an imbalance between free radicals, specifically ROS, and the ability of the human body to neutralize them. Under normal circumstances cells produce ROS for certain physiological roles and as a by-product of oxygen-related metabolism (4, 31). ROS produced by the body are quickly stabilised through the body's antioxidant defence mechanism (31). Failure to do so causes an increase in oxidative stress that consequently leads to various problems such as accelerated skin aging. Excess ROS production in the skin can be induced by UV light and result in "photoaging". ROS generation is mainly brought about by UVA (320-400 nm) since UVB is unable to pass through the deeper section of the epidermis. The energy of UVA which penetrates the skin is absorbed by cellular chromophores that causes it to enter a singlet excited state. In this condition, the chromophore can partake in two possible pathways - either the chromophore falls back into its ground state and releases energy as heat or it can enter an intermediate triplet excited state. As this state is intermediary, the energy is further transferred into a reaction that involves DNA and molecular oxygen, which results in DNA modification or ROS production that increases the oxidative stress of a cell. ROS produced by this mechanism includes superoxide, hydroxyl radicals, singlet oxygen or hydrogen peroxide. Meanwhile the modification of DNA, especially 4977 bp deletion of the mtDNA, leads to an increase in ROS production in the mitochondria (30). There is also evidence for UVB involvement of in photoaging. Wahyono previously demonstrated decreased expression of type I collagen and increased expression of MMP-1 in white rats exposed to 130-150 mJ/cm^2 of UVB (32). Aside from photoaging, there are other mechanisms or conditions which may generate excess ROS; one example is a surplus of D-galactose. This reducing sugar readily reacts with free amines of amino acids through nonenzymatic glycation to form advanced glycation end products. This oxidative metabolism of D-galactose and glycation of the end product reaction generates ROS as a side-product (33).

Nuclear factor kappa B signalling pathway in skin aging

An increase in oxidative stress due to ROS accumulation may lead to skin inflammation and the formation of wrinkles. Induction of skin inflammation by ROS may be mediated by the induction of the nuclear factor kappa B (NF-κB) pathway, typically due to stimulation of IGF1 (34, 35). This consequently leads to the expression of inflammatory cytokines and activation of tumour necrosis factor-α (TNF-α) and MMPs that are responsible for the degradation of various connective tissues, such as the ECM, and this can speed up the skin aging process (34). Degradation of the ECM will lead to expression and activation of activator protein 1 (AP-1), a transcription factor that promotes inflammation and collagen degradation, and consequently increases skin aging (30). The effect of NF-κB inhibition in skin aging has been previously reported by Rui et al. (36) Inhibition of the NF-κB pathway reduced downstream expressions of TNF-α and MMPs in the skin of mice. Hydroxyproline quantification and histopathological assessments also supported these results, and showed that inhibition of NF-κB attenuated MMP-mediated UV-induced photoaging. UV irradiation can decrease type VII collagen, which are anchoring fibrils responsible for stability at the dermal-epidermal junction (4). Li et al. (37) also reported that inhibition of NF-κB could reduce NF-κB-mediated gene expression and production of bFGF and MMP-1. Blockade of NF-κB also reduced UVB-induced proliferation of mice keratinocytes.

DNA/RNA damage and telomere shortening

In addition to ROS and oxidative stress, changes in genetic materials are large contributors toward skin aging. Phenomena such as DNA/RNA damage and telomere shortening are responsible for skin aging. UV irradiation

is one of the mechanisms that result in DNA/RNA damage. Damage in the *COL1A1*, *COL1A2*, *COL3A1*, *COL4A1*, and *COL7A* genes can disrupt collagen synthesis and may accelerate skin aging. The *COL1A1* and *COL1A2* genes are especially important in the maintenance of the skin's mechanical properties, as they encode type I collagen, which is a vital extracellular protein of the skin. Type I collagen does not work alone; it requires the support of type III collagen, which is encoded by *COL3A1*. Both type I and III collagen play a key role in maintaining the elasticity of human skin; therefore, downregulation or damage to their respective genes is thought to cause premature skin aging (38, 39).

Damaged DNA materials are usually repaired through the nucleotide excision repair pathway, such as single-stranded DNA-binding protein RPA, clamp loader PCNA, and polymerase (40). Normally, these proteins are present in the skin, but under certain circumstances they may be deficient. This deficiency contributes to premature skin aging. DNA in human cells is condensed into chromosomes with telomeres that serve as caps to protect the chromosomes from degradation and vital DNA from deletion. The telomeres protect the chromosomes by exposing themselves to degradation and they naturally shorten throughout the aging process. This shortening is balanced by telomerase activity, which extends the telomere ends of a chromosome. It is also thought that deficiency in this enzyme can lead to accelerated aging due to various defects in tissue regeneration and suppression of epidermal stem cell proliferation capacity (4).

Inflammaging

Inflammaging is a phenomenon where chronic, low-intensity inflammation is identified as one of the major characteristics of aging. The mechanism of inflammaging is attributed to oxidised lipid damage of cells. The two play a key role in an inflammatory response by activating macrophages, which cause them to release MMPs that degrade the ECM. One of the contributing factors of inflammaging is repeated exposure to UV radiation. This exposure causes an overdrive in the complement system that overworks the macrophages. These overworked macrophages release ROS and proinflammatory cytokines. This process damages the dermis and, consequently, the skin (4).

Immunosuppression

Chronic low-grade inflammation that may be caused by UV radiation can eventually stimulate immunosuppression of T regulatory cells, regulatory dendritic cells, and myeloid-derived suppressor cells. This immunosuppression causes immunosenescence, which not only decreases immune cell activity but also stimulates degeneration of neighbouring cells (41). Immune cell activity decreases due to the catabolism of L-arginine and tryptophan caused by the activation of the arginase 1 and indoleamine 2,3-dioxygenase enzymes. Degeneration of neighbouring cells are mainly due to impairment of host tissue homeostasis, such as TGF-β signalling, which may lead to degradation of the ECM (34). The immunosuppressed condition leads to a higher risk of infection; since the skin is exposed to a vast array of pathogens, immunosuppressed patients are thought to have higher risk of contracting *tinea pedis* fungal infections, pyoderma bacterial infections, and herpes zoster infection. Normal skin flora such as *Staphylococcus* sp. and *Streptococcus* sp. can become pathologic under immunosuppressed conditions. These opportunistic infections are considered to be a contributing factor towards skin aging because they cause disruptions to the skin's structure (42).

Cellular senescence

Cellular senescence refers to the gradual decrease of a cell's proliferative ability until it enters a state of irreversible cell cycle arrest. Other characteristics of senescent cells are the development of resistance to apoptosis, release of proinflammatory factors, and tissue deterioration factors (43). As many as 20 different cell types in the skin have different proliferative capacities. However, as the skin ages, they turn into senescent skin cells and accumulate over time. Senescent skin cells are formed normally as humans age; they are created by provoking senescence-inducing stimuli. However, the exact mechanism of how the diverse types of skin cells respond to these stimuli are not fully understood. Senescent skin cells can also form under pathologic circumstances, such as ones caused by extrinsic stress signals and oncogene expression (44). This cellular senescence can affect all skin layers and result in changes in their structure and functionality, such as the aging of the epidermal layer which results in decreased barrier and restoration function (43). Various age-related skin pathologies such as hyperpigmented lesions, diabetic wounds, and psoriasis are strongly associated with senescent skin cells (44).

Autophagy

Autophagy is defined as "a starvation-induced cellular recycling pathway" wherein cytoplasmic components undergo lysosomal degradation. It helps maintain the skin's health and plays a key role in controlling skin aging. The main function of autophagy in the aforementioned process involves the elimination of senescent subcellular organelles and proteins as well as regulation of the functions of various skin cells (keratinocytes, dermal fibroblasts, and melanocytes) (45). Physiologically, autophagy has been shown to correlate with the response of keratinocytes to various types of stress, the majority of which contribute to accelerated skin aging. UVB irradiation is the best example among the stressors that can cause inflammation and DNA damage. It has been said to instigate autophagy as primary keratinocyte response to

recognize DNA damage, aiding the process of nucleotide repair (46). A downregulation in autophagy may eventually give rise to unregulated hyperinflammatory skin reactions and lead to accelerated skin aging. Genes that play a major role in modulating autophagy are *BECN1, MAP1LC3B, ATG5, ATGJ,* and *mTOR* (45).

Optimising secretome production

Secretome production is influenced by various factors; intervention in this process can aid in optimising its production. It has been reported that ultrafiltration and freeze-drying techniques can enhance the quality of MSC-secretome production by isolating and purifying the secretomes (47). Molecular priming, tissue engineering, modification of growth medium composition, and hypoxic preconditioning are strategies proposed to increase the production of specific secretomes. Molecular priming with FGF, IL-1, and IFN-ɣ could increase G-CSF, IL-6, TSG-6, and VEGF production. Hypoxic preconditioning and tissue engineering with hydrogels or scaffolds has been shown to increase production of FGF2, HGF, IGF, TGF-β, and VEGF. Changing serum content of the growth medium caused stem cells to enhance the production of BDNF, HGF, IL-6, NGF, PEG2, TGF-β, and VEGF (48). Although these studies showed ways to optimise the production of secretome, they were not specifically applied to skin aging.

Secretomes affected by ascorbic acid and implications in skin aging

Promotion of collagen expression by stem cells has been reported (14-16). The promotion of collagen expression was observed in MSCs derived from human gingival MSCs and rabbit periosteum MSCs. We previously observed increased collagen expression in post-thawed hADMSCs supplemented with 50 and 100 µg/mL of AA. The 50 µg/mL AA demonstrated the greatest increase in collagen expression, although the difference was not statistically significant compared to the 100 µg/mL AA group (11). Collagen expression also increased in periodontal ligament stem cells and tendon-derived stem cells. In Sprague-Dawley rat tendon-derived stem cells, addition of 25 µmol/L of AA resulted in superior collagen arrangement, which was attributed to the greater COL1A1 mRNA expression (15). As previously mentioned, both the decline and degradation in collagen are heavily implicated in skin aging. Decreased collagen content and increased collagen degradation are observed in photoaged skin. Hence, remodelling and replacement of skin collagen along with promotion of collagen expression is hypothesised as a beneficial treatment for skin aging (4).

Fibronectin and β1 integrin expression activity also increased after AA supplementation of periodontal ligament stem cells (14). Fibronectin fibrils form scaffolds that enable proteins such as collagen, elastin, and proteoglycans to bind. Fibronectin is an important part of the ECM that plays a role in ECM maturation and attachment, signalling, and cellular migration (49, 50). Fibronectin matrices also can sequester growth factors, and release them in a timely manner to regulate cell growth and morphogenesis (51). The importance of fibronectin to prevent aging through the loss of stem cells has been reported (52). β1 integrin is a proliferative marker of stem cells, and there is a reduction in epidermal β1 integrin in skin aging (53). AA supplementation may induce stem cell proliferation as evidenced by the increased expression of β1 integrin in periodontal ligament stem cells (14). The result of the author's previous study showed that 75 µg/ml of AA supplementation resulted in the lowest cell spread size, highest cell yield, and fastest doubling time (54).

Pranskunas et al. (21) found that production of cathepsin K was suppressed in rabbit periosteum-derived MSCs supplemented with 25 µg/mL of AA. Cathepsins are elastolytic proteases that cleave elastin fibres. The elastolytic activity of cathepsins is thought to be significantly higher than MMPs. Cathepsins can release elastokines and ECM-degrading enzymes with exacerbation of local tissue damage and aging. As such, cathepsins are also a prospective target for treatment of skin aging (55). The same study also reported suppression of fibrillin-2 in AA-supplemented MSCs (21). Remodelling, reduction, and truncation of fibrillin-rich microfibrils (FRMs) were found to play a role in various pathologies, including photoaging (56). These changes might be caused by its photoreactive nature, which is attributed to the chromophoric amino acid constituents of microfibrils (57). Physiologically, FRMs play a role in the modulation of TGF-β signalling and skin remodelling. A disturbance in the TGF-β signalling pathway may result in aberrant elastin deposition (58). FRMs may also fragment under certain UV doses, which consequently upregulate MMPs and further degrade the ECM (56). UV exposure of the photoreactive FRMs might lead to microfibril exhaustion with simultaneous damage and degradation of the skin ECM. This would explain the concurrent observed phenomena of microfibril reduction and skin aging.

NF-κB is an inflammatory mediator that was elevated in cells treated with 2-hydroxyethylmethacrylate HEMA and in cells treated with *Porphyromonas gingivalis* (*P. gingivalis*) polysaccharide (LPS-G) (17, 20). However, cells treated with AA had decreased NF-κB levels, which was observed through inhibition of the MyD88 and p300 pathway (19). In another study, inhibition of NF-κB translocation was achieved through blockage of NF-κB translocation (17). As previously mentioned, initiation of the NF-κB signalling pathway could lead to skin inflammation and wrinkle formation through the activation of MMPs (34). Overexpression of NF-κB has been observed in aged human fibroblasts. Increased NF-κB levels also decreased dermal fibroblast *COL1A1* gene expression and type I collagen secretion *in vitro* (59).

While telomere shortening is crucial for prevention of abnormal cellular proliferation, it may result in cellular

senesce and skin aging. As such, telomerase activation should theoretically improve skin aging. Telomeres in skin cells may be especially prone to accelerated shortening due to rapid proliferation and damaging agents such as ROS (60). Increased telomerase activity has been observed in human periodontal ligament stem cells (hPDLSCs) treated with AA (14). Nevertheless, it is not known if very long telomeres would be beneficial for cells.

The addition of AA to stem cells also reduced ROS production (17, 19, 20). Irradiation by UVA or UVB generates ROS and activates cell surface receptors that lead to the activation of MAP-kinase p38, JNK, and ERK. The transcription AP-1 is consequently expressed, which results in ECM degradation through the expression of various MMPs in fibroblasts and keratinocytes. AP-1 also has an inhibitory effect on TGF-β, which plays a part in collagen production (30). Yang et al. (60) have shown that AA slowed down MSC senesce via inhibition of the ROS-activated AKT/mTOR signalling pathway. They pretreated bone marrow-derived MSCs with AA followed by subsequent exposure to D-galactose and AA. D-galactose was administered to induce ROS production and activate the Akt/mTOR signalling pathway. The results showed that AA reduced p16 and SA-β-gal expression, a marker of cellular senescence and premature senescence, respectively. While no study exists on the effect of secretome from AA-treated stem cells on autophagy, there is evidence that secretomes from hypoxia-preconditioned hPDLSCs may activate the PI3K/Akt/mTOR signalling pathway, a regulator of the autophagy process (61). mTOR is thought to play an important role in triggering autophagy by its role as a pivotal upstream effector of the PI3K/Akt pathway. Hence, a balance in the PI3K/Akt/mTOR may be essential to achieve optimal skin conditions.

AA-treated human exfoliated deciduous tooth stem cells showed increased secretion of anti-inflammatory cytokines and decreased secretion of proinflammatory cytokines (18). While IL-6 is considered to be both an inflammatory and anti-inflammatory cytokine, it does not exhibit any direct inflammatory activity in the skin, even though its level increases in inflammatory conditions such as rheumatoid arthritis. Under damaging conditions such as exposure to UV radiation, the skin keratinocytes are stimulated to increase IL-6 production because of its ability to assist with keratinocyte proliferation. However, IL-6 also plays a role in the formation of skin wrinkles (62). In the same study, the AA-treated stem cells had increased production of growth factors that possess the ability to assist with ECM repair (19). EGF is a growth factor that has anti-aging properties and the ability to promote skin wound repairs (63). Another growth factor that plays an important role in preventing skin aging is FGF. It is directly correlated with the induction of collagen and elastin synthesis, two compounds essential in skin resistance and elasticity (64).

There is evidence that AA may not only affect the secretomes of stem cells, it may also indirectly modulate epigenetic changes in these stem cells. Human gingiva-derived MSCs treated with LPS-G had evidence of increased p300 levels and decreased DNMT1 levels. Addition of AA prior to exposure to LPS-G facilitated the cells to express physiological levels of p300 and DNMT1 (20). p300 is a histone acetyltransferase that may be implied in the process of skin aging via activation of UV-triggered MMP-1. Overexpression of p300 increased the activity of basal and MMP-1 promoter (65). DNMT1 is a major enzyme involved in DNA methylation. DNMT expression was higher in young human skin fibroblasts compared to their older counterparts. A knockout model of DNMT1 in young human skin fibroblasts induced senescence (66).

Potential for application in humans

Stem cells and their products are extensively used in medical practices as cell-based therapy and as SCS therapy, respectively. A study conducted in 2018 concluded that while cell-based stem cell therapy is helpful, there are a few notable safety issues. Some patients who received cell-based therapy as a treatment of inflammatory bowel disease experienced serious adverse effects and worsening of this disease (67). Another study reported that usage of ADSCs in treating age-related macular degeneration precipitated vision loss in three patients. The vision loss was thought to be caused by the undesired differentiation of the stem cells into myofibroblast-like cells (68). The biggest concern of cell-based therapy is the possibility of stem cell differentiation into undesired tissues such as bones, cartilages and even cancerous tissues. Stem cells, such as MSCs, exhibit an ability to suppress anti-tumour responses as well as the ability to form new blood vessels; these factors may promote tumour growth and metastasis in cancer. Migration of the stem cells towards a primary tumour may accelerate and worsen the cancer (67). To summarise, unpredictability and increased risk of malignancy are some of the primary drawbacks of cell-based therapy.

On the other hand, numerous evidence suggests that SCS are a better method of therapy compared to its cell-based counterpart. The absence of DNA in SCS therapy has overcome the increased risk of cancer found in cell-based therapy; the lack of DNA greatly reduces the risk of mutation and tumour formation in the host. Moreover, secretome production can be controlled; the type that is required can be produced by modifying the condition of the cell culture (69). For instance, cells cultured in a bioreactor secreted secretomes more efficiently (70).

The dosage and safety of SCS are also considered to be more flexible in comparison to cell-based therapy (69). Preclinical studies on the use of SCS in inflammatory bowel disease, an antigen-induced model of arthritis, and Sjögren's syndrome proved to have some therapeutic potential (71). The SCS exhibits anti-inflammatory and anti-fibrotic

activity; it is suggested that SCS likely has the ability to support cell differentiation and could assist damaged tissue repair (1). A clinical case report showed that secretomes of MSCs, specifically the growth factors and cytokines, have great potential in alveolar bone regeneration. The application of the secretome was considered safe, as it showed minimal inflammatory signs and did not present any systemic or local complications in this study (72).

Secretomes are currently being studied for their use in human health. An Indonesian clinical trial assessed secretomes from hypoxia-MSC as treatment for severe COVID-19 patients (73). The evidence collectively suggest that SCS therapy is safer compared to cell-based therapy and has great potential for managing certain diseases.

None of the studies included were designed for secretomes from skin cells. We considered the absence of these studies to be a limitation. Although the sources of the secretomes included in were from non-skin cell sources, the benefit was not limited to stem cells that received AA. Kerscher et al. demonstrated intradermal administration of secretome from non-skin cells to rejuvenate aging skin (7). Wang et al. (6) also reported encouraging results in human dermal fibroblasts cells treated with secretomes from human adipocyte-derived stem cells. This highlights the versatility and potential that SCS have for treatment of skin aging.

To the best of our knowledge, this is the first systematic review that studied the potential application of secretomes from AA-supplemented stem cells as treatment of skin aging. Due to the limited amount of research that specifically studied the effect of AA-supplemented SCS in the context of skin aging, adjustments to the query was made. Thus, the study results were less specific. Because of the decreased amount of literature, we also did not limit our search to a specific stem cell line. However, the scarcity of studies reflects the novelty of this topic.

Conclusion

While the results of our systematic review are promising, further studies are warranted. Modification of SCS with AA may render them better suited for treatment of skin aging. Various methods of secretome administration for skin aging should be studied. The secretome of skin cells treated with AA is necessary to be studied in the context of skin aging. Lastly, we recommend that the potential of secretomes from stem cells supplemented with AA should be confirmed in well-designed *in vivo* and clinical studies.

Acknowledgments

There is no financial support and conflict of interest for this study.

Authors' contributions

K.A.W.; Conceptualization and Data curation. K.A.W., W.I.P., I.W.W., I.G.R.W.; Investigation. K.A.W., W.I.P., I.W.W., I.G.R.W., I.A.I.W.; Wrote the original draft. K.A.W., I.A.I.W.; Wrote, Reviewed, and Edited the manuscript. All authors read and approved the final manuscript.

References

1. Kumar LP, Kandoi S, Misra R, Vijayalakshmi S, Rajagopal K, Verma RS. The mesenchymal stem cell secretome: A new paradigm towards cell-free therapeutic mode in regenerative medicine. Cytokine Growth Factor Rev. 2019; 46: 1-9.
2. González-González A, García-Sánchez D, Dotta M, Rodríguez-Rey JC, Pérez-Campo FM. Mesenchymal stem cells secretome: the cornerstone of cell-free regenerative medicine. World J Stem Cells. 2020; 12(12): 1529-1552.
3. Konala VB, Mamidi MK, Bhonde R, Das AK, Pochampally R, Pal R. The current landscape of the mesenchymal stromal cell secretome: a new paradigm for cell-free regeneration. Cytotherapy. 2016; 18(1): 13-24.
4. Zhang S, Duan E. Fighting against skin aging: the way from bench to bedside. Cell Transplant. 2018; 27(5): 729-738.
5. Damayanti RH, Rusdiana T, Wathoni N. Mesenchymal stem cell secretome for dermatology application: a review. Clin Cosmet Investig Dermatol. 2021; 14: 1401-1412.
6. Wang T, Guo S, Liu X, Xv N, Zhang S. Protective effects of adipose-derived stem cells secretome on human dermal fibroblasts from ageing damages. Int J Clin Exp Pathol. 2015; 8(12): 15739-15748.
7. Kerscher M, Wagner-Schiffler S, Noah EM, Fischer T, Greiner-Krüger D, Sattler S, et al. Cell-free blood cell secretome (BCS) counteracts skin aging: multi-center prospective regenerative aesthetic medicine study using Exokine®. Clin Cosmet Investig Dermatol. 2022; 15: 1157-1173.
8. Hussein MAA, Hussein HAM, Thabet AA, Selim KM, Dawood MA, El-Adly AM, et al. Human wharton's jelly mesenchymal stem cells secretome inhibits human SARS-CoV-2 and avian infectious bronchitis coronaviruses. Cells. 2022; 11(9): 1408.
9. Mendes-Pinheiro B, Anjo SI, Manadas B, Da Silva JD, Marote A, Behie LA, et al. Bone marrow mesenchymal stem cells' secretome exerts neuroprotective effects in a parkinson's disease rat model. Front Bioeng Biotechnol. 2019; 7: 294.
10. Fujisawa K, Hara K, Takami T, Okada S, Matsumoto T, Yamamoto N, et al. Evaluation of the effects of ascorbic acid on metabolism of human mesenchymal stem cells. Stem Cell Res Ther. 2018; 9(1): 93.
11. Wahyuningsih KA, Karina K, Rosadi I, Rosliana I, Subroto WR. Effect of ascorbic acid on morphology of post-thawed human adipose-derived stem cells. Stem Cell Investig. 2020; 7: 16.
12. Page MJ, McKenzie JE, Bossuyt PM, Boutron I, Hoffmann TC, Mulrow CD, et al. The PRISMA 2020 statement: an updated guideline for reporting systematic reviews. BMJ. 2021; 372: n71.
13. Wahyuningsih KA, Pangkahila W, Weta IW, Widiana IGR, Wahyuniari IAI. Systematic review of potential utilization of secretome from ascorbic acid-supplemented stem cells for skin aging. 2023. Available from: https://osf.io/7vjek/ doi: 10.17605/OSF.IO/8S9N7 (6 Jun 2023).
14. Wei F, Qu C, Song T, Ding G, Fan Z, Liu D, et al. Vitamin C treatment promotes mesenchymal stem cell sheet formation and tissue regeneration by elevating telomerase activity. J Cell Physiol. 2012; 227(9): 3216-3224.
15. Lui PP, Wong OT, Lee YW. Transplantation of tendon-derived stem cells pre-treated with connective tissue growth factor and ascorbic acid in vitro promoted better tendon repair in a patellar tendon window injury rat model. Cytotherapy. 2016; 18(1): 99-112.
16. Diomede F, Marconi GD, Serroni M, Pizzicannella G, Trubiani O, Pizzicannella J. Ascorbic acid enhances bone parameter expression in human gingival mesenchymal stem cells. J Biol Regul Homeost Agents. 2019; 33(6): 1715-1723.
17. Diomede F, Marconi GD, Guarnieri S, D'Attilio M, Cavalcanti MFXB, Mariggiò MA, et al. A Novel role of ascorbic acid in anti-inflammatory pathway and ROS generation in HEMA treated dental pulp stem cells. Materials (Basel). 2019; 13(1): 130.
18. Bhandi S, Alkahtani A, Mashyakhy M, Abumelha AS, Albar NHM,

Renugalakshmi A, et al. Effect of ascorbic acid on differentiation, secretome and stemness of stem cells from human exfoliated deciduous tooth (SHEDs). J Pers Med. 2021; 11(7): 589.
19. Marconi GD, Fonticoli L, Guarnieri S, Cavalcanti MFXB, Franchi S, Gatta V, et al. Ascorbic acid: a new player of epigenetic regulation in LPS-gingivalis treated human periodontal ligament stem cells. Oxid Med Cell Longev. 2021; 2021: 6679708.
20. Pizzicannella J, Marconi GD, Guarnieri S, Fonticoli L, Della Rocca Y, Konstantinidou F, et al. Role of ascorbic acid in the regulation of epigenetic processes induced by Porphyromonas gingivalis in endothelial-committed oral stem cells. Histochem Cell Biol. 2021; 156(5): 423-436.
21. Pranskunas M, Šimoliūnas E, Alksne M, Martin V, Gomes PS, Puisys A, et al. Assessment of the bone healing process mediated by periosteum-derived mesenchymal stem cells' secretome and a xenogenic bioceramic-an in vivo study in the rabbit critical size calvarial defect model. Materials (Basel). 2021; 14(13): 3512.
22. Bacakova L, Zarubova J, Travnickova M, Musilkova J, Pajorova J, Slepicka P, et al. Stem cells: their source, potency and use in regenerative therapies with focus on adipose-derived stem cells - a review. Biotechnol Adv. 2018; 36(4): 1111-1126.
23. Sandonà M, Di Pietro L, Esposito F, Ventura A, Silini AR, Parolini O, et al. Mesenchymal stromal cells and their secretome: new therapeutic perspectives for skeletal muscle regeneration. Front Bioeng Biotechnol. 2021; 9: 652970.
24. Ahangar P, Mills SJ, Cowin AJ. Mesenchymal stem cell secretome as an emerging cell-free alternative for improving wound repair. Int J Mol Sci. 2020; 21(19): 7038.
25. Sriramulu S, Banerjee A, Di Liddo R, Jothimani G, Gopinath M, Murugesan R, et al. Concise review on clinical applications of conditioned medium derived from human umbilical cord-mesenchymal stem cells (UC-MSCs). Int J Hematol Oncol Stem Cell Res. 2018; 12(3): 230-234.
26. Sjerobabski-Masnec I, Situm M. Skin aging. Acta Clin Croat. 2010; 49(4): 515-518.
27. Wong QYA, Chew FT. Defining skin aging and its risk factors: a systematic review and meta-analysis. Sci Rep. 2021; 11(1): 22075.
28. Bonta M, Daina L, Mețiu G. The process of ageing reflected by histological changes in the skin. Rom J Morphol Embryol. 2013; 54 Suppl 3: 797-804.
29. Lee H, Hong Y, Kim M. Structural and functional changes and possible molecular mechanisms in aged skin. Int J Mol Sci. 2021; 22(22): 12489.
30. Rinnerthaler M, Bischof J, Streubel MK, Trost A, Richter K. Oxidative stress in aging human skin. Biomolecules. 2015; 5(2): 545-589.
31. Pizzino G, Irrera N, Cucinotta M, Pallio G, Mannino F, Arcoraci V, et al. Oxidative stress: harms and benefits for human health. Oxid Med Cell Longev. 2017; 2017: 8416763.
32. Wahyono P. Impact of Uv-b rays on photoaging. Int J Innov Eng Res Technol. 2020; 7(6): 143-147.
33. Han H, Liu Z, Yin J, Gao J, He L, Wang C, et al. D-galactose induces chronic oxidative stress and alters gut microbiota in weaned piglets. Front Physiol. 2021; 12: 634283.
34. Wang Y, Wang L, Wen X, Hao D, Zhang N, He G, et al. NF-κB signaling in skin aging. Mech Ageing Dev. 2019; 184: 111160.
35. García-García VA, Alameda JP, Page A, Casanova ML. Role of NF-κB in ageing and age-related diseases: lessons from genetically modified mouse models. Cells. 2021; 10(8): 1906.
36. Rui Y, Zhaohui Z, Wenshan S, Bafang L, Hu H. Protective effect of MAAs extracted from Porphyra tenera against UV irradiation-induced photoaging in mouse skin. J Photochem Photobiol B. 2019; 192: 26-33.
37. Li J, Yoshida Y, Kurita M, Usuki T. Cynaropicrin and inhibition of NF-κB activation: a structure activity relationship study. Bioorg Med Chem Lett. 2019; 29(12): 1518-1521.
38. Lago JC, Puzzi MB. The effect of aging in primary human dermal fibroblasts. PLoS One. 2019; 14(7): e0219165.
39. Al-Atif H. Collagen supplements for aging and wrinkles: a paradigm shift in the fields of dermatology and cosmetics. Dermatol Pract Concept. 2022; 12(1): e2022018.
40. Slade D. Maneuvers on PCNA rings during DNA replication and repair. Genes (Basel). 2018; 9(8): 416.
41. Salminen A, Kaarniranta K, Kauppinen A. Photoaging: UV radiation-induced inflammation and immunosuppression accelerate the aging process in the skin. Inflamm Res. 2022; 71(7-8): 817-831.
42. Sergeyenko AM, Rosenfeld DJ, Tsoukas MM. Chronic immunosuppression in the mature patient. Clin Dermatol. 2018; 36(2): 255-263.
43. Csekes E, Račková L. Skin aging, cellular senescence and natural polyphenols. Int J Mol Sci. 2021; 22(23): 12641.
44. Ho CY, Dreesen O. Faces of cellular senescence in skin aging. Mech Ageing Dev. 2021; 198: 111525.
45. Jeong D, Qomaladewi NP, Lee J, Park SH, Cho JY. The role of autophagy in skin fibroblasts, keratinocytes, melanocytes, and epidermal stem cells. J Invest Dermatol. 2020; 140(9): 1691-1697.
46. Eckhart L, Tschachler E, Gruber F. Autophagic control of skin aging. Front Cell Dev Biol. 2019; 7: 143.
47. Mocchi M, Bari E, Marrubini G, Bonda AF, Perteghella S, Tartara F, et al. Freeze-dried mesenchymal stem cell-secretome pharmaceuticalization: optimization of formulation and manufacturing process robustness. Pharmaceutics. 2021; 13(8): 1129.
48. Meiliana A, Dewi NM, Wijaya A. Mesenchymal stem cell secretome: cell-free therapeutic strategy in regenerative medicine. Indones Biomed J. 2019; 11(2): 113-124.
49. Dalton CJ, Lemmon CA. Fibronectin: molecular structure, fibrillar structure and mechanochemical signaling. Cells. 2021; 10(9): 2443.
50. Gimeno-LLuch I, Benito-Jardón M, Guerrero-Barberà G, Burday N, Costell M. The role of the fibronectin synergy site for skin wound healing. Cells. 2022; 11(13): 2100.
51. Patten J, Wang K. Fibronectin in development and wound healing. Adv Drug Deliv Rev. 2021; 170: 353-368.
52. Lukjanenko L, Jung MJ, Hegde N, Perruisseau-Carrier C, Migliavacca E, Rozo M, et al. Loss of fibronectin from the aged stem cell niche affects the regenerative capacity of skeletal muscle in mice. Nat Med. 2016; 22(8): 897-905.
53. You J, Roh KB, Li Z, Liu G, Tang J, Shin S, et al. The antiaging properties of andrographis paniculata by activation epidermal cell stemness. Molecules. 2015; 20(9): 17557-17569.
54. Wahyuningsih KA. Effect of L-ascorbic acid-2-phosphate towards proliferation rate of human adipose-derived stem cells. Sapporo Med J. 2020; 54(7): 1-10.
55. Panwar P, Hedtke T, Heinz A, Andrault PM, Hoehenwarter W, Granville DJ, et al. Expression of elastolytic cathepsins in human skin and their involvement in age-dependent elastin degradation. Biochim Biophys Acta Gen Subj. 2020; 1864(5): 129544.
56. Langton AK, Hann M, Costello P, Halai P, Griffiths CEM, Sherratt MJ, et al. Remodelling of fibrillin-rich microfibrils by solar-simulated radiation: impact of skin ethnicity. Photochem Photobiol Sci. 2020; 19(9): 1160-1167.
57. Sherratt MJ, Bayley CP, Reilly SM, Gibbs NK, Griffiths CE, Watson RE. Low-dose ultraviolet radiation selectively degrades chromophore-rich extracellular matrix components. J Pathol. 2010; 222(1): 32-40.
58. Mellody KT. The intrinsic ageing of cutaneous fibrillin-rich microfibrils and the impact of photodamage upon their role as biosignalling molecules. Presented as Ph.D., Manchester. University of Manchester. 2019.
59. Soydas T, Sayitoglu M, Sarac EY, Cınar S, Solakoglu S, Tiryaki T, et al. Metformin reverses the effects of high glucose on human dermal fibroblasts of aged skin via downregulating RELA/p65 expression. J Physiol Biochem. 2021; 77(3): 443-450.
60. Yang M, Teng S, Ma C, Yu Y, Wang P, Yi C. Ascorbic acid inhibits senescence in mesenchymal stem cells through ROS and AKT/mTOR signaling. Cytotechnology. 2018; 70(5): 1301-1313.
61. Giacoppo S, Thangavelu SR, Diomede F, Bramanti P, Conti P, Trubiani O, et al. Anti-inflammatory effects of hypoxia-preconditioned human periodontal ligament cell secretome in an experimental model of multiple sclerosis: a key role of IL-37. FASEB J. 2017; 31(12): 5592-5608.
62. Park KM, Yoo YJ, Ryu S, Lee SH. Nelumbo Nucifera leaf protects against UVB-induced wrinkle formation and loss of subcutaneous fat through suppression of MCP3, IL-6 and IL-8 expression. J Photochem Photobiol B. 2016; 161: 211-216.
63. Miller-Kobisher B, Suárez-Vega DV, Velazco de Maldonado GJ. Epidermal growth factor in aesthetics and regenerative medicine: systematic review. J Cutan Aesthet Surg. 2021; 14(2): 137-146.
64. de Araújo R, Lôbo M, Trindade K, Silva DF, Pereira N. Fibroblast growth factors: a controlling mechanism of skin aging. Skin Pharmacol Physiol. 2019; 32(5): 275-282.

65. Lu YE, Chen YJ. Resveratrol inhibits matrix metalloproteinase-1 and -3 expression by suppressing of p300/NFκB acetylation in TNF-α-treated human dermal fibroblasts. Chem Biol Interact. 2021; 337: 109395.
66. Xie HF, Liu YZ, Du R, Wang B, Chen MT, Zhang YY, et al. miR-377 induces senescence in human skin fibroblasts by targeting DNA methyltransferase 1. Cell Death Dis. 2017; 8(3): e2663.
67. Volarevic V, Markovic BS, Gazdic M, Volarevic A, Jovicic N, Arsenijevic N, et al. Ethical and safety issues of stem cell-based therapy. Int J Med Sci. 2018; 15(1): 36-45.
68. Kuriyan AE, Albini TA, Townsend JH, Rodriguez M, Pandya HK, Leonard RE 2nd, et al. Vision loss after intravitreal injection of autologous "Stem Cells" for AMD. N Engl J Med. 2017; 376(11): 1047-1053.
69. Foo JB, Looi QH, Chong PP, Hassan NH, Yeo GEC, Ng CY, et al. Comparing the therapeutic potential of stem cells and their secretory products in regenerative medicine. Stem Cells Int. 2021; 2021: 2616807.
70. Park YM, Lee M, Jeon S, Hrůzová D. In vitro effects of conditioned medium from bioreactor cultured human umbilical cord-derived mesenchymal stem cells (hUC-MSCs) on skin-derived cell lines. Regen Ther. 2021; 18: 281-291.
71. Ogata K, Matsumura-Kawashima M, Moriyama M, Kawado T, Nakamura S. Dental pulp-derived stem cell-conditioned media attenuates secondary Sjögren's syndrome via suppression of inflammatory cytokines in the submandibular glands. Regen Ther. 2021; 16: 73-80.
72. Katagiri W, Osugi M, Kawai T, Hibi H. First-in-human study and clinical case reports of the alveolar bone regeneration with the secretome from human mesenchymal stem cells. Head Face Med. 2016; 12: 5.
73. Putra A, Widyatmoko A, Ibrahim S, Amansyah F, Amansyah F, Berlian MA, et al. Case series of the first three severe COVID-19 patients treated with the secretome of hypoxia-mesenchymal stem cells in Indonesia. F1000Res. 2021; 10: 228.

Cell J
Cell Journal (Yakhteh)
Homepage: https://www.celljournal.org/
Original Article
Vol 25, No 9, September 2023, Pages: 603-612

Gallic Acid Ameliorates Cadmium Effect on Osteogenesis by Activation of Alkaline Phosphatase and Collagen Synthesis

Mohammad Hossein Abnosi, Ph.D.*, Javad Sargolzaei, Ph.D., Farshid Nazari, M.Sc.

Department of Biology, Faculty of Sciences, Arak University, Arak, Iran

Abstract

Objective: We previously reported that cadmium (Cd) inhibits osteogenic differentiation of bone marrow mesenchymal stem cells (BMSCs). In addition, gallic acid (GA) improves BMSC differentiation. Here, we aim to study the ability of GA to prevent osteogenic inhibition induced by Cd.

Materials and Methods: In this experimental study, BMSCs were extracted and purified from Wistar rats and their viability was determined in the presence of Cd and GA. The results indicated that 1.5 µM Cd and 0.25 µM of GA were appropriate for further investigation. After 20 days in osteogenic medium, matrix production was analysed by alizarin red, calcium content, and alkaline phosphatase (ALP) activity. Osteogenic-related genes and collagen 1A1 (COL1A1) protein expressions were investigated. The preventive effect of GA on oxidative stress and metabolic change induced by Cd was estimated.

Results: GA counteracted the inhibitory effect of Cd on matrix production and significantly (P=0.0001) improved the osteogenic differentiation ability of BMSCs. Also, GA prevented the toxic effect of Cd on osteogenic-related gene expressions and nullified the reducing effect of Cd on COL1AI and ALP activity. A significant reduction (P=0.0001) in malondialdehyde and lactic acid concentration showed that GA counteracted both oxidative stress and metabolic changes caused by Cd.

Conclusion: GA prevented the toxic effect of Cd, an environmental pollutant and a factor in osteoporosis.

Keywords: Cadmium, Gallic Acid, Mesenchymal Stem Cell, Osteoblasts

Citation: Abnosi MH, Sargolzaei J, Nazari F. Gallic acid ameliorates cadmium effect on osteogenesis by activation of alkaline phosphatase and collagen synthesis. Cell J. 2023; 25(9): 603-612. doi: 10.22074/CELLJ.2023.1999110.1263

Introduction

Cadmium (Cd) is a heavy metal that has a half-life of more than 20 years in biological systems (1, 2). It is an environmental pollutant released mostly via human activities that contaminate soil and water. Cd enters the food chain (3) and causes contamination after consumption of vegetables and aquatic animals. Various adverse effects, including bone complications, have been reported following consumption of Cd contaminated food and water. Exposure to high concentrations of Cd decreases bone mineral density (BMD) and this may result in osteomalacia and osteoporosis (4). Bones undergo dynamic self-renovation attributed to activity governed by bone cells, osteoblasts, and osteoclasts (5). Osteoclasts resorb bone, whereas osteoblasts, which are differentiated form bone marrow mesenchymal stem cells (BMSCs), synthesise the bone matrix to assist with bone repair and renovation (6). Proposed mechanisms that explain bone-related Cd toxicity include: inactivation of the parathyroid hormone (7); significant increase in osteoclast activity (8); reduction in 1,25-dihydroxy vitamin D biosynthesis via inactivation of 1-hydroxylase (9); inhibition of collagen production in the bone (9); and reduction in proliferation and differentiation ability of MSCs (10-12).

Several investigations have shown that Cd toxicity can generate reactive oxygen species (ROS) both *in vivo* and *in vitro* (4, 13-15). Cd induction of oxidative stress can deplete the cell's total antioxidant status and inactivate antioxidant enzymes, which lead to an accumulation of hydroxyl ($HO^{\cdot}$) radicals, superoxide ions ($O_2^{\cdot}$), and hydrogen peroxide (13, 16) that cause damage to membrane phospholipids, functional proteins, and DNA (17).

Antioxidants are endogenous or exogenous molecules that neutralise ROS and prevent its effects. Cells lack the ability to fight radicals when there is excessive use of endogenous antioxidants or a decrease in exogenous antioxidant intake, and this results in oxidative stress (18). The cell antioxidant system includes vitamin E, vitamin C and glutathione, and enzymes such as catalase (CAT), superoxide dismutase (SOD), and glutathione peroxidase (19). This antioxidant system inhibits the formation or neutralisation of free radicals; therefore, it protects

Received: 28/March/2023, Revised: 17/July/2023, Accepted: 26/July/2023
*Corresponding Address: P.O.Box: 3848177584, Department of Biology, Faculty of Sciences, Arak University, Arak, Iran
Email: m-abnosi@araku.ac.ir

Royan Institute
Cell Journal (Yakhteh)

the cells from oxidative stress and ultimately prevents membrane lipid peroxidation and DNA/protein damage. Cd toxicity disrupts the balance between free radicals and antioxidants (20); this imbalance may cause osteoporosis by reducing the proliferation and differentiation properties of BMSCs.

Plant antioxidants are the first line of consideration to increase a cell's antioxidant capacity. Natural plant products are present in a variety of foods such as grapes, apples, plums, berries, and other vegetables. Phenolic acids are a family of phytonutrients found in tomatoes, apples, strawberries, peppers, bananas, and many other plants (21). A member of this family is trihydroxybenzoic acid, which is also called gallic acid (GA). GA efficiently prevents oxidative damage caused by hydroxyl ($HO^{\cdot}$), superoxide ($O_2^{\cdot}$), peroxyl ($ROO^{\cdot}$) and the non-radical hydrogen peroxide (H_2O_2) free radicals (22).

BMSCs play an important role in bone repair and regeneration, and impairment of these cells has a tremendous impact on bone matrix production. Therefore, protection of BMSCs is very important after Cd toxicity. To the best of our knowledge, there is no published report that discusses the preventive effect of GA on Cd inhibition of osteogenic differentiation of BMSCs. The aim of the present study is to examine the toxic impact of Cd on osteogenic differentiation of BMSCs and assess the protective effect of GA on metabolic activity, oxidative stress, and matrix production as well as expressions of the genes involved in osteogenic differentiation after Cd exposure.

Materials and Methods

Extraction and rat bone marrow cell culture

This research was approved by the Ethics Committee of Arak Medical University, Arak, Iran (IR.ARAKMU.REC.1401.026). Wistar rats (6-8 weeks old) were obtained from Pasteur Institute (Tehran, Iran) and kept in an animal house at Arak University (Arak, Iran) under standard conditions for food and temperature. After a one-week acclimation period, the rats were euthanised using chloroform inhalation and their tibias and femurs were surgically removed. Under sterile conditions, the connective tissues were removed from the bones under sterile conditions and transferred to a clean room. The ends of the bones were removed and the bone marrow was extracted by a 2 ml syringe that contained Dulbecco's Modified Eagle Medium (DMEM) media [DMEM, 15% foetal bovine serum (FBS), and 1% penicillin/streptomycin (all from Gibco, Germany)]. The extracted bone marrow was centrifuged at 250 g for 5 minutes, then the cells were suspended in fresh medium and placed in T25 culture flasks. The flasks were incubated in an incubator at 37°C, 5% CO_2, and 95% humidity. The medium was replaced every three days by fresh medium until the bottom of the flask was covered by a cell monolayer. At this time the cells were detached using trypsin-EDTA (Gibco, Germany), centrifuged, and washed with phosphate-buffered saline (PBS, 20 mM, pH=7.2), then placed in new T25 culture flasks. This sub-culture was carried out two more times; at the third passage, flow cytometer [Germany, PARTEC (PAS)] analysis confirmed the purity of these cells. These passage-3 cells were kept for further analysis.

Cell viability

Cell viability was assessed by the trypan blue method under non-osteogenic conditions in order to select an effective concentration for further analysis. Passage-3 cells were treated with different concentrations (0.5, 1, 1.5, 2, 4, and 5 µM) of Cd (Merck Company, Germany) and GA (0.06, 0.12, 0.25, 0.5, 1, 20, and 30 µM; Sigma-Aldrich, USA) in the presence of a control group. After 20 days, the cells were removed from the flask by trypsin-EDTA and homogenized in fresh medium. Then, 50 µl of the homogenized cell was mixed with 50 µl (40 mg/ml in PBS) of trypan blue (Sigma-Aldrich, USA); after two minutes of incubation, the cells were counted using a haemocytometer chamber. Trypan blue passes through the cell membrane of nonviable cells (blue). The percentage of live cells was recorded.

We sought to study the effect of the selected concentrations, both individually and in combination, under osteogenic conditions. Cell viability was determined by the 3-(4, 5 dimethylthiazol-2-yl)-2,5-diphenyl tetrazolium bromide (MTT, Sigma-Aldrich, USA) assay. Briefly, BMSCs were cultured in a 24-well sterile plate, then treated individually with 1.5 µM (IC_{50}) of Cd or 0.25 µM of GA, or their combination (1.5 µM Cd+0.25 µM GA). After 20 days the cells were washed with PBS and then incubated for 4 hours with 100 µL of MTT (5 mg/ml in PBS) and 1 ml of culture media (without FBS). The culture media was removed and we added DMSO to dissolve the formazan crystals (30 minutes at 25°C). Then, 100 µl of the extracted solution was transferred to an ELISA plate and absorption was read at 505 nm by an ELISA plate reader (Medical SCO GmbH, Germany). We used the linear formula Y=0.0032X+0.0073 with R^2=9983 to calculate the number of viable cells. In this formula, Y represents absorption and X is the number of viable cells.

Proliferation assay

We used the population doubling number (PDN) formula to determine the proliferation ability of BMSCs in the presence of Cd, GA, and Cd+GA under non-osteogenic conditions.

$$PDN=\log N/N0+3.32,$$

Where: N0 is the initial number of cells cultured and N is the final number of cells harvested.

After 20 days of treatment, the total number of cells were counted using a haemocytometer chamber.

Osteogenic induction and detection

Osteogenic differentiation was induced in complete DMEM medium that contained 1 mM sodium glycerophosphate, 50 µg/mL L-ascorbic acid, and 10 nM dexamethasone (all from Sigma-Aldrich Company). The six-well plates were incubated at 37º C and 5% CO_2 and the media was replaced every three days. After 20 days, mineralisation was detected and quantified by alizarin red analysis. The plates were washed with PBS and fixed in 10% formaldehyde for 15 minutes. Then, we added 1 mL alizarin red solution (ARS, 40 mM, pH=4.2) and the plates were incubated for 40 minutes. The excess dye was washed with PBS, and images were acquired with an inverted microscope (Olympus, Japan) equipped with a camera (DP-70, Japan). In order to perform quantitative alizarin red staining, 800 µL of 10% acetic acid was added to each well of the plate; after 30 minutes, the cells were removed with a cell scraper and collected in a 1.5 mL tube. The content of each tube was vortexed for 30 seconds, overlaid with 500 µL of mineral oil (Sigma-Aldrich), and then heated in a water bath (85ºC) for 10 minutes. The micro-tubes were transferred to an ice bath for five minutes and centrifuged at 10 000 g for 15 minutes. We removed the supernatant (500 µL) and mixed it with 200 µL of 10% ammonium hydroxide to neutralise the solution. Absorption was read at 405 nm by a microplate reader (SCO Thec., Germany). Next, a stock solution of ARS was diluted with mixture of 10% acetic acid and 10% ammonium hydroxide (5:2) to give a final concentration of 2 mM, after which a series of five different dilutions were made. A standard graph of the known concentrations of ARS was plotted and we used the linear formula Y=0.0093X+0.3607 with R^2=0.9985, where Y is absorbance and X is concentration (µM) of the ARS, to determine the absorption of the unknown.

Determination of calcium concentration

The plates were washed with PBS and once with double-distilled water (ddH_2O). The cells were scraped off the plates and collected in a preweighed 1.5 mL microcentrifuge tube to determining their weight by subtraction. An equal weight of the cells was used to extract the calcium with 50 µL of 0.5 N hydrochloric acid (HCl) for 24 hours at 4ºC. Total calcium concentration was measured using a commercial kit (Pars Azmoon, Iran) and a spectrophotometer (T80 spectrophotometer, PG Instruments, Ltd., UK) at 630 nm. A standard graph was plotted using various concentrations of CaCl2 and the concentration of unknown was determined using the linear formula Y=0.0145X+0.0256 with R^2=0.9982, where Y is absorption and X is the concentration of calcium (mg/dL).

Extraction of cell content for further analysis

After osteogenic differentiation, the T25 flasks were washed with tris-HCl buffer (TB; 20 mM tris-HCl, pH=7.2) and the cells were removed from the flask with a cell scraper. The cells were added to a microcentrifuge tube that contained 500 µl of TB. After freezing and thawing, the cell membranes were broken and centrifuged at 12 000g for 10 minutes. The protein content was collected and estimated using the Lowry method. We used bovine serum albumin to plot a standard graph and the linear formula Y=0.00004X+0.0015 with R^2=0.9973 was used to calculate the protein concentration of each sample. In this formula, Y stands for absorbance and X is the concentration of protein (µg). Further biochemical analysis was performed based on the equal amount of protein in each sample.

Determination of alanine transaminase, aspartate transaminase, and lactate dehydrogenase activities

We used a commercial kit (Pars Azmoon, Iran) to estimate the activities of aspartate transaminase (AST), lactate dehydrogenase (LDH), and alanine transaminase (ALT) according to the manufacturer's protocol. A standard graph was plotted and the linear formulas Y=0.0016X+0.0003 with R^2=0.9996, Y=0.0013X+0.0119 with R^2=0.9854, and Y=0.0015X+0.0006 with R^2=0.9986 were used to calculate the AST, LDH, and ALT activities, respectively, for each sample. In the formula, Y stands for absorbance and X for the enzyme activity (IU/L).

Determination of alkaline phosphatase activity

Alkaline phosphatase (ALP) activity was estimated according to a commercial kit (Pars Azmoon, Iran) by using the same amount of protein. The measurement was taken at 410 nm with a spectrophotometer (T80 spectrophotometer, PG Instruments, Ltd., UK). A standard graph was plotted and the linear formula, Y=0.0015X+0.0004 with R^2=0.9993, was used to calculate the enzyme activity of each sample. In the formula Y stands for absorbance and X for the enzyme activity (IU/L).

Determination of superoxide dismutase activity

Nitro blue tetrazolium (NBT; Sigma-Aldrich, N6876 was used to determine SOD activity. Briefly, 50 µL of sample was added to 1 ml of the reaction mixture (6.1 mg NBT, 1.9 mg methionine, 7.9 mg riboflavin, and 3.3 mg EDTA dissolved in 10 mL potassium phosphate); after 10 minutes of incubation in a light box, absorbance of each sample was read at 560 nm. The blank and control tubes were also prepared in the same manner without the sample. The blank was kept in the dark and after 10 minutes, the spectrophotometer (T80 spectrophotometer, PG Instruments, Ltd., UK) was adjusted to zero using the same tube. Activity of the enzyme was calculated as unit per minute for mg of protein required to cause 50% inhibition.

Determination of catalase activity

We estimated CAT activity with a reaction mixture that consisted of 300 µL of H_2O_2 and 200 µL of 25 mM potassium phosphate buffer (pH=7.0) with an absorption of the solution adjusted to 0.4 prior to the measurement. CAT activity was determined by adding the 50 µl) of samples

to the mixture. Absorption was read after two minutes at 240 nm by a spectrophotometer (T80 spectrophotometer, PG Instruments, Ltd., UK). CAT activity was calculated for one minute using 39.4 $mM^{-1}cm^{-1}$ as the extinction coefficient.

Determination of lipid peroxidation

The level of malondialdehyde (MDA), as an indicator, was determined to estimate lipid peroxidation. 50 µl of sample was added to 1 ml of reaction mixture (0.5% thiobarbituric acid and 20% trichloroacetic acid in HCl) and kept in a boiling water bath for 30 minutes. Then, the mixture was placed on ice for 15 minutes and centrifuged at 10 000 g for 15 minutes. Absorption of the samples was determined first at 523 nm then at 600 nm with a spectrophotometer (T80 spectrophotometer, PG Instruments, Ltd., UK). The absorption values were subtracted and we used the extinction coefficient (155 mM-1 cm-1) to determine the concentration of MDA (µM/mL).

Measurement of total antioxidant content

Total antioxidant content (TAC) was estimated based on an equal amount of protein. First, 150 µL of the sample was mixed with 1700 µL of the reaction solution [300 mM sodium acetate buffer (pH=6.3), 10 mM 2,4,6-Tris(2-pyridyl)-s-triazine; (Sigma-Aldrich, USA) dissolved in 40 mM HCl and 20 mM iron chloride] and 850 µL distilled water. The mixture was incubated in the dark for 10 minutes, and absorbance at 593 nm was measured using a spectrophotometer (T80 spectrophotometer, PG Instruments, Ltd., UK). A standard graph was plotted using different concentrations of iron sulphate ($FeSO_4.7H_2O$; Merck, Germany). TAC of the sample was calculated using the linear formula, Y=0.0007X+0.0103 with R^2=0.997, where Y stands for absorption and X for concentration.

Protein extraction and Western blot analysis

Western blot was used to evaluate the level of collagen-1A1 (COL-1A1) in the protein extract. The cells were removed after trypsinization and lysed by freezing and thawing, after which the protein concentrations of the cell extracts were determined by the Bradford method. Protein cell extracts were isolated on 12% SDS-PAGE gels and electro-transferred onto a polyvinylidene difluoride membrane. The membrane was blocked with 5% non-fat powdered milk and probed with antibodies for COL-1A1 (Invitrogen, Cat# PA5-86862) and β-actin as the internal control (Santa Cruz Biotechnology, sc-53483) overnight at 4°C. The procedure was followed by incubation with horseradish peroxidase-conjugated secondary antibody for one hour. The blots were developed using an enhanced chemiluminescence reagent and detected by X-ray. The intensity of the colour on the membrane was quantified using ImageJ software and presented as arbitrary units.

Gene expression analysis

Reverse transcription polymerase chain reaction (RT-PCR) was conducted after total RNA extraction (Super RNA Extraction kit YT9080) and cDNA synthesis using a BioFACT (BR631-096) commercial kit. *ALP*, osteocalcin (*OC*), runt-related transcription factor 2 *(RUNX2), SMAD1,* bone morphogenetic protein 2 *(BMP2), COL1A1* and glyceraldehyde dehydrogenase (*GAPDH)* were amplified three times with an Eppendorf Mastercycler Gradient (Eppendorf Co., Hamburg, Germany) and specific primers (Table S1, See Supplementary Online Information at www.celljournal.org). The program was: 95°C for five minutes, 95°C for one minute, annealing temperature of the specific primer for one minute, 72°C for one minute and a final elongation temperature of 72°C for seven minutes. Amplification was repeated for 35 cycles and the product was run on a 1.5% agarose gel. The bands were photographed with a gel documentation system (Gene Flash, Syngene Bio Imaging, England) and analysed by GelQuant software (GelQuant: 1.8.2).

Statistical analysis

Data analysis was performed using one-way analysis of variance (ANOVA) and Tukey's tests with the help of SPSS software (version 20, IBM, USA). GraphPad Prism was used to plot the graphs (version 8.4.3 (686), GraphPad Software, Inc., USA). The results are shown as mean ± standard deviation, and the minimum level of significance is P<0.05.

Results

Cell viability

Cd treatment caused a significant (P=0.001), concentration dependent reduction of cell viability from 1 µM. GA significantly increased cell viability from 0.25 µM (P=0.04). Although the highest increase in cell viability was observed with the 0.25 µM GA treatment, the 30 µM concentration significantly reduced cell viability (P=0.0001, Fig.1A). Cell proliferation analysis revealed that cells treated with Cd had a significant (P=0.001) reduction in PDN from 1 µM; the highest reduction was observed at 5 µM. Treatment with GA showed no significant changes at the 0.625 µM concentration compared with the control; however, a significant increase in PDN was observed from the 0.125 µM concentration (P=0.04). The highest increase in PDN was observed with 0.25 µM of GA. We observed a highly significant reduction (P=0.001) at 30 µM (Fig.1B). The 1.5 µM concentration of Cd caused an almost 50% reduction in cell viability; therefore, we considered this concentration to be the IC_{50} and selected it for further analysis. PDN results indicated that 0.25 µM of GA had maximum proliferation, and this concentration was also chosen for further analysis.

We used the MTT assay to study cell viability under osteogenic conditions. Co-treatment of the cells for 20 days with 1.5 µM of Cd and 0.25 µM of GA counteracted the toxic effect of Cd. Therefore, the change in cell viability in the co-treatment group was non-significant (P=0.06) compared to the control group (Fig.1C).

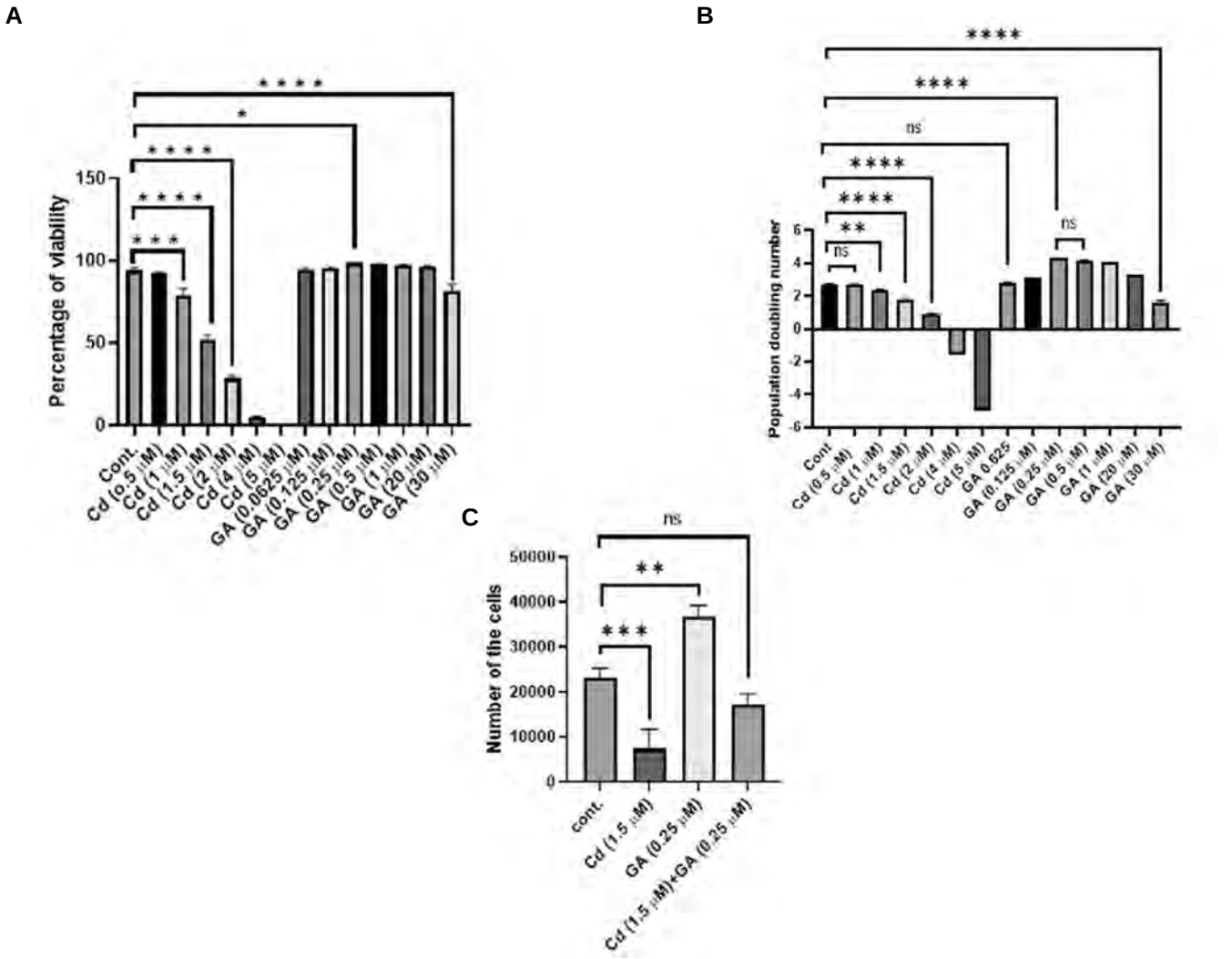

Fig.1: Cell viability and proliferation. **A.** Effects of Cd and GA individually on cell viability of BMSCs after 20 days of treatment under non-osteogenic conditions (trypan blue assay). **B.** Effects of Cd and GA individually on BMSCs proliferation after 20 days of treatment. **C.** Effects of Cd, GA, and Cd+GA on cell viability of BMSCs after 20 days of treatment in osteogenic media using the 3-(4, 5 dimethylthiazol-2-yl)-2,5-diphenyl tetrazolium bromide (MTT) assay. Data are shown as mean ± SD for three replicates. Cd; Cadmium, GA; Gallic acid, BMSCs; Bone marrow mesenchymal stem cells, ns; Not significant, *; P<0.05, **; P<0.01, ***; P<0.001, and ****; P<0.0001.

Osteogenic differentiation

Alizarin red staining of the cell matrix showed that Cd treatment reduced the osteogenic differentiation ability of the BMSCs compared with the control group (Fig.2IA, B). Treatment with GA increased the osteogenic ability (Fig.2IC) and co-treatment of the cells with Cd and GA counteracted the toxic effect of Cd (Fig.2ID). Statistical analysis confirmed this effect of GA in the co-treatment group. Alizarin red analysis results showed that GA treatment significantly improved matrix production (P=0.0001), whereas treatment with Cd significantly reduced matrix production (P=0.001, Fig.2IIA).

Calcium content (Fig.2IIB) and ALP activity (Fig.2IIC) analyses showed that co-treatment of the cells with 1.5 μM of Cd and 0.25 μM of GA improved the toxic effect of Cd. No changes could be observed in comparison to the control group. Treatment of the cells with only GA significantly increased ALP and matrix extracted calcium content compared with the control group (P=0.0001).

Oxidative stress

Cells treated with Cd had a significant (P=0.00001) increase in MDA (Fig.3A), whereas the level of TAC and activity of CAT and SOD were significantly reduced (P=0.01, Fig.3B-D). Treatment of the cells with GA significantly (P<0.001) reduced MDA levels and significantly increased TAC levels and CAT and SOD activity (P=0.001). In the co-treatment group, we observed that the level of MDA was non-significant (P=0.06) in comparison with the control group. In addition, co-treatment of the cells counteracted the toxic effect of Cd with respect to TAC levels and antioxidant enzyme activities. SOD levels were significant compared to the control group.

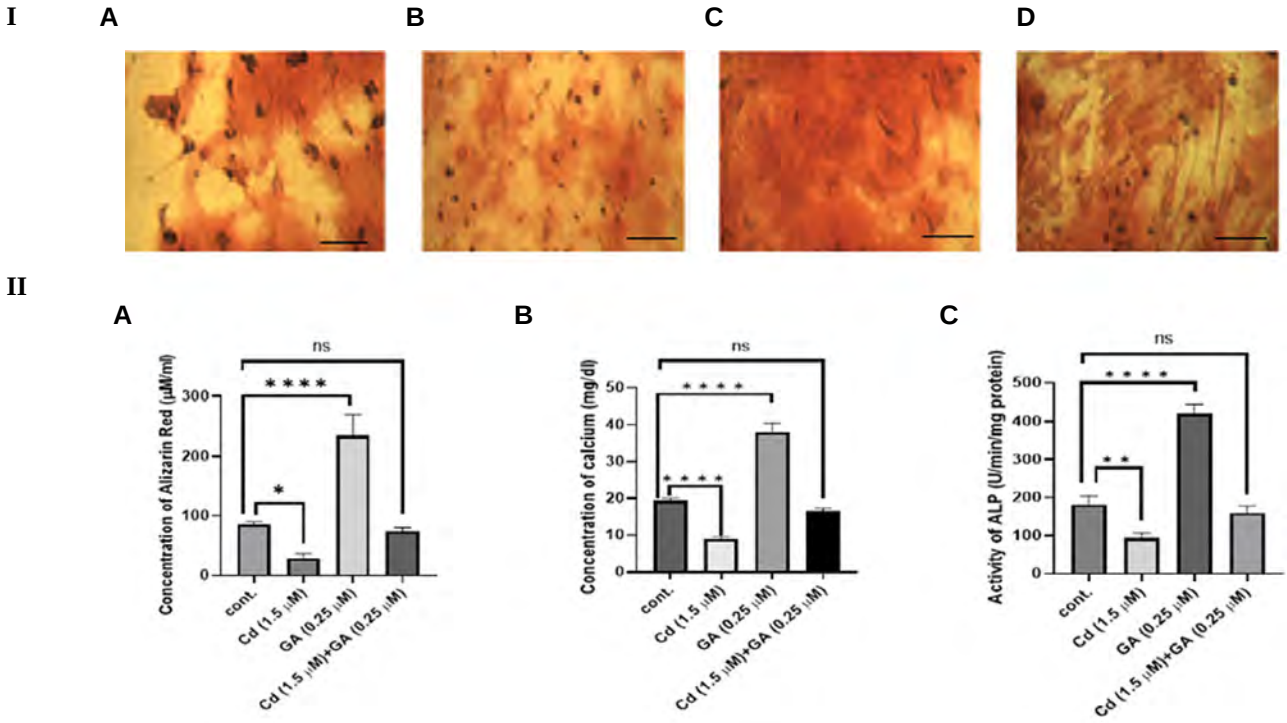

Fig.2: Osteogenic differentiation. **I.** Alizarin red staining of BMSCs after 20 days of treatment under an osteogenic condition. **A.** Control. Treatment with **B.** Cd, **C.** GA, and **D.** Cd+GA (magnification: 20x, scale bar: 200 µm). **II.** Effects of Cd and GA on differentiation ability of BMSCs based on **A.** Alizarin red, **B.** Calcium concentration, and **C.** ALP activity after 20 days of treatment under an osteogenic condition. Data are shown as mean ± SD for three replicates. BMSCs; Bone marrow mesenchymal stem cells, Cd; Cadmium, GA; Gallic acid, ALP; Alkaline phosphatase, ns; Not significant, *; P<0.05, **; P<0.01, and ****; P<0.0001.

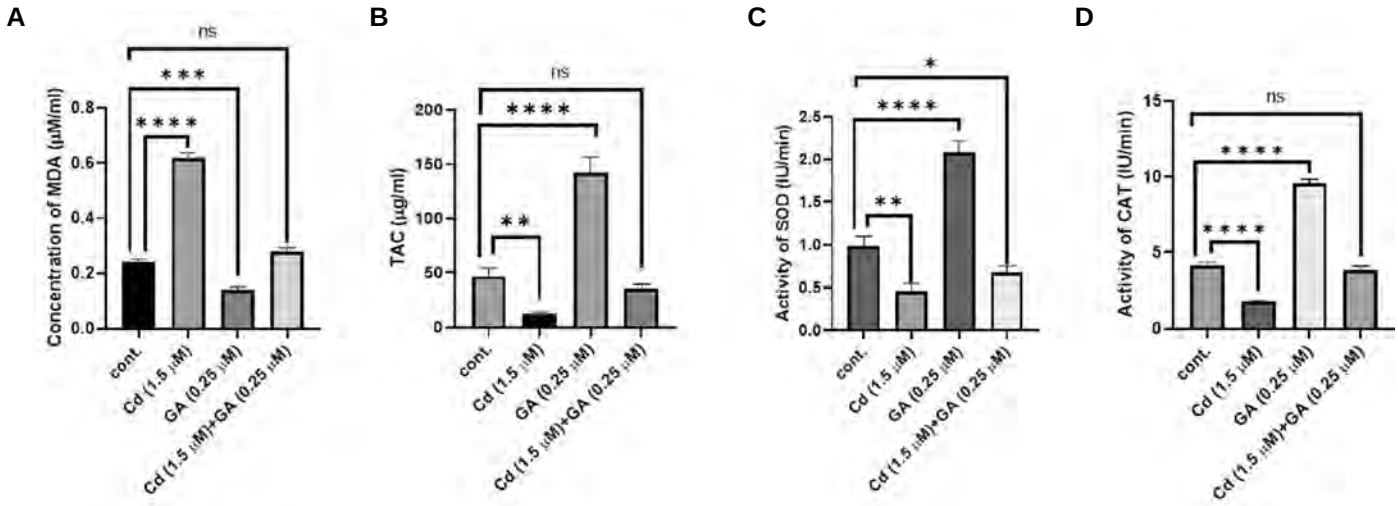

Fig.3: Effect of Cd and GA on BMSCs. **A.** MDA concentration, **B.** TAC, **C.** SOD activity, and **D.** CAT activity after 20 days of treatment under an osteogenic condition. Data are shown as mean ± SD for three replicates. Cd; Cadmium, GA; Gallic acid, BMSCs; Bone marrow mesenchymal stem cells, MDA; Malondialdehyde, TAC; Total antioxidant content, SOD; Superoxide dismutase, CAT; Catalase, ns; Not significant, *; P<0.05, **; P<0.01, ***; P<0.001, and ****; P<0.0001.

Metabolic activity

When compared with control group, Cd (1.5 µM) caused a significant (P=0.001) elevation in LDH, AST and ALT levels in the treated cells; however, 0.25 µM of GA significantly reduced the activities of these enzymes (P=0.001). Although co-treatment of the cells counteracted the toxic effect of Cd, it only restored ALT activity (Fig.4).

Western blot analysis

Western blot analysis of the cell extract showed that the Cd caused a highly significant reduction of COL1A1 (P=0.0001), whereas GA significantly increased COL1A1 expression in the osteogenic differentiated BMSCs (P=0.01). Co-treatment of the cells could significantly (P=0.001) replenish COL1Al expression in the cell extract compared with the Cd treated group (Fig.5).

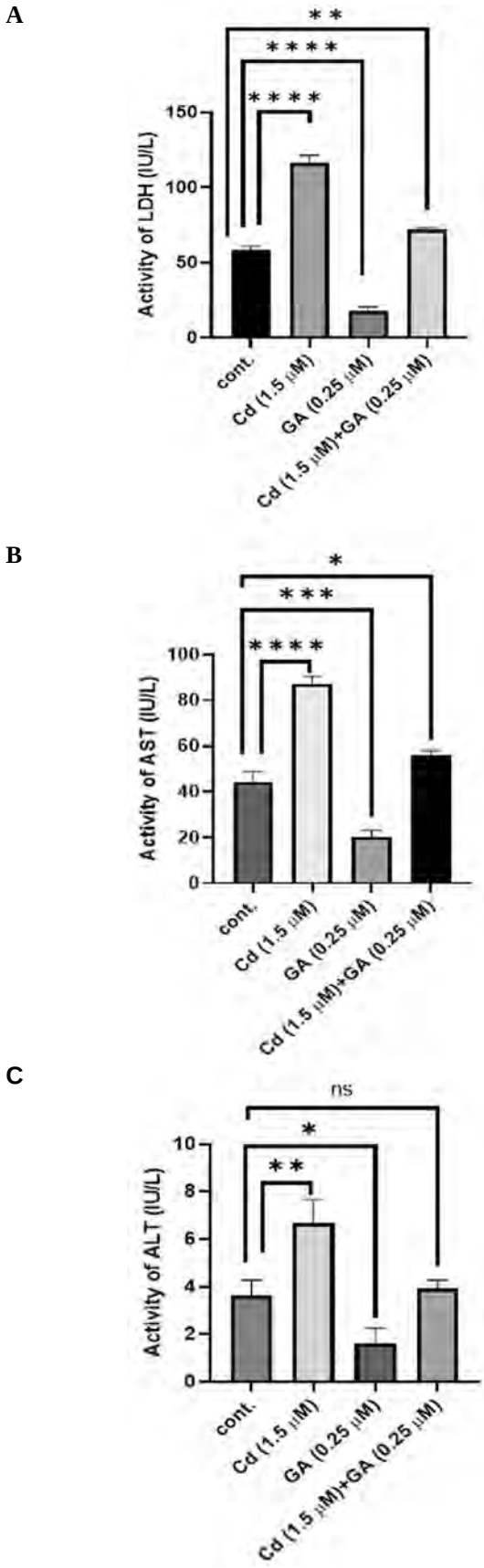

Fig.4: Effects of Cd and GA on metabolic activity of BMSCs. **A**. LDH, **B.** AST, and **C.** ALT activities after 20 days of treatment under an osteogenic condition. Data are shown as mean ± SD for three replicates. Cd; Cadmium, GA; Gallic acid, BMSCs; Bone marrow mesenchymal stem cells, LDH; Lactate dehydrogenase, AST; Aspartate transaminase, ALT; Alanine transaminase, ns; Not significant, *; P<0.05, **; P<0.01, ***; P<0.001, and ****; P<0.0001.

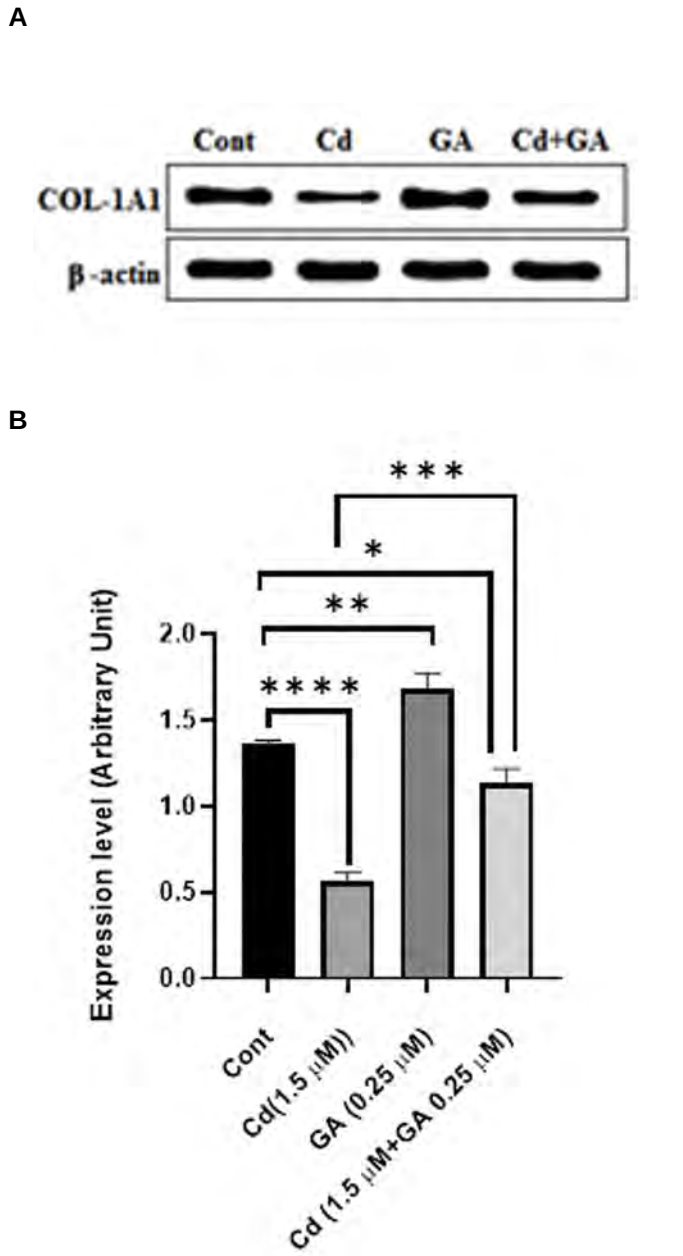

Fig.5: Effects of Cd and GA on expression of COL1A1 protein in BMSCs. **A.** Western blot of COL1Al and β-actin (internal control). **B.** Protein expression level (arbitrary unit) after 20 days of treatment under an osteogenic condition. Data are shown as mean ± SD for three replicates. Cd; Cadmium, GA; Gallic acid, BMSCs; Bone marrow mesenchymal stem cells, ns; Not significant, *; P<0.05, **; P<0.01, ***; P<0.001, and ****; P<0.0001.

Osteogenic-related gene expressions

There was a highly significant reduction in expression of the osteogenic-related genes after treatment with Cd (P=0.0001, Fig.6). In the co-treatment group, GA counteracted the effect of Cd and restored *OC*, *RUNX2*, *BMP2*, *COL1A1* and *ALP* expressions compared with the control group. Treatment of the cells with only GA caused a significant increase (P=0.001) in *OC*, *RUNX2*, *SMAD1*, *COL1A1* and *ALP* expressions (Fig.6).

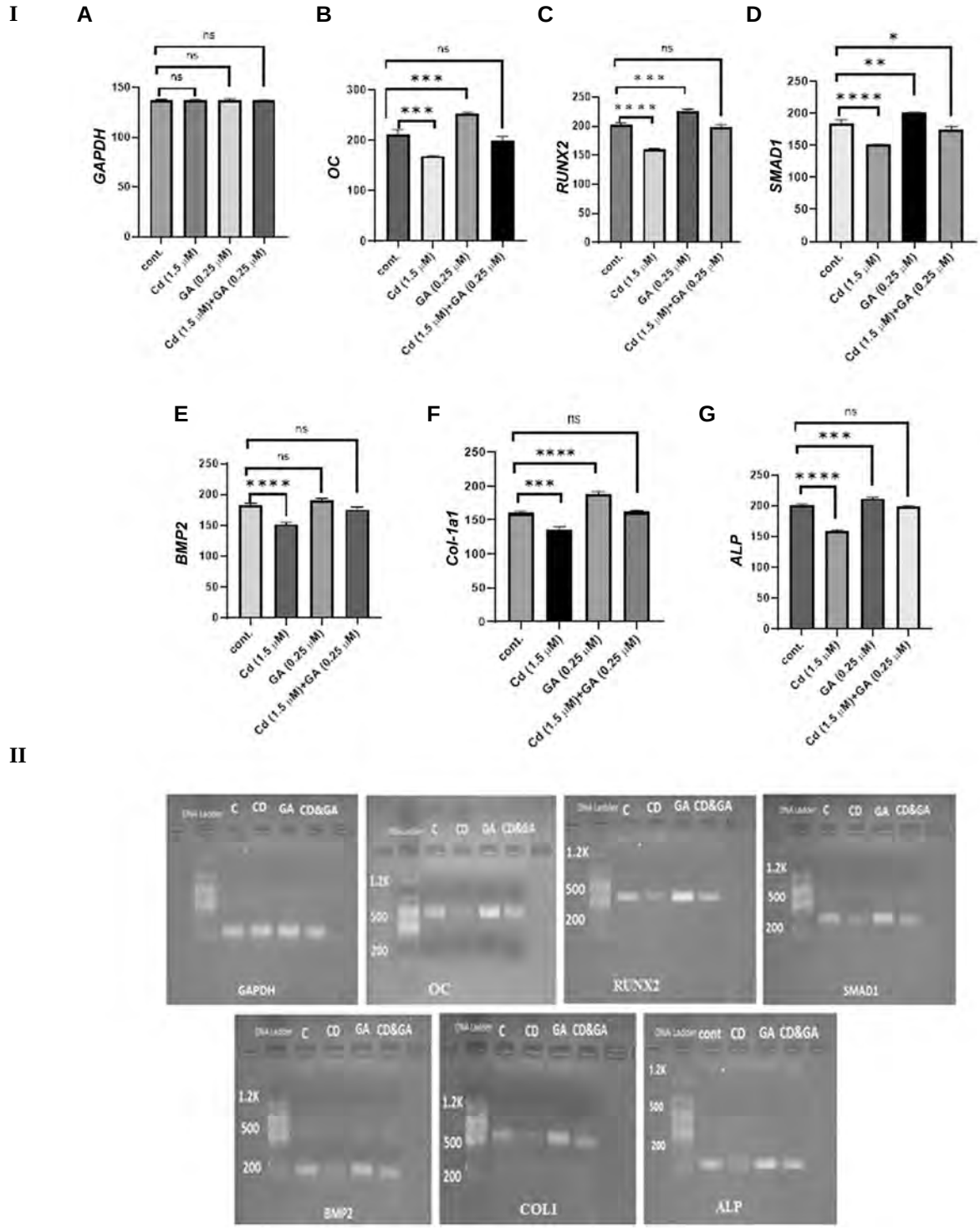

Fig.6: I. Graph presents the effects of Cd and GA on gene expression (arbitrary unit). **A.** *GAPDH*, **B.** *OC*, **C.** *RUNX2*, **D.** *SMAD1*, **E.** *BMP2*, **F.** *BMP7,* and **G.** *ALP* of BMSCs after 20 days of treatment under an osteogenic condition. **II.** Image presents the agarose gel electrophoresis of the PCR product of the osteogenic-related genes of BMSCs after 20 days of treatment. Data are shown as mean ± SD for three replicates. Cd; Cadmium, GA; Gallic acid, BMSCs; Bone marrow mesenchymal stem cells, ns; Not significant, *; P<0.05, **; P<0.01, ***; P<0.001, ****; P< 0.0001, C; Control, Cd, GA, and Cd+GA; Combination of Cd and GA.

Discussion

In the present study, we observed that Cd suppressed osteogenic differentiation while GA increased this property in BMSCs. Osteogenic-related gene expressions significantly reduced following treatment of BMSCs with $CdCl_2$. ALP activity, alizarin red staining, the calcium concentration of matrix, and COL1A1 expression all confirmed the suppressing effect of Cd. On the other hand, treatment with GA significantly increased expressions of these osteogenic-related genes, and also increased the ALP enzyme and COL1A1 protein in osteoblasts that produce matrix. The increase in matrix formation

attributed to GA treatment was confirmed by alizarin red staining and measurements of calcium content, ALP activity, and COL1A1 expression.

Cd has been shown to reduce BMD in several different populations. In animal studies, Cd treatment resulted in changes to the bone microstructure, including an elevation in trabecular separation and reduction of bone vascularization (13, 14). Investigations in humans revealed that low Cd exposure had a significantly negative impact on cortical area and thickness as well as trabecular bone volume fraction, and an increase in trabecular separation (4). Cd causes direct and indirect effects on bone tissue; it reduces bone formation by inhibition of osteoblasts and activation of osteoclasts (11, 15, 16). The specific mechanism of bone damage by Cd is unclear, especially for osteogenic differentiation of BMSCs. We have previously reported that Cd causes membrane damage and metabolic impairment in BMSCs (10, 12). In the present study, Cd induction of peroxidation of membrane lipids increased the amount of MDA and reduced both antioxidant enzyme activities and TAC concentration in the BMSC-derived osteoblasts. Cd toxicity also altered the metabolic state of osteogenic differentiated BMSCs by activation of LDH to convert pyruvate and produce more lactic acid, which facilitates glycolysis (17).

Cd toxicity is related to a depletion in cell antioxidant capacity (18, 19) and generation of ROS (O_2, H_2O_2, and HO.) radicals (20). Plant antioxidants may prevent lipid peroxidation due to ROS overproduction (21-23). GA is a potent plant antioxidant found in many fruits and vegetables; therefore, it is easily available to the public. GA has an oxidative preventive effect and an osteogenic improvement ability, whereas Cd inhibits BMSC osteogenesis (24). Here, we used GA to overcome the toxic effect of Cd. In this study, GA improved TAC of the osteogenic differentiated BMSCs and increased antioxidant enzyme activities. There was a significantly low level of MDA generated in the presence of GA compared to the control group. Therefore, GA in the co-treatment group could counteract the oxidative effect of Cd and prevent oxidative stress compared to the control group. In addition to lipid peroxidation, ROS can react with functional groups of proteins and inactivate enzymes (25). DNA and RNA damage has been reported in the presence of ROS generating agents (26). Thus, prevention of oxidation of macromolecule by ROS is a prime step to prevent the deleterious effect of free radicals.

Cells treated with GA improved BMSC osteogenesis after oxidative damage from Cd. We observed that Cd inhibition of osteogenic differentiation of BMSCs was reduced by GA treatment at the gene and protein levels. *RUNX2* is a key gene in the progression of osteogenic differentiation (27), which is regulated by *BMP2* and the *SMAD* family (28). Consequently, *RUNX2* activates *OC, COL1A1* and *ALP*, the genes that control matrix formation in newly produced osteoblasts (29). In the present study, following osteoinduction, expressions of *BMP2*, *SMAD1*, *RUNX2*, *COL1A1*, *ALP* and *OC* up-regulated after GA treatment. Cd treatment resulted in down-regulation of the osteogenesis-related genes, whereas treatment with GA overcame the inhibitory effect of Cd on gene regulation and at the protein level of COL1A1 and ALP.

In bone remodelling the balance between osteoblast-mediated bone formation and osteoclast-mediated bone resorption is important. Differentiation of BMSCs to osteoblasts ensures the availability of bone matrix to produce a strong and healthy bone. Therefore, any imbalance in osteogenic differentiation would result in decreased bone density (30), which is the main reason for osteoporosis. Osteogenic-related gene activation results in production of organic and inorganic components of bone matrix (31). Cd down-regulated gene expressions; as a result, it inhibited the organic (COL1A1) and inorganic (calcium) components required for matrix production. GA improved the gene expressions and restored COL1A1 levels and ALP activity, which are main factors for production of bone matrix.

Previously, we reported the toxic effect of Cd on osteogenic differentiation of BMSCs (11, 32), The results of the current study support previous reports about the osteogenic induction property of GA (33, 34). Here, we confirmed the ability of GA to prevent the osteogenic inhibitory effect of Cd. In our previous study, we showed that the Cd changed the metabolic situation of BMSCs from an aerobic to an anaerobic state (10-12). We also showed that GA could restore the metabolic activity of differentiated BMSCs, as the cells in the osteogenic differentiated state need more energy for production via aerobic respiration.

Conclusion

Cd induces oxidative stress that results in inhibition of osteogenic gene expressions. Cd also prevents COL1A1 production and inhibits ALP activity, which prevents the production of organic and inorganic components of the bone matrix. GA is a strong antioxidant that prevents the oxidative effect of Cd and restores gene expressions. It also counteracts the inhibitory effect of Cd on matrix production by increasing ALP activity to deposit more calcium on the organic component (COL1A1).

Acknowledgements

This project was conducted in the Department of Biology, Arak University as a M.Sc. research program; therefore, we wish to cordially acknowledge the authorities who approved this research work. There is no financial support and conflict of interest in this study.

Authors' Contributions

M.H.A.; Conceived the study, supervised the overall

direction and planning, designed the experiments, and wrote the manuscript. J.S.; Conducted statistical and gene analyses. F.N.; Performed the laboratory experiments and statistical analysis. All authors read and approved the final version of this manuscript.

References

1. Mori C, Lee JY, Tokumoto M, Satoh M. Cadmium toxicity is regulated by peroxisome proliferator-activated receptor δ in human proximal tubular cells. Int J Mol Sci. 2022; 23(15): 8652.
2. Suwazono Y, Kido T, Nakagawa H, Nishijo M, Honda R, Kobayashi E, et al. Biological half-life of cadmium in the urine of inhabitants after cessation of cadmium exposure. Biomarkers. 2009; 14(2): 77-81.
3. Chunhabundit R. Cadmium exposure and potential health risk from foods in contaminated area, Thailand. Toxicol Res. 2016; 32(1): 65-72.
4. Wallin M, Barregard L, Sallsten G, Lundh T, Sundh D, Lorentzon M, et al. Low-level cadmium exposure is associated with decreased cortical thickness, cortical area and trabecular bone volume fraction in elderly men: The MrOS Sweden study. Bone. 2021; 143: 115768.
5. Wang L, You X, Zhang L, Zhang C, Zou W. Mechanical regulation of bone remodeling. Bone Res. 2022; 10(1): 16.
6. Qin Q, Liu Y, Yang Z, Aimaijiang M, Ma R, Yang Y, et al. Hypoxia-inducible factors signaling in osteogenesis and skeletal repair. Int J Mol Sci. 2022; 23(19): 11201.
7. Babić Leko M, Pleić N, Gunjača I, Zemunik T. Environmental factors that affect parathyroid hormone and calcitonin levels. Int J Mol Sci. 2021; 23(1): 44.
8. He S, Zhuo L, Cao Y, Liu G, Zhao H, Song R, et al. Effect of cadmium on osteoclast differentiation during bone injury in female mice. Environ Toxicol. 2020; 35(4): 487-494.
9. Kjellström T. Mechanism and epidemiology of bone effects of cadmium. IARC Sci Publ. 1992; (118): 301-310.
10. Hussein AM, Hasan S. Cadmium affects viability of bone marrow mesenchymal stem cells through membrane impairment, intracellular calcium elevation and DNA breakage. Indian J Med Sci. 2010; 64(4): 177-186.
11. Abnosi MH, Gholami S. Cadmium treatment of rats caused impairment of osteogenic potential of bone marrow mesenchymal stem cells: a possible mechanism of cadmium related osteoporosis. Iran J Toxicol. 2017; 11(1): 1-9.
12. Abnosi MH, Golami S. Cadmium chloride treatment of rats significantly impairs membrane integrity of mesenchymal stem cells via electrolyte imbalance and lipid peroxidation, a possible explanation of Cd related osteoporosis. Iran J Basic Med Sci. 2017; 20(3): 280-287.
13. Duranova H, Martiniakova M, Omelka R, Grosskopf B, Bobonova I, Toman R. Changes in compact bone microstructure of rats subchronically exposed to cadmium. Acta Vet Scand. 2014; 56(1): 64.
14. Chen X, Zhu G, Shao C, Jin T, Tan M, Gu S, et al. Effects of cadmium on bone microstructure and serum tartrate-resistant acid phosphatase 5b in male rats. Exp Biol Med (Maywood). 2011; 236(11): 1298-1305.
15. Chen X, Zhu G, Gu S, Jin T, Shao C. Effects of cadmium on osteoblasts and osteoclasts in vitro. Environ Toxicol Pharmacol. 2009; 28(2): 232-236.
16. Chen X, Zhu G, Jin T, Zhou Z, Gu S, Qiu J, et al. Cadmium stimulates the osteoclastic differentiation of RAW264.7 cells in presence of osteoblasts. Biol Trace Elem Res. 2012; 146(3): 349-353.
17. Parra-Bonilla G, Alvarez DF, Al-Mehdi AB, Alexeyev M, Stevens T. Critical role for lactate dehydrogenase A in aerobic glycolysis that sustains pulmonary microvascular endothelial cell proliferation. Am J Physiol Lung Cell Mol Physiol. 2010; 299(4): L513-L522.
18. Branca JJV, Fiorillo C, Carrino D, Paternostro F, Taddei N, Gulisano M, et al. Cadmium-induced oxidative stress: focus on the central nervous system. Antioxidants (Basel). 2020; 9(6): 492.
19. Genchi G, Sinicropi MS, Lauria G, Carocci A, Catalano A. The effects of cadmium toxicity. Int J Environ Res Public Health. 2020; 17(11): 3782.
20. Liu J, Qu W, Kadiiska MB. Role of oxidative stress in cadmium toxicity and carcinogenesis. Toxicol Appl Pharmacol. 2009; 238(3): 209-214.
21. Tenyang N, Zambou GT, Ponka R, Womeni H. Antioxidant effect of plants aqueous extract on lipid stability of oreochromis niloticus during traditional sun and smoke drying in far-north cameroon. Food Sci Nutr. 2020; 11(8): 854-871.
22. Veskoukis AS, Tsatsakis AM, Kouretas D. Dietary oxidative stress and antioxidant defense with an emphasis on plant extract administration. Cell Stress Chaperones. 2012; 17(1): 11-21.
23. Maqsood S, Benjakul S, Abushelaibi A, Alam A. Phenolic compounds and plant phenolic extracts as natural antioxidants in prevention of lipid oxidation in seafood: a detailed review. Compr Rev Food Sci Food Saf. 2014; 13(6): 1125-1140.
24. Oh Y, Ahn CB, Marasinghe MPCK, Je JY. Insertion of gallic acid onto chitosan promotes the differentiation of osteoblasts from murine bone marrow-derived mesenchymal stem cells. Int J Biol Macromol. 2021; 183: 1410-1418.
25. Grimsrud PA, Xie H, Griffin TJ, Bernlohr DA. Oxidative stress and covalent modification of protein with bioactive aldehydes. J Biol Chem. 2008; 283(32): 21837-21841.
26. Guo C, Ding P, Xie C, Ye C, Ye M, Pan C, et al. Potential application of the oxidative nucleic acid damage biomarkers in detection of diseases. Oncotarget. 2017; 8(43): 75767-75777.
27. Bruderer M, Richards RG, Alini M, Stoddart MJ. Role and regulation of RUNX2 in osteogenesis. Eur Cell Mater. 2014; 28: 269-286.
28. Hassan MQ, Tare RS, Lee SH, Mandeville M, Morasso MI, Javed A, et al. BMP2 commitment to the osteogenic lineage involves activation of Runx2 by DLX3 and a homeodomain transcriptional network. J Biol Chem. 2006; 281(52): 40515-40526.
29. Liu TM, Lee EH. Transcriptional regulatory cascades in Runx2-dependent bone development. Tissue Eng Part B Rev. 2013; 19(3): 254-263.
30. Valenti MT, Dalle Carbonare L, Mottes M. Osteogenic differentiation in healthy and pathological conditions. Int J Mol Sci. 2016; 18(1): 41.
31. Blair HC, Larrouture QC, Li Y, Lin H, Beer-Stoltz D, Liu L, et al. Osteoblast differentiation and bone matrix formation in vivo and in vitro. Tissue Eng Part B Rev. 2017; 23(3): 268-280.
32. Mehranjani MS, Mosavi M. Cadmium chloride toxicity suppresses osteogenic potential of rat bone marrow mesenchymal stem cells through reducing cell viability and bone matrix mineralization. Indian J Med Sci. 2011; 65(4): 157-167.
33. Jiang J, Hai J, Liu W, Luo Y, Chen K, Xin Y, et al. Gallic acid induces neural stem cell differentiation into neurons and proliferation through the MAPK/ERK pathway. J Agric Food Chem. 2021; 69(42): 12456-12464.
34. Chauhan S, Sharma A, Upadhyay NK, Singh G, Lal UR, Goyal R. In-vitro osteoblast proliferation and in-vivo anti-osteoporotic activity of Bombax ceiba with quantification of Lupeol, gallic acid and β-sitosterol by HPTLC and HPLC. BMC Complement Altern Med. 2018; 18(1): 233.

Cell J
Cell Journal (Yakhteh)
Homepage: https://www.celljournal.org/
Original Article
Vol 25, No 9, September 2023, Pages: 613-624

Bioinformatic Analysis of The Prognostic Value of A Panel of Six Amino Acid Transporters in Human Cancers

Yaqi Liu, B.Sc.[1, 2, 3, 4#], Haijuan Xiong, B.Sc.[1, 2, 3, 4#], Chenhui Yan, M.Sc.[1, 2, 3, 4], Yalei Wang, M.Sc.[1, 2, 3, 4], Wenfeng Cao, M.D., Ph.D.[1, 2, 3, 4], Shuo Qie, M.D., Ph.D.[1, 2, 3, 4*]

1. Department of Pathology, Tianjin Medical University Cancer Institute and Hospital, Tianjin, China
2. National Clinical Research Center for Cancer, Tianjin, China
3. Key Laboratory of Cancer Prevention and Therapy (Tianjin), Tianjin, China
4. Tianjin's Clinical Research Center for Cancer, Tianjin, China

Abstract

Objective: Solid tumor cells utilize amino acid transporters (AATs) to increase amino acid uptake in response to nutrient-insufficiency. The upregulation of AATs is therefore critical for tumor development and progression. This study identifies the upregulated AATs under amino acid deprived conditions, and further determines the clinicopathological importance of these AATs in evaluating the prognosis of patients with cancers.

Materials and Methods: In this experimental study, the Gene Expression Omnibus (GEO) datasets (GSE62673, GSE26370, GSE125782 and GSE150874) were downloaded from the NCBI website and utilized for integrated differential expression and pathway analysis v0.96, Gene Set Enrichment Analysis (GSEA), and REACTOME analyses to identify the AATs upregulated in response to amino acid deprivation. In addition, The Cancer Genome Atlas (TCGA) datasets with prognostic information were assessed and employed to evaluate the association of identified AATs with patients' prognoses using SurvExpress analysis.

Results: Using analysis of NCBI GEO data, this study shows that amino acid deprivation leads to the upregulation of six AAT genes; SLC3A2, SLC7A5, SLC7A1, SLC1A4, SLC7A11 and SLC1A5. GSEA and REACTOME analyses identified altered signaling in cells exposed to amino acid deprivation, such as pathways related to stress responses, the cell cycle and apoptosis. In addition, Principal Component Analysis showed these six AAT genes to be well divided into two distinct clusters in relation to TCGA tumor tissues versus normal counterparts. Finally, Log-Rank analysis confirmed the upregulation of this panel of six AAT genes is correlated with poor prognosis in patients with colorectal, esophageal, kidney and lung cancers.

Conclusion: The upregulation of a panel of six AATs is common in several human cancers and may provide a valuable diagnostic tool to evaluate the prognosis of patients with colorectal, esophageal, kidney and lung cancers.

Keywords: Amino Acid Transporters, Glutamine, Prognosis, Tumorigenesis

Citation: Liu Y, Xiong H, Yan C, Wang Y, Cao W, Qie S. Bioinformatic analysis of the prognostic value of a panel of six amino acid transporters in human cancers. Cell J. 2023; 25(9): 613-624. doi: 10.22074/CELLJ.2023.2004011.1319

Introduction

Tumor development and progression includes a series of interconnected steps such as the activation of oncogenes and/or the loss of tumor suppressors leading to replicative immortality and constitutive cell proliferation (1). As solid tumors grow larger and larger, the angiogenic switch is turned on to induce blood vessel formation (2) which provides both nutrients and a route for tumor metastasis. The processes outlined above are defined as the hallmarks of human cancers. Recently, two emerging hallmarks and two enabling characteristics have been illustrated and characterized in human cancers. An example is dysregulated cellular metabolism which has been widely investigated and considered as one of the emerging hallmarks (3, 4). The Warburg effect and active glutaminolysis represent the most common characteristics of tumor metabolism (5, 6). Glutaminolysis is mainly the conversion of glutamine to glutamate. Generally, tumor cells are addicted to glutamine, thus glutamine is considered as a conditionally essential amino acid. Besides glutamine, there are twenty other proteinogenic amino acids in eukaryotes. Biologically, amino acids participate in a variety of cellular processes that contribute to tumor development and progression. Amino acids are precursors in energy production, biosynthetic and reductive processes. They also participate in epigenetic regulation and ammonia detoxification processes (7-12). Accordingly there is a high demand for amino acids in tumor cells, with increased proliferation leading to overexpression of amino acid transporters (AATs) (13). In normal cells, the expression of AATs is finely adjusted to control the uptake and distribution of amino acids. In

Received: 05/June/2023, Revised: 05/July/2023, Accepted: 06/August/2023
#These authors contributed equally in this study.
*Corresponding Address: Department of Pathology, Tianjin Medical University Cancer Institute and Hospital, Tianjin, China
Email: shuoqie@tmu.edu.cn

Royan Institute
Cell Journal (Yakhteh)

contrast, tumor cells acquire a large quantity of amino acids, mainly through the upregulation of AATs; the expression of AATs being reprogrammed to promote the absorption of amino acids in accordance with the elevated level of cellular proliferation.

The AATs are a group of membrane-bound proteins that facilitate the uptake or excretion of amino acids at cellular or organelle levels (14). They belong to the solute carrier (SLC) superfamily and are grouped into different categories based on their substrate specificity and different working mechanisms (15). Biologically, AATs regulate a variety of processes, such as, energy production, biosynthesis, redox homeostasis, gene transcription and translation, signaling pathways, and cell proliferation. Due to their critical roles in controlling various biological functions, the dysregulation of AATs leads to the development of pathologies, such as, tumors, neurodegenerative diseases, metabolic diseases, etc. In human tumors the dysregulation of AATs facilitates the metabolic reprogramming that controls autophagy and cell proliferation through ATP generation, protein & nucleotide synthesis, and NADPH production.

Normally, solid tumors have defective blood vessel systems that lead to insufficient nutrient supplies, such as low amino acid or glucose levels, and hypoxia (12). A recent paper identified that SLC7A5 can be induced when cells are exposed to media low in histidine, tyrosine, and methionine levels (16). Under stress conditions, tumor cells resort to conserved signaling to upregulate AATs. For example, amino acid deprivation can activate eukaryotic translation initiation factor 2α (eIF2α)-activating transcription factor 4 (ATF4) signaling through general control nondepressible 2 (GCN2). Therefore, it is common that AAT promotion includes amino acid response elements (AAREs) that can be bound by ATF4 transcription factor leading to increased transcription of AATs (17-20). This study identifies the upregulated AATs under amino acid deprived conditions, and further determines the clinicopathological importance of these AATs in evaluating the prognosis of patients with cancers.

Materials and Methods

Collection of published and open-access datasets

In this experimental study, mRNA expression and RNA-Seq data were obtained from the Gene Expression Omnibus (GEO) on the NCBI website (https://www.ncbi.nlm.nih.gov/geo/). MCF7 breast cancer cells in the GSE62673 dataset were first exposed to complete medium or medium without one/all amino acid(s) for 24 hours. mRNAs were then extracted and analyzed using the Affymetrix Human Genome U133A 2.0 Array. MDA-MB-231 breast cancer cells from the GSE26370 dataset were cultured in medium with/without glutamine for 24 hours and the mRNA levels were also analyzed using the Affymetrix Human Genome U133A 2.0 Array. Wild-type 3T3 cells from the GSE125782 dataset were maintained in the presence or absence of glutamine for 18 hours and the RNAs sequenced using the Illumina HiSeq 2500 platform. KPC pancreatic ductal adenocarcinoma cells from the GSE150874 dataset were cultured in regular or glutamine-free medium for 24 hours, and the RNA sequencing was conducted using the Illumina NextSeq 500 platform.

Analysis of the microarray or RNA-Seq data using the iDEP v0.96 online tool

The microarray or RNA-Seq datasets were normalized and analyzed using the iDEP v0.96 online tool (http://bioinformatics.sdstate.edu/idep/) (21). iDEP (integrated differential expression and pathway analysis) is an online tool that facilitates analyzing transcriptomic profiling like microarray or RNA-Seq data. iDEP can be applied for exploratory analysis, identification of differentially expressed genes, and pathway analysis.

Normalization of microarray data and Gene Set Enrichment Analysis

GEO datasets (GSE62673, GSE26370, GSE125782 and GSE150874) were uploaded to the R-Project Bioconductor and standardized using the Robust Multiarray Average (RMA) method. The signal intensities were shown on a Log^2 scale and the normalization of gene expression was evaluated using the LIMMA package from the R Bioconductor. In this study, R-Project Bioconductor (ver. 4.1.0, 09/10/2021) was performed to normalize the Affymetrix data. The detailed codes are the same as those in our previous paper (4).

The normalized datasets were processed according to the instructions on the GSEA website (http://software.broadinstitute.org/gsea/index.jsp). Thereafter, GSEA was applied to analyze gene signatures using the Hallmark gene sets. NES was applied to rank the gene-set enrichment. The FDR q-value was calculated to estimate the probability of a false positive finding. In addition, the FWER P value was utilized to estimate the probability of a false positive finding for NES.

REACTOME analysis

REACTOME (https://reactome.org/) is an open-access, manually curated pathway database that provides interpretation and visualization of relevant pathways based on the microarray or RNA-Seq data (22, 23). The data were prepared following the requirements published on the website: https://reactome.org/userguide/analysis. The normalized microarray dataset GSE62673 was uploaded to the online system and underwent PADOG analysis, which down-weighs the genes existing in different pathways.

Pathway analysis using ShinyGO v0.741

ShinyGO (http://bioinformatics.sdstate.edu/go/)

was developed using R-Bioconductor packages that facilitate data analysis and the visualization of results in a graphical way (24). For ShinyGO analysis, the six AAT genes ENSG00000168003, ENSG00000103257, ENSG00000139514, ENSG00000115902, ENSG00000151012 and ENSG00000105281 were listed and applied to build the pathway networks.

DepMap analysis

DepMap analysis was conducted using the online portal (https://depmap.org). The Cancer Dependency Map project provides all the data available to the public under a Creative Commons license in order to create open science. The generated datasets are posted on the DepMap portal prior to publication every three months.

Identification of the alteration in glutamine-deprivation related signaling pathways

Glutamine was selected to validate the repeatability of the response of cells to amino acid deprivation because a plethora of studies have focused on investigating how cells reprogram gene expression to adapt to glutamine-deprivation. For this analysis, the most affected genes were listed to generate and compare the enrichment plots.

GEPIA2 analysis

GEPIA2 is an online tool that helps to explore the large TCGA and GTEx datasets (http://gepia2.cancer-pku.cn/#index) (25). The expression of one single gene can be compared via Boxplots in multiple cancers and their normal counterparts, and the expression of multiple genes can be compared using a matrix plot. GEPIA2 can also be applied to Principal Component Analysis (PCA) of multiple genes in different cancer types through presenting the results in either 2D or 3D plots.

Analysis of gene expression in human samples using cBioportal

The six AAT genes were analyzed according to gene mutations, copy number variations and mRNA levels on the cBioportal website: http://www.cbioportal.org/.

Establishing the clinical significance of the six AAT genes using SurvExpress

The SurvExpress database (http://bioinformatica.mty.itesm.mx:8080/Biomatec/Surviva X.jsp) was applied to investigate the correlation between the expression of six AAT genes with the prognosis of patients. The six AAT genes included SLC3A2, SLC7A5, SLC7A1, SLC1A4, SLC7A11 and SLC1A5.

Dissection of prognostic importance using ENCORI Pan-Cancer survival analysis

This analysis was performed using the ENCORI Pan-Cancer survival analysis online tool: http://starbase.sysu.edu.cn/panGeneSurvivalExp.php# by searching on the six AAT genes. The p values were presented as Dot plots.

Results

Comparison of gene expression under conditions of amino acid-deprivation

Dataset # GSE62673 was identified by searching the NCBI GEO website. This study was performed to dissect unique transcriptional responses to the withdrawal of one amino acid or all amino acids at one time while the control cells were maintained in regular complete medium. The dataset also provides useful information on how tumor cells respond to amino acid-deprivation. In particular, it will help identify factors that can evaluate patients' prognoses. The iDEP v0.96 online tool was employed to compare the range of log ratios associated with replicate spots (Fig. S1A, See Supplementary Online Information at www.celljournal.org), especially for the group with minor variation in data distribution, an indicator of the good quality of the dataset. Next, a heatmap was generated using the 1,000 most variable genes in all groups. The heatmap demonstrates glycine-deprivation leads to almost no alteration in gene expression relative to the control group while methionine-deprivation causes the most changes relative to the control group compared to other amino acid(s) deprivation (Fig.1A). These results were also validated by the PCA analysis (Fig.S1B, See Supplementary Online Information at www.celljournal.org) and the number of differentially expressed genes in each group (Fig.1B).

k-Means clustering enrichment analysis

k-Means enrichment analysis was performed using the 2,000 most variable genes through comparing a total of five pathways on the iDEP v0.96 website. These include Gene Ontology (GO) Cellular Component, GO Biological Process, GO Molecular Function, Curated Reactome and Kyoto Encyclopedia of Genes, and Genomes (KEGG) Metabolic Pathways. The exported results of the k-Means analysis were used to generate waterfall plots based on the number of changed genes (Fig.2, Fig.S2, See Supplementary Online Information at www.celljournal.org). Amino acid deprivation activates the conserved signaling pathways, for example the GCN2-mediated eIF2α phosphorylation that drives ATF4 expression to maintain cellular homeostasis (26). Accordingly, k-Means clustering enrichment detected activation of CHOP-ATF4 and CHOP-C/EBP complexes in the absence of amino acid(s) (Fig.2A). Under amino acid-depleted conditions, cells can activate the signaling related to apoptotic processes (Fig.2B, Fig.S2B, See Supplementary Online Information at www.celljournal.org) and the binding of transcription or

translation factors to relevant DNA or RNA targets (Fig.2C). Importantly, the restriction of amino acid availability also leads to the alteration of cell cycle related pathways like Mitotic G_1-G_1/S phases, Mitotic G_2-G_2/M phases and Mitotic prometaphase (Fig.S2B, See Supplementary Online Information at www.celljournal.org). Taken together, these results indicate that cells will first activate the evolutionally conserved signaling to effectively alleviate apoptosis when cells are exposed to short-term and acute nutrient-depletion. However, with long-term treatment, the cells will undergo apoptosis even with induction of the protective signaling due to the irreversible damage to the cells.

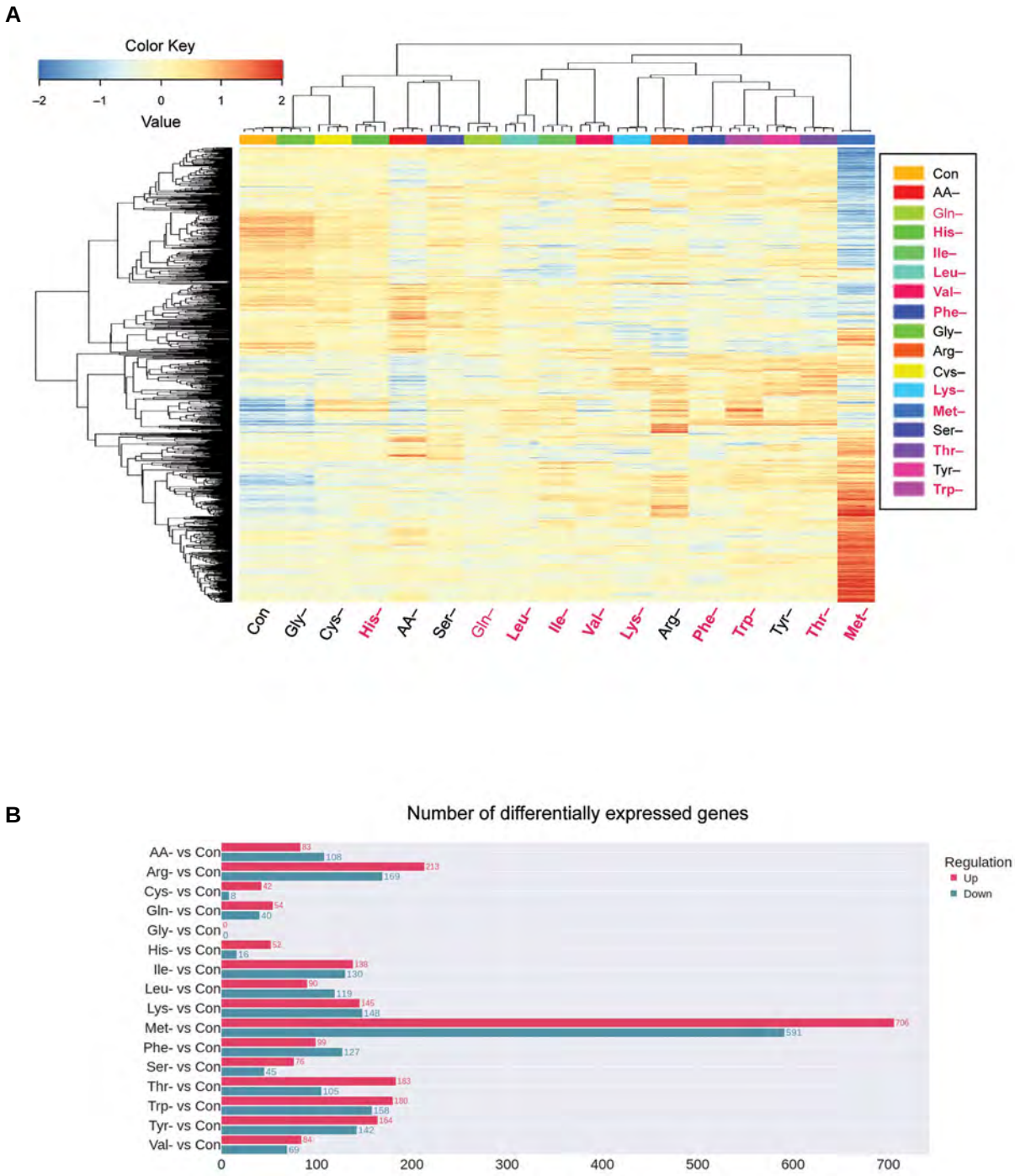

Fig.1: Comparison of the most variable genes between amino acid(s)-deprived groups and control group. **A.** The heatmap, generated using the iDEP v0.96 online tool, shows the gene expression pattern in different groups. Red font indicates the essential amino acids and conditionally essential amino acids. "Con" stands for "Control" group with cells maintained in regular culture medium. **B.** The numbers of differentially expressed genes (either up- or down-regulated) among different groups without one or all amino acid(s) versus that in control group.

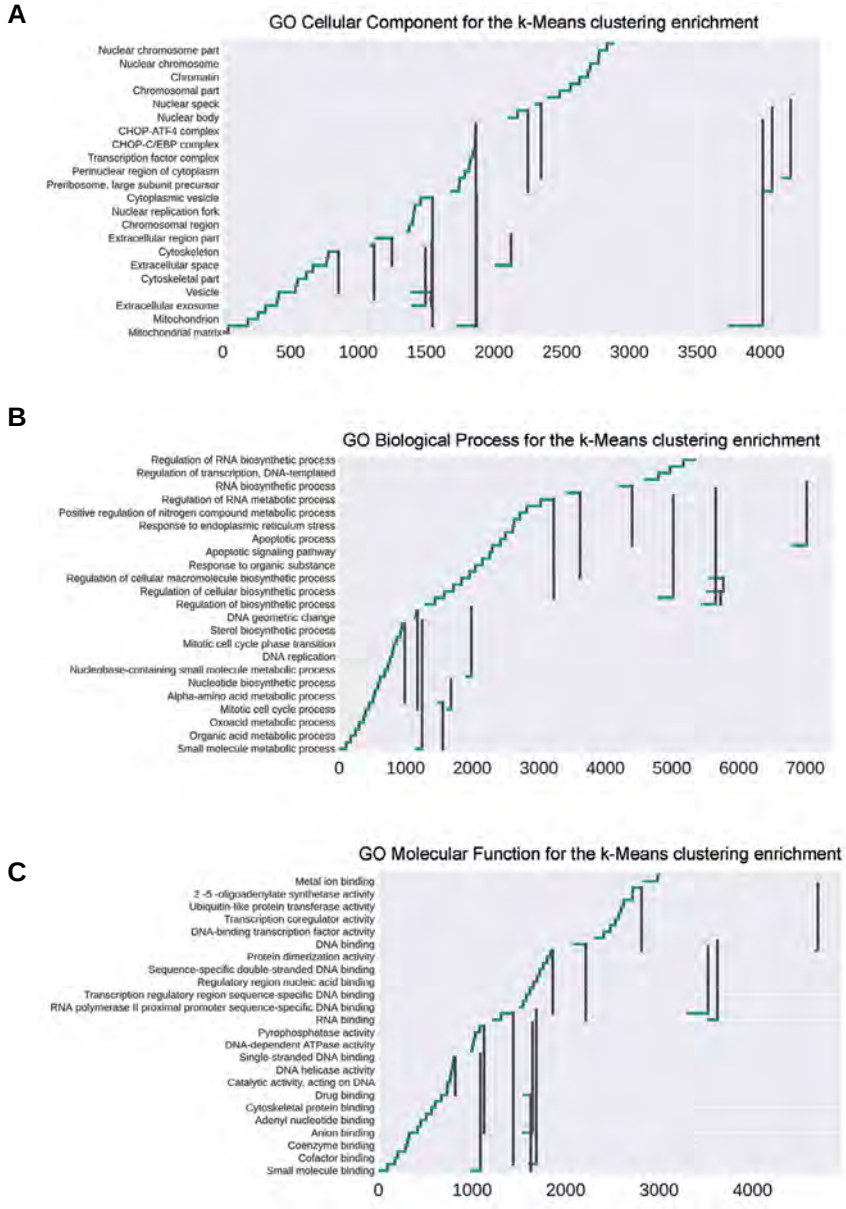

Fig.2: The waterfall plots demonstrate the k-Means clustering enrichment. **A.** The number of genes for pathway alteration in GO Cellular Component for the k-Means clustering enrichment. **B.** The number of genes for pathway alteration in GO Biological Process for the k-Means clustering enrichment. **C.** The number of genes for pathway alteration in GO Molecular Function for the k-Means clustering enrichment.

REACTOME analysis of different responses under conditions of amino acid-deprivation

REACTOME provides a platform for interpreting signaling, metabolic molecules and their relations with biological pathways and processes. For example, it facilitates establishing reaction networks through dissecting the metabolism of proteins, nucleic acids, complexes, vaccines, anti-cancer therapeutics and small molecules. The withdrawal of amino acids leads to the alteration of pathways like metabolism, the cell cycle, DNA Replication, DNA Repair, metabolism of proteins, programmed cell death, cellular responses to stimuli and so forth. Generally, there is a clear reduction in pathways related to the cell cycle, DNA Replication and DNA Repair, suggesting the amino acid deprivations affect cell cycle progression by interfering with the supply of molecules for DNA replication and reducing the building blocks for cell proliferation. Accordingly, reduction in amino acid levels can activate cellular responses to stimuli. For example, GSEA analysis showed the activation of unfolded protein response as one of the hallmark pathways generated by the deprivation of one/all amino acid(s) (Fig.S3, See Supplementary Online Information at www.celljournal.org). The REACTOME analysis also identified the upregulation of apoptosis-related signaling on deprivation of Arginine, Cystine, Glutamine, Isoleucine, Leucine, Lysine, Phenylalanine, Threonine, Tyrosine or Valine (Fig.S3, See Supplementary Online Information at www.celljournal.org), including both essential and non-essential amino acids.

Expression of AAT genes under amino acid-deprived conditions

Mammalian cells have a family of SLC membrane transporters, such as amino acids or glucose, to uptake organic molecules, inorganic ions and ammonia. It remains unknown what kinds of AATs will be altered in tumor cells on amino acid withdrawal. To address this question, SLC family member genes were listed from the GSE62673 dataset and analyzed using the iDEP v0.96 online tool. In accordance with the whole genome alterations, the glycine-deprived group had the lowest number of differentially expressed genes, while methionine-deprived group had the most alterations when compared with the control group (Fig.3A). PCA analysis also showed a pretty similar pattern of genes in the glycine-deprived group and the most changes in the methionine-deprived group (Fig.3B). Methionine initiates protein synthesis in eukaryotes, as seen in the PCA analysis, restriction of methionine demonstrates the greatest effects on global gene translation. For this reason, the expression of SLC family membrane transporters were analyzed and compared excluding the all-amino-acid-deprived group and the methionine-deprived group. Normally, solid tumors have insufficient blood supply, leading to low amino acid levels. Under this condition, the upregulated genes are supposed to play important roles in maintaining cell survival and proliferation. Based on this hypothesis, upregulated genes were analyzed under the depletion of different amino acids. Following this process, six AAT genes were identified as consistently upregulated; SLC3A2, SLC7A5, SLC7A1, SLC1A4, SLC7A11 and SLC1A5, when comparing the amino acid-deprived group to the control group (Fig.3C, Fig.S4, See Supplementary Online Information at www.celljournal.org). According to the biological functions of the six transporters, the pathway network was generated using ShinyGO (Fig.3D), highlighting that these AAT genes regulate various aspects of cellular functions that contribute to tumor development and progression.

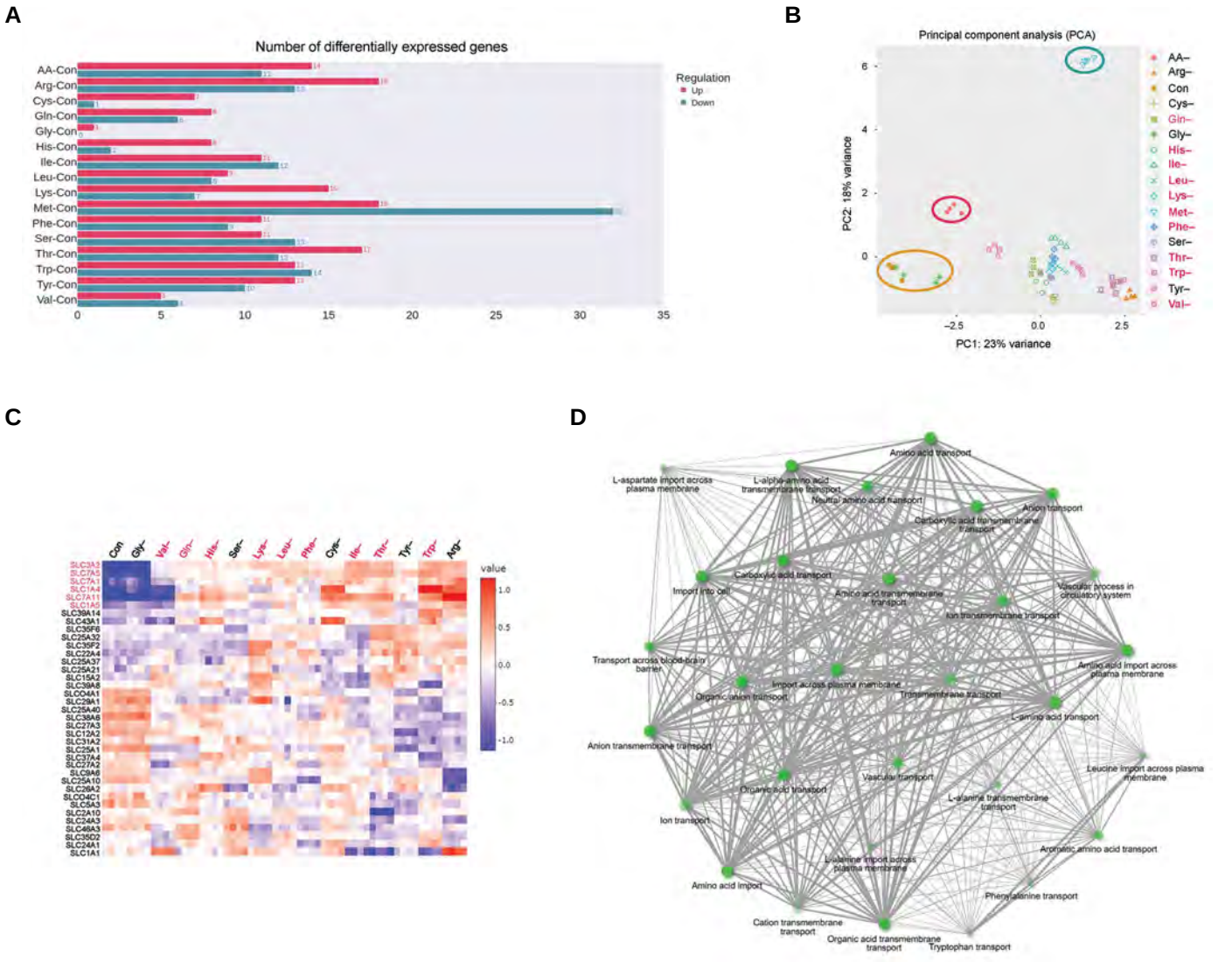

Fig.3: Upregulation of the six AAT genes in amino acid-deprivation. **A.** Comparison of the number of differentially expressed transporter genes among different groups. **B.** The PCA analysis indicates the alteration of AAT genes under different amino acid-depleted conditions. **C.** The heatmap demonstrates the most-altered AATs in amino acid-deprived conditions except that for methionine- and all amino acid- depletion. **D.** The ShinyGO online tool establishes the pathway network based on the six AAT genes.

Comparison of gene expression under glutamine-deprivation in independent studies

Glutamine is a widely investigated amino acid since it functions as a conditionally essential amino acid in tumor cells. Glutamine-deprivation leads to the upregulation of genes like ASNS, DDIT3, DDIT4, TRIB3, ATF3 and ATF4 (Fig.4A), which are well-known for their involvement in the integrated stress response. Importantly, glutamine-deprivation enhances the expression of genes related to cellular response to stress and apoptosis while reducing those related to DNA replication and cell cycle progression (Fig.4B, C). To further validate the findings from MCF7 cells in the GSE62673 dataset, three other datasets that included glutamine-deprivation were collected and analyzed to examine the alteration of genes related to the stress response and cell cycle progression (Fig.S5, See Supplementary Online Information at www.celljournal.org). These analyses showed that glutamine-deprivation induces the expression of the six AAT genes in both human and mouse cells, except for SLC1A4 and SLC1A5 in mouse pancreatic ductal adenocarcinoma KPC cells (Fig.4D), highlighting that upregulation of these six AAT genes function as conserved factors to mediate cellular response to the withdrawal of amino acids.

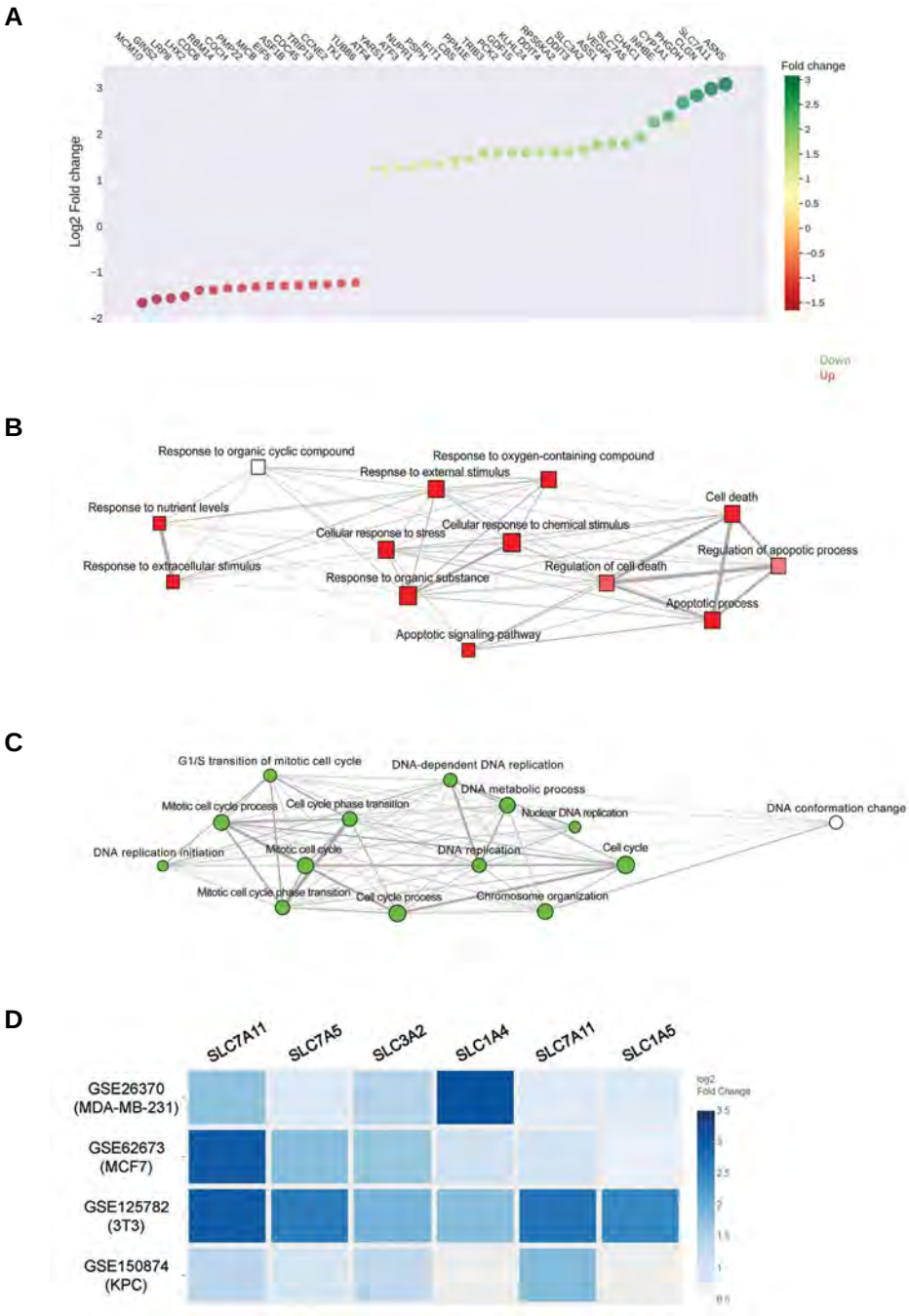

Fig.4: Comparison of gene expression pattern in glutamine-deprivation in independent studies. **A.** The most altered genes under glutamine-deprivation in the GSE62673 dataset. **B**, **C.** The activated or inactivated signaling pathways under glutamine-deprivation. **D.** The matrix plot indicates the log2 fold change of listed AATs in these datasets: GSE26370 (MDA-MB-231), GSE62673 (MCF7), GSE125782 (3T3) and GSE150874 (KPC).

Distinct expression of the six AATs in human tumor and normal tissues

Expression of the six AAT genes was compared using the GEPIA2 online tool regarding to the TCGA tumor tissues and their normal counterparts. Interestingly, there is an obvious upregulation of six AAT genes in different tumors relative to their normal counterparts (Fig.5A, Fig.S6, See Supplementary Online Information at www.celljournal.org). To further demonstrate the importance of these six AAT genes, PCA analysis was performed to study their enrichment in TCGA tumor samples versus normal tissues. Out of the twenty-three tumor types, there are six types of tumors that demonstrate a distinct separation of signals between tumor and normal tissue on both 2D and 3D plots (Fig.5, Fig.S7, See Supplementary Online Information at www.celljournal.org). These tumors include colon adenocarcinoma (COAD), esophageal cancer (ESCA), kidney renal clear cell carcinoma (KIRC), lung adenocarcinoma (LUAD), lung squamous cell carcinoma (LUSC) and rectal adenocarcinoma (READ). In accordance, cBioportal analysis also suggests there is a pattern of co-expression of these six AAT genes in human tumors like COAD, KIRC, LUAD, LUSC and esophageal adenocarcinoma (Fig.S8, See Supplementary Online Information at www.celljournal.org).

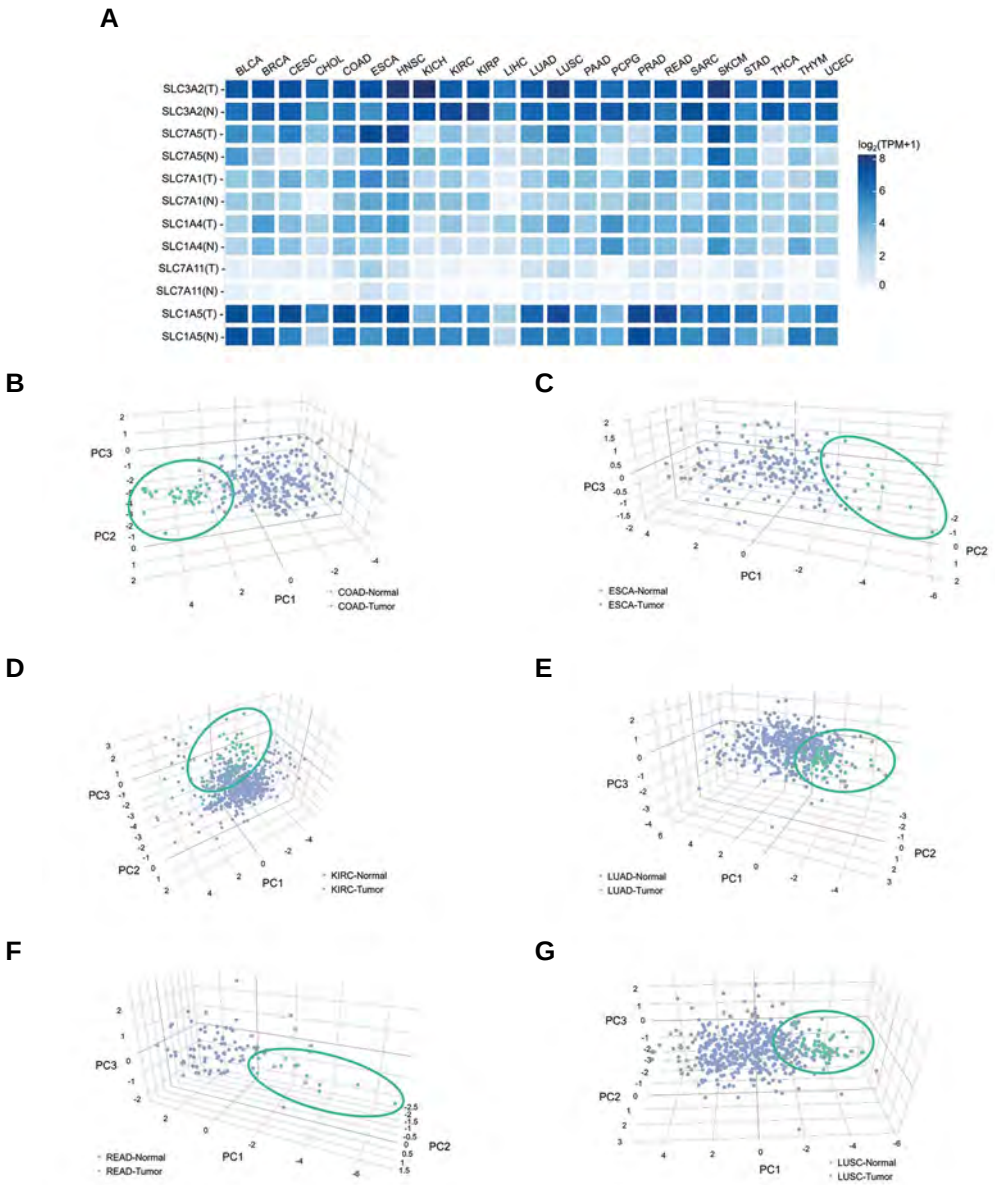

Fig.5: Expression of the six AAT genes in human tumors. **A.** The matrix plot compares expression of the indicated AAT genes in TCGA tumor tissues and in normal counterparts. This matrix is produced using the Multiple Gene Comparison function of the online tool GEPIA2. Generally, the gene list was uploaded first, and the TCGA tumor and normal data were chosen for further analysis. The comparison was performed using log2(TPM+1) for the log scale. **B**-**G.** The PCA analysis demonstrates this panel of six AAT genes is well separated into two distinct clusters when comparing normal and corresponding tumors including **B.** COAD, **C.** ESCA, **D.** KIRC, **E.** LUAD, **F.** READ, and **G.** LUSC. TPM; Transcripts per million, COAD; Colon adenocarcinoma, ESCA; Esophageal cancer, KIRC; Kidney clear cell carcinoma, LUAD; Lung adenocarcinoma, LUSC; Lung squamous cell carcinoma, and READ; Rectal adenocarcinoma.

Analysis of the prognostic importance of the six AAT genes in human cancers

For most TCGA tumors, overexpression of any one of the six AAT genes is significantly correlated with a poor prognosis (Fig.S9, See Supplementary Online Information at www.celljournal.org). SurvExpress analysis was applied to investigate correlation between the six AAT genes as a panel and the patients' prognoses. Particular attention was paid to those tumors characterized by a distinct expression pattern for the six AAT genes compared to that for their normal counterparts in the PCA analysis (Fig.5). Dysregulated expression, particularly overexpression, of the six AAT genes as a panel was significantly correlated with a poor prognosis in patients with COAD, ESCA, KIRC, LUAD and COADREAD. Although there is no significance of dysregulated expression of those six AAT genes in evaluating prognosis of patients with LUSC when setting the p value at 0.05, the general pattern remains consistent with that of COAD, ESCA, KIRC, LUAD and COADREAD (Fig.6). Taken together, the survival analyses identified the clinicopathological importance of these six AAT genes in assessing patients' prognoses.

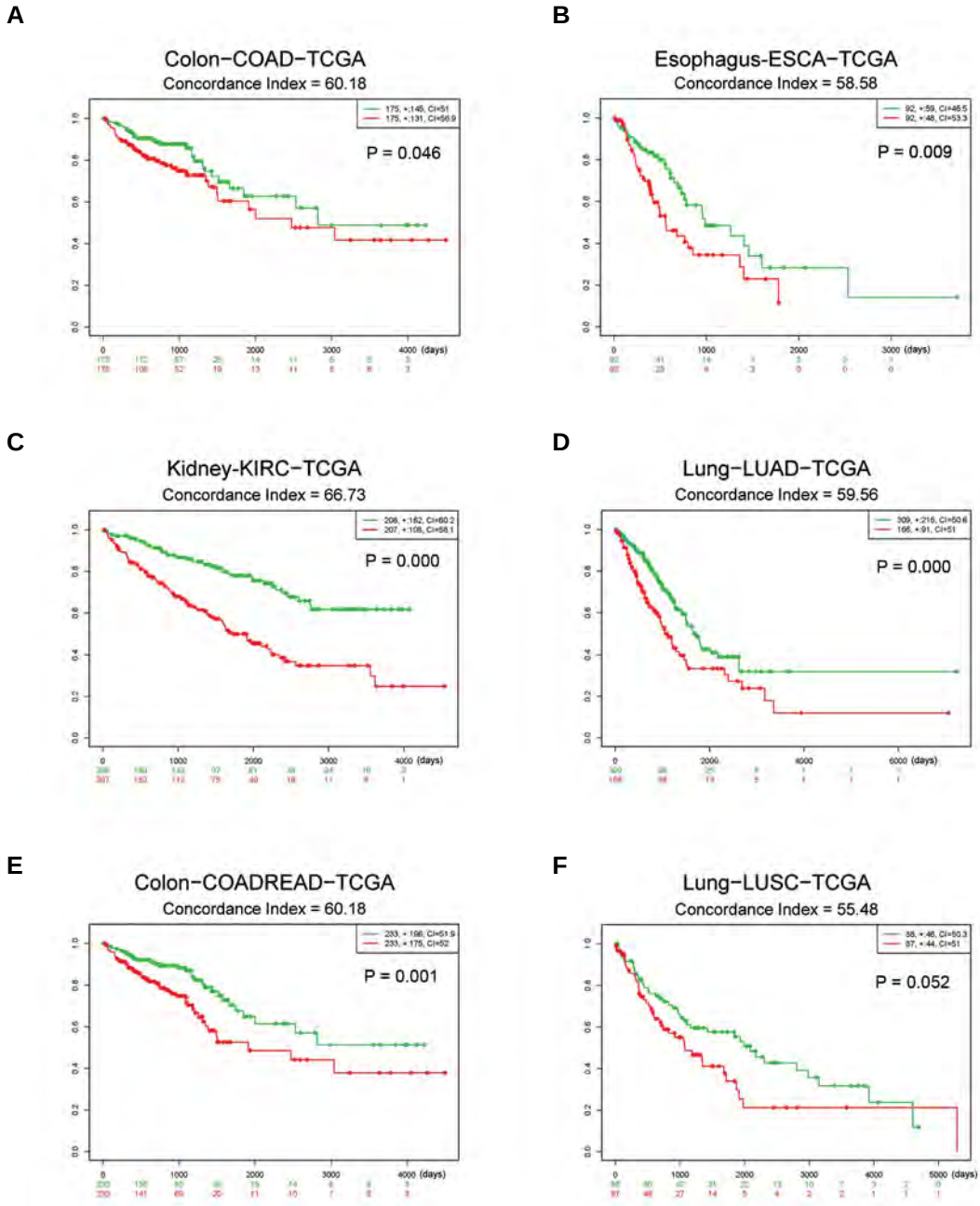

Fig.6: Survival analysis based on the expression of six AAT genes in human tumors. The Log-Rank analysis shows that expression of the panel of six AAT genes (SLC3A2, SLC7A5, SLC7A1, SLC1A4, SLC7A11 and SLC1A5) can be applied to evaluate the prognosis of patients with **A.** COAD, **B.** ESCA, **C.** KIRC, **D.** LUAD, **E.** COADREAD, and **F.** LUSC. The green lines indicate tumors with reduced expression while the red lines are for tumors with overexpression of the panel of six AAT genes. Statistical analyses were performed using the Log Rank test.

DepMap analysis indicates the biological importance of these six AAT genes in human cancers

The biological importance of these six AAT genes was evaluated using DepMap analysis. DepMap determines the genes required for cell growth by performing genome-wide RNAi or CRISPR loss-of-function screening analyses in more than 1,000 cancer cell lines. The RNAi screening employs DEMETER2, a method based on large-scale RNAi data, to demonstrate the effect of knockdown of the six AAT genes on cell growth (27). For all cell lines tested, transient knockdown of SLC3A2, SLC7A5, SLC1A5 and SLC7A1 demonstrated stronger effects than knockdown of SLC1A4 and SLC7A11 (Fig.S10, See Supplementary Online Information at www.celljournal.org). In accordance with previous reports, SLC3A2, SLC7A5 and SLC1A5 were related to uptake of glutamine, a well-known amino acid contributing to cell survival and proliferation.

Discussion

Recent studies have focused on glutamine instead of other amino acids because tumor cells undergo more apoptosis in the absence of glutamine than other amino acids. However, this doesn't mean that other amino acids are not important for tumor cells. To culture mammalian cells, formulated medium is utilized that makes it easier to test the response of tumor cells to the deprivation of a single amino acid or all amino acids at one time. In the GSE62673 dataset, amino acids are removed to investigate whether there is a conserved response in tumor cells under single amino acid- or all amino acid- deprived conditions. iDEP v0.96 analysis was applied this dataset to show glycine-deprivation results in minor changes in gene expression relative to the control group while methionine-deprivation leads to the most dramatic alterations, suggesting the effects of methionine-deprivation on gene transcription are exaggerated because it is coded by the start codon that contributes to the synthesis of most polypeptides. The k-Means clustering enrichment, REACTOME and GSEA analyses showed activation of the integrated stress response. This response enhances the adaptivity of cells to acute stresses but is lost under chronic stress conditions, finally inducing apoptotic signaling. In addition, amino acid withdrawal attenuates cell proliferation through blocking cell cycle progression due to reduced DNA replication and elongated DNA repair time. After validating the reliability of this dataset (GSE62673), the expression of AATs was further analyzed and a panel of six AAT genes was identified to be upregulated; SLC3A2, SLC7A5, SLC7A1, SLC1A4, SLC7A11 and SLC1A5. The analyses also demonstrated that a distinctive enrichment pattern exists for these six AAT genes in tumor tissues relative to normal counterparts.

LAT1/SLC7A5 is an obligatory amino acid exchanger that can transport leucine, isoleucine, valine, phenylalanine, methionine, tyrosine, histidine and tryptophan into cells with the efflux of glutamine (14). In order to perform its biological function, LAT1 forms a heterodimer with 4F2 cell-surface antigen heavy chain (4F2hc, also termed CD98hc/SLC3A2) (28). LAT1 activates mTORC1 signaling through enhancing leucine uptake. The expression of LAT1/SLC7A5 is elevated and associated with poor prognosis in colorectal cancer, esophageal cancer, renal cell carcinoma, lung cancer, breast cancer and pancreatic cancer, etc. (29). xCT/SLC7A11, linked by a covalent disulfide bond to CD98hc/SLC3A2, functions as a bidirectional AAT that mediates cysteine uptake with the excretion of glutamate (30). xCT thus provides cysteine for the synthesis of glutathione, which maintains the intracellular oxidative/reductive balance. There is an obvious upregulation of xCT/SLC7A11 in human cancers including colorectal cancer, esophageal cancer, lung cancer, pancreatic cancer, head and neck cancer among others (31, 32). CD98hc/SLC3A2 controls amino acid transport and integrin signaling, which play critical roles in driving tumor development and progression (33). CD98hc forms a heterodimer with LAT1, LAT2 or xCT to promote the uptake of relevant amino acids. Besides contributing to amino acid uptake, CD98hc can also bind to β1 or β3 integrin to mediate cell survival, proliferation, and migration. CD98hc is highly expressed in human tumors like renal cell carcinoma, lung cancer, breast cancer, sarcoma, head and neck cancer, among others (34).

ASCT1/SLC1A4 is specifically expressed in the cell plasma membrane. As a serine and cysteine transporter ASCT1 is linked with brain homeostasis (35). The full-length form of ASCT2/SLC1A5 is predominantly localized in the plasma membrane while the short variant is localized in the inner membrane of mitochondria (36). ASCT2 is a Na^+-dependent transmembrane transporter that works to uptake neutral amino acids, such as glutamine, particularly in cancer cells. ASTC2 expression is elevated in colorectal cancer, gastric cancer, head and neck cancer and leukemia (37). CAT1/SLC7A1 is a plasma membrane transporter that is glycosylated but not associated with an ancillary protein to perform its functions. CAT1 facilitates the uptake of proteinogenic amino acids like arginine and lysine and non-proteinogenic ones such as ornithine. CAT1 is mainly overexpressed in colorectal and breast cancers (38). Like indicated above, the six AAT genes are overexpressed at both mRNA and protein levels in various human cancers. Consistently, the six AATs can be considered as a panel to evaluate patients' prognoses. However, a lot of unknown questions remain to be further investigated, for example, how these six AAT genes are induced when deprived of amino acids, whether there is functional redundancy in these AAT genes at cellular levels, and what is the therapeutic potential of the dysregulation of the six AAT genes.

As already mentioned, any of the six single AATs can be involved in regulating a variety of processes including cell cycle progression, proliferation, migration, invasion, survival and the production of factors in response to stress conditions. Importantly, although the six AATs are upregulated together when cells are exposed to amino acid deprivation, their clinical importance as a panel

in evaluating patients' prognoses remains unclear. Our current study showed their importance in determining the prognosis of patients with colorectal, esophageal, kidney and lung cancers. The next step will be to further validate these bioinformatic findings in real world human specimens using IHC staining. In the event of good validation, this panel of AATs could be used as diagnostic markers. Moreover, we anticipate that the expression of these six AATs can be applied to assess patients' response to treatments like anti-angiogenic treatment, which generally leads to an insufficient supply of amino acids in solid tumors.

Conclusion

To sum up, solid tumor cells employ conserved signaling to upregulate the expression of a panel of six AATs in order to enhance the uptake of amino acids to maintain homeostasis. This study identifies these AATs include SLC3A2, SLC7A5, SLC7A1, SLC1A4, SLC7A11 and SLC1A5. Clinically, the upregulation of these AATs is significantly correlated with poor prognosis in patients with colorectal, esophageal, kidney and lung cancers. Future studies are required to further determine their biological roles and their potential as therapeutic targets.

Acknowledgments

This study is supported by the Start-up funding awarded to S.Q. from the Tianjin Medical University Cancer Institute and Hospital (No.: 2021-1-7), 2021 Tianjin Medical University Cancer Institute and Hospital Talent Program and Start-up Grant for Doctors awarded to S.Q. (No.: B2102), 2023 Tianjin Municipal Education Commission Key Project Program (No.: 2022ZD065) to S.Q., and Tianjin Key Medical Discipline (Pathology) Construction Project (TJYXZDXK-012A). There is no conflict of interest in this study.

Authors' Contributions

S.Q.; Conception, Data analysis, Interpretation, Preparation, Revision of manuscript, and supervision. W.C.; Data analysis and Interpretation. Y.L., H.X., C.Y., Y.W.; Data analysis, Interpretation, Preparation, and Revision of manuscript. All authors read and approved the final manuscript.

References

1. Sanchez-Vega F, Mina M, Armenia J, Chatila WK, Luna A, La KC, et al. Oncogenic signaling pathways in the cancer genome atlas. Cell. 2018; 173(2): 321-337. e10.
2. Batlle R, Andrés E, Gonzalez L, Llonch E, Igea A, Gutierrez-Prat N, et al. Regulation of tumor angiogenesis and mesenchymal-endothelial transition by p38α through TGF-β and JNK signaling. Nat Commun. 2019; 10(1): 3071.
3. Qie S, Diehl JA. Glutamine addiction: an Achilles heel in esophageal cancers with dysregulation of CDK4/6. Mol Cell Oncol. 2019; 6(4): 1610257.
4. Qie S, Yoshida A, Parnham S, Oleinik N, Beeson GC, Beeson CC, et al. Targeting glutamine-addiction and overcoming CDK4/6 inhibitor resistance in human esophageal squamous cell carcinoma. Nat Commun. 2019; 10(1): 1296.
5. Qie S, He D, Sang N. Overview of glutamine dependency and metabolic rescue protocols. Methods Mol Biol. 2019; 1928: 427-439.
6. Dong M, Miao L, Zhang F, Li S, Han J, Yu R, et al. Nuclear factor-κB p65 regulates glutaminase 1 expression in human hepatocellular carcinoma. Onco Targets Ther. 2018; 11: 3721-3729.
7. Lee JS, Adler L, Karathia H, Carmel N, Rabinovich S, Auslander N,et al. Urea cycle dysregulation generates clinically relevant genomic and biochemical signatures. Cell. 2018; 174(6): 1559-1570. e22.
8. Micaily I, Roche M, Ibrahim MY, Martinez-Outschoorn U, Mallick AB. Metabolic pathways and targets in chondrosarcoma. Front Oncol. 2021; 11: 772263.
9. Papalazarou V, Maddocks ODK. Supply and demand: cellular nutrient uptake and exchange in cancer. Mol Cell. 2021; 81(18): 3731-3748.
10. Qie S, Diehl JA. Cyclin D degradation by E3 ligases in cancer progression and treatment. Semin Cancer Biol. 2020; 67(Pt 2): 159-170.
11. Xiong G, Stewart RL, Chen J, Gao T, Scott TL, Samayoa LM, et al. Collagen prolyl 4-hydroxylase 1 is essential for HIF-1α stabilization and TNBC chemoresistance. Nat Commun. 2018; 9(1): 4456.
12. Wei Z, Liu X, Cheng C, Yu W, Yi P. Metabolism of amino acids in cancer. Front Cell Dev Biol. 2021; 8: 603837.
13. Fultang L, Gneo L, De Santo C, Mussai FJ. Targeting amino acid metabolic vulnerabilities in myeloid malignancies. Front Oncol. 2021; 11: 674720.
14. Kandasamy P, Gyimesi G, Kanai Y, Hediger MA. Amino acid transporters revisited: new views in health and disease. Trends Biochem Sci. 2018; 43(10): 752-789.
15. Huang X, Anderle P, Hostettler L, Baumann MU, Surbek DV, Ontsouka EC, et al. Identification of placental nutrient transporters associated with intrauterine growth restriction and pre-eclampsia. BMC Genomics. 2018; 19(1): 173.
16. Rebsamen M, Girardi E, Sedlyarov V, Scorzoni S, Papakostas K, Vollert M, et al. Gain-of-function genetic screens in human cells identify SLC transporters overcoming environmental nutrient restrictions. Life Sci Alliance. 2022; 5(11): e202201404.
17. Liu C, Li X, Li C, Zhang Z, Gao X, Jia Z, et al. SLC3A2 is a novel endoplasmic reticulum stress-related signaling protein that regulates the unfolded protein response and apoptosis. PLoS One. 2018; 13(12): e0208993.
18. Kahlhofer J, Teis D. The human LAT1-4F2hc (SLC7A5-SLC3A2) transporter complex: Physiological and pathophysiological implications. Basic Clin Pharmacol Toxicol. 2022 (ahead of print).
19. Torrence ME, MacArthur MR, Hosios AM, Valvezan AJ, Asara JM, Mitchell JR, et al. The mTORC1-mediated activation of ATF4 promotes protein and glutathione synthesis downstream of growth signals. Elife. 2021; 10: e63326.
20. Sikalidis AK, Lee JI, Stipanuk MH. Gene expression and integrated stress response in HepG2/C3A cells cultured in amino acid deficient medium. Amino Acids. 2011; 41(1): 159-171.
21. Ge SX, Son EW, Yao R. iDEP: an integrated web application for differential expression and pathway analysis of RNA-Seq data. BMC Bioinformatics. 2018; 19(1): 534.
22. Wu G, Haw R. Functional interaction network construction and analysis for disease discovery. Methods Mol Biol. 2017; 1558: 235-253.
23. Jassal B, Matthews L, Viteri G, Gong C, Lorente P, Fabregat A, et al. The reactome pathway knowledgebase. Nucleic Acids Res. 2020; 48(D1): D498-D503.
24. Ge SX, Jung D, Yao R. ShinyGO: a graphical gene-set enrichment tool for animals and plants. Bioinformatics. 2020; 36(8): 2628-2629.
25. Tang Z, Kang B, Li C, Chen T, Zhang Z. GEPIA2: an enhanced web server for large-scale expression profiling and interactive analysis. Nucleic Acids Res. 2019; 47(W1): W556-W560.
26. Yuan F, Jiang H, Yin H, Jiang X, Jiao F, Chen S, et al. Activation of GCN2/ATF4 signals in amygdalar PKC-δ neurons promotes WAT browning under leucine deprivation. Nat Commun. 2020; 11(1): 2847.
27. McFarland JM, Ho ZV, Kugener G, Dempster JM, Montgomery PG, Bryan JG, et al. Improved estimation of cancer dependencies from large-scale RNAi screens using model-based normalization and data integration. Nat Commun. 2018; 9(1): 4610.
28. Rosario FJ, Dimasuay KG, Kanai Y, Powell TL, Jansson T. Regulation of amino acid transporter trafficking by mTORC1 in primary human trophoblast cells is mediated by the ubiquitin ligase Nedd4-2. Clin Sci (Lond). 2016; 130(7): 499-512.
29. Honjo H, Kaira K, Miyazaki T, Yokobori T, Kanai Y, Nagamori S, et al. Clinicopathological significance of LAT1 and ASCT2 in patients with surgically resected esophageal squamous cell carcinoma. J

Surg Oncol. 2016; 113(4): 381-389.
30. Oda K, Lee Y, Wiriyasermkul P, Tanaka Y, Takemoto M, Yamashita K, et al. Consensus mutagenesis approach improves the thermal stability of system x_c^- transporter, xCT, and enables cryo-EM analyses. Protein Sci. 2020; 29(12): 2398-2407.
31. Badgley MA, Kremer DM, Maurer HC, DelGiorno KE, Lee HJ, Purohit V, et al. Cysteine depletion induces pancreatic tumor ferroptosis in mice. Science. 2020; 368(6486): 85-89.
32. Ji X, Qian J, Rahman SMJ, Siska PJ, Zou Y, Harris BK, et al. xCT (SLC7A11)-mediated metabolic reprogramming promotes non-small cell lung cancer progression. Oncogene. 2018; 37(36): 5007-5019.
33. Canup BSB, Song H, Laroui H. Role of CD98 in liver disease. Ann Hepatol. 2020; 19(6): 602-607.
34. Ip H, Sethi T. CD98 signals controlling tumorigenesis. Int J Biochem Cell Biol. 2016; 81(Pt A): 148-150.
35. Scalise M, Console L, Cosco J, Pochini L, Galluccio M, Indiveri C. ASCT1 and ASCT2: Brother and Sister? SLAS Discov. 2021; 26(9): 1148-1163.
36. Yoo HC, Park SJ, Nam M, Kang J, Kim K, Yeo JH, et al. A variant of SLC1A5 Is a mitochondrial glutamine transporter for metabolic reprogramming in cancer cells. Cell Metab. 2020; 31(2): 267-283. e12.
37. Teixeira E, Silva C, Martel F. The role of the glutamine transporter ASCT2 in antineoplastic therapy. Cancer Chemother Pharmacol. 2021; 87(4): 447-464.
38. Okita K, Hara Y, Okura H, Hayashi H, Sasaki Y, Masuko S, et al. Antitumor effects of novel mAbs against cationic amino acid transporter 1 (CAT1) on human CRC with amplified CAT1 gene. Cancer Sci. 2021; 112(2): 563-574.

Cell J
Cell Journal (Yakhteh)
Homepage: https://www.celljournal.org/
Original Article
Vol 25, No 9, September 2023, Pages: 625-632

Protective Effects of Relaxin 2 (RLXH2) against Hypoxia-Induced Oxidative Damage and Cell Death via Activation of The Nrf2/HO-1 Signalling Pathway in Gastric Cancer Cells

Liguo Wang, Ph.D.#, Yi Zhou, Ph.D.#, Hui Lin, Ph.D, Kezhu Hou, Ph.D.*

Department of General Surgery, Shidong Hospital, Yangpu District, Shanghai, China

Abstract

Objective: This study aims to investigate the potential role of relaxin, a peptide hormone, in preventing cellular deterioration and death in gastric carcinoma cells under hypoxic conditions. It explores the effects of recombinant relaxin 2 (RLXH2) on growth, cell differentiation, invasive potential, and oxidative damage in these cells.

Materials and Methods: In this experimental study, the NCI-N87 cell line was cultured under normal conditions and then subjected to hypoxia using cobalt chloride ($CoCl_2$). The cells were treated with RLXH2, and various assays were performed to assess cellular deterioration, death, and oxidative stress. Western blot and quantitative real time polymerase chain reaction (qRT-PCR) were used to measure the expression levels of nuclear factor erythroid 2-related factor 2 (Nrf2) and HO-1, and the translocation of Nrf2 to the nucleus was confirmed through Western blot analysis.

Results: This study demonstrates, for the first time, that RLXH2 significantly reduces the formation of reactive oxygen species (ROS) and the release of lactate dehydrogenase (LDH) in gastric cancer cells under hypoxic conditions. RLXH2 also enhances the activities of superoxide dismutase (SOD), glutathione peroxidase (GPX), and catalase (CAT), leading to a decrease in hypoxia-induced oxidative damage. RLXH2 promotes the translocation of Nrf2 to the nucleus, resulting in HO-1 expression.

Conclusion: Our findings suggest that RLXH2 plays a significant protective role against hypoxia-induced oxidative damage in gastric carcinoma cells through the Nrf2/HO-1 signalling pathway. This research contributes to a better understanding of the potential therapeutic applications of RLXH2 in gastric cancer treatment.

Keywords: Gastric Cancer, HO-1, Hypoxia, Nrf2, Relaxin

Citation: Wang L, Zhou Y, Lin H, Hou K. Protective effects of relaxin 2 (RLXH2) against hypoxia-induced oxidative damage and cell death via activation of the Nrf2/HO-1 signalling pathway in gastric cancer cells. Cell J. 2023; 25(9): 625-632. doi: 10.22074/CELLJ.2023.2000342.1287

Introduction

Relaxin, a peptide hormone, was initially found to be associated with pregnancy (1). Over time, relaxin was determined to carry out diverse functions in different diseases like cancer, heart failure, and diabetes (2-4). Three types of relaxin peptides are expressed in humans-relaxin 1 (RLXH1), relaxin 2 (RLXH2), and relaxin 3 (RLN3). Each type performs a different function (5). RLXH1 and RLXH2 act via binding to their respective receptors, RXFP1 and RXFP2, respectively. These receptors are a unique type of G-protein coupled receptors that consist of a large ectodomain and an N-terminal module. RLXH2 is a pleiotropic peptide hormone that is overexpressed in various types of cancers (6). RLXH2 helps in proliferation, invasiveness, and metastasis in cancer cells.

Hypoxia is a commonly observed phenomenon in different cancers, which causes activation of hypoxia-associated pathways in these cells (7, 8). Cancerous cells adapt to this hypoxic environment by stimulating metabolic alterations and angiogenesis in order to survive the hypoxic conditions. Response of cancerous cells to hypoxia leads to an aggressive phenotypic behaviour, chemotherapy resistance, and poor clinical outcomes (9). Hypoxia is a well-known phenomenon in different types of cancers like gastric cancer (10). The hypoxic environment within cells is associated with increased production of reactive oxygen species (ROS) (11). The enhanced ROS production is responsible for cellular injuries and often results in cell death (12). Therefore, to prevent hypoxia-associated injuries and death, cells often activate responses by scavenging ROS (13).

Nuclear factor erythroid 2-related factor 2 (Nrf2) is a transcription factor that plays a crucial role in cellular defence against oxidative stress and xenobiotic insults (14). Its activation is essential for maintaining cellular homeostasis, and dysregulation of Nrf2 signalling has been implicated in various cancers (15). Aberrant activation of the Nrf2 pathway has been observed in many cancer types, including lung, breast, prostate, colorectal, and liver cancers (16). The persistent activation of Nrf2 in cancer cells is associated with several tumour-promoting effects (17). Nrf2 activation enhances the cellular antioxidant capacity by upregulating

Received: 17/April/2023, Revised: 05/July/2023, Accepted: 06/August/2023
#These authors contributed equally in this study.
*Corresponding Address: Department of General Surgery, Shidong Hospital, Yangpu District, Shanghai, China
Email: kezhuhou235@gmail.com

Royan Institute
Cell Journal (Yakhteh)

the expression of genes that encode antioxidant enzymes (18). This increased antioxidant defence allows cancer cells to counteract oxidative stress and maintain a redox balance, which promotes cell survival and resistance to chemotherapy and radiotherapy.

The involvement of Nrf2 in cancer extends beyond its effects on oxidative stress, cell survival, and metabolism. Nrf2 is implicated in promoting cancer cell invasion, metastasis, and resistance to anti-cancer therapies. Nrf2 can modulate the expression of genes involved in epithelial-mesenchymal transition, extracellular matrix remodelling, angiogenesis, and drug efflux transporters, and it contributes to cancer cell migration, invasion, and therapy resistance.

In summary, while Nrf2 activation serves as a critical defence mechanism against oxidative stress and xenobiotic insults in normal cells, dysregulated Nrf2 signalling in cancers can confer numerous advantages to tumour cells, including increased antioxidant capacity, enhanced cell survival and proliferation, metabolic reprogramming, and resistance to therapies. Therefore, targeting the Nrf2 pathway is a potential therapeutic strategy to overcome therapy resistance and improve cancer treatment outcomes. The present work aims to explore the protective role of RLXH2 against hypoxia-associated cellular damage and death in gastric cancer cells.

Materials and Methods

The study has been approved by the Research Review and Ethics Board (RREB) of Shidong Hospital (SH/2018/0029).

Cell culture, treatments, and transient transfection

In this experimental study, the NCI-N87 gastric carcinoma cell line (ATCC) was grown in DMEM medium with 5% FBS and culture conditions of 37°C and 5% CO_2. The cells were grown in culture for 24 hours and either left untreated or treated with RLXH2 (Abcam, MA, USA) in 12-well plates. For the hypoxia-related experiments, we grew the cells in DMEM without serum and glucose, and treated them with 200 µM cobalt chloride ($CoCl_2$, Sigma-Aldrich, USA) for 12 or 24 hours with or without RLXH2 (15 nmol/l, Sigma-Aldrich, USA). Inhibition and activation of the Nrf2 pathway was carried out chemically. The NCI-N87 cells were grown overnight and treated with trigonelline (5 nM, Sigma-Aldrich, USA) or 100 µM tert-butylhydroquinone (tBHQ, Sigma-Aldrich, USA), respectively, according to a previously published protocol (19). Chemical inhibition of HO-1 was carried out by growing NCI-N87 cells for 24 hours and subsequently treating them with 2 µM zinc protoporphyrin IX (ZnPPIX, Sigma-Aldrich, USA) for 12 hours. siRNA technology was used to silence Nrf2. For that purpose, NCI-N87 cells were grown for 24 hours and then transiently transfected with 1 µM Nrf2-siRNA (Santa Cruz, Biotechnology, USA) using calcium phosphate (Sigma-Aldrich, USA).

Lactate dehydrogenase leakage assay

The gastric carcinoma cells were grown in a 12-well plate (2 ml medium/well) for 24 hours. The cells were treated under hypoxic only or hypoxic with RLXH2 (15 nmol/L) conditions for 12 hours. Then, 300 µl of the medium was removed and analysed for lactate dehydrogenase (LDH) activity using an LDH Cytotoxicity Assay kit (ThermoFisher Scientific, Waltham, MA, USA) according to the manufacturer's protocol.

Antioxidant assays

The gastric carcinoma cells were grown in a 12-well plate (5×10^5 per well) for 24 hours. The cells were treated under hypoxic only or hypoxic with RLXH2 (15 nmol/L) conditions for 12 hours. The cells were then washed three times in wash buffer (PBS with 0.05 mM EDTA), followed by sonication to disrupt the cells. Centrifugation at 3000 rpm for 10 minutes was carried out to separate the supernatant from the cell lysate. The resultant supernatant was assayed for superoxide dismutase (SOD, ThermoFisher Scientific, USA, cat. no. EIASODC), glutathione peroxidase (GPX, Sunlong, China, cat.no. SL2786Hu), and catalase (CAT, Biocompare, USA, cat. no. ELH-CAT-1) activities by following the manufacturers' instructions. The standards, controls, and working solutions were prepared according to the manufacturer's instructions in the ELISA kit.

Reactive oxygen species measurement

Gastric carcinoma cells were cultured in a 96-well plate (0.42×10^5 cells/well) for 24 hours. For analysis purposes, the treated cells were washed with 1X wash buffer followed by the addition of diluted DCFDA solution (100 µl/well) at 37°C. After 30 minutes of incubation, the DCFDA solution was aspirated and the cells underwent hypoxic treatment alone or together with RLXH2 for 12 hours. Finally, the amount of fluorescence in the cells was assessed.

Extraction of RNA and quantitative real time polymerase chain reaction

Total RNA was extracted from cultured cells using TRIzol-T Reagent (ThermoFisher Scientific, USA) followed by cDNA strand synthesis. The extracted cDNA was subjected to quantitative real time polymerase chain reaction (qRT-PCR) using primers against *Nrf2* and *HO-1*. *β-actin* was used for loading control purposes. The following primer sequences were used:

Nrf2-

F: 5′-CCTCAACTATAGCGATGCTGAATCT-3′
R: 5′-AGGAGTTGGGCATGAGTGAGTAG-3′

HO-1-

F: 5′-GGGCCAGCAACAAAGTG-3′
R: 5′-AGTGTAAGGACCCATCGGAGAA-3′

β-actin-

F: 5′-AGGCATCCTCACCCTGAAGTA-3′
R: 5′-CACACGCAGCTCATTGTAGA-3′

Protein extraction

Cell lysate was prepared from the NCI-N87 cells using NP-40 lysis buffer. In order to inhibit proteolysis, the Halt

Protease Inhibitor Cocktail (ThermoFisher Scientific, USA) was incorporated into the lysis buffer. The cell lysate was subjected to centrifugation at 3000 rpm for 10 minutes, and the supernatant was collected. The protein concentration in the obtained lysate was determined by the Bradford assay method.

Nuclear fraction preparation

A Nuclear Extraction kit (ThermoFisher Scientific, USA) was used to prepare nuclear extracts of the NCI-N87 cells and the Bradfords assay was used to determine protein concentrations. Western blot analysis was used to determine the purity of the nuclear fractions using specific antibodies according to a previously published protocol (20).

Western blot analysis

Protein samples were prepared according to a previously published protocol (21). The proteins were separated on sodium dodecyl sulphate-polyacrylamide gel electrophoresis (SDS-PAGE) and later transferred to a polyvinylidene difluoride (PVDF) membrane. The membrane was incubated overnight with the following primary antibodies: anti-Nrf2 (CST, #12721, 1:1000), anti-HO-1 (CST, #5853, 1:1000), anti-β actin (Abcam, #ab8227, 1:1000), anti-GAPDH (Sigma-Aldrich, #G8795, 1:1000), and anti-histone 4 (H4) (CST, #2592, 1:1000). The membranes were rinsed with PBS and further incubated with fluorescent-labelled secondary antibodies (LI-COR, fluorescent anti-mouse IRDye 680, 1:20 000 and LI-COR, anti-rabbit IRDye 800, 1:10 000). The LI-COR system (Biosciences, Lincoln, NE, USA) was used for secondary detection.

Quantification of immunoblots

Protein band quantification was performed using a LI-COR scanner. In order to create a standard plot, fluorescent spots from various concentrations of fluorescent-labelled secondary antibodies were measured. The fluorescence levels of the individual blot bands were measured and compared to standard plot to quantify the protein bands on the immunoblots.

Apoptotic assay

The gastric carcinoma cells were grown in 96-well plates for 24 hours. Then, the cells were either treated under hypoxic alone or hypoxic plus RLXH2 conditions for 12 hours. A Cell Death Detection ELISAPLUS kit (CELLDETH-RO Roche, USA) was used to determine apoptosis according to the manufacturer's instructions.

Statistical analysis

Statistical analysis was conducted using GraphPad Prism (version 9, GraphPad Software, Inc. USA). The data were analysed using One-way ANOVA followed by Duncan's test for multiple comparisons. The experimental values are presented as mean ± standard error of the mean with a statistical significance of $P<0.05$.

Results

Impact of relaxin 2 on lactate dehydrogenase and reactive oxygen species

Figure 1A shows successful induction of hypoxia after treatment with $CoCl_2$. The hypoxia resulted in membrane damage to the NCI-N87 cells, which was confirmed by LDH release. However, RLXH2 treatment significantly prevented LDH release and excessive ROS production from the hypoxia-damaged NCI-N87 cells (Fig.1B, C).

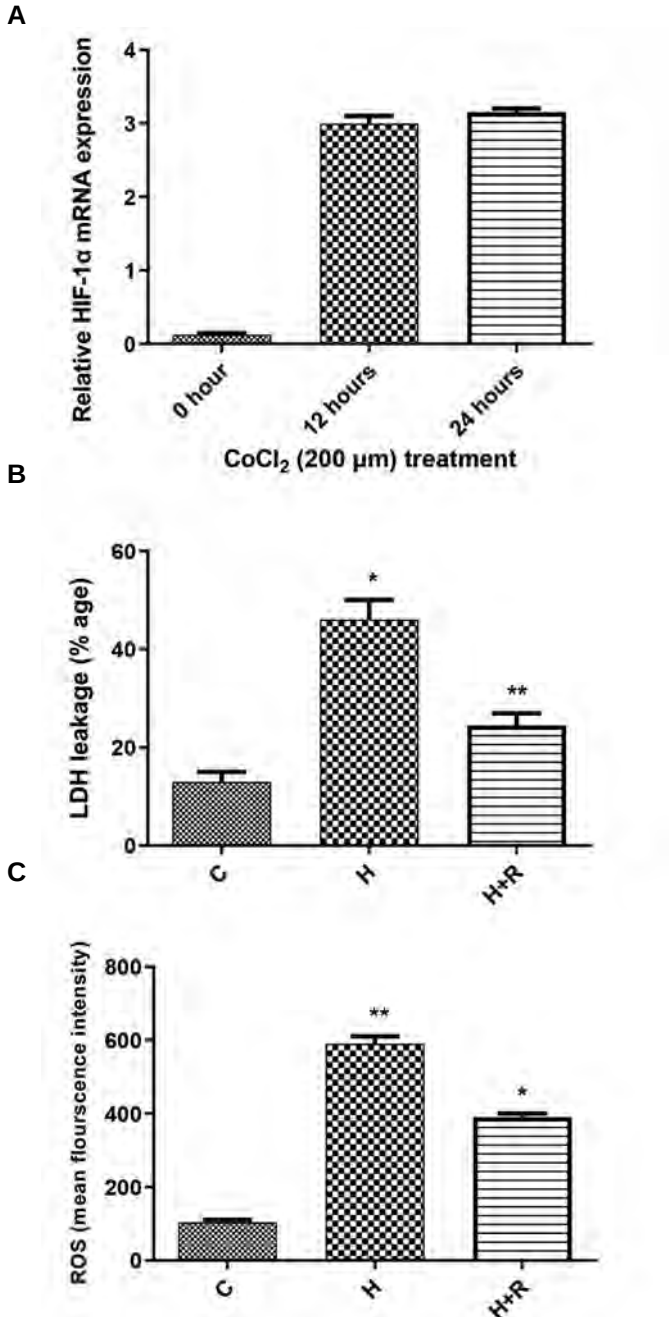

Fig.1: Impact of relaxin 2 (RLXH2) on lactate dehydrogenase (LDH) release and reactive oxygen species (ROS) formation. **A.** Induction of HIF-1α expression after hypoxia treatment for 12 and 24 hours. **B.** RLXH2 significantly decreased LDH release from the NCI-N87 cells in the hypoxia (H) group compared to the control (C) group ($P<0.05$). A $P<0.01$ was obtained from the hypoxia plus RLXH2 treatment group (H+R) compared to the H group. **C.** RLXH2 significantly decreased ROS production in the NCI-N87 cells in the H group compared to the control group (**; $P<0.01$) and in the H+R group compared to the H group (*; $P<0.05$). The results are the average of the three independent experiments.

Impact of Relaxin 2 treatment on hypoxia-associated oxidative damage

The administration of RLXH2 treatment resulted in a noteworthy augmentation of the activities of various antioxidant enzymes, as illustrated in Table 1. This outcome underscores the pivotal role played by RLXH2 in bolstering the cellular defence mechanisms against oxidative stress. In effect, the treatment with RLXH2 emerges as a safeguarding strategy for gastric cancer cells, as it triggers a robust upregulation in the expression levels of antioxidant enzymes.

Table 1: Assessment of antioxidant enzyme activities in the study groups

Antioxidant enzymes	Control*	Hypoxia*	Hypoxia+RLXH2*
SOD	80 ± 3.2	52 ± 2.7	67 ± 3.4
CAT	51 ± 2.5	19 ± 1.6	34 ± 1.9
GPX	31 ± 2.1	13 ± 1.2	25 ± 1.4

RLXH2; Relaxin 2, SOD; Superoxide dismutase, CAT; Catalase, GPX; Glutathione peroxidase, and *; U/mg protein.

Relaxin 2 increases nuclear factor erythroid 2-related factor 2 expression

We assessed the impact of RLXH2 on total Nrf2 levels in the gastric cancer cells. Western blot analysis was performed to determine Nrf2 expression before and after RLXH2 treatment by using specific antibodies against Nrf2 and a control (β-actin). RLXH2 increased expression of the Nrf2 protein compared to the control sample (Fig.2A). As shown in Figure 2B, there was an approximately six-fold increase in Nrf2 protein expression in the RLXH2 treated cells compared to the control (0 hour).

There was a significant increase in Nrf2 mRNA in the NCI-N87 cells after RLXH2 treatment compared to the control (Fig.2B).

Nuclear factor erythroid 2-related factor 2 translocation and HO-1 levels

Western blot analysis was carried out to determine nuclear fraction purity by using primary antibodies against GAPDH and the histone 4 proteins. The antibody against GAPDH did not show any band in the nuclear fraction; on the other hand, the antibody against histone 4 caused a clear band (Fig.3A).

The possible nuclear translocation of Nrf2 after RLXH2 treatment was assessed by Western blot. We cultured the NCI-N87 cells in 60 mm plates for 24 hours, and then treated them with RLXH2 (12 hours). Our analysis of Nrf2 expression indicated that the untreated nuclear fraction did not show any Nrf2 protein band, whereas there was a protein band for Nrf2 expression in the RLXH2 treated nuclear fraction at 12 and 24 hours (Fig.3B).

Inside the nucleus, Nrf2 can activate a wide range of genes and promote cell survival against oxidative stress. Enzymes activated by the Nrf2/ARE pathway include HO-1, GPX, CAT, SOD, GST, thioredoxin, and NQO-1. HO-1 is the main protein activated by Nrf2 (22). Therefore, we assessed the protein levels of HO-1 in the NCI-N87 cells. Figure 3C and D shows HO-1 time-dependent expression levels in the RLXH2-treated gastric carcinoma cells. HO-1 expression significantly increased in the RLXH2-activated gastric carcinoma cells.

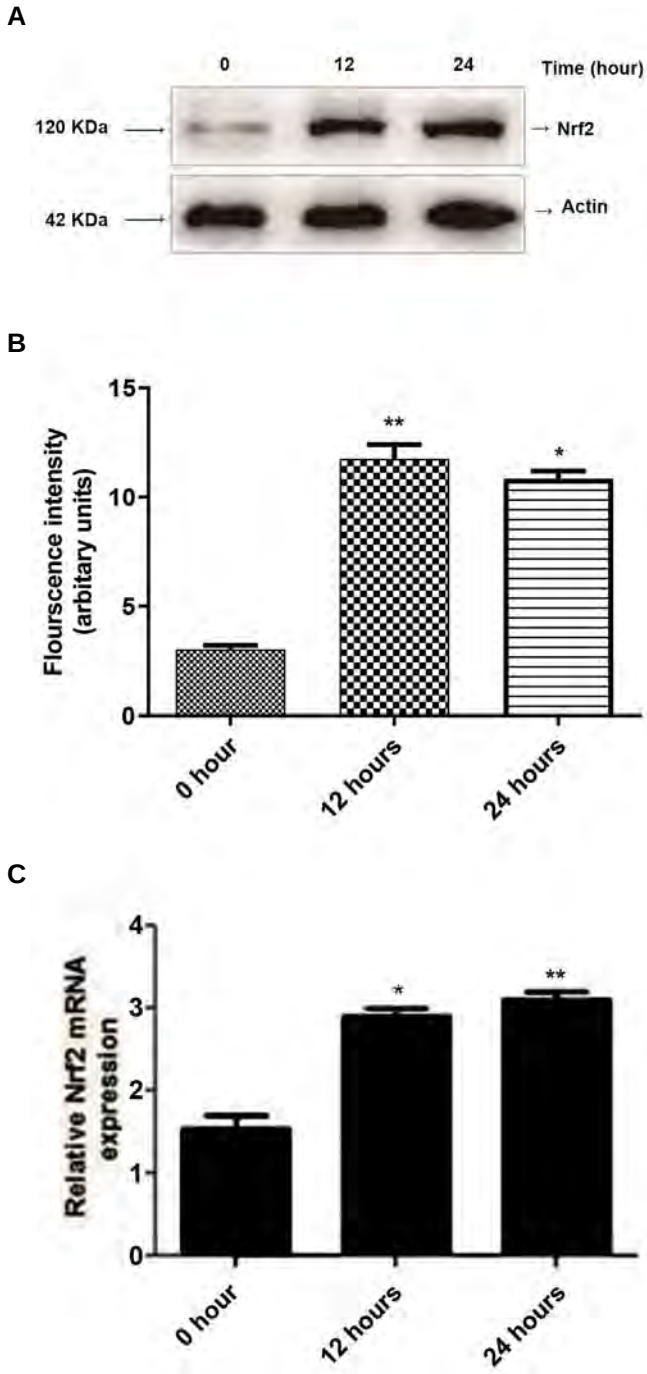

Fig.2: Nuclear factor erythroid 2-related factor 2 protein and mRNA levels. **A.** Nrf2 expression before and after relaxin 2 (RLXH2) treatment. **B.** Densitometry of Nrf2 bands (**; P<0.01 at 12 hours compared to 0 hours, and P<0.05 at 24 hours compared to 12 hours). **C.** Nrf2 mRNA levels significantly increased after RLXH2 treatment (*; P<0.05 both for 12 hours compared to 0 hour and for 24 hours compared to 12 hours). The results are the average of an independent experiment.

Impact of nuclear factor erythroid 2-related factor 2 silencing on relaxin 2 treatment

Figure 4A shows western blot of nuclear (N) and cytosolic (C) protein fractions. Nuclear fraction did not detect any GAPDH band; however a prominent protein band of Histone 4 was detected. As shown in Figure 4B (top panel), Nrf2 antibody detected a protein band in the control, while the Nrf2 protein was appreciably down-regulated in the siRNA transfected cells. We also assessed nuclear factor erythroid 2-related factor 2 (Nrf2) silencing on relaxin 2 (RLXH2) induced antioxidant enzymes in these NCI-N87 cells (Table 2). The results indicated that Nrf2 silencing partially blocked the RLXH2 induced antioxidant enzymes.

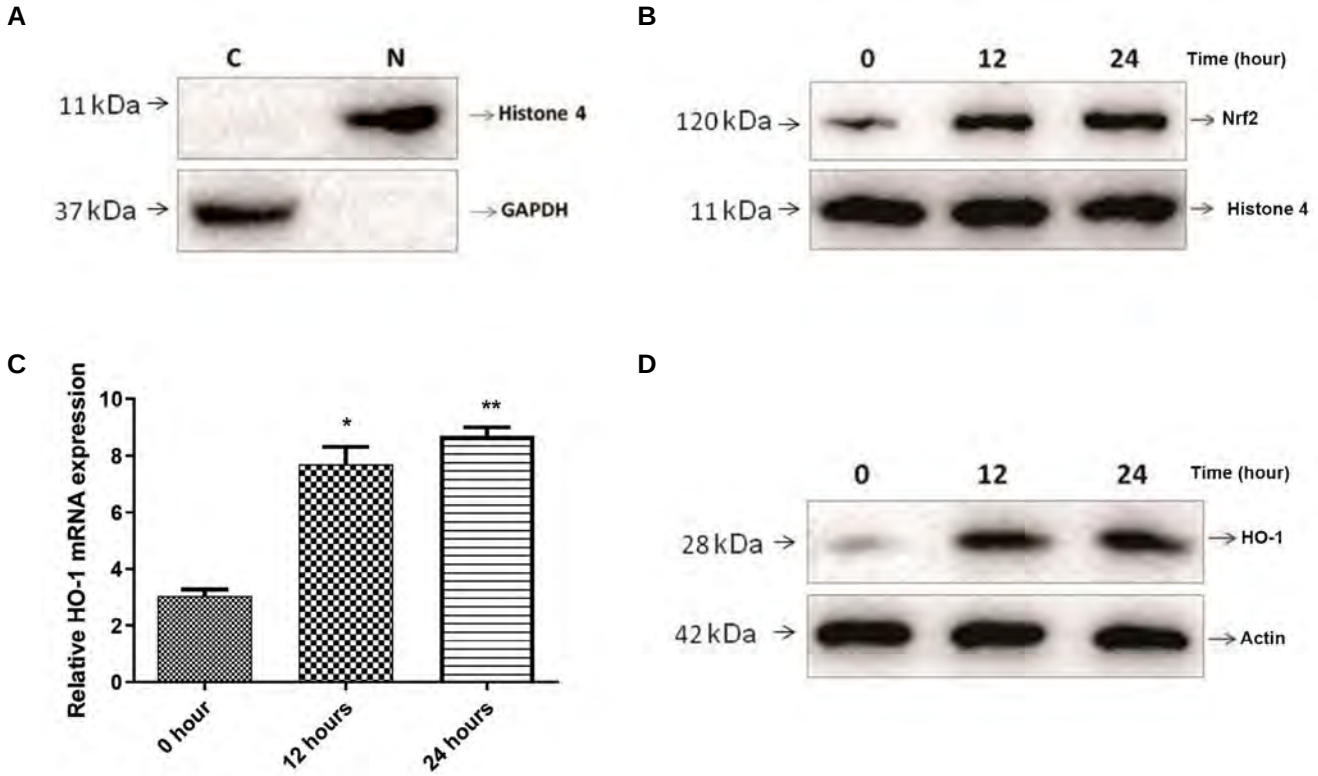

Fig.3: Nuclear factor erythroid 2-related factor 2 (Nrf2) translocation to the nucleus. **A.** Western blot assessment of nuclear (N) and cytosolic (C) protein fractions. The nuclear fraction did not detect any GAPDH band; however, there was a prominent protein band for histone 4. **B.** Western blot assessment of relaxin 2 (RLXH2) activated nuclear fraction. The untreated nuclear fraction did not show any band with the Nrf2 antibody; however, there was a protein band for Nrf2 in the RLXH2-activated nuclear fraction at 12 and 24 hours. **C.** There is increased expression of HO-1 mRNA in the RLXH2-activated NCI-N87 cells (12 hours and 24 hours) with P<0.05 at 12 hours compared to 0 hours, and P<0.01 at 24 hours compared to 12 hours). **D.** There is a significant increase in HO-1 expression level in the RLXH2-activated NCI-N87 cells (12 hours and 24 hours). The results are the average of an independent experiment. *; P<0.05 and **; P<0.01.

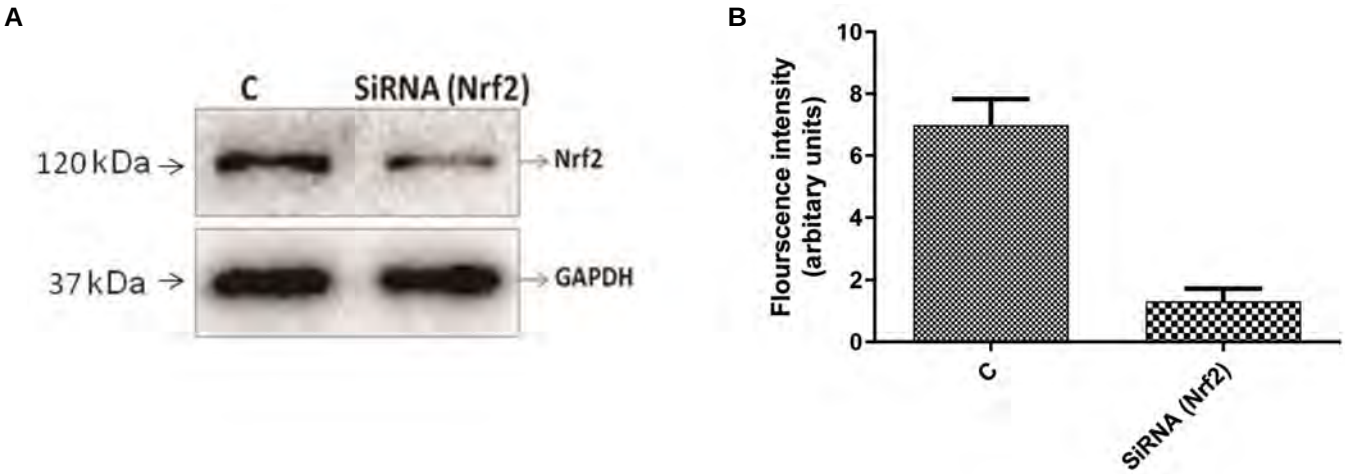

Fig.4: siRNA mediated down-regulation of nuclear factor erythroid 2-related factor 2 (Nrf2) in NCI-N87 cells. **A.** The cells were transfected with Nrf2-specific siRNA or with control siRNA (C). **B.** Immunoblotting was used to confirm down-regulation of Nrf2 with GAPDH as the control. The results are the average of an independent experiment.

Table 2: Impact of nuclear factor erythroid 2-related factor 2 silencing on relaxin 2 induced antioxidant enzymes in NCI-N87 cells

Antioxidant enzymes*	Control	Hypoxia	Hypoxia+RLXH2	Hypoxia+RLXH2+Nrf2-siRNA
SOD	78 ± 3.1	42 ± 2.3	51 ± 2.9	46 ± 1.9
CAT	55 ± 1.9	21 ± 1.6	32 ± 2.6	25 ± 2.1
GPX	30 ± 2.8	15 ± 1.3	24 ± 1.7	19 ± 2.0

SOD; Superoxide dismutase, GPX; Glutathione peroxidase, CAT; Catalase, *; Results are reported as U/mg protein.

Impact of relaxin 2 on hypoxia-associated cell apoptosis

We examined the impact of Nrf2 translocation cell death. NCI-N87 cells were cultured and incubated with agents that either inhibited or increased Nrf2 nuclear translocation. Figure 5A shows that the hypoxic condition significantly resulted in cell death. However, treatment of cells with RLXH2 (H+R) significantly reduced hypoxic-associated cell death compared to the hypoxia (H) group. In order to further prove the protective role of RLXH2 in NCI-N87 cells, we treated some of the cells with an Nrf2 inhibitor and others with tBHQ, an Nrf2 enhancer. Figure 5A shows that the Nrf2 inhibitor (trigonelline) eliminated RLXH2 associated cell protection, whereas treatment with the Nrf2 activator (tBHQ) increased cellular protection against hypoxia-associated cell death compared to RLXH2 treatment only.

HO-1 increased in the presence of RLXH2 in the NCI-N87 cells. Therefore, we sought to examine the role of HO-1 activation on hypoxia-associated cell death. The cells were cultured overnight and the next day, they were treated as RLXH2 only or RLXH2 with ZnPPIX. There was acute cell death in the NCI-N87 cells of the hypoxia group (H, Fig.5B). Treatment with RLXH2 (H+R) significantly reduced hypoxia-associated cell death. Inhibition of HO-1 expression significantly eliminated RLXH2 mediated cell protection.

A

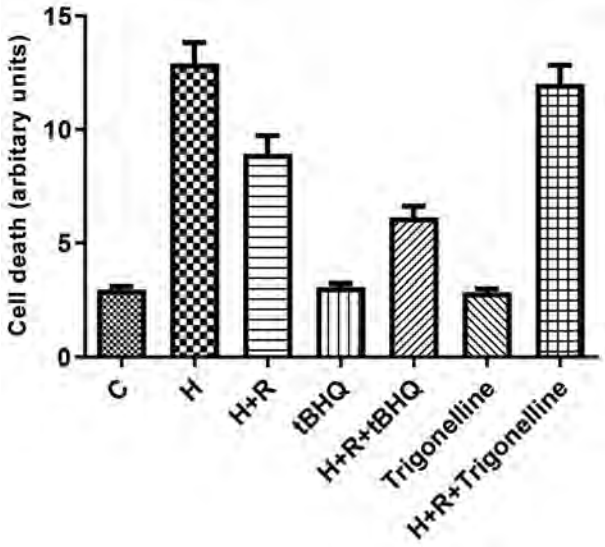

B

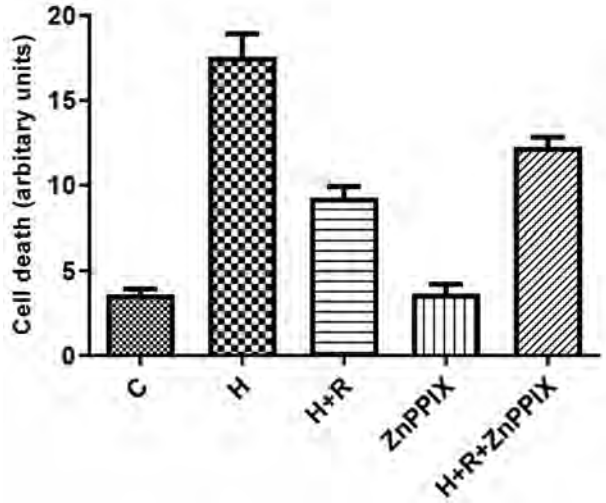

Fig.5: Hypoxia-associated cell apoptosis and role of nuclear factor erythroid 2-related factor 2 (Nrf2). **A.** Treatment with relaxin 2 (RLXH2) significantly reduces cell apoptosis. The protection offered by RLXH2 is eliminated when Nrf2 is inhibited and increases during activation of Nrf2. **B.** RLXH2 mediated cell protection and HO-1 inhibition. NCI-N87 cells cultured overnight are treated with RLXH2 only or RLXH2 with ZnPPIX. Treatment with ZnPPIX eliminates RLXH2 mediated cell protection. The results are the average of an independent experiment. C; Control group, H; Hypoxia group, and H+R; Hypoxia with RLXH2 treatment group.

Discussion

Hypoxia is common in different types of cancers and it causes activation of hypoxia-associated pathways in these cancer cells. Hypoxia within cells often results in oxidative stress, which can result in cellular damage and death. It has been reported that relaxin protect cells against hypoxia-associated cellular damage and death in different types of cancer cells (6, 23). Relaxin-associated cancer growth and invasion is a well-known phenomenon in thyroid, prostate, breast and other cancer models (24-26). In most, over-expression of relaxin has been observed, and this activates different protective signalling pathways (27-29). The role of relaxin in cancers is not fully understood but has recently emerged as a therapeutic target to counter the pro-cancer effects of enhanced relaxin levels (3). It has been reported in prostate cancer cells that down-regulation of relaxin decreases tumour formation in nude mice. LDH release by the cultured cells is a marker of cell death (11). Waza et al. (19) have reported

that RLXH2 successfully suppressed LDH release from cells with hypoxia. Here, we observed that treatment of RLXH2 prevented LDH release from hypoxia challenged gastric cancer cells.

Normally, cells remain safe from oxidative damage by the presence of various antioxidant enzymes along with GST, GSH, vitamin C, GPX, CAT, and SOD, among others (30). A proper balance of ROS is important for cells to function normally; however, the imbalance in ROS formation results in oxidative stress (31). Excessive production of ROS is linked with cellular damage, which is mainly due to enzyme inactivation, lipid peroxidation, and changes in nucleic acids (32). Hypoxia can cause excessive ROS production within cells (33) and oxidative damage to the cells, which eventually induces apoptosis or necrosis (34). Waza et al. (19) have reported that RLXH2 successfully suppressed hypoxia-associated ROS production and apoptosis. In the current study, treatment of NCI-N87 cells with RLXH2 (15 nmol/L) activated different antioxidant enzymes, and thereby decreased hypoxia-associated ROS formation in the NCI-N87 cells.

Nrf2 regulates the expression of different antioxidant enzymes (HO-1, GST, COX-2) (35, 36). It is a major defensive protein to combat oxidative stress in cancer cells (37). Nrf2 knockout cells are more prone to H_2O_2 induced cellular injury (38) and its over-expression within cells protects against injury from oxidative stress (14). Waza et al. (19) have reported that RLXH2 successfully activated the Nrf2/HO-1 signalling pathway. Since relaxin offered cellular protection against oxidative damage, we designed the current experiment to investigate the impact of RLXH2 on the Nrf2/HO-1 pathway (a major cellular defence against oxidative stress). We observed increased Nrf2 expression after RLXH2 treatment in the gastric cancer cells. Treatment with RLXH2 treatment enhanced nuclear translocation of Nrf2 in gastric cancer cells, and subsequently increased HO-1 levels. Furthermore, we observed that RLXH2 significantly eliminated hypoxia-induced apoptosis in these gastric cancer cells. The translocation of Nrf2 has been observed to undergo enhancement and inhibition upon exposure to tBHQ and trigonelline, respectively (39, 40). We found that incubation with tBHQ increased RLXH2 cell protection, while trigonelline abrogated this protection.

Conclusion

RLXH2 appears to be a promising therapeutic candidate for gastric cancer treatment because it offers protection against hypoxia-induced oxidative damage and cell death. Activation of the Nrf2/HO-1 pathway by RLXH2 provides a potential avenue for the development of targeted therapies that can enhance cellular antioxidant defences and counteract the detrimental effects of hypoxia. Further research and clinical investigations are necessary to fully exploit the therapeutic potential of RLXH2 and bring it closer to clinical application, and ultimately benefit patients with gastric cancer and other hypoxia-related disorders.

Acknowledgements

There is no financial support and conflict of interest in this study.

Authors' Contributions

L.W.; Conception, design of the manuscript, and experimental work. Y.Z.; Data acquisition or data analysis and interpretation. H.L.; Experimental work and drafting of the manuscript. K.H.; Final approval of the manuscript and repeatation of experimental work. All authors read and approved the final manuscript.

References

1. Sherwood OD. Relaxin's physiological roles and other diverse actions. Endocr Rev. 2004; 25(2): 205-234.
2. Wei X, Yang Y, Jiang YJ, Lei JM, Guo JW, Xiao H. Relaxin ameliorates high glucose-induced cardiomyocyte hypertrophy and apoptosis via the Notch1 pathway. Exp Ther Med. 2018; 15(1): 691-698.
3. Thanasupawat T, Glogowska A, Nivedita-Krishnan S, Wilson B, Klonisch T, Hombach-Klonisch S. Emerging roles for the relaxin/RXFP1 system in cancer therapy. Mol Cell Endocrinol. 2019; 487: 85-93.
4. Bani D, Pini A, Yue SK. Relaxin, insulin and diabetes: an intriguing connection. Curr Diabetes Rev. 2012; 8(5): 329-335.
5. Bruell S, Sethi A, Smith N, Scott DJ, Hossain MA, Wu QP, et al. Distinct activation modes of the relaxin family peptide receptor 2 in response to insulin-like peptide 3 and relaxin. Sci Rep. 2017; 7(1): 3294.
6. Radestock Y, Hoang-Vu C, Hombach-Klonisch S. Relaxin reduces xenograft tumour growth of human MDA-MB-231 breast cancer cells. Breast Cancer Res. 2008; 10(4): R71.
7. Harris AL. Hypoxia--a key regulatory factor in tumour growth. Nat Rev Cancer. 2002; 2(1): 38-47.
8. Pouysségur J, Dayan F, Mazure NM. Hypoxia signalling in cancer and approaches to enforce tumour regression. Nature. 2006; 441(7092): 437-443.
9. Nordgren IK, Tavassoli A. Targeting tumour angiogenesis with small molecule inhibitors of hypoxia inducible factor. Chem Soc Rev. 2011; 40(8): 4307-4317.
10. Tarnawski A, Pai R, Deng X, Ahluwalia A, Khomenko T, Tanigawa T, et al. Aging gastropathy-novel mechanisms: hypoxia, up-regulation of multifunctional phosphatase PTEN, and proapoptotic factors. Gastroenterology. 2007; 133(6): 1938-1947.
11. Jing L, Li Q, He L, Sun W, Jia Z, Ma H. Protective effect of tempol against hypoxia-induced oxidative stress and apoptosis in H9c2 cells. Med Sci Monit Basic Res. 2017; 23: 159-165.
12. Hensley K, Robinson KA, Gabbita SP, Salsman S, Floyd RA. Reactive oxygen species, cell signaling, and cell injury. Free Radic Biol Med. 2000; 28(10): 1456-1462.
13. Granger DN, Kvietys PR. Reperfusion injury and reactive oxygen species: the evolution of a concept. Redox Biol. 2015; 6: 524-551.
14. Ma Q. Role of nrf2 in oxidative stress and toxicity. Annu Rev Pharmacol Toxicol. 2013; 53: 401-426.
15. Jung BJ, Yoo HS, Shin S, Park YJ, Jeon SM. Dysregulation of NRF2 in cancer: from molecular mechanisms to therapeutic opportunities. Biomol Ther (Seoul). 2018; 26(1): 57-68.
16. Pouremamali F, Pouremamali A, Dadashpour M, Soozangar N, Jeddi F. An update of Nrf2 activators and inhibitors in cancer prevention/promotion. Cell Commun Signal. 2022; 20(1): 100.
17. Kitamura H, Motohashi H. NRF2 addiction in cancer cells. Cancer Sci. 2018; 109(4): 900-911.
18. Zhang M, An C, Gao Y, Leak RK, Chen J, Zhang F. Emerging roles of Nrf2 and phase II antioxidant enzymes in neuroprotection. Prog Neurobiol. 2013; 100: 30-47.
19. Waza AA, Hamid Z, Bhat SA, Shah NUD, Bhat M, Ganai B. Relaxin protects cardiomyocytes against hypoxia-induced damage in in-vitro conditions: Involvement of Nrf2/HO-1 signaling pathway. Life Sci. 2018; 213: 25-31.
20. Waza AA, Andrabi K, Hussain MU. Protein kinase C (PKC) mediated interaction between conexin43 (Cx43) and K(+)(ATP) channel subunit (Kir6.1) in cardiomyocyte mitochondria: Implications in cytoprotection against hypoxia induced cell apoptosis. Cell Signal.

2014; 26(9): 1909-1917.
21. Ahmad Waza A, Andrabi K, Ul Hussain M. Adenosine-triphosphate-sensitive K+ channel (Kir6.1): a novel phosphospecific interaction partner of connexin 43 (Cx43). Exp Cell Res. 2012; 318(20): 2559-2566.
22. Waza AA, Hamid Z, Ali S, Bhat SA, Bhat MA. A review on heme oxygenase-1 induction: is it a necessary evil. Inflamm Res. 2018; 67(7): 579-588.
23. Chen TY, Li X, Hung CH, Bahudhanapati H, Tan J, Kass DJ, et al. The relaxin family peptide receptor 1 (RXFP1): An emerging player in human health and disease. Mol Genet Genomic Med. 2020; 8(4): e1194.
24. Vinall RL, Mahaffey CM, Davis RR, Luo Z, Gandour-Edwards R, Ghosh PM, et al. Dual blockade of PKA and NF-κB inhibits H2 relaxin-mediated castrate-resistant growth of prostate cancer sublines and induces apoptosis. Horm Cancer. 2011; 2(4): 224-238.
25. Hombach-Klonisch S, Bialek J, Trojanowicz B, Weber E, Holzhausen HJ, Silvertown JD, et al. Relaxin enhances the oncogenic potential of human thyroid carcinoma cells. Am J Pathol. 2006; 169(2): 617-632.
26. Cao WH, Liu HM, Liu X, Li JG, Liang J, Liu M, et al. Relaxin enhances in-vitro invasiveness of breast cancer cell lines by upregulation of S100A4/MMPs signaling. Eur Rev Med Pharmacol Sci. 2013; 17(5): 609-617.
27. Hombach-Klonisch S, Buchmann J, Sarun S, Fischer B, Klonisch T. Relaxin-like factor (RLF) is differentially expressed in the normal and neoplastic human mammary gland. Cancer. 2000; 89(11): 2161-2168.
28. Bigazzi M, Brandi ML, Bani G, Sacchi TB. Relaxin influences the growth of MCF-7 breast cancer cells. Mitogenic and antimitogenic action depends on peptide concentration. Cancer. 1992; 70(3): 639-643.
29. Tashima LS, Mazoujian G, Bryant-Greenwood GD. Human relaxins in normal, benign and neoplastic breast tissue. J Mol Endocrinol. 1994; 12(3): 351-364.
30. Bhattacharyya A, Chattopadhyay R, Mitra S, Crowe SE. Oxidative stress: an essential factor in the pathogenesis of gastrointestinal mucosal diseases. Physiol Rev. 2014; 94(2): 329-354.
31. Nita M, Grzybowski A. The role of the reactive oxygen species and oxidative stress in the pathomechanism of the age-related ocular diseases and other pathologies of the anterior and posterior eye segments in adults. Oxid Med Cell Longev. 2016; 2016: 3164734.
32. Ray PD, Huang BW, Tsuji Y. Reactive oxygen species (ROS) homeostasis and redox regulation in cellular signaling. Cell Signal. 2012; 24(5): 981-990.
33. Görlach A, Dimova EY, Petry A, Martínez-Ruiz A, Hernansanz-Agustín P, Rolo AP, et al. Reactive oxygen species, nutrition, hypoxia and diseases: Problems solved? Redox Biol. 2015; 6: 372-385.
34. Balderas-Villalobos J, Molina-Muñoz T, Mailloux-Salinas P, Bravo G, Carvajal K, Gómez-Viquez NL. Oxidative stress in cardiomyocytes contributes to decreased SERCA2a activity in rats with metabolic syndrome. Am J Physiol Heart Circ Physiol. 2013; 305(9): H1344-H1353.
35. Kim JH, Xu EY, Sacks DB, Lee J, Shu L, Xia B, et al. Identification and functional studies of a new Nrf2 partner IQGAP1: a critical role in the stability and transactivation of Nrf2. Antioxid Redox Signal. 2013; 19(2): 89-101.
36. Waza AA, Hamid Z, Ali S, Bhat SA, Bhat MA. A review on heme oxygenase-1 induction: is it a necessary evil. Inflamm Res. 2018; 67(7): 579-588.
37. Vomund S, Schäfer A, Parnham MJ, Brüne B, von Knethen A. Nrf2, the Master regulator of anti-oxidative responses. Int J Mol Sci. 2017; 18(12): 2772.
38. Zhu H, Itoh K, Yamamoto M, Zweier JL, Li Y. Role of Nrf2 signaling in regulation of antioxidants and phase 2 enzymes in cardiac fibroblasts: protection against reactive oxygen and nitrogen species-induced cell injury. FEBS Lett. 2005; 579(14): 3029-3036.
39. Zagorski JW, Turley AE, Dover HE, VanDenBerg KR, Compton JR, Rockwell CE. The Nrf2 activator, tBHQ, differentially affects early events following stimulation of Jurkat cells. Toxicol Sci. 2013; 136(1): 63-71.
40. Arlt A, Sebens S, Krebs S, Geismann C, Grossmann M, Kruse ML, et al. Inhibition of the Nrf2 transcription factor by the alkaloid trigonelline renders pancreatic cancer cells more susceptible to apoptosis through decreased proteasomal gene expression and proteasome activity. Oncogene. 2013; 32(40): 4825-4835.

Cell J
Cell Journal (Yakhteh)
Homepage: https://www.celljournal.org/
Original Article
Vol 25, No 9, September 2023, Pages: 633-644

Reversing T Cell Exhaustion by Converting Membrane PD-1 to Its Soluble form in Jurkat Cells; Applying The CRISPR/Cas9 Exon Skipping Strategy

Zeinab Yousefi-Najafabadi, Ph.D.[1, 2], Zohreh Mehmandoostli, Ph.D.[2], Yazdan Asgari, Ph.D.[1], Saeed Kaboli, Ph.D.[3], Reza Falak, Ph.D.[4], Gholam Ali Kardar, Ph.D.[1, 2*]

1. Department of Medical Biotechnology, School of Advanced Technologies in Medicine, Tehran University of Medical Sciences, Tehran, Iran
2. Immunology, Asthma and Allergy Research Institute (IAARI), Tehran University of Medical Sciences, Tehran, Iran
3. Department of Medical Biotechnology, School of Medicine, Zanjan University of Medical Sciences, Zanjan, Iran
4. Department of Immunology, School of Medicine, Iran University of Medical Sciences, Tehran, Iran

Abstract

Objective: T-cells express two functional forms of the programmed cell death protein 1 (PD-1): membrane (mPD-1) and soluble (sPD-1). The binding of mPD-1 and its ligand (PD-L1) on tumor cells could lead activated lymphocytes toward exhaustion. Selective deletion of the transmembrane domain via alternative splicing of exon-3 in PD-1 mRNA could generate sPD-1. Overexpression of sPD-1 could disrupt the mPD-1/PD-L1 interaction in tumor-specific T cells. We investigated the effect of secreted sPD-1 from pooled engineered and non-engineered T cell supernatant on survival and proliferation of lymphocytes in the tumor microenvironment (TME).

Materials and Methods: In this experimental study, we designed two sgRNA sequences upstream and downstream of exon-3 in the *PDCD1* gene. The lentiCRISPRv2 puro vector was used to clone the dual sgRNAs and produce lentiviral particles to transduce Jurkat T cells. Analysis assays were used to clarify the change in PD-1 expression pattern in the pooled (engineered and non-engineered) Jurkat cells. Co-culture conditions were established with PD-L1+ cancer cells and lymphocytes.

Results: CRISPR/Cas9 could delete exon-3 of the *PDCD1* gene in the engineered cells based on the tracking of indels by decomposition (TIDE) and interference of CRISPR edit (ICE) sequencing analysis reports. Our results showed a 12% reduction in mPD-1 positive cell population after CRISPR manipulation and increment in sPD-1 concentration in the supernatant. The increased sPD-1 confirmed its positive effect on proliferation of lymphocytes co-cultured with PD-L1+ cancer cells. The survival percent of lymphocytes co-cultured with the pooled cells supernatant was 12.5% more than the control.

Conclusion: The CRISPR/Cas9 exon skipping approach could be used in adoptive cell immunotherapies to change PD-1 expression patterns and overcome exhaustion.

Keywords: CRISPR-Cas Systems, Exhaustion, Exons, PD-1-PD-L1 Blockade, Programmed Cell Death 1 Receptor

Citation: Yousefi-Najafabadi Z, Mehmandoostli Z, Asgari Y, Kaboli S, Falak R, Kardar GA. Reversing T cell exhaustion by converting membrane PD-1 to its soluble form in jurkat cells; applying the CRISPR/Cas9 exon skipping strategy. Cell J. 2023; 25(9): 633-644. doi: 10.22074/CELLJ.2023.1999548.1269

Introduction

The physiological condition of the tumor microenvironment (TME) could lead the tumor-specific T lymphocytes, $CD8^+$ and $CD4^+$, towards exhaustion. The most significant T lymphocyte exhaustion hallmarks, depending on their progenitor or terminal status, are the expression of one or more inhibitory markers such as programmed cell death protein 1 (PD-1), cytotoxic T-lymphocyte-associated protein 4 (CTLA4); T-cell immunoglobulin and mucin-domain containing-3 (TIM3); lymphocyte-activation gene 3 (LAG3); B- and T-lymphocyte attenuator (BTLA); T cell immunoreceptor with Ig and immunoreceptor tyrosine-based inhibitory motif (ITIM) domains (TIGIT); 2B4; and SLAM family member 6 (SLAMF6) (1-3). Exhaustion could be a transient state in T lymphocytes, and blocking the inhibitory markers or their ligands could distort the inhibitory signalling pathways and reverse this condition (4, 5). The PD-1 protein is the first inhibitory coreceptor expressed on the surface of effector T cells in the TME (6). Therefore, immunotherapy methods that include anti-PD-1/anti-PD-L1 monoclonal antibodies (7), siRNA-mediated down-regulation of PD-1 expression (8), and programmed cell death 1 (*PDCD1*) gene knock-out

Received: 05/April/2023, Revised: 28/May/2023, Accepted: 17/June/2023
*Corresponding Address: P.O.Box: 14177-55469, Department of Medical Biotechnology, School of Advanced Technologies in Medicine, Tehran University of Medical Sciences, Tehran, Iran
Email: gakardar@tums.ac.ir

Royan Institute
Cell Journal (Yakhteh)

methods by zinc finger nucleases (ZFNs) (9); clustered regularly interspaced short palindromic repeats and CRISPR-associated protein 9 (CRISPR/Cas9) (10-12) are developed to disrupt the PD-1/PD-L1 axis. These methods could be used with traditional cancer treatments and adoptive cell transfer (ACT) therapies to improve their functions as combinational therapies (13).

Recent studies demonstrated that in addition to the full-length membrane PD-1 isoform (mPD-1), the PD-1 mRNA transcript has four alternative splice variants. In mPD-1, exon-2 is responsible for the extracellular IgV-like domain expression, which is crucial for PD-1/PD-L1 binding. Exon-3 is in charge of transmembrane domain expression. The full-length PD-1 also retains an intracellular domain with an ITIM and an immunoreceptor tyrosine-based switch motif (ITSM) as signalling motifs, by exons 4 and 5. Transformation of PD-1 from the mPD-1 form to the soluble form (sPD-1) is the result of exon-3 deletion due to alternative splicing of the PD-1 mRNA transcript (14). The sPD-1 transcript has prognostic, diagnostic, and therapeutic values and is regarded as a biomarker in human cancers (15). Notably, sPD-1 can block the mPD-1/PD-L1 interaction and decrease immunosuppressive signalling in exhausted T cells (16). In cancer therapy methods, overexpression of sPD-1 as an adjuvant along with cancer vaccines (17) and secretion of sPD-1 from oncolytic virus-infected cells in TME (18) could enhance the proliferation and immunological cytotoxicity of T cells against PD-L1$^+$ tumor cells.

In recent years, CRISPR/Cas9 technology is the most practical advancement in biotechnology to manipulate the genome with high accuracy. CRISPR/Cas9 systems have been applied in several studies for genetic editing of lymphocytes. A disruption in the *PDCD1* gene sequence through the non-homologous end joining (NHEJ) approach of CRISPR/Cas9 to knock-out PD-1 expression is a new therapeutic strategy that has been used in chimeric antigen receptor (CAR)-T cell therapy and tumor infiltrated lymphocytes (TILs) therapy. The intention of this strategy is to promote an immune system response and eliminate tumor cells (10, 11, 19). Some of these developed CRISPR-engineered T cells are in clinical trial phase 1 studies (20).

Based on recent studies using sPD-1 to improve the functionality of the T cells, besides the positive effect of blocking mPD-1 expression by the CRISPR/Cas9 system, we hypothesize that deletion of exon-3 (transmembrane domain) from the *PDCD1* gene of the T cells could interrupt full-length mPD-1 expression and increase sPD-1 production to overcome exhaustion. The exon-2 sequence was considered a target location for manipulating the *PDCD1* gene to block all transcripts of the PD-1 protein in recent studies. We intend to keep both exon-1 and exon-2 intact to have an IgV-like domain and skip exon-3 of PD-1 mRNA to delete the transmembrane domain in this protein sequence.

We used the CRISPR/Cas9 system in this study because of the promising results of this system for targeted exon skipping. The CRISPR/Cas9 studies show two approaches for exon skipping. The first approach is to design sgRNAs for the splicing sites to create random insertion and deletion (indel) mutations at the specified intron-exon edge and remove the exon at the splicing level through selective alternative splicing. The second approach is to design two sgRNAs for the upstream and downstream regions of the specified exon, which could ultimately lead to the deletion of the exon at the genome level (21-23). Here, we designed two sgRNAs for the upstream and downstream sequences of exon-3 in the *PDCD1* gene. At least one sgRNA targeted the splicing site to change the structure of the expressed protein from the membrane to the soluble form by skipping the target exon and remove the transmembrane domain of PD-1. Finally, we investigated the effect of secreted sPD-1 from pooled engineered and non-engineered T cell supernatant on survival and proliferation of lymphocytes in the TME.

Materials and Methods

Soluble PD-1 protein in the in-silico laboratory

In this experimental study, bioinformatic tools were used to compare the mPD-1 and sPD-1 protein structures and their locations in the cells. The location of the PD-1 protein before and after exon-3 deletion in CELLO v.2.5 and LocTree v.3, the protein subcellular localization prediction web servers, were compared (Tables S1-S4, See Supplementary Online Information at www.celljournal.org). Prediction of membrane helices and a plot of the protein sequence with TMHMM Server v.2.0 confirmed the removal of transmembrane helices in exon-3 deleted PD-1 protein (Figs.S1, S2, See Supplementary Online Information at www.celljournal.org). CD-search online software from the NCBI database was used to predict the conserved domains in the mPD-1 and sPD-1 proteins. IgV-PD1, a functional domain from the Ig superfamily, was detected in both natural (mPD-1) and exon-3 deleted PD-1 (sPd-1) proteins, and this indicated the functionality of these proteins (Figs.S3, S4, See Supplementary Online Information at www.celljournal.org).

Prediction of splicing sites, sgRNA design, and dual cloning

Prediction of splicing regions in intron 2-3/exon-3 edge and exon-3/ intron 3-4 edge was done through NetGene2 Server v.2.42 based on a neural network prediction algorithm to determine target regions to design the sgRNAs (Table S5, See Supplementary Online Information at www.celljournal.org).

CHOPCHOP v.3.0.0 (chopchop.cbu.uib.no) (24) and CRISPOR v.5.01 (crispor.tefor.net) (25) tools were used to design the sgRNAs. The closest protospacer adjacent motif (PAM) to the splicing regions in the upstream and downstream introns (intron 2-3 and intron 3-4) of exon-3 were defined. The best sgRNA sequences with the highest specificity and efficiency scores and low off-targets were

candidate. The final selected sgRNA sequences for this study were 5′CTGGAAGGGCACAAAGGTCA3′ (right sgRNA) and 5′TTAGTCCAGGGGCCTTCATC3′ (left sgRNA). Tables S6-S8 (See Supplementary Online Information at www.celljournal.org) provides information about the sgRNAs.

We intended to transfer the CRISPR/Cas9 structure to lymphocytes. Therefore, we selected a lentiviral vector to improve the transduction result. Sense and antisense sequences of sgRNAs with the BsmBI restriction enzyme (RE) sites for cloning into the lentiCRISPRv2 puro vector (Addgene; #98290) were synthesised by Metabion AG, Germany. Each sgRNA was separately cloned into the lentiCRISPRv2 puro vector construct by digestion with BsmBI Fast Digest enzyme (Esp3I RE, Thermo Scientific™, USA, cat no: FD0454) and ligation with a T4 ligase enzyme (Thermo Scientific™, USA, cat no: EL0014). In order to produce the dual sgRNAs/lentiCRISPRv2 puro vector, we first performed PCR using forward and reverse primers (5′TTTCTAGAGAGGGCCTATTTCCCA3′ and 5′TTTCAAGACCTAGCTAGCGAATTC3′), which included cutting regions for XbaI and NheI enzymes, respectively, to target the beginning and end of the right sgRNA construct and propagate the U6 promoter, right sgRNA, and its scaffold. Next, the PCR product was cleaned with an EZ-10 Spin Column PCR Product Purification Kit (Bio Basic, Inc., Canada, cat no:BS363), then double digested with NheI enzyme (Thermo Scientific™, USA, cat no: FD0684) and XbaI enzyme (Thermo Scientific™, USA, cat no: FD0974). Finally, the lentiCRISPRv2 puro vector that included left sgRNA was restricted with NheI enzyme and subcloned by ligation of the double-digested PCR product using T4 ligase enzyme. The final cloned dual sgRNAs/lentiCRISPRv2 puro vector sequence was confirmed by forward and reverse Sanger sequencing of the right and left sgRNA sequences.

Cell culture

The HEK293T cell line was cultured for transfection of the viral vectors to produce lentiviral particles with DMEM complete medium that included 10% FBS and 1X Pen/Strep (all from Gibco™, USA) in a 5% CO_2 incubator at 37°C and 95% humidity.

The Jurkat cell line ($CD4^+$ T cells) is a suitable cell line for immuno-oncology research. This cell line could be used as the exhausted T cells with PD-1 protein expression after activation. We used the Jurkat T cells for transduction of the lentiviral particles and manipulation of the *PDCD1* gene by the CRISPR/Cas9 system. The Jurkat cells were cultured in RPMI complete medium (Gibco™, USA) that included 10% FBS and 1X Pen/Strep at 37°C with 95% humidity in a 5% CO_2 incubator.

We used the MDA-MB-231 ($PD\text{-}L^+$) cell line for the co-culture tests in DMEM medium. All of the cell lines were purchased from the Cell Bank at Pasteur Institute of Iran.

Renal carcinoma cells (RCC) were extracted from a patient's renal tumor tissue after filtering through a cell strainer without digestion. The filtered cells were washed twice with PBS and cultured in RPMI medium with 15% FBS and 1X Pen/Strep in a 5% CO_2 incubator with 37°C and 95% humidity for 72 hours. The suspended cells were removed by washing with sterile PBS, and the adherent cells were cultured in fresh RPMI medium that included 10% FBS and 1X Pen/Strep for one week to enable the cells to reach 90% confluency. Ethical certification for the use of the patient's primary cells is provided in the Ethical Consideration section.

Lentiviral packaging, titration, transduction, and activation

We seeded 3.8×10^6 HEK-293T cells on a 10 cm plate (SPL, Korea) in DMEM complete medium. After 24 hours, the supernatant of the cells was completely removed and the medium was replaced by DMEM that included 2% FBS without antibiotics, and again incubated for 2 hours. We mixed 1:2:3 ratios of the lentiviral vectors in Opti-MEM media (Gibco™), which equalled 15 µg dual sgRNAs/lentiCRISPRv2 puro (Addgene #98290), 10 µg psPAX2 (Addgene #12260), and 5 µg pMD2G (Addgene #12259) vectors, respectively. Next, 1 mg/mL of branched polyethyleneimine (PEI) transfection reagent (Sigma-Aldrich, USA) was combined with the vector mixture in a 1:2 (PEI: vector) ratio in Opti-MEM media and incubated for 20 minutes at room temperature (RT). Finally, the transfection mix was transferred to the HEK-293T cells. After an 18-hour incubation, the media was replaced by DMEM complete medium. The supernatant that included the lentiviral particles was harvested at 72 hours post-transfection and centrifuged for 10 minutes at 2000×g to pellet any packaging cells; then, the supernatant was filtered through a 0.45 µm polyethersulfone (PES) filter (Jet Bio-Filtration Co., Ltd., China). Finally, the lentiviral particles were concentrated with polyethylene glycol (PEG) 6000 (Sigma-Aldrich, USA) and NaCl. The concentrated viral particles were aliquoted in PBS and stored at -80°C.

In order to indicate the viral particle titration, the viral RNA was extracted with a BehPrep Viral RNA Extraction Kit (BehGene Biotech Co., Iran). cDNA synthesis was done using a RT-ROSET Kit (ROJE Technologies Co., Iran). A pair of primers that targeted the LTR region of the lentiCRISPRv2 puro vector was designed to titrate the produced lentiviral particles by standard quantitative polymeras chai reaction (qPCR). The primer sequences were 5′TGTGTGCCCGTCTGTTGTGT3′ (forward) and 5′GAGTCCTGCGTCGAGAGAGC3′ (reverse).

A total of 5×10^5 Jurkat cells were seeded per well in a 24-well plate (SPL, Korea) and transduced with dual sgRNAs/CRISPR lentiviral particles at Multiplicity of infection (MOI) of ten diluted in RPMI medium with 5% FBS and 8 µg/mL polybrene (Sigma-Aldrich). The polybrene concentration for transduction was determined by the MTT assay results (data not shown). The transduction mixture was incubated for 20 minutes at RT, then the plate was centrifuged at 800 ×g for 90 minutes

at 32°C according to the spinoculation protocol (26). The media was replaced at 24 hours post-transduction, and the plate was incubated again. After 24 hours, 50 ng/mL PMA and 1 µg/mL PHA were added to the media to enable cell activation. At 96 hours post-transduction the Jurkat cell population of active transduced and non-transduced cells (engineered and non-engineered cells) were collected and called the pooled cell group. The positive control cell group consisted of 5×10^5 Jurkat cells seeded per well in a 24-well plate that was activated with PMA and PHA for 48 hours. Jurkat cells without transduction and activation were cultured as negative control cell group. The cells and their supernatants from the pooled and control groups were collected separately for subsequent analysis.

Analysis of extracted DNA

DNA from the pooled cells and negative control groups were extracted using a DNA Extraction Kit (Gene Transfer Pioneers Co., Iran). A forward primer targeting intron 2-3 upstream of exon-3 and reverse primer targeting intron 4-5 downstream of exon-3 with the primer sequences of 5′TCTGTCCTCTAGCTCTGGAAGC3′ and 5′AGAATGTGAGTCCTGCA3′, respectively, were used for PCR. The PCR was done with Taq DNA Polymerase 2x Master Mix, 1.5 mM $MgCl_2$ (Ampliqon, Denmark) by the standard program and at 58°C for annealing of the primers. The PCR products were sequenced by Pishgam Co., Iran. Sanger sequencing data from the PCR products of the pooled cells and control groups were analysed with Chromas Lite v.2.5 by focusing on nucleotide peaks in the sequencing chromatogram. Alignment was done between the pooled cells group and the control group sequencing data with CLC DNA Workbench v.6 in order to survey indel mutation in the targeting locations of the sgRNAs. In addition, tracking of indels by decomposition (TIDE) (https://tide.nki.nl) tool v.3.3.0 (27) and interference of CRISPR edits (ICE) (https://ice.synthego.com) tool v.3.0 from Synthego were used for Sanger sequencing data analysis. The purpose of decomposing and aligning based on the TIDE and ICE tools was a visualisation of the indel spectrums and estimation of the overall editing efficiency from the sequencing data of the pooled cells in the comparison control group.

Analysis of synthesised cDNA

RNA from the pooled cells group and the positive control group were extracted using a SanPrep Column MicroRNA Mini-Prep Kit (Bio Basic, Inc. Canada). cDNA synthesis was carried out with the RT-ROSET Kit (ROJE Technologies Co., Iran) protocol. The reverse PCR was designed to check the exon-3 deletion in the PD-1 mRNAs. The forward primer for targeting exon-2 was 5′CTTCCGTGTCACACAACTGC3′ and reverse primer for targeting exon-4 was 5′GAGGGGTCCTCCTTCAGG3′. The PCR was performed with Taq DNA Polymerase 2x Master Mix at 58°C to anneal the primers by a standard program. The size of the PCR product band on 3% gel agarose in the presence and absence of exon-3 must be 360 bp and 204 bp, respectively.

Real-time polymerase chain reaction PCR (RT-PCR) was used to investigate the PD-1 expression pattern in mRNA from the pooled cell group and compare them with the positive control group. The control primers 5′CTTAGACTCCCCAGACAGG3′ (forward) and 5′GATGTGTTGGAGAAGCTGC3′ (reverse) were used for targeting upstream exons located at the junction of exon 1-2 and exon 2, which were continually expressed in the mPD-1 and sPD-1 transcripts. Test primers [5′TGCTGCTAGTCTGGGTCCT3′ (forward) and 5′GAGGGGTCCTCCTTCAGG3′ (reverse)] were used to target exon-3 and the exon 4-5 junction, which were continually expressed in the mPD-1 transcript and had reduced expression in the sPD-1 transcript. The relative expression calculation from the RT-PCR results enabled us to determine the change in PD-1 expression pattern. RT-PCR was performed using with RealQ Plus Master Mix Green High ROX™ (Ampliqon, Denmark) at 58°C for annealing of the primers through a standard program.

Co-culture conditions

The PBMCs were separated from healthy donor blood by Ficol-Lymphodex (Innotrain, Germany) and labelled with 5 µM carboxyfluorescein succinimidyl ester (CFSE, Sigma-Aldrich) for 10 minutes at 37°C in PBS. Labelling was stopped by the addition of a 10-fold volume of PBS and the PBMCs were subsequently washed for three times in PBS. The labelled cells were placed in a 24-well plate in RPMI complete medium to incubate for 10 hours. The next day, the suspended cells were collected as CFSE-labelled lymphocytes for co-culture.

RCC and MDA-MB-231 cancer cells, as PD-L^+ cells, were seeded in 24-well plates to achieve 50% confluency. Then, the CFSE-labelled lymphocytes were added to each well for co-culture with the cancer cells. The effector to target cell ratio was determined as 10:1. A total of 150 µl of supernatant from the pooled cell group (collected from the transduction step) was added to the medium of the cells according to the panels in Table 1. After 72 hours, the suspended and adherent cells were collected for the proliferation and apoptosis assays by flow cytometry.

Flow cytometry assay

Flow cytometry was performed using the FITC anti-human CD279 (PD-1) antibody (Sina Biotech Co., Iran) for analysis of mPD-1 expression on the surfaces of the pooled cells, and the positive and negative controls.

The proliferation assay was done with APC anti-human CD3 antibody (OKT-3, Elabscience, USA) and CFSE label for positive gating of lymphocytes by flow cytometry.

The collected cells were prepared with an Annexin V-FITC/7-AAD Kit (Elabscience, USA) according to the manufacturer's protocol for the apoptosis assay. The flow cytometry results were analysed by FlowJo™ software v.10.

Table 1: Co-culture states for the intended assays

Co-culture panels	Co-culture conditions	Assay
Lymphocyte panel	Lymphocyte CFSE-label	Negative control for proliferation assay
	Lymphocyte CFSE-label culture with PHA and PMA	Positive control for proliferation assay
	Lymphocyte CFSE-label culture with supernatant of pooled cell group	Proliferation assay
RCC panel	Lymphocyte CFSE-label co-culture with RCC	Proliferation and apoptosis assays
	Lymphocyte CFSE-label co-culture with RCC and supernatant of pooled cell group	Proliferation and apoptosis assays
MDA-MB-231 cell line panel	Lymphocyte CFSE-label co-culture with MDA-MB-231 cell line	Apoptosis assay
	Lymphocyte CFSE-label co-culture with MDA-MB-231 and supernatant of pooled cell group	Apoptosis assay

RCC; Renal carcinoma cells and CFSE: Carboxyfluorescein succinimidyl ester.

Dot blot assay

A total of 4 µl of the cell supernatants were spotted on the PVDF strip for the dot blot assay. The detection procedure was done with biotinylated anti-human PD-1 antibody (Sina Biotech Co., Iran), streptavidin-POD (Sigma-Aldrich), and a DAB substrate (Roche, USA), respectively. Intensity of the brown spots were captured and quantified with ImageJ v.2 software.

Statistical analysis

Statistical analysis was performed using Prism 9 software (GraphPad Software, LLC, USA). $P<0.05$ indicated statistical significance.

Ethical consideration

The Vice Chancellor of Research Affairs, Tehran University of Medical Sciences, Tehran, Iran approved the acquisition of the primary cell culture in this study (IR.TUMS.VCR.REC.1397.524).

Results

Cloning, viral packaging, and dual sgRNAs/CRISPR lentiviral particles transduction

Figure 1A shows successful cloning of the sgRNAs into the lentiCRISPRv2 puro and sub-cloning of the right sgRNA construct (U6 promoter, sgRNA, and scaffold) into the lentiCRISPRv2 puro vector, including the left sgRNA. Both forward and reverse Sanger sequencing confirmed the accuracy of the dual sgRNAs/lentiCRISPRv2 puro vector sequence (results not shown).

We transfected the viral vectors (lentiCRISPRv2 puro, psPAX2, pMD2.G) into the HEK-293T cell line and the packaging processes were done. qPCR titration results showed that there were 22×10^6 RNA copy number/mL of collected dual sgRNAs/CRISPR lentiviral particles after concentration with PEG 6000. The lentiviral particles with MOI of 10 were transduced to the Jurkat cell line. We noted that 96 hours after viral transduction and PMA/PHA activation, the Jurkat cells formed clumps with less than 50% viability because of the activation procedure effect (Fig.1B). The experimental groups are also shown in Figure 1B.

Sanger sequencing data analysis confirmed indels in the pooled genome

Figure 2A1 shows the changes in nucleotide peaks of the DNA sequencing chromatogram of the pooled cells compared to control cells. There were noises near the double strand break (DSB) region of the left sgRNA targeting location in the *PDCD1* gene, which indicated indel in the specified location. The alignment results between the pooled and control group sequences near the DSB regions of the left sgRNA confirmed changes in several nucleotides (Fig.2A1). However, we did not detect any nucleotide changes in the chromatogram signal plot and alignment result in the right sgRNA (Fig.2A2).

Sanger sequencing data analysis in TIDE separately for each sgRNA estimated that the overall editing efficiency for the left and right sgRNAs were 87.2 and 84.9% with R^2 model fit of 0.87 and 0.85 in order. The TIDE tool results showed that 78% of the pooled cells had one nucleotide deletion in charge of the left sgRNA and 66% in the right sgRNA ($P<0.001$, Fig.2B1, B2). The ICE tool was used to simultaneously check the two sgRNA. ICE results showed 100% indel efficiency with 0.06 R^2 model fit. We noted that 99% of the indels occurred through the contribution of the left sgRNA; their indel sites were in the edge of the intron 2-3/exon-3 splicing region. One percent of the pooled cells were estimated that have large deletions, 311bp, which could be referred to as exon-3 deletion at the genome level with the simultaneous contribution of left and right sgRNAs (Fig.2C).

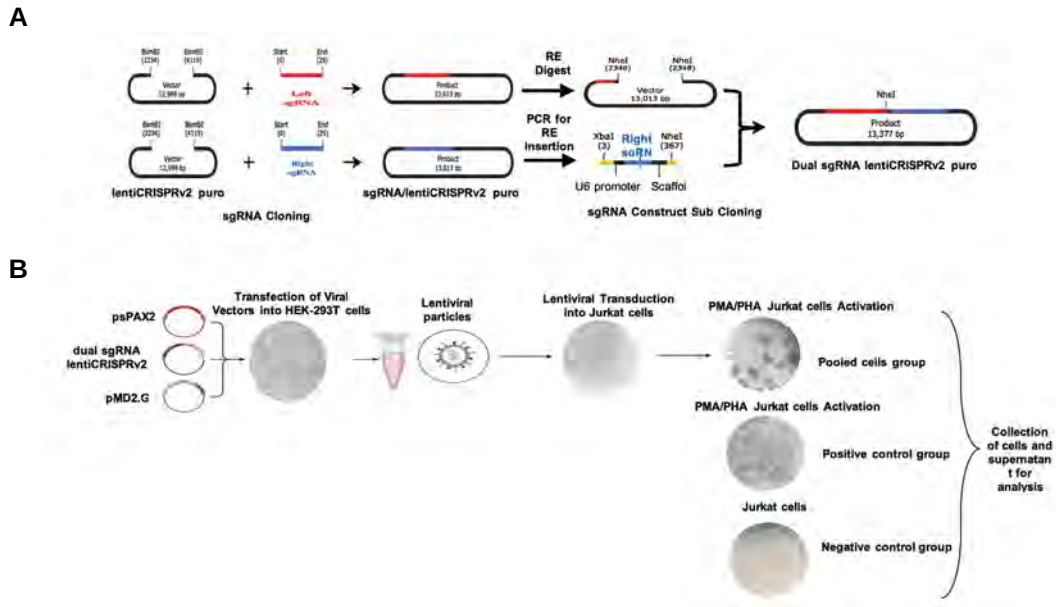

Fig.1: From cloning to lentiviral particle production processes are depicted. **A.** Cloning of the dual sgRNAs construct in the lentiCRISPRv2 puro vector. First, each sgRNA is cloned into the lentiCRISPRv2 puro vector, then the right sgRNA construct with a U6 promoter and its scaffold is cloned into the left sgRNA lentiCRISPRv2 puro vector with the XbaI/NheI RE sites. **B.** Production of the lentiviral particles and transduction pathway. Transfection of plasmids into HEK-293T for lentiviral packaging, transduction into the Jurkat cell line, and activation process for the pooled cell and control groups are shown.

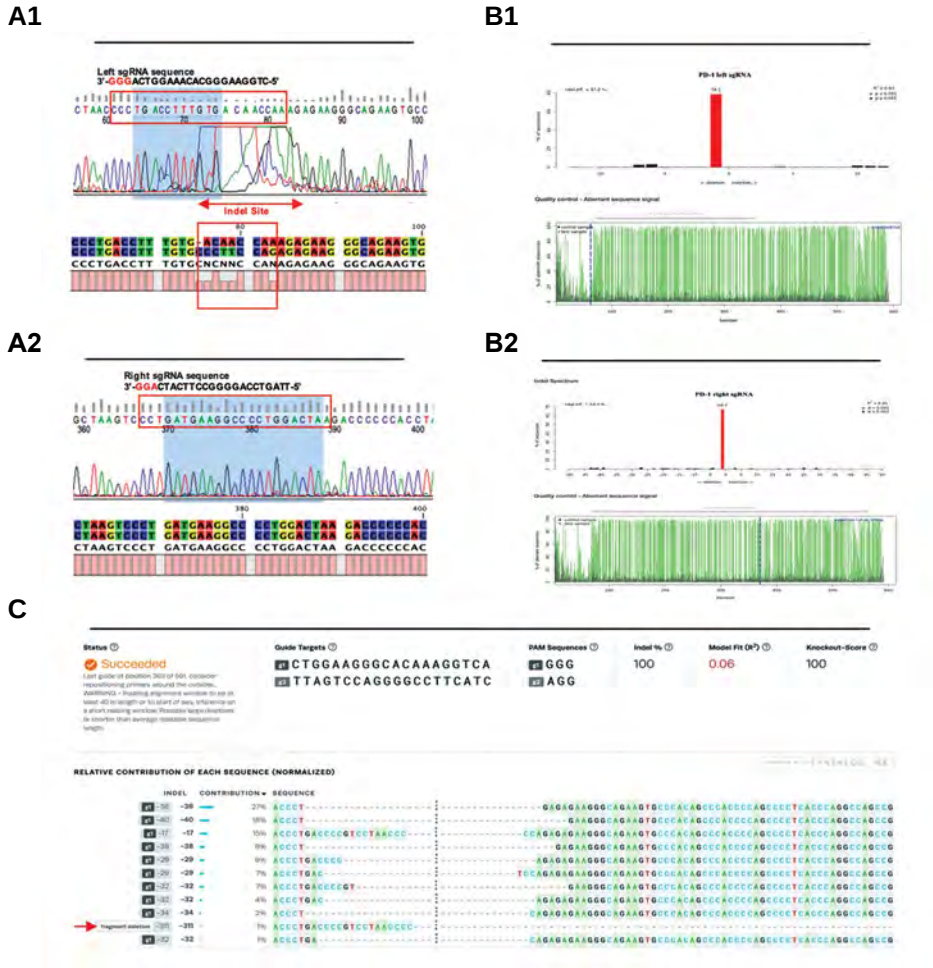

Fig.2: Sanger sequencing data analysis are reported the changes in target sequence. **A1.** Chromatogram plot of left sgRNA and alignment result determines the nucleotide changes in the target region. **A2.** The chromatogram plot and alignment result of the right sgRNA does not show any detectable signs. **B1, B2.** Tracking of indels by decomposition (TIDE) analysis plot of each sgRNA separately with total efficiency of 78.2% for the left and 84.9% for the right sgRNA. **C.** Simultaneous interference of CRISPR edits (ICE) analysis of dual sgRNAs with 100% efficiency. The arrow indicates a large fragment deletion in the pooled cells that could be referred to as an exon-3 deletion at the genome level.

Changes in expression pattern of the PD-1 transcripts in pooled mRNA

Reverse PCR was performed to confirm the exon-3 deletion at the mRNA level in the pooled cell group compared to the positive control group. Figure 3A1 shows the designed primers for reverse PCR, and the band sizes in the presence and absence of exon-3 are shown. The PCR product of the positive control group had only a 360 bp band on 3% agarose gel. The PCR product of the pooled group had 360 bp and 204 bp bands that referred to the mPD-1 and sPD-1 transcripts, respectively (Fig.3A2).

Two primer pairs were used for RT-PCR to investigate the change in PD-1 expression pattern. Figure 3B1 shows the control primer and test primer pairs, and their target sites. According to the results obtained from RT-PCR and their relative expression calculation, it was determined that the mPD-1 expression decreased by 50% in the pooled cells compared to the positive control group (Fig.3B2).

Reduction of membrane PD-1 expression versus increased soluble PD-1 in pooled cells using CRISPR/Cas9

Flow cytometry was performed using FITC anti-human PD-1 antibody to investigate the expression level of mPD-1 on the surfaces of the pooled cells and control groups. Only 5% of Jurkat cells expressed mPD-1 in the negative control group. However, 70.91% of the cells expressed mPD-1 after activation of Jurkat cells in the positive group. The pooled group, after transduction and activation of Jurkat cells, only 58.33% of the cells were mPD-1 positive. There was a 12.85% reduction in mPD-1 positive cells after manipulation. Figure 4A1, A2 show the flow cytometry results and related diagram of the percentage of Jurkat cells that expressed mPD-1.

Biotinylated anti-human PD-1 antibody was used in a dot blot to check sPD-1 protein expression in the supernatant of the pooled cells group compared to the control positive and negative groups. Brown dots were observed with the pooled group and control positive supernatants. Therefore, both groups had different intensities of sPD-1 expression (Fig.4B1). The captured image of the dot blot strip was quantified using ImageJ software. The results showed that the increased level of soluble protein expression in the supernatant was 9.7%, from 28.26% for the control positive group to 37.96% for the pooled cells group (Fig.4B2).

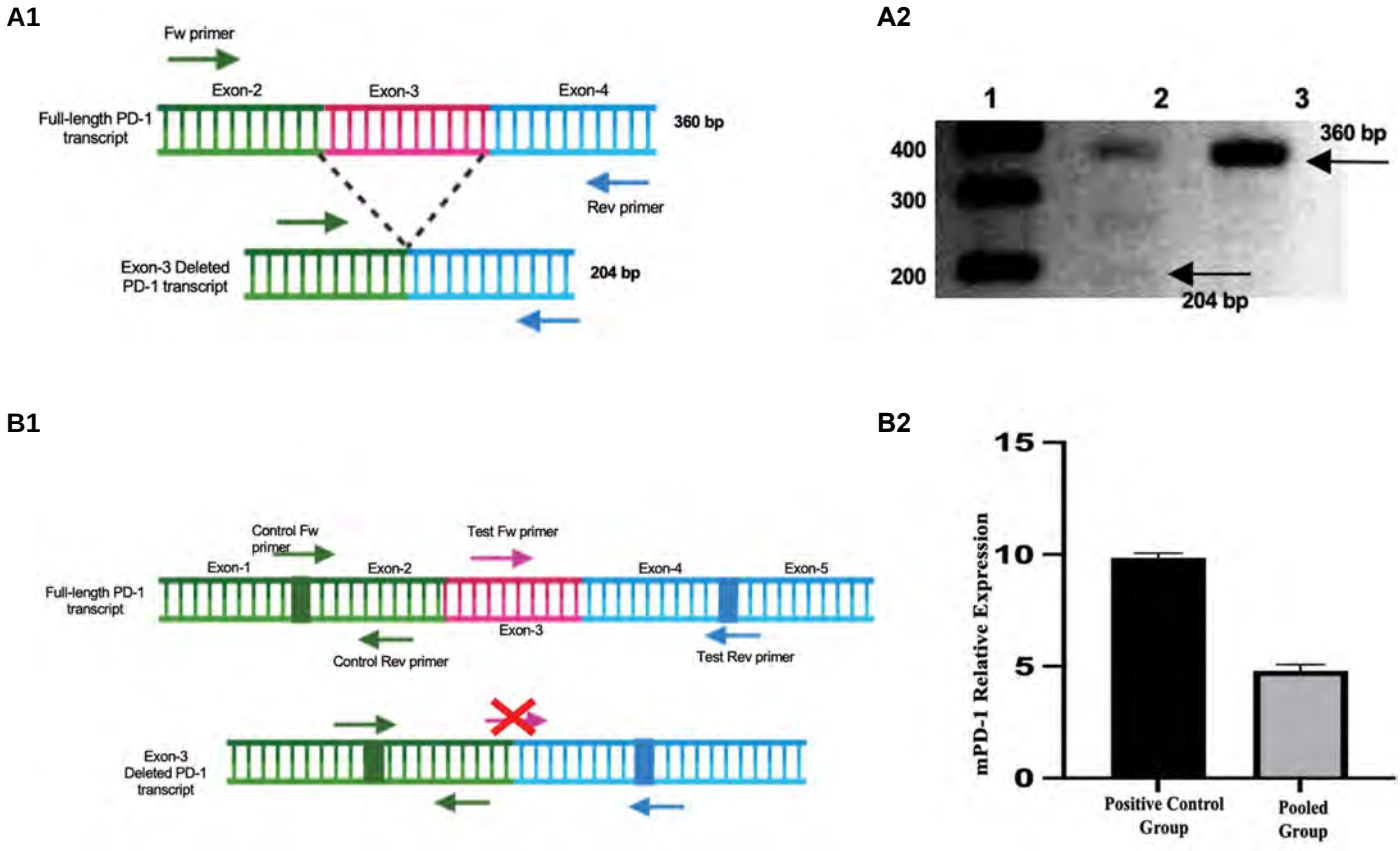

Fig.3: PD-1 transcript expression patterns are analysed. **A1.** Full-length and exon-3 deletion PD-1 transcripts are shown. A pair of primers for reverse-PCR upstream (exon-2) and downstream (exon-4) of exon-3 are depicted. **A2.** The result of the reverse PCR product was run on 3% agarose gel electrophoresis. Lane 1: 100 bp DNA ladder (Yekta Tajhiz Azma, Iran), lane 2: PCR product of the pooled cells group, and lane 3: PCR product of the positive control group. Arrows show the 360 bp and 240 bp bands. The middle band is an unwanted band that also appeared in the control. **B1.** Schematic picture of real-time PCR (RT-PCR) with two primer sets. Control primers target upstream exons of PD-1 mRNA with stable expression for membrane PD-1 and soluble PD-1. The test primers target exon-3 of PD-1 mRNA for checking the membrane PD-1 reduction after exon deletion. **B2.** Results of RT-PCR with two sets of primers for the positive control and pooled cells, analysed with relative expression calculation in Prism with two sample sizes and P=0.0024. PCR; polymerase chain reaction.

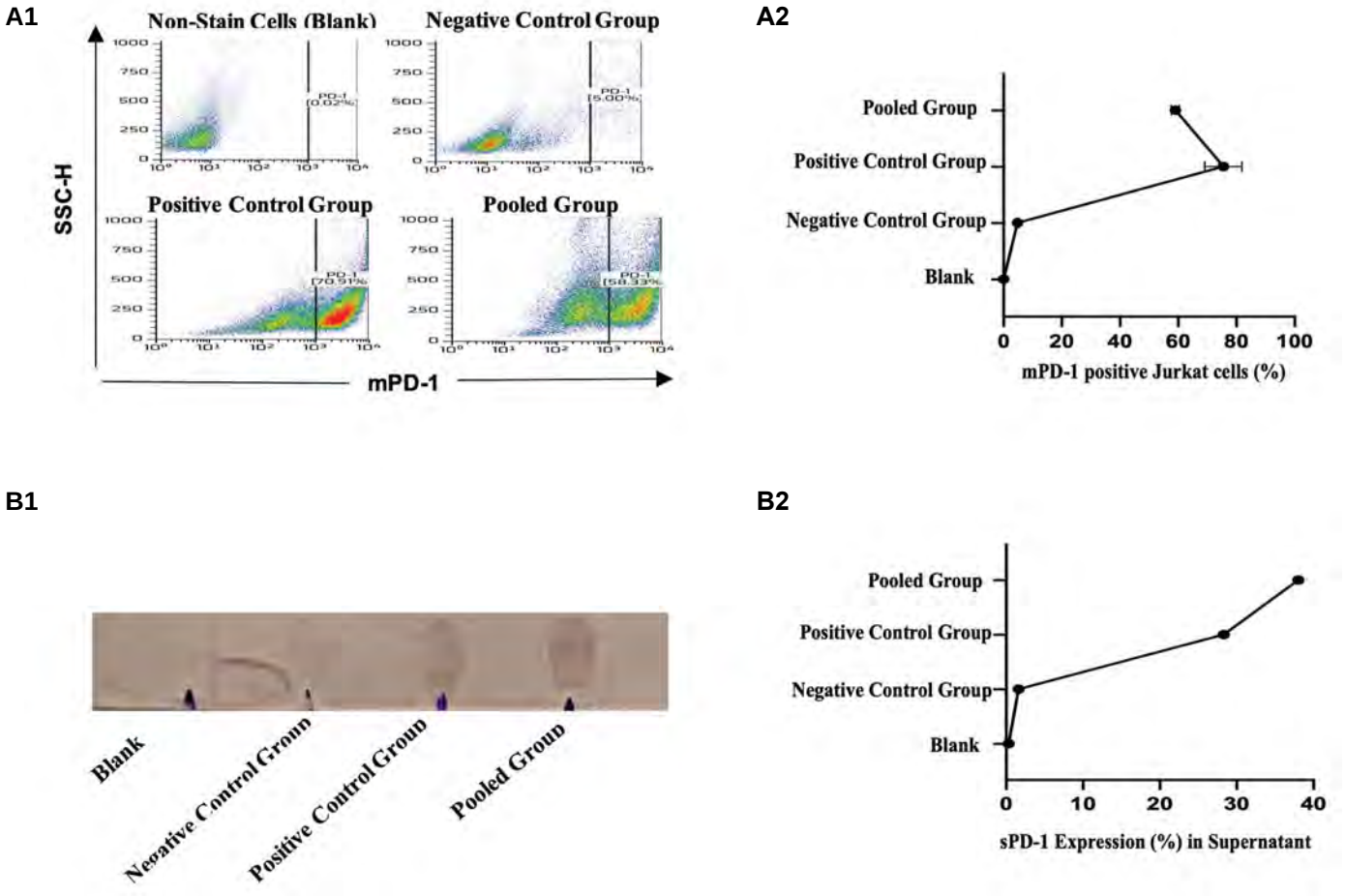

Fig.4: Effect of dual sgRNAs/CRISPR lentiviral particles on PD-1 protein expression in Jurkat cells versus control groups are reported. **A1.** Flow cytometry results for four groups stained with FITC-anti-PD-1 antibody. **A2.** The percentage of membrane PD-1 (mPD-1) positive Jurkat cells derived from flow cytometry results, with two sample sizes and P<0.0001. **B1.** Strip image of dot blot assay for detection of soluble PD-1 (sPD-1) in the supernatant. **B2.** The dots on the strip were quantified with ImageJ software. The results are reported as percentages.

Lymphocyte proliferation and apoptosis assay in the co-cultures

The selection of candidate cancer cells was based on surface PD-L1 protein expression. It has been reported that the MDA-MB-231 breast cancer cell line has a high expression level of PD-L1. RCC was selected as a primary cancer cell that expresses PD-L1. High expression level of PD-L1 in these cells was confirmed by qPCR (data not shown).

We sought to examine the effect of sPD-1 in the supernatant of the pooled cells group on the proliferation and apoptosis of lymphocytes, alone and in co-culture with PD-L1$^+$ cancer cells. Therefore, we designed co-culture panel tests (Table 1) that had an effector to target cell ratio of 10:1. CFSE-labelled lymphocytes were collected after 72 hours of co-culture with or without RCC. Supernatant from the pooled cells group was assessed by flow cytometry to evaluate CD3-CFSE$^+$ gated cell proliferation. The proliferation histograms were analysed with FlowJo™ v.10 software. CFSE-labelled lymphocytes were considered to be the negative control and non-stained lymphocytes comprised the blank that did not have any proliferation peaks in the histogram. The histogram of PHA/PMA activated CFSE-labelled lymphocytes was the positive control for proliferation, which separated into divided peaks of proliferated cells and an undivided peak of non-proliferated cells. Histograms of other co-culture groups were compared with the positive and negative control histograms (Fig.5A1). The percentage of proliferated lymphocytes or cells with lower CFSE in the divided peaks of each condition is shown in Figure 5A2. In lymphocytes co-cultured with RCC, we observed that ~37% of cells were proliferated; in the co-culture of lymphocytes and supernatant, this rate was ~45%. In the lymphocyte, RCC, and supernatant co-culture, the proliferated CD3-CFSE$^+$ lymphocytes increased to ~55%. The supernatant, including sPD-1, had a positive effect on lymphocyte proliferation with or without tumor cells (Fig.5A2).

We tested apoptosis of the CFSE$^+$ gated lymphocytes by flow cytometry and an Annexin V-FITC/7-AAD kit. In the first step, the cells were gated by CFSE positivity. Then, these cells were defined by 7-AAD and Annexin V-FITC. The percentage of late and early apoptosis (Q2: Annexin V positive and 7-AAD positive and Q3: Annexin V positive and 7-AAD negative, respectively)

after CFSE$^+$ gating of lymphocytes co-cultured with RCC was 13.36%. The apoptosis percentage of CFSE$^+$ lymphocytes co-cultured with RCC and supernatant was 3.3%. There was a 10% reduction in the percentage of lymphocytes that underwent apoptosis after the addition of supernatant to the co-culture. There were 12.5% more viable lymphocytes in the presence of supernatant than viable lymphocytes co-cultured with only RCC. This positive function on lymphocytes could be attributed to the influence of sPD-1 in the supernatant. Figure 5B1 shows the percentages of lymphocytes (live, necrotic, late apoptosis, and early apoptosis). The percent of surviving CFSE$^+$ gated lymphocytes co-cultured with the MDA-MB-231 cell line in the presence and absence of supernatant had a 14.8% difference (Fig.5B2). The percentages of lymphocytes (live, necrosis, late apoptosis, and early apoptosis) in the different co-culture conditions are shown in Figure 5B2.

Microscopic cell images of the co-culture conditions confirmed the proliferation and apoptosis results of the lymphocytes. Furthermore, we observed morphological changes indicative of apoptosis in the tumor cells in the presence of supernatant (Fig.5C).

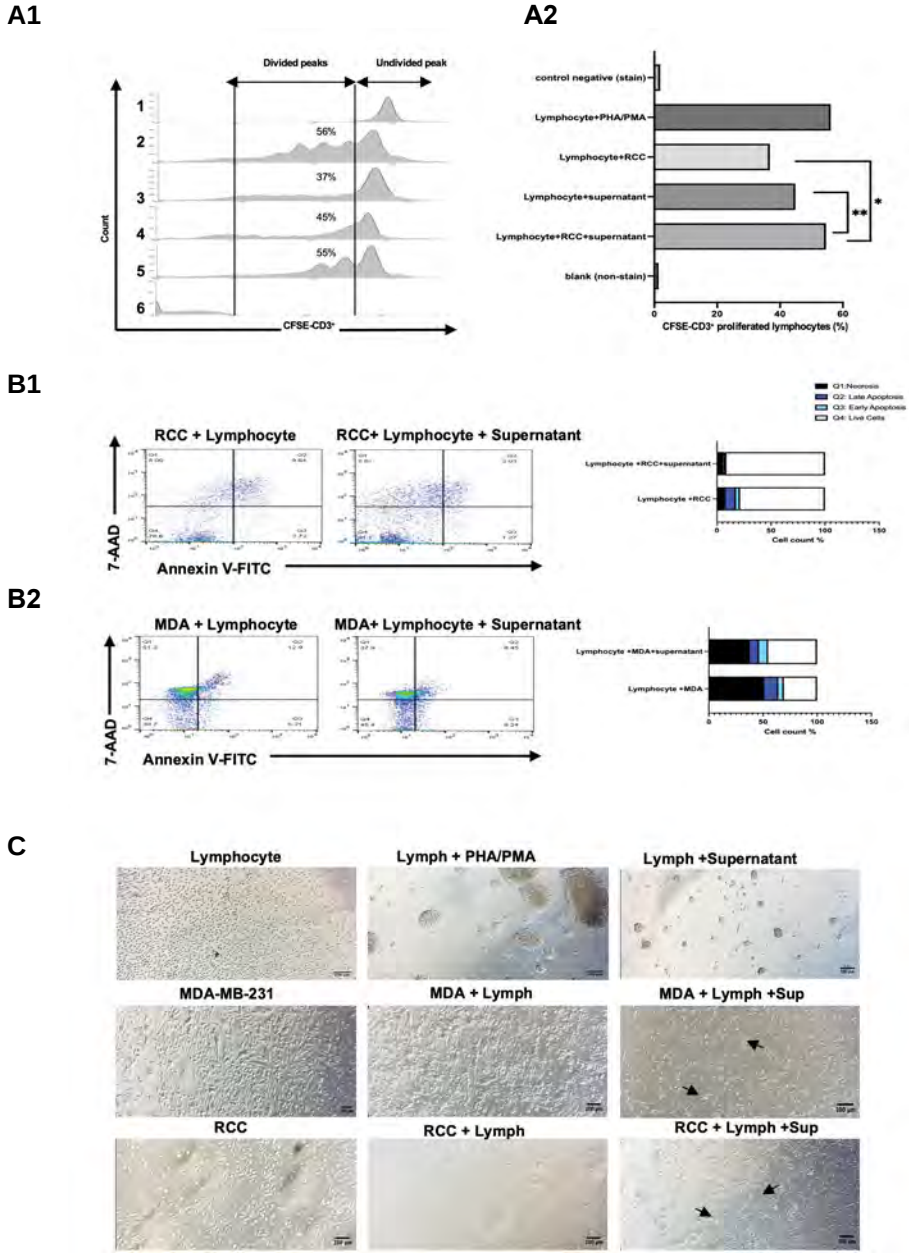

Fig.5: Effect of sPD-1 in supernatant on proliferation and apoptosis of lymphocytes are reported. **A1.** Histogram plot for proliferation of CD3-CFSE$^+$ gated cells. 1; Negative control (CFSE-labelled lymphocytes), 2; Positive control (CFSE-labelled lymphocytes activated with PHA/PMA), 3; CFSE-CD3$^+$ gated lymphocytes co-cultured with renal carcinoma cells (RCC), 4; CFSE-CD3$^+$ gated lymphocytes co-cultured with supernatant, 5; CFSE-CD3$^+$ gated lymphocytes co-cultured with RCC and supernatant, and 6; Blank (unstained lymphocytes). **A2.** Percentage of proliferated cells. *; ~18% difference, **; ~9.5% difference). **B1, B2.** Apoptosis assay for the CFSE$^+$ gated cells. Co-culture states are shown. Four states for the cells are shown in the diagram (live, late apoptosis, early apoptosis, and necrosis). **C.** Cell images (scale bar: 100 µm, magnification: 10x). Arrows show the changes in cancer cell morphology. CFSE; Carboxyfluorescein succinimidyl ester and RCC; Renal carcinoma cell.

Discussion

In general, the infiltrated T-cells in the heterogeneous tumor cell population are classified into different levels of functionality. Cell-intrinsic processes, such as the negative signalling pathway of immune checkpoint inhibitors (ICIs), and cell-extrinsic factors, such as immunosuppressive factors in TME, cause a reduction in T cell function and lead to exhaustion. Interventional treatments that include immune checkpoint blockade (ICB) therapy could be effective in restoring exhausted T cell activity. Interruption of the PD-1/PD-L1 negative signalling pathway via designed monoclonal antibodies showed better responses in comparison with other antibodies against inhibitory receptors, such as CTLA4 and TIM3 (28, 29). We took into consideration the latest studies of PD-1 and, in this experiment, targeted the pattern of PD-1 molecule expression in T cells that affected the PD-1/PD-L1 signalling pathway. Our approach used knocked-out mPD-1 versus increasing sPD-1 expression. Then, we used a dual sgRNAs/CRISPR system to skip exon-3 in the *PDCD1* gene of Jurkat T cells. Our results from DNA sequencing data of the pooled cells (population of transduced and non-transduced T cells) confirmed the deletion of exon-3 from *PDCD1* gene in parts of the cell population. A reduction in the mPD-1 transcript in the pooled cells was confirmed by flow cytometry and RT-PCR. Increased sPD-1 expression in the supernatant of pooled Jurkat cells was another outcome of this study. The co-culture conditions that included the supernatant of pooled cells confirmed the effect of sPD-1 on boosting lymphocyte proliferation and reducing their apoptosis.

Aside from $CD8^+$ T cells, tumor antigen-specific $CD4^+$ T cells that have an anti-tumor function also accumulate in the tumor environment. These $CD4^+$ T cells have similar exhaustion patterns due to the high expression level of inhibitory receptors. Studies show that the scRNA-Seq panel of the $CD4^+$ TILs and it's phenotype analyses are parallel to $CD8^+$ TILs; therefore, the exhaustion process and related hallmarks are similar (30). The phenotypes of exhausted T cells are not homogeneous, and this lack of homogeneity is observed in both $CD8^+$ and $CD4^+$ T cells. PD-1 expression, as the first inhibitory marker, is the important point in these cells. Therefore, the use of anti-PD-1/PD-L1 therapies can be a front line ICB to restore T cell function, both in progenitor cells to prevent exhaustion and in terminal cells to return exhaustion (2). The Jurkat cells are immortalized human $CD4^+$ T lymphocyte cells that can be a model for exhaustion research because of the importance of $CD4^+$ T cells in the exhaustion process and the importance of blocking and changing PD-1 expression in these cells. The Jurkat cell line has been used in several studies for genetic engineering purposes, Including studies of the interactions between PD-1 and PD-L1 (31, 32). Our flow cytometry results showed stimulation of mPD-1 expression after PMA/PHA activation of Jurkat cells. Therefore, we chose this cell line for genomic editing of the *PDCD1* gene sequence.

The PD-1 molecule has a soluble form that is translated after alternative splicing in addition to the membrane form responsible for binding to its ligands on the surface of cancer cells. Among four splice variants of PD-1 mRNA, the exon-3 deleted variant expresses a soluble transcript variant. The sPD-1 variant tends to bind PD-L1 through its IgV-like domain and compete with mPD-1. sPD-1 could block the negative signalling pathway of mPD-1/PD-L1 to reduce apoptotic death of tumor-specific T cells and increase their survival and proliferation (16, 33). The inhibitory function of sPD-1 molecule in TME is similar to anti-PD-L1 monoclonal antibody functions (7, 34). The therapeutic value of the sPD-1 molecule in combination with cancer peptide vaccines and CAR-T cells, as an adjuvant, has been proven to improve the quality of cancer immunotherapy (35, 36). The structure of sPD-1 used in recent studies was the transgene construct that included exon-1 and 2 of the *PDCD1* gene that expressed in target cells, besides the natural expression of mPD-1 in lymphocytes. We used the exon skipping approach of the CRISPR/Cas9 system to target the *PDCD1* gene in T cells and mimic natural alternative splicing by removing exon-3 and changing the protein expression pattern permanently from its membrane to its soluble form. We observed that active Jurkat cells had baseline sPD-1 expression in their supernatant in addition to mPD-1 on their surface; after engineering of the cells and removal of PDCD1 exon-3 with dual sgRNAs/CRISPR, the expression pattern showed increased sPD-1 and decreased mPD-1 in the pooled cells.

CRISPR gene knock-out methods used in recent studies caused disruption of the *PDCD1* gene and blocked both sPD-1 and mPD-1 expression (10-12, 19). However, in our method, mPD-1 expression was distorted and the soluble form of the *PDCD1* gene was expressed. Therefore, negative signalling and mPD-1/PD-L1 in T cells would be blocked. Total sPD-1 expressed by engineered T cells could interfere with the binding of mPD-1/PD-L1/2 and PD-L1/CD80 (B7-1), and block their inhibitory action in T cells (37).

We used a combination of two approaches for exon skipping level based on the latest studies of CRISPR/Cas9 (22). Here, we used a dual sgRNAs/CRISPR construct. The selected left sgRNA could target the splicing site and the right one could not. We expected to have an exon-3 deletion in the genome if both of the sgRNAs were functional. Conversely, we expected to have an exon-3 deletion in the mRNA transcript after splicing if only the left sgRNA was functional, and result in indels upstream of the splicing site. The results of DNA sequencing analysis from the pooled cells showed changes in the chromatogram plot sequence. TIDE analysis of the pooled cell DNA sequences did not show any exon deletion due to the limitations of the tools; however, we observed changes upstream and downstream of exon-3 at the DNA level due to both sgRNAs. The limitations of TIDE analysis are the inability to analyses two sgRNAs and the incapability to calculate indel size range greater than 50 bp which would not be able to estimate large deletions. Therefore, this

tool could not analyse large deletions in sequences, which would be expected in our pooled cell genomes. The ICE tool could simultaneously analyse both sgRNAs in the pooled manipulated cells compared to control sequences. Our results from ICE showed deletions that ranged from 17 bp to 311 bp, which confirmed changes in the genome level of the pooled cells. The low R^2 model fit in the result of ICE was attributed to the indel size range limitation in this tool. Ultimately the sequencing data could confirm the indels in target sequence. In order to improve the results and show the exact change at the genome level in each cell, we should do clonal selection with puromycin. We will take this into consideration in our future study.

According to our design, exon skipping could be expected at the mRNA level based on alternative splicing of exon-3. We detected the deleted exon-3 sequences with reverse PCR in the pooled mRNA and did not detect any deletion in the positive control. RT-PCR and flow cytometry results showed a reduction in mPD-1 transcript expression in the pooled cells compared to the controls, which confirmed the change in pattern expression. Dot blot results showed an increase in sPD-1 in the pooled cells. Dot blot, as a semi-quantified method, also detected and confirmed the functionality of the sPD-1 secreted in the supernatant. Overall, there was a significant change in pattern between mPD-1 in the population of pooled cells and sPD-1 in its supernatant. A considerable point in this study was the proof of positive function of the sPD-1 protein in the collected pooled cell supernatant on proliferation and survival of $CD3^+$ lymphocytes co-cultured with PD-$L1^+$ cancer cells.

Conclusion

The positive results obtained by using the CRISPR/Cas9 system for exon-3 skipping of the *PDCD1* gene in T cells to knock-out mPD-1 expression and increase sPD-1 in the supernatant to overcome exhaustion should be further confirmed. This experiment could be improved by the use of clonal selection, single-cell analysis, optimisation of lentiviral transduction efficiency or non-viral methods, and investigation of off-targets. Furthermore, our recommended method could engage with ACT therapies such as TILs and CAR-T cell therapy to overcome their exhaustion instead of anti-PD-1/PD-L1 antibodies or PD-1 knock-out. The advantage of this method is the ability for local treatment, which prevents the cytotoxic side effects and autoimmunity in systemic ICB therapies. This method could be generalized for other inhibitory receptors to produce soluble forms by using the CRISPR/Cas9 exon skipping strategy.

Acknowledgments

This study was Ph.D. thesis supported by Tehran University of Medical Sciences, Tehran, Iran (grant: 97-03-87-39820). The authors gratefully acknowledge support from the Iran National Science Foundation (INSF grant: 97011707). The authors declare no conflict of interest.

Authors' Contributions

Z.Y.-N.; Formal analysis, Investigation, Data curation, Visualisation, and Preparation of the original draft of this manuscript. Z.Y-N., G.A.K.; Conceptualisation, Methodology, Validation, and Project administration. Z.Y.-N., Y.A.; Software. Z.Y.-N., Z.M.; Resources. Z.Y.-N., G.A.K., Y.A., S.K., R.F.; Wrote, reviewed and edited the manuscript. R.F.; Consultation. G.A.K.; Supervision and funding acquisition. All authors read and approved the final manuscript.

References

1. Schietinger A, Greenberg PD. Tolerance and exhaustion: defining mechanisms of T cell dysfunction. Trends Immunol. 2014; 35(2): 51-60.
2. Miggelbrink AM, Jackson JD, Lorrey SJ, Srinivasan ES, Waibl-Polania J, Wilkinson DS, et al. CD4 T-cell exhaustion: does it exist and what are its roles in cancer? Clin Cancer Res. 2021; 27(21): 5742-5752.
3. Wherry EJ, Kurachi M. Molecular and cellular insights into T cell exhaustion. Nat Rev Immunol. 2015; 15(8): 486-499.
4. Bonorino C, Mognol G. Editorial: T cell exhaustion. Front Immunol. 2020; 11: 920.
5. Guram K, Kim SS, Wu V, Sanders PD, Patel S, Schoenberger SP, et al. A threshold model for T-Cell activation in the era of checkpoint blockade immunotherapy. Front Immunol. 2019; 10: 491.
6. Torphy RJ, Schulick RD, Zhu Y. Newly emerging immune checkpoints: promises for future cancer therapy. Int J Mol Sci. 2017; 18(12): 2642.
7. Yan T, Yu L, Shangguan D, Li W, Liu N, Chen Y, et al. Advances in pharmacokinetics and pharmacodynamics of PD-1/PD-L1 inhibitors. Int Immunopharmacol. 2023; 115: 109638.
8. Simon B, Harrer DC, Schuler-Thurner B, Schaft N, Schuler G, Dörrie J, et al. The siRNA-mediated downregulation of PD-1 alone or simultaneously with CTLA-4 shows enhanced in vitro CAR-T-cell functionality for further clinical development towards the potential use in immunotherapy of melanoma. Exp Dermatol. 2018; 27(7): 769-778.
9. Beane JD, Lee G, Zheng Z, Mendel M, Abate-Daga D, Bharathan M, et al. Clinical scale zinc finger nuclease-mediated gene editing of PD-1 in tumor infiltrating lymphocytes for the treatment of metastatic melanoma. Mol Ther. 2015; 23(8): 1380-1390.
10. Su S, Zou Z, Chen F, Ding N, Du J, Shao J, et al. CRISPR-Cas9-mediated disruption of PD-1 on human T cells for adoptive cellular therapies of EBV positive gastric cancer. Oncoimmunology. 2016; 6(1): e1249558.
11. Rupp LJ, Schumann K, Roybal KT, Gate RE, Ye CJ, Lim WA, et al. CRISPR/Cas9-mediated PD-1 disruption enhances anti-tumor efficacy of human chimeric antigen receptor T cells. Sci Rep. 2017; 7(1): 737.
12. Nakazawa T, Natsume A, Nishimura F, Morimoto T, Matsuda R, Nakamura M, et al. Effect of CRISPR/Cas9-mediated PD-1-disrupted primary human third-generation CAR-T cells targeting EGFRvIII on in vitro human glioblastoma cell growth. Cells. 2020; 9(4): 998.
13. Ureña-Bailén G, Lamsfus-Calle A, Daniel-Moreno A, Raju J, Schlegel P, Seitz C, et al. CRISPR/Cas9 technology: towards a new generation of improved CAR-T cells for anticancer therapies. Brief Funct Genomics. 2020; 19(3): 191-200.
14. Nielsen C, Ohm-Laursen L, Barington T, Husby S, Lillevang ST. Alternative splice variants of the human PD-1 gene. Cell Immunol. 2005; 235(2): 109-116.
15. Zhu X, Lang J. Soluble PD-1 and PD-L1: predictive and prognostic significance in cancer. Oncotarget. 2017; 8(57): 97671-97682.
16. Khan M, Zhao Z, Arooj S, Fu Y, Liao G. Soluble PD-1: predictive, prognostic, and therapeutic value for cancer immunotherapy. Front Immunol. 2020; 11: 587460.
17. Song MY, Park SH, Nam HJ, Choi DH, Sung YC. Enhancement of vaccine-induced primary and memory CD8(+) T-cell responses by soluble PD-1. J Immunother. 2011; 34(3): 297-306.
18. Bartee MY, Dunlap KM, Bartee E. Tumor-localized secretion of soluble PD1 enhances oncolytic virotherapy. Cancer Res. 2017; 77(11): 2952-2963
19. Chamberlain CA, Bennett EP, Kverneland AH, Svane IM, Donia

M, Met Ö. Highly efficient PD-1-targeted CRISPR-Cas9 for tumor-infiltrating lymphocyte-based adoptive T cell therapy. Mol Ther Oncolytics. 2022; 24: 417-428.
20. Stadtmauer EA, Fraietta JA, Davis MM, Cohen AD, Weber KL, Lancaster E, et al. CRISPR-engineered T cells in patients with refractory cancer. Science. 2020; 367(6481): eaba7365.
21. Gapinske M, Luu A, Winter J, Woods WS, Kostan KA, Shiva N, et al. CRISPR-SKIP: programmable gene splicing with single base editors. Genome Biol. 2018; 19(1): 107.
22. Mou H, Smith JL, Peng L, Yin H, Moore J, Zhang XO, et al. CRISPR/Cas9-mediated genome editing induces exon skipping by alternative splicing or exon deletion. Genome Biol. 2017; 18(1): 108.
23. Togashi Y, Mizuuchi H, Tomida S, Terashima M, Hayashi H, Nishio K, et al. MET gene exon 14 deletion created using the CRISPR/Cas9 system enhances cellular growth and sensitivity to a MET inhibitor. Lung Cancer. 2015; 90(3): 590-597.
24. Labun K, Montague TG, Krause M, Torres Cleuren YN, Tjeldnes H, Valen E. CHOPCHOP v3: expanding the CRISPR web toolbox beyond genome editing. Nucleic Acids Res. 2019; 47(W1): W171-W174.
25. Concordet JP, Haeussler M. CRISPOR: intuitive guide selection for CRISPR/Cas9 genome editing experiments and screens. Nucleic Acids Res. 2018; 46(W1): W242-W245.
26. Rajabzadeh A, Hamidieh AA, Rahbarizadeh F. Spinoculation and retronectin highly enhance the gene transduction efficiency of Mucin-1-specific chimeric antigen receptor (CAR) in human primary T cells. BMC Mol Cell Biol. 2021; 22(1): 57.
27. Brinkman EK, Chen T, Amendola M, van Steensel B. Easy quantitative assessment of genome editing by sequence trace decomposition. Nucleic Acids Res. 2014; 42(22): e168.
28. Nagasaki J, Togashi Y. A variety of 'exhausted' T cells in the tumor microenvironment. Int Immunol. 2022; 34(11): 563-570.
29. Yu Y, Cui J. Present and future of cancer immunotherapy: a tumor microenvironmental perspective. Oncol Lett. 2018; 16(4): 4105-4113.
30. Balança CC, Salvioni A, Scarlata CM, Michelas M, Martinez-Gomez C, Gomez-Roca C, et al. PD-1 blockade restores helper activity of tumor-infiltrating, exhausted PD-1hiCD39+ CD4 T cells. JCI Insight. 2021; 6(2): e142513.
31. Bloemberg D, Nguyen T, MacLean S, Zafer A, Gadoury C, Gurnani K, et al. A high-throughput method for characterizing novel chimeric antigen receptors in Jurkat cells. Mol Ther Methods Clin Dev. 2020; 16: 238-254.
32. Yang W, Chen PW, Li H, Alizadeh H, Niederkorn JY. PD-L1: PD-1 interaction contributes to the functional suppression of T-cell responses to human uveal melanoma cells in vitro. Invest Ophthalmol Vis Sci. 2008; 49(6): 2518-2525.
33. Niu M, Liu Y, Yi M, Jiao D, Wu K. Biological characteristics and clinical significance of soluble PD-1/PD-L1 and exosomal PD-L1 in cancer. Front Immunol. 2022; 13: 827921.
34. He L, Zhang G, He Y, Zhu H, Zhang H, Feng Z. Blockade of B7-H1 with sPD-1 improves immunity against murine hepatocarcinoma. Anticancer Res. 2005; 25(5): 3309-3313.
35. Qiu H, Liu S, Xie C, Long J, Feng Z. Regulating immunity and inhibiting tumor growth by the recombinant peptide sPD-1-CH50. Anticancer Res. 2009; 29(12): 5089-5094.
36. Zhang A, Sun Y, Wang S, Du J, Gao X, Yuan Y, et al. Secretion of human soluble programmed cell death protein 1 by chimeric antigen receptor-modified T cells enhances anti-tumor efficacy. Cytotherapy. 2020; 22(12): 734-743.
37. Keir ME, Butte MJ, Freeman GJ, Sharpe AH. PD-1 and its ligands in tolerance and immunity. Annu Rev Immunol. 2008; 26: 677-704.

Cell J
Cell Journal (Yakhteh)
Homepage: https://www.celljournal.org/
Original Article
Vol 25, No 9, September 2023, Pages: 645-654

β-Glucan Regulates Lipopolysaccharide Induced Genotoxic Damage to The Liver through The Induction of BRCA1 Protein Expression

Gözde Aydoğan Kılıç, Ph.D.*, Mojahed Alsafi, Ph.D.

Department of Biology, Faculty of Science, Eskişehir Technical University, Eskişehir, Turkey

Abstract

Objective: The present study aims to investigate the role of breast cancer-susceptibility gene 1 (*BRCA1*) protein in the β-Glucan (βG) molecule mediated regulation of lipopolysaccharide (LPS)-induced liver genotoxicity.

Materials and Methods: In this experimental study, totally, 32 male Swiss Albino mice were randomly divided into 4 equal groups: control (C), LPS-administered (LPS), βG-administered (βG) and βG-pre-administered/LPS-administered (βG+LPS). The βG was injected at the dose of 150 mg/kg/day intraperitoneally (i.p.) for 3 days. A single dose of 4 mg/kg (i.p.) LPS was administered 24 hours after the last βG injection. BRCA1 expression was determined by western blot analysis and confirmed by quantitative immunofluorescence. Proliferating cell nuclear antigen (PCNA), nuclear factor erythroid 2–related factor (Nrf2) and 8-OHdG protein levels were also determined by the immunofluorescence analysis. The alkaline comet assay was performed. superoxide dismutase (SOD), catalase (CAT) and membrane lipid peroxidation were biochemically measured, and light microscopic histology was evaluated.

Results: The BRCA1 expression level was significantly decreased in the LPS group. However, in the βG+LPS group, expression of BRCA1 protein was over 2 folds higher than the control. After the LPS induction, the DNA strand breaks, oxidative DNA lesions and abnormal proliferation of the liver cells were almost entirely suppressed in βG pre-administrated animals, indicating the BRCA1 mediated ubiquitination of PCNA and activation of the DNA damage repair pathways. Activation of Nrf2 in the βG+LPS group resulted in an increase in the levels of Nrf2 pathway dependent antioxidant enzymes SOD and CAT, prevented the peroxidation of membrane lipids and maintained the histological architecture of the liver.

Conclusion: The results manifested that the βG is a strong inducer of the BRCA1 protein expression in the LPS-induced hepatic stress and the protein constitutes the key component of a βG mediated liver protection against an LPS-induced genotoxic and pathological damage.

Keywords: Beta-Glucan, BRCA1, Genotoxicity, Lipopolysaccharide, Liver

Citation: Kılıç GA, Alsafi M. β-Glucan regulates lipopolysaccharide induced genotoxic damage to the liver through the induction of BRCA1 protein expression. Cell J. 2023; 25(9): 645-654. doi: 10.22074/CELLJ.2023.1989382.1226

Introduction

The lipopolysaccharide (LPS) is the major surface membrane component of the gram-negative bacterial cell wall and the main pathogenic factor of endotoxemia. The liver is particularly susceptible to an LPS-induced damage since hepatocytes are the main players in the elimination of the endotoxin (1, 2). LPS-induced damage to the liver is a result of the dysregulated immune response to the pathogenic factor, and the following induction of oxygen free radicals such as superoxide anion radical (O_2•-), and non-radical but highly reactive molecules like hydrogen peroxide (H_2O_2). The resulting oxidative stress (OS) leads to the depletion of an intracellular storage of endogenous antioxidants, while inducing a damage to protein, membrane lipid and DNA (3, 4). LPS-induced single (SSB) and double (DSB) strand breaks can cause malfunctions in the cell cycle. These changes can constitute the potential cause of carcinogenesis after severe infections (5, 6). Compounds of anti-oxidative and anti-genotoxic are considered a potent agent can prevent the LPS-induced hepatic injury and the risk of developing a subsequent cancer (7, 8).

Beta-glucans (βGs) are a group of biologically active natural compounds that commonly are found in the cell walls of fungi, yeast, algae, and cereals. They are well-known for their immune-modulator and anti-oxidative functions (9). The anti-genotoxic potential of βGs have been subjected to previous studies, their controversial results led to need a better understanding of the mechanism of βGs (10, 11). The βGs have been shown to have an anti-proliferative action on different cancer cell types (12-14). As a suitable target for cancer prevention, breast cancer susceptibility gene 1 (*BRCA1*) gene has potentially associated with DNA replication, damage, repair, cell proliferation and

Received: 07/February/2023, Revised: 20/April/2023, Accepted: 14/May/2023
*Corresponding Address: P.O.Box: 26470, Department of Biology, Faculty of Science, Eskişehir Technical University, Eskişehir, Turkey
Email: gozdea@eskisehir.edu.tr

Royan Institute
Cell Journal (Yakhteh)

antioxidant pathways. The effects of dietary compounds on the expression of BRCA1 protein have been subjected to some of the recent studies. The necessity of further investigation on the role of dietary compounds involved in the regulation of the expression of the gene has been pointed out (15-17).

To the best of our knowledge, an anti-genotoxic mechanism of the βG has not been evaluated in association with the functions of BRCA1 protein. Besides, an anti-genotoxic potential of the βG against the LPS-induced hepatic damage has not been subjected to previous studies. Hence, the present study aims to investigate the multifunctional role of the BRCA1 protein on the βG mediated regulation of genotoxic damage. For this aim, LPS-induced liver is chosen as the organ that can firstly reflect the effects of toxic compounds, and due to the risk of subsequent carcinogenesis development.

Materials and Methods

Ethics approval code

The present experiments were approved by the Local Ethical Committee at Animal Experimentation of the Anadolu University, Eskisehir, Turkey (2018-1) in accordance with the National Institutes of Health Guidelines for the use of Laboratory Animals.

Materials

In this experimental study, LPS (L2630) and *Saccharomyces cerevisiae* β-glucan (from baker's yeast) (9012-72-0) were both purchased from Sigma (St Louis, MO, USA). Primary antibodies for BRCA1 (9010S) and proliferating cell nuclear antigen (PCNA, 2586S) were purchased from Cell Signaling Technology (Danvers, MA, USA) and Nrf-2 (NBP1-32822) was from Novus Biologicals (Littleton, CO, USA). The 8-oxoguanine (8- oxoG) antibody was obtained from Santa Cruz Biotechnology (CA, USA).

Animals and treatment

Totally, 32 Male Swiss Albino mice were obtained from the Experimental Animals Research Center, Anadolu University, Eskişehir, Turkey. Animals with a weight between 30-40 g were acclimatized to the laboratory conditions for 3 days before the experiments onset. During this period, all animals were kept at the 25 ± 3˚C with a 12 hours light-dark cycle condition and fed ad libitum with Purina Chow pellets (022-5022 Nestlé Purina. PetCare, St Louis. MO, USA). In succession, all animals were randomly divided into four equal groups (n=8); including control (C), LPS-administered (LPS), β-Glucan-administered (βG) and βG-pre-administered/LPS-administered (βG+LPS). The total treatment period lasted for 6 days. The control group received vehicle, 0.9% saline (S0817 Merck, Darmstadt, Germany) intraperitoneally (i.p.). The prophylactic βG (9012-72-0, Sigma, St Louis, MO, USA) was injected to both groups, βG and βG+LPS, at the dose of 150 mg/kg/day intraperitoneally (i.p.) for 3 days. A single dose of LPS (4 mg/kg i.p.) (Cat No: L2630, Sigma, St Louis, MO, USA) was injected into the animals in the LPS group and βG+LPS group on the fourth day of the experimental period (The βG+LPS group received its LPS dose 24 hours after the last βG injection). All the animals in control and experimental groups were sacrificed at the end of the experimental period under ketamine (K-113, Sigma, St Louis, MO, USA) anesthesia (80 mg/kg i.p.) and their livers were dissected for the analysis by using standard procedure. The treatment strategies, doses, days and duration of the βG and LPS intervention were conducted based on previous studies (18, 19).

BRCA1 protein western blot assay

The protein lysates of the liver tissue were subjected to western blot analysis with both a specific rabbit polyclonal antibody BRCA1 (9010S, Cell Signaling Technology, Danvers, MA, USA), against BRCA1 protein as well as an appropriate HRP-conjugated secondary antibody (7074, Cell Signaling Technology, Danvers, MA, USA). Using Bradford technique, the total protein content of all samples was measured spectrophotometrically at 595 nm (Shimadzu UV-2101PC, Japan) (20). Upon being quantified, samples (60 µg of each) were resolved by SDS-PAGE (Bio-Rad Mini Protean System, USA) and transferred to the specific membrane (88018, Thermo Fisher Scientific, USA) by a Dry Blotting System (I Blot 2, Thermo Fisher Scientific, Waltham, MA, USA). Successively, the administration of antibodies to the membrane was performed (Invitrogen™ iBind™ Flex Western device, Thermo Fisher Scientific, USA). During this process, all applied solutions were checked for their compatibility with the device before being applied to the device. β-actin was measured as a loading control (21). An ECL system (GEN-BOX imagER CFx, ER Biotech Ltd., Ankara, Turkey) was used to visualize the protein bands. The band intensity of BRCA1 was measured with the ImageJ software (version 1.53t, NIH, USA).

Immunofluorescence assay

In a first step, 5 µm thick sections were taken from the tissue blocks which were previously prepared for the histological examinations (22). An indirect immunofluorescence method was applied to the samples by using a rabbit polyclonal antibody against BRCA1 (9010S, Cell Signaling Technology, Danvers, MA, USA), a rabbit monoclonal antibody against PCNA (2586S, Cell Signaling Technology, Danvers, MA, USA) and a mouse polyclonal antibody against Nrf-2 (NBP1-32822, Novus Biologicals, Littleton, CO, USA) (23). The 8- oxoguanine (8- oxoG) labelling protocol was applied by using a mouse 8- oxoguanine (8- oxoG) antibody (sc-516176, Santa Cruz Biotechnology, CA, USA) according to the method of Kemeleva et al. (23). For the immunofluorescence assay, the liver sections were incubated in the blocking solution for 30 minutes at room temperature. Tissues were incubated together with the primary antibody at an appropriate degree of dilution (1:200 v/v) with a 1% BSA (Cat No: A3294, Sigma, St Louis, MO, USA) in the PBS buffer (P7059, Sigma, St Louis, MO, USA) and at a consistent temperature of 4°C overnight. After washing with PBS (3×5

minutes), liver sections were incubated with the appropriate secondary antibody (labelled with Alexaflor 488) (ab150113, ab150077, Ab Chem, Cambridge, UK) at an appropriate degree of dilution (1:1000 v/v) in PBS buffer for one hour, at consistent room temperature and in the dark. Positive controls were mouse brain, regenerating rat liver, piceatannol induced mouse liver and Al-induced rat liver for BRCA1, PCNA and Nrf-2 proteins and 8- oxoG lesion sites respectively. Negative controls were the same tissues that were prepared by avoiding the use of primary antibodies. Subsequently, immunofluorescence examinations were performed under a Leica DM 6000B fluorescence motorized microscope (Leica microsystems, Wetzlar, Germany). At least 20 different areas from the liver sections of all animals were randomly selected from each experimental group (n=160) and analyzed using the Image J software (version 1.53t, NIH, USA).

Comet assay procedure

The 0.1 g of liver tissues was homogenized in the Merchant EDTA buffer (0.5 mM NaEDTA, 10 % DMSO in phosphate buffered saline, pH=7.4) with a Potter Elvehjem homogenizator. Totally, 1×10^5/ml liver tissue cells were suspended in a low melting point agarose (75 µl of 1%, w/v) (Cat No: A9095, Sigma, St Louis MO, USA). A microgel was formed on a microscope slide (precoated with 1% normal melting point agarose) by using 85 µl of the cell suspension and allowed to set at 4°C for 5 minutes. Samples were treated with the cell lysis buffer (2.5 mol l^{-1} NaCl, 100 mmol l^{-1} EDTA, 10 mmol l^{-1} Tris-HCl, pH=10.0, containing 1% Triton X-100 added just before use, and 40 mmol l^{-1} dithiothreitol) for 24 hours at room temperature. To remove salt and detergent, slides were washed with deionized water (C7684, Merck- Milipore, Darmstadt, Germany) three times in a 10 minutes intervals between washes. Slides were allowed to equilibrate for 20 minutes in a horizontal electrophoresis unit with a running buffer (500 mmol l^{-1} NaCl, 100 mmol l^{-1} Tris-HCl and 1 mmol l^{-1} EDTA, pH 9.0) before electrophoresis (0.60 V cm^{-1}, 250 mA) for 30 minutes. They were then neutralized with the 0.4 mol l^{-1} Tris (pH=7.5) and stained with SYBR Green I (1:10.000, S9430 Sigma, St Louis, MO, USA) for 1 hour. Fluorescent microscopic examinations were performed under a Leica DM 6000B microscope (Leica microsystems, Wetzlar, Germany). Analysis of the gels was performed by using the Comet IV Software (Perceptive Instruments, Wiltshire, UK). An average of 100 cells from each slide was counted. The results were given as 'tail moment' which is a product of the tail length and the tail DNA% (Tail moment=tail length× % of DNA in the tail) (24).

Biochemical evaluation

For the superoxide dismutase (SOD) activity measurement, an experiment was conducted in accordance with the method of Nebot et al. (25), which was previously standardized. This method is based on the measurement of the formation rate of the chromophore resulted from the SOD enzyme-dependent autooxidation of 5,6,6a,11btetrahydro-3,9,10-trihydroxybenzo[c]fluorine (BXT-01050) in an aqueous alkaline solution. One unit of an enzyme is defined as the amount of enzyme that allows the autoxidation of one micromole of the BXT-01050 reagent at 37°C, pH=8.8 in one minute. The catalase (CAT) activity was determined according to the method of Beers and Sizer (26). The method is based on the absorbance measurement of the hydrogen peroxide at 240 nm. Therefore, one unit of an enzyme is defined as the amount of an enzyme that is degraded to a 1.0 micromole of the hydrogen peroxide in one minute at 25°C and pH=7.0. Furthermore, the lipid peroxidation (LP) level was measured at 532 nm, according to the method of Ohkawa and Ohishi from the n-butanol and pyridine (15:1, v/v) extract of the malondialdehyde (MDA) (27).

Histological assay

All tissues were fixed in a solution containing 4% paraformaldehyde in PBS buffer (EMS 15712, Electron Microscopy Sciences Hatfield, PA, USA) (pH=7.2-7.3). Then, each sample was passed through a graded series of the alcohol (1012768, Sigma, St Louis, MO, USA) to remove the water. In addition, the samples were infiltrated with a mixture of LR White medium grade kit (14380, Electron Microscopy Sciences Hatfield, PA, USA) and 70% ethanol (2: 1; v/v) with a following treatment in pure LR White. Consecutively, all tissue blocks were polymerized in an 60°C oven overnight and sectioned (700 nm) by using a Leica EM UC7 ultramicrotome. These sections prepared for light microscopic observations were then stained with 1% toluidine blue/borax (pH=8.4, 104172, Merck, Germany). As a final step, light microscopic examinations were performed under a Leica DM 6000B light microscope (Leica microsystems, Wetzlar, Germany) (22).

Statistical analysis

Statistical analyses were performed by using SPSS 20.0 Software (IBM Corp., NY, USA). The one-way analysis of variance (ANOVA) was followed by the Dunnett's T3. Values of $P<0.05$ were considered as statistically significant. All data are expressed as the mean ± standard error (SE).

Results

BRCA1 western blot analysis results

BRCA1 western blot analysis was performed in order to compare the expression levels of the protein among groups (Fig.1A). The protein expression of *BRCA1* gene of the LPS group was significantly lower than the control group ($P<0.05$). The BRCA1 protein expression level was not significantly different in the βG group in comparison with the control group, while the βG+LPS group showed an over 2-fold increase in comparison with the control group ($P<0.05$). This increase in the BRCA1 protein expression level, particularly takes place in the Kupffer cells. Our immunofluorescence findings also confirmed our Western blot results (Fig.1B). As it is demonstrated in Figure 1, βG pre-administration resulted in an overexpression of *BRCA1* gene. βG-stimulated significant increase in the level of BRCA1 protein took place only in LPS-induced stress conditions.

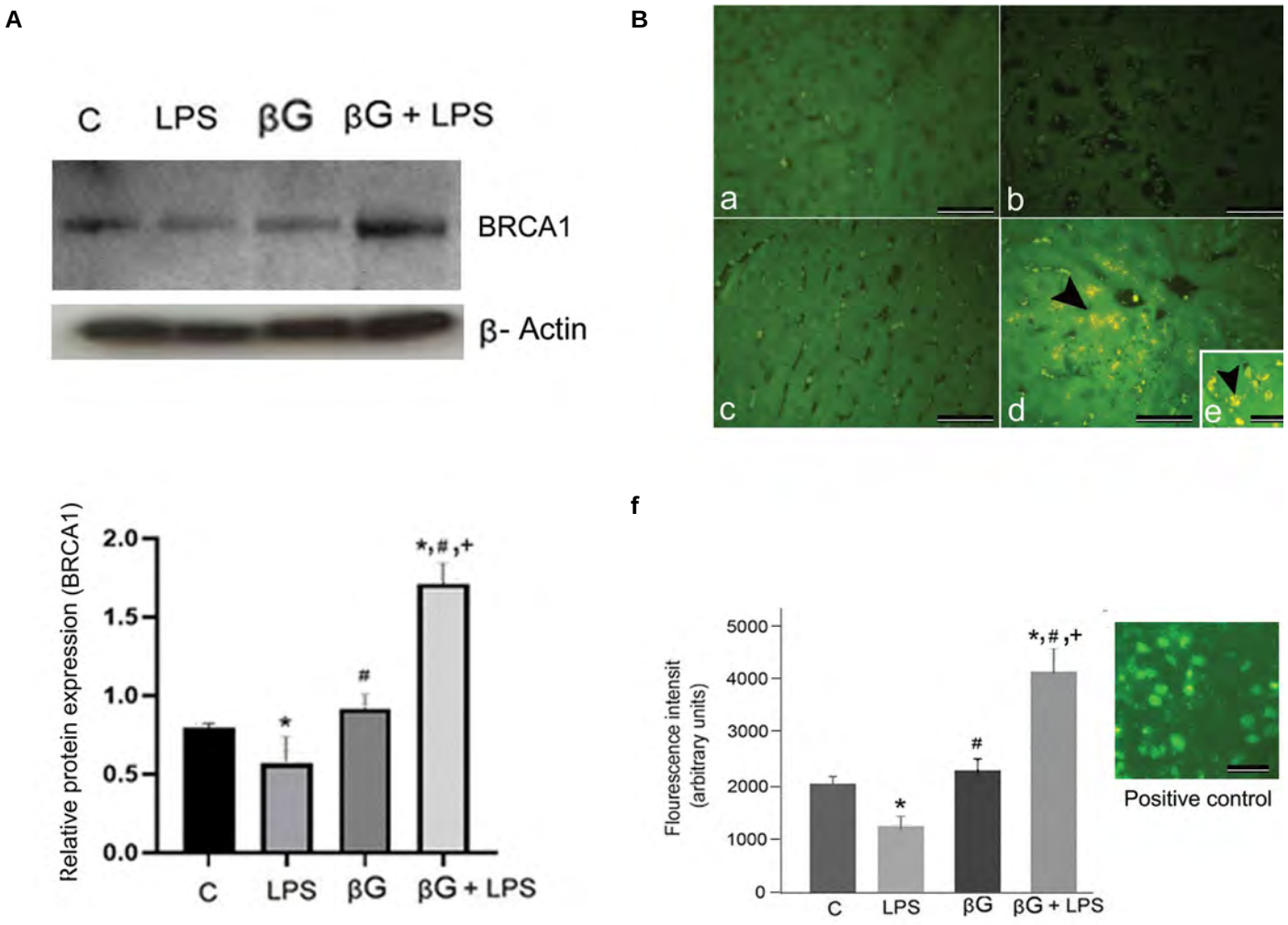

Fig.1: BRCA1 protein expression and immunofluorescence results**. A.** Western blot analysis results of BRCA1. **B.** Representative images of immunohistochemical staining of BRCA1 protein. a; Control (0.9% saline), b; LPS (4 mg/kg single dose i.p.), c; βG (150 mg/kg/d for 3 days i.p.), d; βG+LPS (150 mg/kg/d for 3 days βG i.p. and 4 mg/kg single dose LPS i.p), e; Increased fluorescence signal in the Kupffer cells, and f. Fluorescence intensity graph of the Image J analysis (scale bar: 100 µm). C; Control, LPS; Lipopolysaccharide, βG; Beta glucan, Black arrow; Increased fluorescence signal of BRCA1 protein, *; Significant differences when compared to control, #; Significant differences when compared to the LPS group, +; Significant differences when compared to the βG group.

BRCA1, PCNA and Nrf2 immunofluorescence

Using immunofluorescence assay, we confirm our western blot results for BRCA1 protein expression. On the other hand, PCNA is a multifunctional essential protein for DNA replication and repair that is also in association with the BRCA1 protein at various levels. Therefore, PCNA immunofluorescence levels were analyzed to determine the levels of liver cell proliferation. The Nrf2 immunofluorescence was also examined due to its role in mediating the expression levels of endogenous antioxidants in association to BRCA1. A base level of signal was observed in the control group that confirmed our western blot outcomes (Fig.1Ba). The fluorescence signal in the LPS group was significantly lower than the control group ($P<0.05$). In the βG group, the signal was equal with the control group (Fig.1Bb, c, f). However, the fluorescence signal intensity of the βG+LPS group was over 2-fold higher than the control group ($P<0.05$), and the fluorescence intensity was observed to be higher in the Kupffer cells (Fig.1Bd). Figure 2A shows the PCNA immunofluorescence assay results as a marker of a hepatocellular proliferation. There were not any observable nuclear signals in the control group (Fig.2Aa). A fluorescence signal was observed in the tissue sections of the LPS group, while indicating approximately 4 folds higher active proliferation rate of hepatocytes, in comparison with the control group ($P<0.05$, Fig.2Ab, e). However, there was not a significant signal in either βG group or βG+LPS group (Fig.2Ac, d). The basal level of cytoplasmic expression of Nrf2 protein in hepatocytes was observed in the control group (Fig.2Ba). In the LPS group of animals, low level but significant induction of Nrf2 protein expression was observed ($P<0.05$, Fig.2Bb). The βG+LPS group showed a significant increase in the Nrf2 protein expression level (over 2-fold) ($P<0.05$), while there was not a significant difference between control and βG groups (Fig.2Bc, d). Taken together, the results of the immunofluorescence findings revealed that the βG stimulated the overexpression of BRCA1 protein, normalized the protein level of PCNA and significantly induced the protein level of Nrf2 in the βG+LPS group of animals.

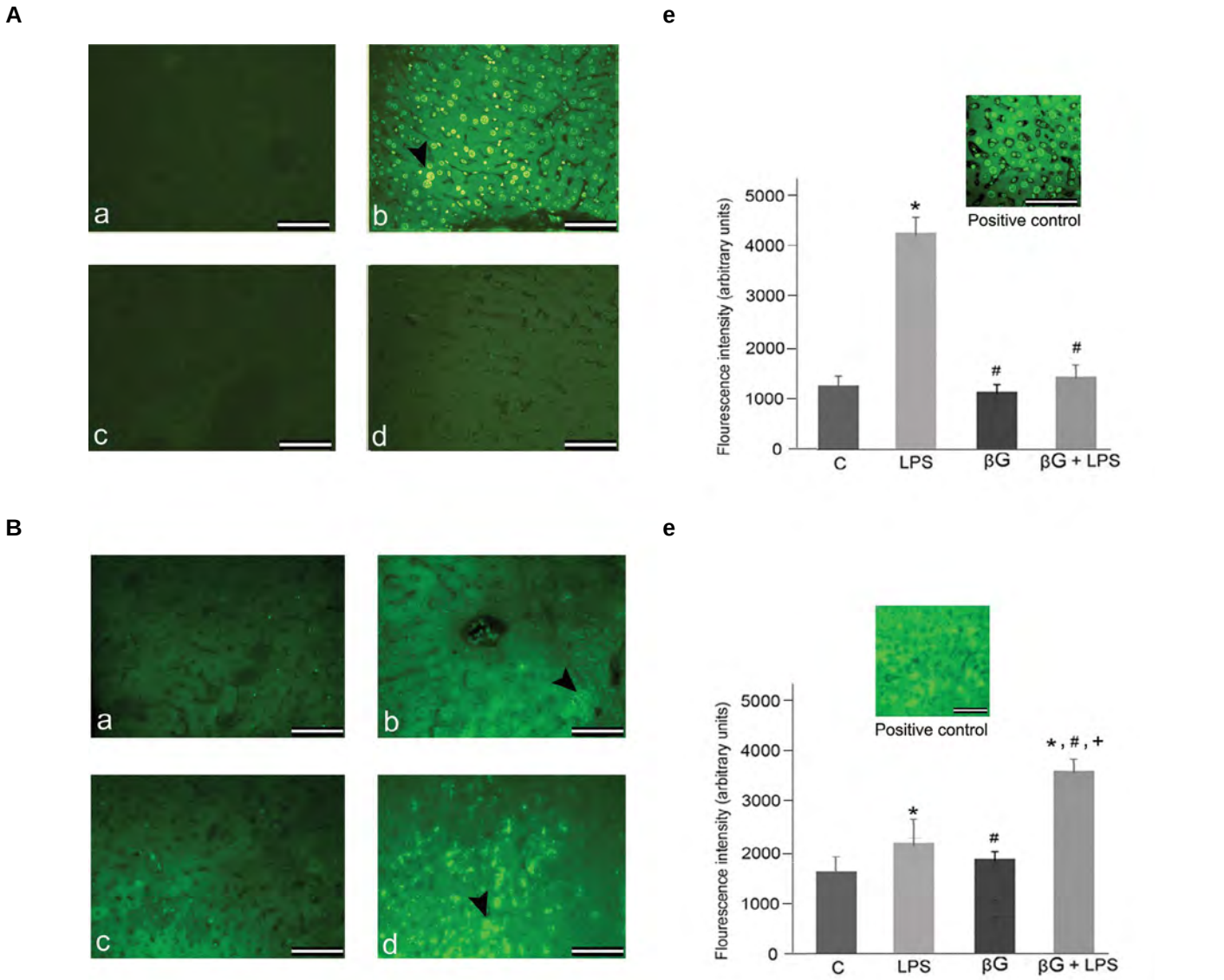

Fig.2: Results of PCNA and Nrf2 immunofluorescence analysis. **A.** Representative images of immunofluorescence staining of PCNA. a; Control (0.9% saline), b; LPS (4 mg/kg single dose i.p.), c; βG (150 mg/kg/d for 3 days i.p.), d; βG+LPS (150 mg/kg/d for 3 days i.p. βG and 4 mg/kg single dose i.p. LPS), and e; Fluorescence intensity graph of Image J analysis**. B.** Representative images of immunohistochemical staining of Nrf2 analysis. a; Control (0.9% saline), b; LPS (4 mg/kg single dose i.p.), c; βG (150 mg/kg/d for 3 days i.p.), d; βG+LPS (150 mg/kg/d for 3 days i.p., βG and 4 mg/kg single dose i.p. LPS), and e; Fluorescence intensity graph of Image J analysis (scale bar: 100 µm). C; Control, LPS; Lipopolysaccharide, βG; Beta glucan, Black arrow; Increased fluorescence signal of PCNA and Nrf2 proteins, *; Significant differences when compared to control; #; significant differences when compared to the LPS group, and +; Significant differences when compared to the βG group.

DNA damage results

Single (SSB) and double (DSB) strand breaks and alkali labile sites of the DNA damage were analyzed by the alkaline comet assay. The 8-oxoG lesion was also analyzed in order to determine the oxidative stress-induced lesions in DNA (Fig.3). Typical control nuclei were observed in Figure 3Aa characterized by a regular round structure. Based on tail moment calculations, LPS pre-administration resulted in a significant DNA damage which is to about three-fold in comparison with the control group (P<0.05, Fig.3Ab, e). In the βG group, there was no significant difference between tail moments in comparison with the control group (Fig.3Ac, e). The βG pre-administration significantly regulated DNA damage with a reduction of ~ 63 % in comparison with the LPS group of animals (P<0.05). Furthermore, there was no significant difference in comparison with the control group (Fig.3Ad, e). Figure 3B represents the results of 8-oxoG immunofluorescence. Our control group showed a pale background immunofluorescence (Fig.3Ba). In the LPS group of animals, the overall fluorescence intensity was significantly increased. Also, 8-oxoG DNA lesions in the LPS group were about two times higher than the control group (P<0.05). Lesions were particularly observed in Kupffer cells and hepatocytes upon being localized at the damaged sites of the liver tissue (Fig.3Bb, e). The βG group did not show significant differences in the fluorescence intensity rate in comparison with the control group (Fig.3Bc, e). We observed a decrease of ~34 % in fluorescence intensity in the βG+LPS group in comparison with the LPS group (P<0.05). The difference in fluorescence

intensity between βG+LPS group and control group was not significant, very rare signals were mostly observed in the Kupffer cells (Fig.3Bd, e). As a result, a βG pre-administration was evidently efficient in protecting against DNA damage in both analyses.

Biochemical findings

SOD and CAT levels were evaluated to demonstrate the capacity of endogenous antioxidants. The LP was evaluated in order to show the OS levels (Fig.4). The LPS administration resulted in a significant decrease in the activities of SOD and CAT, 52% and ~57%, respectively, in comparison with the control group (P<0.05). The levels of SOD and CAT, (~13 and ~31% respectively) were observed significantly higher in the βG group in comparison with the control group (P<0.05) (Fig.4A, B). In the LPS group, the LP level was significantly increased (~60 %) in comparison with the control (P<0.05, Fig.4C). In the βG+LPS group, a decrease was observed in the LP rate, that it reached to the control group level (Fig.4C).

Histological findings

Light microscopic observations were performed to demonstrate the histopathological differences among groups (Fig.5). The control group showed a normal histological architecture of the liver (Fig.5A). Steatosis was observed in the LPS group sections, accompanied by apoptotic and necrotic changes (Fig.5B). In the βG group, there were no observable changes in the pattern of hepatocytes (Fig.5C). In βG+LPS group, mild microvesicular fatty change and rare apoptotic events were observed (Fig.5D). Generally, normal histological architecture of the liver was preserved in the βG pre-administered group.

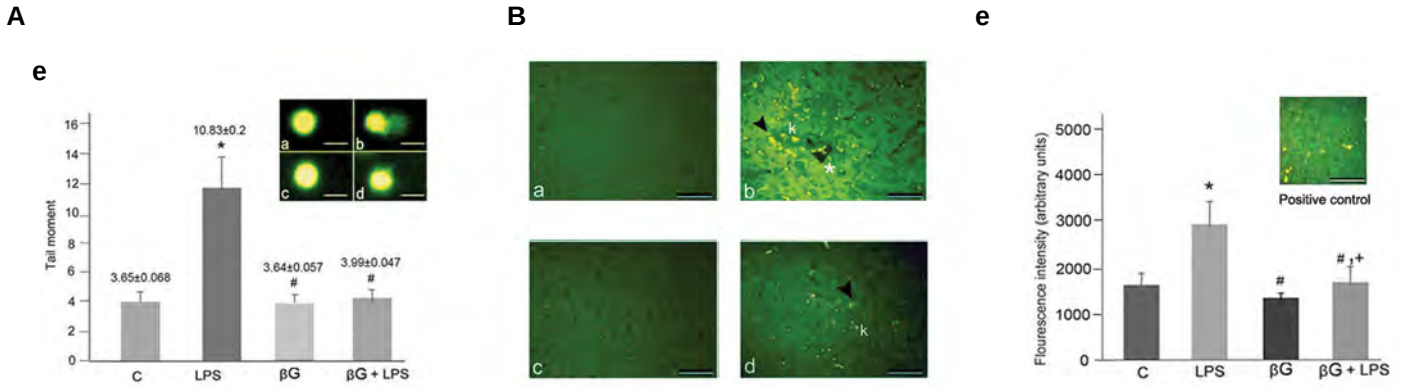

Fig.3. Comet assay analysis and 8-oxoG labelling results**. A.** Representative images of the comet assay results and graphical illustration of tail moment comparisons. a; Control (0.9% saline i.p.), b; LPS (single dose of 4 mg/kg i.p.), c; βG (150 mg/kg/day i.p.), d; βG+LPS (150 mg/kg/day i.p. for 3 days; 24 hours later, a single 4 mg/kg dose of LPS i.p.), and e; Tail moment graph. **B.** Representative images of 8-oxoG labelling. a; Control (0.9% saline i.p.), b; LPS (single dose of 4 mg/kg i.p.), c; βG (150 mg/kg/day i.p.), d; βG+LPS (150 mg/kg/day i.p. for 3 days; 24 hours later, a single 4 mg/kg dose of LPS i.p.), and e; Fluorescence intensity graph of Image J analysis. C; Control, LPS; Lipopolysaccharide, βG; Beta glucan, Black arrow; 8-oxoG lesion Immunofluorescence, White star; Damaged sites, k, Kupffer cells, *; Significant differences when compared to control, #; Significant differences when compared to the LPS group, and +; Significant differences when compared to the βG group.

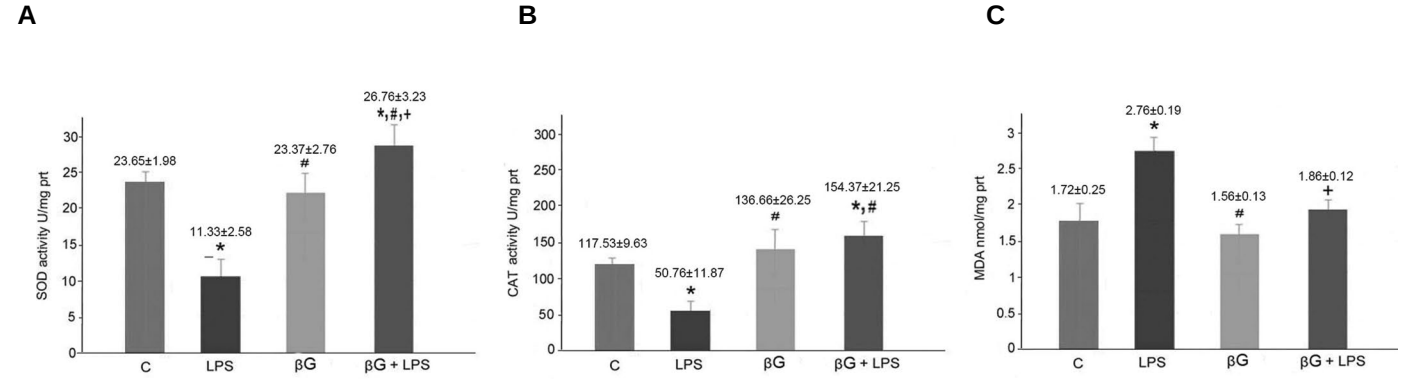

Fig.4: Results of the biochemical measurements. **A.** SOD activity (U/mg/prt). **B.** CAT activity (U/mg prt). **C.** MDA levels (nmol/mg/prt). SOD; Superoxide dismutase, CAT; Catalase, MDA; Malondialdehyde, C; Control, LPS; Lipopolysaccharide, βG; Beta glucan, *; Significant differences when compared with the control group (P<0.05), #; Significant differences when compared with LPS group (P<0.05), and +; Significant differences when compared with βG group.

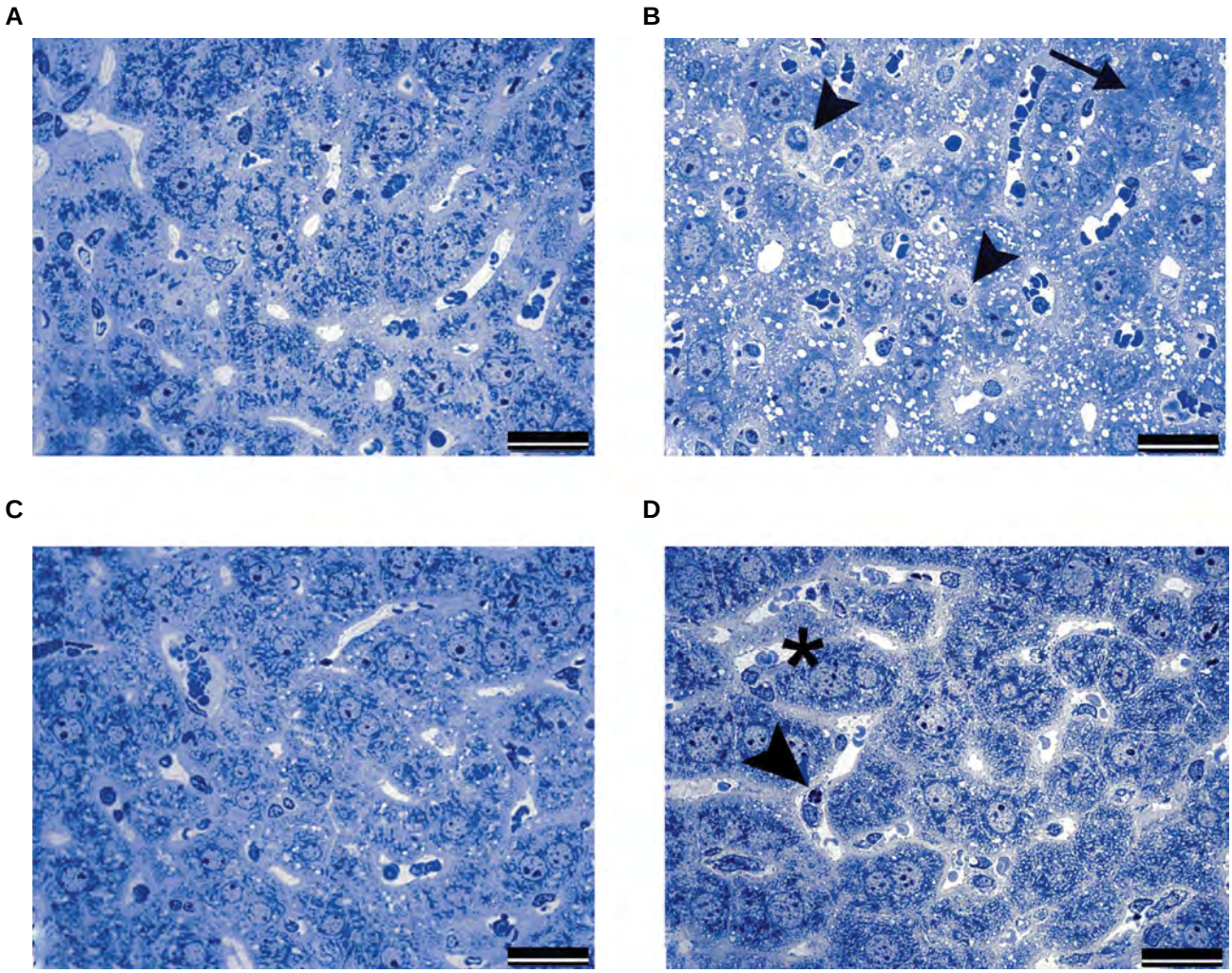

Fig.5: Representative images of light microscopic observations of the liver tissue. **A.** Control (0.9% saline i.p.): normal histological architecture of the liver tissue. **B.** LPS (single dose of 4 mg/kg i.p.): steatosis with discernible apoptotic (▶) and necrotic (→) appearance in individual hepatocytes. **C.** βG (150 mg/kg/day i.p.): liver tissue with normal histological appearance. **D.** βG+LPS (150 mg/kg/day i.p. for 3 days: 24 hours later, a single 4 mg/kg dose of LPS i.p.): liver tissue with no observable pathologies with the exception of mild swelling of hepatocytes (*) and rare apoptotic events (scale bar: 20 µm).

Discussion

The LPS-induced damage to DNA is an early event in severe bacterial infections. The administration of compounds with a natural origin, applies to managing damages and subsequent complications, such as cancer formation (28, 29). As a gatekeeper of genome stability, *BRCA1* is considered to be a critical target of regulation. Although a variety of bioactive food compounds, such as βGs, have been reported as a gene modulator in cancer cells (30, 31), there is a lack of evidence on the βGs molecular effect on the *BRCA1* gene, in normal and stress-induced cells. According to the present study, it seems that the BRCA1 protein expression is significantly down-regulated with a mechanism that reversely is controlled by the *lncRNA MALAT1* in the LPS group of animals. The mechanism of this down-regulation was formerly reported by Yong et al. in their study (32).

However, a dramatic increase in the expression of BRCA1 protein was observed in the βG+LPS group (over 2-fold when compared with the control). The fluorescence intensity was observed to be higher in the Kupffer cells in this group. The LPS is a potent stimulator of the Kupffer cell tumor necrosis factor alpha (TNF-α) production and the following increase in the inflammation and oxidative stress. Therefore, Kupffer cells become more susceptible to damage. Bennett et al. (33) provided evidence that Kupffer cells give the first hand response to an LPS intoxication which is consistent with our findings. In the βG group of animals, BRCA1 protein expression level which was not statistically different from the control, indicated an induction of the gene by βG only in stress conditions. BRCA1 is a stress response protein which mediates both cell-cycle arrest and apoptosis, beside regulating DNA damage repair following different types of injury in a cell (34).

LPS-induced damage to the DNA was observed to be effectively decreased by the pre-administration of βG as long as the non-significant difference in the DNA

damage between the βG+LPS group and the control group are considered. Associated with its potential to trigger significant damage to DNA, LPS can promote hepatocellular carcinoma by activating TLR-4 mediated proliferative and anti-apoptotic signals (35). In parallel with the downregulation of BRCA1 protein expression, we observed an abnormal proliferation rate of the hepatocytes that was exerted with the significant increase in the protein levels of PCNA in the LPS group of animals. In the βG+LPS group, the βG treatment mediated BRCA1 protein expression increase was accompanied by the suppression of abnormal hepatocyte proliferation. Besides being a useful marker of cells with proliferative potential, PCNA protein is an essential tool for the DNA replication pathways. It is involved in the DNA excision repair pathways as well as mismatch repair pathways, when it is ubiquitinated with the mechanisms promoted by *BRCA1* (36). BRCA1 protein functions in a number of cellular pathways in the nucleus and cytoplasm in association with PCNA at various levels. By the control of DNA damage-induced cell cycle checkpoint activation and repair of the damaged DNA, these pathways maintain stability of the genome. The products of these genes also function in the ubiquitination of the proteins, chromatin remodeling, transcriptional regulation, apoptosis and cell survival in relation to each other. The *BRCA1* gene mediated PCNA ubiquitination results in the replication blockade, and also increases the translesion polymerases recruitment and DNA damage repair (37). The present study findings manifest that the βG molecule acts its role by its ability to stimulate BRCA1 protein expression. The ubiquitination of G2/M cell cycle proteins, such as PCNA, and transcriptional regulation of the genes in the DNA repair pathways of the BRCA1 protein are suggested to be the primary routes of the βG's molecular protection against LPS-induced genotoxicity in the liver cells.

On the other hand, we observed an LPS-driven decrease in the antioxidant capacity that was balanced with the βG administration. The endogenous antioxidant system was fairly insufficient to deal with the increased OS in the LPS group of animals, as shown by the increase in the LP level and a significant decrease in the levels of antioxidant enzymes SOD and CAT. However, in the βG+LPS group SOD and CAT enzyme levels were higher than the LPS group and also slightly but significantly higher than the control as a sign of a regulation in the antioxidative defense system. The LP, which was observed in control levels in the βG+LPS group of animals is concrete evidence that the βG pre-administration treatment efficiently regulated these enzymes to overcome the increasing radical formation. The BRCA1 induction in this group is also suggested to be involved in the mechanisms of βG molecules to overcome LPS-induced oxidative stress. Previous studies revealed that BRCA1 protein plays an active role in the regulation of OS to prevent carcinogenesis in normal cells by interacting with the transcription factor nuclear factor erythroid 2-like 2 (Nrf2). Gorrini et al. (38) reported that the BRCA1 protein binds to the Nrf2 protein to control the Keap1-mediated ubiquitination activity, while this binding results in the increased stability and activation of Nrf2 protein. As a master regulator of anti-oxidative responses, an increase in the Nrf2 protein expression, enhances the expression of the endogenous antioxidants (39).

We observed a low significant increase in the Nrf2 protein expression in the LPS group. However, the stability and activity of the Nrf-2 protein seem to be declining as a result of decreased BRCA1 protein level in this group. The decrease in the levels of SOD and CAT supported this observation, indicating the impairment of Nrf2-driven antioxidant signaling in LPS-exposed animals. On the other hand, the βG pre-administration resulted in a significant increase in BRCA1/Nrf2 protein expressions and SOD/CAT enzyme levels resulting in the reduced levels of OS and DNA damage. Based on the supporting histological evidence, the βG pre-administration treatment prevented an intense cytoplasmic vacuolation, inflammatory infiltrates, hyperplasia, and necrosis of the individual hepatocytes which are the common signs of the LPS intoxication in the liver. Apart from having very few vacuoles and rare apoptotic events for the elimination of the damaged cells, livers from the βG+LPS group of animals were almost always normal in the term of their tissue architecture. Herein, in the βG pre-administered group, βG-induced BRCA1 protein expression increased the antioxidant capacity of the liver. It seems that BRCA1 interacting with the Nrf2, promotes the stability and activation of the Nrf2 protein. Although, the βG molecule, itself could serve as a molecular scavenger of free radicals and support the endogenous antioxidant capacity of the liver (40), the replenishment of the antioxidant enzymes by the mechanisms shaped on the βG-driven induction of BRCA1 protein interaction of the molecule is manifested to be the most efficient route of OS reduction in LPS-exposed animals. The present study findings strongly suggest that the BRCA1 protein expression stimulation by the βG molecule is the underlying factor in the protection against an LPS-induced DNA damage to the liver. However, mechanisms of this protection are needed to be further investigated, since many other related molecular pathways could contribute to this protection in different ways.

Conclusion

The present study demonstrated that prophylactic βG protects against the LPS-induced genotoxicity and pathological damage of the liver tissue, through the induction of BRCA1 protein expression. The βG molecule alone do not change the expression of BRCA1 protein while, the protein level solely arises during the LPS-induced hepatic stress conditions. In the LPS-exposed liver with an increase in DNA damage and hepatocytes with abnormal proliferation, a βG-stimulated BRCA1 protein as a key factor of the protection, mediates the ubiquitination of PCNA which results in the arrest of the cell-cycle at the S-phase. The BRCA1-promoted pathway dependent repair of the damaged DNA efficiently reduces LPS-induced DNA strand breaks and maintains

the genomic stability of the liver. The βG molecule also regulates and supports the antioxidant capacity of the liver via BRCA1 interaction with Nrf2, that results in the activation and stabilization of the transcription factor. Activation of Nrf2-driven antioxidative pathway supports the endogenous antioxidative capacity of the liver and prevents the LPS-induced oxidative stress, associated DNA lesions, membrane lipid damages and also pathological damage to the liver. These results support the potential use of the βG as an early management tool to prevent a genotoxic damage and subsequent carcinogenic nature in the endotoxemia liver tissue. The present study provides knowledge for future studies subjected to the development of the βG-based drugs that aims *BRCA1* gene targeted therapy. Further studies on other possible molecular targets and pathways could be useful for the development of different therapeutic strategies.

Acknowledgements

This study was supported by the Eskisehir Technical University Scientific Research Projects Comission under the grant no:1705F229. The authors gratefully acknowledge to Şeyda Uçarcan for her laboratory technical assistance. The authors declare that they have no conflicts of interest in this study.

Authors' Contributions

G.A.K.; Conceptualization, Methodology, Validation, Formal analysis, Investigation, Resources, Writing – Original Draft. M.A.; Writing- Reviewing and Editing, Visulalization, and Investigation. All authors have read and approved the manuscript.

References

1. Yan J, Li S, Li S. The role of the liver in sepsis. Int Rev Immunol. 2014; 33(6): 498-510.
2. Guerville M, Boudry G. Gastrointestinal and hepatic mechanisms limiting entry and dissemination of lipopolysaccharide into the systemic circulation. Am J Physiol Gastrointest Liver Physiol. 2016; 311(1): G1-G15.
3. Xu T, Liu R, Zhu H, Zhou Y, Pei T, Yang Z. The inhibition of LPS-induced oxidative stress and inflammatory responses is associated with the protective effect of (-)-Epigallocatechin-3-Gallate on bovine hepatocytes and murine liver. Antioxidants (Basel). 2022; 11(5): 914.
4. van Elsland D, Neefjes J. Bacterial infections and cancer. EMBO Rep. 2018; 19(11): e46632.
5. Liu Z, Mahale P, Engels EA. Sepsis and risk of cancer among elderly adults in the United States. Clin Infect Dis. 2019; 68(5): 717-724.
6. Samivel R, Subramanian U, Ali Khan A, Kirat O, Masmali A, Almubrad T, et al. Lipopolysaccharide enhances genotoxicity by activating GADD45G and NF-κB in human corneal epithelial cells. Oxid Med Cell Longev. 2022; 2022: 4328116.
7. Hamzawy MA, El-Denshary ESM, Abdel-Wahhab MA. Effects of natural compounds in treatment and prevention of hepatotoxicity and hepatocellular carcinoma. Hepatoma Res. 2015; 1: 111-118.
8. Li S, Tan HY, Wang N, Zhang ZJ, Lao L, Wong CW, et al. The role of oxidative stress and antioxidants in liver diseases. Int J Mol Sci. 2015; 16(11): 26087-26124.
9. Kofuji K, Aoki A, Tsubaki K, Konishi M, Isobe T, Murata Y. Antioxidant activity of β-glucan. ISRN Pharm. 2012; 2012: 125864.
10. da Silva AF, Sartori D, Macedo FC Jr, Ribeiro LR, Fungaro MH, Mantovani MS. Effects of β-glucan extracted from Agaricus blazei on the expression of ERCC5, CASP9, and CYP1A1 genes and metabolic profile in HepG2 cells. Hum Exp Toxicol. 2013; 32(6): 647-654.
11. Madrigal-Bujaidar E, Morales-González JA, Sánchez-Gutiérrez M, Izquierdo-Vega JA, Reyes-Arellano A, Álvarez-González I, et al. Prevention of aflatoxin B□-induced DNA breaks by β-D-glucan. Toxins (Basel). 2015; 7(6): 2145-2158.
12. Oliveira RJ, Salles MJ, da Silva AF, Kanno TY, Lourenço AC, Leite Vda S, et al. In vivo evaluation of the antimutagenic and antigenotoxic effects of β-glucan extracted from Saccharomyces cerevisiae in acute treatment with multiple doses. Genet Mol Biol. 2013; 36(3): 413-424.
13. Queiroz EA, Fortes ZB, da Cunha MA, Barbosa AM, Khaper N, Dekker RF. Antiproliferative and pro-apoptotic effects of three fungal exocellular β-glucans in MCF-7 breast cancer cells is mediated by oxidative stress, AMP-activated protein kinase (AMPK) and the Forkhead transcription factor, FOXO3a. Int J Biochem Cell Biol. 2015; 67: 14-24.
14. Binmama S, Dang CP, Visitchanakun P, Hiengrach P, Somboonna N, Cheibchalard T, et al. Beta-glucan from S. cerevisiae protected AOM-induced colon cancer in cGAS-deficient mice partly through dectin-1-manipulated macrophage cell energy. Int J Mol Sci. 2022; 23(18): 10951.
15. Lagunas-Rangel FA, Bermúdez-Cruz RM. Natural compounds that target DNA repair pathways and their therapeutic potential to counteract cancer cells. Front Oncol. 2020; 10: 598174.
16. Kang HJ, Hong YB, Kim HJ, Wang A, Bae I. Bioactive food components prevent carcinogenic stress via Nrf2 activation in BRCA1 deficient breast epithelial cells. Toxicol Lett. 2012; 209(2): 154-160.
17. Dalmasso B, Puccini A, Catalano F, Borea R, Iaia ML, Bruno W et al. Beyond BRCA: the emerging significance of DNA damage response and personalized treatment in pancreatic and prostate cancer patients. Int J Mol Sci. 2022; 23(9): 4709.
18. Oliveira RJ, Salles MJ, da Silva AF, Kanno TY, Lourenço AC, Freiria GA, et al. Effects of the polysaccharide beta-glucan on clastogenicity and teratogenicity caused by acute exposure to cyclophosphamide in mice. Regul Toxicol Pharmacol. 2009; 53(3): 164-173.
19. Hamesch K, Borkham-Kamphorst E, Strnad P, Weiskirchen R. Lipopolysaccharide-induced inflammatory liver injury in mice. Lab Anim. 2015; 49(1): 37-46.
20. Bradford MM. A rapid and sensitive method for the quantitation of microgram quantities of protein utilizing the principle of protein-dye binding. Anal Biochem. 1976; 7 (72):248-54.
21. Tu H, Zhang ZW, Qiu L, Lin Y, Jiang M, Chia SY et al. Increased expression of pathological markers in Parkinson's disease dementia post-mortem brains compared to dementia with Lewy bodies. BMC Neurosci. 2022; 23(1): 3.
22. El Shawi OE, Abd El-Rahman SS, El Hameed MA. In: Bancroft JD, Gamble M, editors. Theory and practice of histological techniques. 6th Ed. China: Churchill Livingstone, Elsevier; 2008.
23. Kemeleva EA, Sinitsyna OI, Kolosova NG, Vasyunina EA, Zharkov DO, Conlon KA, et al. Immunofluorescent detection of 8-oxoguanine DNA lesions in liver cells from aging OXYS rats, a strain prone to overproduction of free radicals. Mutat Res. 2006; 599(1-2): 88-97.
24. Singh NP, McCoy MT, Tice RR, Schneider EL. A simple technique for quantitation of low levels of DNA damage in individual cells. Exp Cell Res. 1988; 175(1): 184-191.
25. Nebot C, Moutet M, Huet P, Xu JZ, Yadan JC, Chaudiere J. Spectrophotometric assay of superoxide dismutase activity based on the activated autoxidation of a tetracyclic catechol. Anal Biochem. 1993; 214(2): 442-451.
26. Beers RF Jr, Sizer IW. A spectrophotometric method for measuring the breakdown of hydrogen peroxide by catalase. J Biol Chem. 1952; 195(1): 133-140.
27. Ohkawa H, Ohishi N, Yagi K. Assay for lipid peroxides in animal tissues by thiobarbituric acid reaction. Anal Biochem. 1979; 95(2): 351-358.
28. Aisa-Alvarez A, Soto ME, Guarner-Lans V, Camarena-Alejo G, Franco-Granillo J, Martínez-Rodríguez EA, et al. Usefulness of antioxidants as adjuvant therapy for septic shock: a randomized clinical trial. Medicina (Kaunas). 2020; 56(11): 619.
29. Gugliandolo E, Cordaro M, Siracusa R, D'Amico R, Peritore AF, Genovese T, et al. Novel combination of COX-2 inhibitor and antioxidant therapy for modulating oxidative stress associated with intestinal ischemic reperfusion injury and endotoxemia. Antioxidants (Basel). 2020; 9(10): 930.
30. Khan H, Labanca F, Ullah H, Hussain Y, Tzvetkov NT, Akkol EK et al. Advances and challenges in cancer treatment and nutraceutical prevention: the possible role of dietary phenols in BRCA regulation.

Phytochem Rev. 2022; 21: 385–400.
31. Huff MO, Klinge CM, Regulation of gene expression by β-Glucans. Am J Immunol. 2017; 13(1): 1-10.
32. Yong H, Wu G, Chen J, Liu X, Bai Y, Tang N, et al. lncRNA MALAT1 accelerates skeletal muscle cell apoptosis and inflammatory response in sepsis by decreasing BRCA1 expression by recruiting EZH2. Mol Ther Nucleic Acids. 2020; 19: 97-108.
33. Bennett H, Troutman TD, Sakai M, Glass CK. Epigenetic regulation of kupffer cell function in health and disease. Front Immunol. 2021; 11: 609618.
34. Gilmore PM, Quinn JE, Mullan PB, Andrews HN, McCabe N, Carty M, Kennedy RD, Harkin DP. Role played by BRCA1 in regulating the cellular response to stress. Biochem Soc Trans. 2003; 31(Pt 1): 257-262.
35. Singh A, Koduru B, Carlisle C, Akhter H, Liu RM, Schroder K, et al. NADPH oxidase 4 modulates hepatic responses to lipopolysaccharide mediated by Toll-like receptor-4. Sci Rep. 2017; 7(1): 14346.
36. Thakar T, Dhoonmoon A, Straka J, Schleicher EM, Nicolae CM, Moldovan GL. Lagging strand gap suppression connects BRCA-mediated fork protection to nucleosome assembly through PCNA-dependent CAF-1 recycling. Nat Commun. 2022; 13(1): 5323.
37. Tarsounas M, Sung P. The antitumorigenic roles of BRCA1–BARD1 in DNA repair and replication. Nat Rev Mol Cell Biol. 2020; 21(5): 284-299.
38. Gorrini C, Baniasadi PS, Harris IS, Silvester J, Inoue S, Snow B et al. BRCA1 interacts with Nrf2 to regulate antioxidant signaling and cell survival. J Exp Med. 2013; 210(8): 1529-1544.
39. He F, Ru X, Wen T. NRF2, a transcription factor for stress response and beyond. Int J Mol Sci. 2020; 21(13): 4777.
40. Giese EC, Gascon J, Anzelmo G, Barbosa AM, da Cunha MA, Dekker RF. Free-radical scavenging properties and antioxidant activities of botryosphaeran and some other β-D-glucans. Int J Biol Macromol. 2015; 72: 125-130.

Cell J
Cell Journal (Yakhteh)
Homepage: https://www.celljournal.org/
Short Communication
Vol 25, No 9, September 2023, Pages: 655-659

Generation of Mouse Model of Hemophilia A by Introducing Novel Mutations, Using CRISPR/Nickase Gene Targeting System

Mehdi Shamsara, Ph.D.[1], Abbas Jamshidizad, M.Sc.[1], Aidin Rahim-Tayfeh, D.V.M.[1], Maliheh Davari, Ph.D.[2], Ali Rajabi Zangi, Pharm.D.[3], Fatemeh Masoumi, M.Sc.[2], Alireza Zomorodipour, Ph.D.[2]*

1. Department of Animal Biotechnology, Institute Agricultural Biotechnology, National Institute of Genetic Engineering and Biotechnology, Tehran, Iran
2. Department of Molecular Medicine, Institute of Medical Genetics, National Institute of Genetic Engineering and Biotechnology, Tehran, Iran
3. Department of Pharmaceutics, Faculty of Pharmacy, Tabriz University of Medical Sciences, Tabriz, Iran

Abstract

Developing mouse models of hemophilia A has been shown to facilitate *in vivo* studies to explore the probable mechanism(s) underlying the disease and to examine the efficiency of the relevant potential therapeutics. This study aimed to knockout (KO) the *coagulation factor viii* (*fviii*) gene in NMRI mice, using CRISPR/Cas9 (D10A/nickase) system, to generate a mouse model of hemophilia A. Two single guide RNAs (sgRNAs), designed from two distinct regions on NMRI mouse *FVIII* (*mFVIII*) exon 3, were designed and inserted in the pX335 vector, expressing both sgRNAs and nickase. The recombinant construct was delivered into mouse zygotes and implanted into the pseudopregnant female mice's uterus. Mutant mice were identified by genotyping, genomic sequencing, and mFVIII activity assessment. Two separate lines of hemophilia A were obtained through interbreeding the offspring of the female mice receiving potential CRISPR-Cas9-edited zygotes. Genomic DNA analysis revealed disruptions of the *mfviii* gene reading frame through a 22-bp deletion and a 23-bp insertion in two separate founder mice. The founder mice showed all the clinical signs of hemophilia A including; excessive bleeding after injuries, and spontaneous bleeding in joints and other organs. Coagulation test data showed that mFVIII coagulation activity was significantly diminished in the mFVIII knockout ($FVIII_{KO}$) mice compared to normal mice. The CRISPR/nickase system was successfully applied to generate mouse lines with the knockout *fviii* gene. The two novel $FVIII_{KO}$ mice demonstrated all clinical symptoms of hemophilia A, which could be successfully inherited. Therefore, both of the developed $FVIII_{KO}$ mouse lines are eligible for being considered as proper mouse models of hemophilia A for *in vivo* therapeutic studies.

Keywords: CRISPR-Cas9, Factor VIII, Hemophilia A, Knockout Gene, Mouse Models

Citation: **Shamsara M, Jamshidizad A, Rahim-Tayfeh A, Davari M, Rajabi Zangi A, Masoumi F, Zomorodipour A. Generation of mouse model of hemophilia a by introducing novel mutations, using crispr/nickase gene targeting system. Cell J. 2023; 25(9): 655-659. doi: 10.22074/CELLJ.2023.1999800.1278**

Hemophilia A, as an X-linked recessive bleeding disorder, caused by deficiency or dysfunction of coagulation factor VIII (FVIII), is one of the most well-known hereditary disorders (1). Replacement therapy is a common treatment for hemophilia A, done by infusion of either human plasma-derived or recombinant FVIII protein (2, 3). In the continuation of the previous attempts, ongoing efforts have been made to improve hemophilia treatment approaches through the development of upgraded products, cell therapy strategies, and powerful gene delivery vectors (4, 5). In the cases of hemophilia A and other hemorrhagic diseases, animal models facilitate studying the pathophysiology and homeostasis of the blood coagulation cascade and improve the therapeutic methods. Till now, several hemophilic animal models harboring various mutations in the *fviii* gene have been developed, including rat (6, 7), pig (8), dog (9), sheep (10), mouse (11), cow (12), and a transient hemophilic rabbit (13). In the past decade, transgenic mouse models have been added to the animal models of hemophilia (14). Bi et al. (15) reported the development of a mouse line defective in the *fviii* gene and showed that the hemophilia A phenotype in the hemophilic mice is less severe than what is observed in human patients suffering from this disease. Therefore, in light of the fact that mice lacking functional FVIII are able to live a healthy life and present a grade of hemophilic phenotypes, they could be considered suitable models for studies focusing on FVIII activity restoration in hemophilia A. Two well-characterized $fviii_{KO}$ strains of mice have been previously generated by inserting a neo-expression cassette in exons 16 (E16-/- line) and 17 (E17-/- line) of the *fviii* gene (15, 16), which are currently being used extensively in hemophilia A studies (17). The classical approach for

Received: 11/April/2023, Revised: 08/June/2023, Accepted: 18/June/2023
***Corresponding Address: P.O.Box: 161/14965, Department of Molecular Medicine, Institute of Medical Genetics, National Institute of Genetic Engineering and Biotechnology, Tehran, Iran**
Email: zomorodi@nigeb.ac.ir

Royan Institute
Cell Journal (Yakhteh)

gene knockout was based on homologous recombination-based techniques (18, 19). With the advent of a nuclease-based method for genome editing, named clustered regularly interspaced short palindromic repeats/Cas9 (CRISPR/Cas9), it is now possible to create animal models more simply and in a considerably shorter time (20). An improvement in this technique was the development of a modified version of Cas9, namely Cas9(D10A) or Nickase, to reduce the nonspecific incisions, referred to as off-target. Nikase can only produce single-stranded breaks in the targeted genomic DNA, reducing the rate of off-targets. However, it requires two guide RNAs simultaneously, to finally introduce breaks in both DNA strands (21). This study aimed to generate an NMRI mouse model of hemophilia A by targeting mouse *fviii* (*mfviii*) exo3 and consequently knocking out the *mfviii* gene utilizing CRISPR/Nickase editing system.

Normal 4-week-old male and female NMRI mice were purchased from the Pasteur Institute of Iran and housed in standard animal rooms equipped with proper air-conditioning systems, regular 12 hour-cycles of light and dark, and free access to food and water. All animal experiments were performed in accordance with the institutional guidelines and the standard protocols approved by the Ethic (Animal Care and Use) Committee of NIGEB (IR.NIGEB.EC.1401.12.14.C).

Before designing the gRNAs, the probable genetic variations in the desired target site located in mFVIII exon 3 among NMRI mice were examined. To do this, genomic DNAs were extracted from three NMRI mice's tails according to available standard protocols. DNA samples were then used as PCR templates to amplify a 631-bp fragment including the target site in mFVIII exon 3 using a specific primer pair (Table S1, See Supplementary Online Information at www.celljournal.org). Next, PCR products were sequenced by ABI 373A Applied Biosystems automated DNA sequencer (MWG-Germany).

To design gRNAs, the sequence of the *mfviii* gene (Accession number: NC_000086) was obtained from Genbank (NCBI) and then two short guide RNA (sgRNA) oligonucleotides were designed by using the CRISPOR website (http://crispor.tefor.net/) to target parts of exon 3 of the *mfviii* gene (Table S1, See Supplementary Online Information at www.celljournal.org). Two gRNA fragments were cloned into a region flanked by restriction sites of BbsI enzyme on the pX335-U6-Chimeric_BB-CBh-hSpCas9n (hereinafter pX335) vector (Addgene ID # 42335).

To knock out the *mfviii* gene, superovulated normal female NMRI mice (4 weeks old) were mated to NMRI males, and the fertilized oocytes were collected from oviducts. The recombinant vectors were mixed at 4 ng/µl concentration and injected into the male pronucleus of the fertilized zygotes (Fig.S1, See Supplementary Online Information at www.celljournal.org). The microinjected zygotes were then incubated in M16 medium at 37°C for 1 hour. The surviving oocytes were transferred to the oviduct of pseudopregnant female NMRI mice (foster mother) at 12 hours post-coitus.

To detect the introduced CRISPR-mediated mutations in the *mfviii* gene, genomic DNA samples were isolated from finger biopsies obtained from mouse pups aged 2-3 weeks old. The *mfviii* target site of gRNAs was amplified by PCR using specific primers (Mutfviii primers) flanking a 259-bp fragment containing the target site and then visualized by agarose gel electrophoresis. The genotypes of the mice were determined by sequencing the PCR products amplified from the genomic DNAs of both normal and mutant mice, using ABI 373A Applied Biosystems automated DNA sequencer (MWG-Germany).

The coagulation activity of the mFVIII in the mouse serum was measured by the activated partial thromboplastin time (APTT) method, using the COATEST SP4 FVIII kit (Chromogenic, Bedford, MA), as previously described by Chao et al. (22). The FVIII-deficient plasma pool (HRF Inc., Raleigh, NC), needed for the FVIII assay, contained <0.4% FVIII. Normal mouse plasma was considered as a standard sample with 100% activity equal to 1 IU/ml mFVIII.

To exclude any possible polymorphic regions in the gRNA design, a 631-bp fragment of the *mfviii* gene covering exon 3 was amplified and sequenced from three randomly selected NMRI mice (Fig.S2A, B, See Supplementary Online Information at www.celljournal.org). The multiple sequence alignment data showed no nucleotide difference among the sequenced fragments (Fig.S2C, See Supplementary Online Information at www.celljournal.org). The nucleotide BLAST analysis also showed a complete match between the sequenced fragments and the recorded sequence in NCBI GenBank as the reference sequence.

In order to generate $mFVIII_{KO}$ mice, two gRNAs were designed using CRISPOR tool to target exon 3 of the *mfviii* gene. The gRNA fragments were separately cloned between the *Bsb*I sites of the pX335 vector and were confirmed by sequencing (Fig.S3A, B, See Supplementary Online Information at www.celljournal.org). The fertilized oocytes were injected with the recombinant vectors encoding both gRNAs and nickase. The surviving oocytes were transferred into the oviduct of pseudopregnant females, resulting in 67 newborns. The sequencing data of the target region on the *fviii* gene detected 7 mutant mice (Fig.1A). The mutants mainly carried deletions, as insertion was detected only in one mouse. Two out of seven *fviii*-mutant mice, including +23 and -22 founders, carried the frameshift mutations. The first founder (designated as +23) was a heterozygous female. As shown in Figure 1B (lane +/-), three distinct bands were amplified by PCR, where the bottom band corresponds to wild type, the middle band corresponds to mutant and the upper band was the hybrid of wild type and mutant strands. Sequencing of the middle band detected a 23-bp insertion in one of the *mfviii* alleles (Fig.1A). Crossing of the +23 founder with a normal male resulted in a hemophilic male in the F1 generation, demonstrated by PCR (Fig.1B). The second founder (designated as

-22) was again a female with a heterozygous pattern of *fviii* alleles (Fig.1C, lane +/). Crossing this founder with normal males resulted in the transfer of defective genes to half of the F1 males (25% of offspring) (Fig.1C, lane Y/-). The inheritances of the mutant alleles for each mutant were verified by sequencing of target regions of the F1 males (Fig.1D).

One of the most problematic symptoms, which occur in hemophilic patients is spontaneous bleeding in the joints. The hemophilia males displayed hemarthrosis (joint bleeding) occasionally in their hip and toe joints (Fig.2).

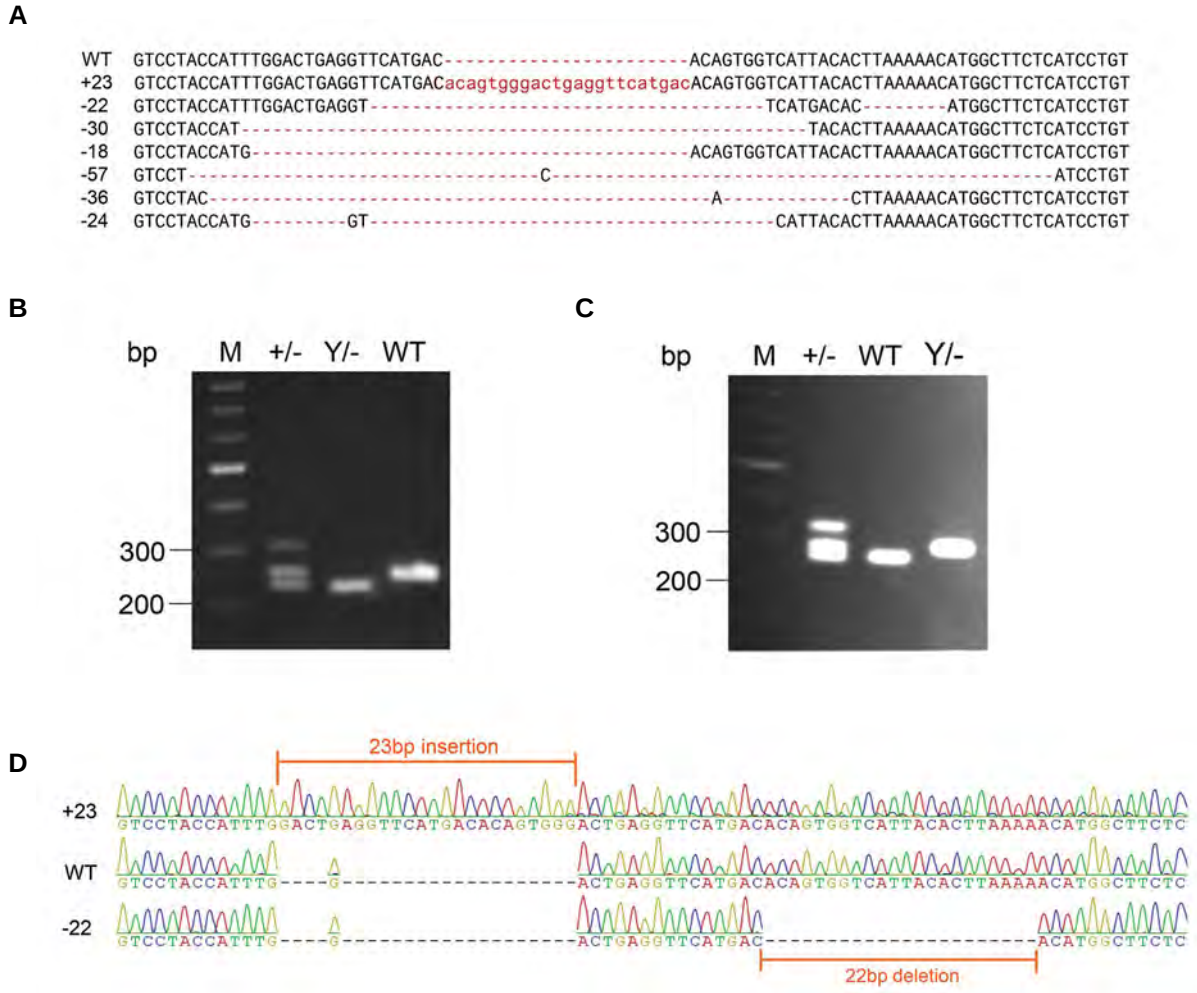

Fig.1: The genotypes of the mutant mice, determined by sequencing the PCR products from the genomic DNAs. **A.** Multiple sequence alignments of mutant mice. PCR followed by sequencing detected 7 mutants. Indel mutations were detected in the mutants. **B.** The PCR product, obtained from the genomic DNA, of the mutant mouse with a 22-bp deletion at the target site of the *mfviii* gene. **C.** The PCR product, obtained from the genomic DNA, of the mutant mouse with a 23-bp insertion at the target site of the *mfviii* gene. **D.** Genotyping of F1 generation mice from both female founders verified the inheritance of the mutant alleles in the male offspring. PCR; Polymerase chain reaction, +/-; Heterozygous female, Y/-; Hemophilic male, and WT; Wild-type mouse.

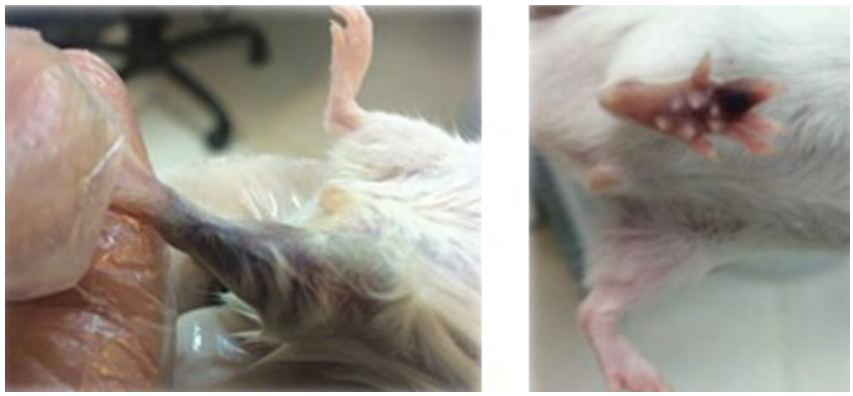

Fig.2: Hemorrhage in the joints of hemophilic males.

The effects of the mutations in the $FVIII_{KO}$ mice were first studied *in silico*. Accordingly, the computational translation of transcripts of both of the mutant alleles produced truncated polypeptides. In this regard, in the first mutant mouse the allele interrupted with a 22-bp deletion encoded a 153-amino acid polypeptide instead of the full-length protein. In the second mutant, the allele was disrupted by a 23-bp insertion and produced a defective protein of 168 amino acids. Both proteins were much shorter than the full-length protein to have a normal function (Fig.3A). The activity of the FVIII protein was experimentally assayed in the plasma of male mice using a coagulation test (Fig.3B). The results showed a significant decline in the mFVIII coagulation activities in the plasma samples derived from $FVIII_{KO}$ mice, compared to that in the normal mouse plasma.

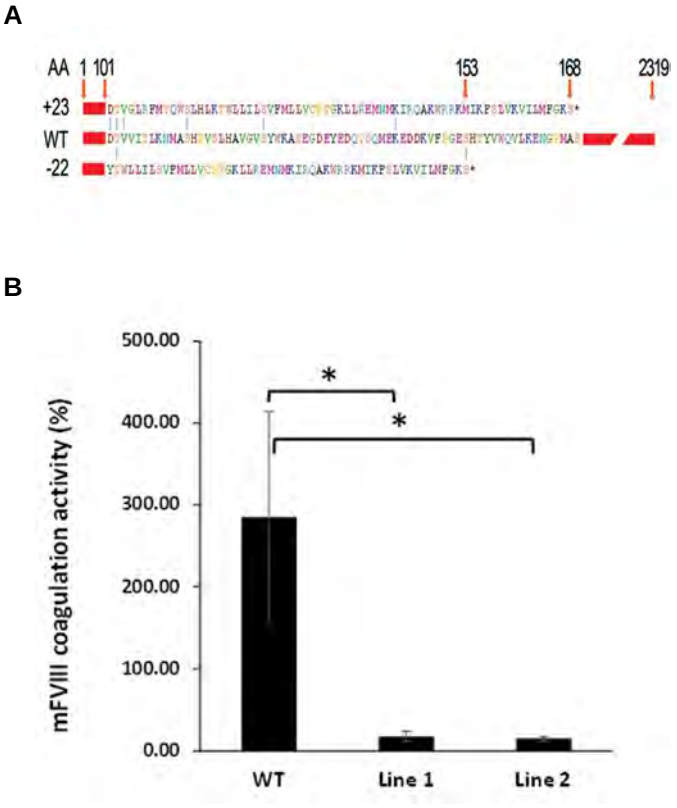

Fig.3: *In silico* and experimental evaluation of mFVIII fate as a result of mutations. **A.** *In silico* data showed that the indel mutations lead to the translation of mutant genes to truncated FVIII proteins. The 23-bp insertion resulted in a 168-aa polypeptide and the 22-bp deletion led to the production of a 153-aa protein. **B**. FVIII coagulation test (lines 1 and 2 corresponding to mutants 1 and 2, respectively) and wild type. Asterisks indicate samples that are significant differences (P<0.05), compared to wildtype.

In this work, we considered the mouse as an appropriate animal to develop a hemophilia A model. It has been known that male mice with FVIII deficiency continue to survive well and are eligible for studies dealing with FVIII correction and other in vivo therapies (15). The present hemophilia A model has been generated using CRISPR/Cas9 (nickase) tool. The previous hemophilia A mouse models, including exon 16 or exon 17 knockout models, have been generated by conventional gene targeting approaches (23). In 2016, a genetically engineered mouse model of hemophilia A was developed by complete deletion of the the *fviii* gene using the cre-loxp recombination technique (22). A recently published study reported the application of CRISPR/Cas9 in the generation of hemophilia A model via inversion of intron 22 of the *fviii* gene. In our study, the third exon of the *fviii* gene has been targeted by microinjection of all-in-one plasmids harboring both Cas9 (D10A) and sgRNAs. The mFVIII protein start site, located in exon 3, has not been already used as a target site for the generation of hemophilia A mice. When this site is disrupted, it is basically expected that the *fviii* gene to be knocked out (24). Besides, the occurrence of mutations in the *FVIII* exon 3 has been detected in several patients suffering from hemophilia A (25, 26). According to literature, the use of nickase enhances the specificity of genome editing (27). Moreover, the advantages of genome editing approaches, such as high efficiency and ease of use, in development of new animal models have been previously discussed.

Following the gRNA design and construction of the CRISPR/nickase-based gRNA expressing vectors, microinjection of the mouse fertilized oocytes with the recombinant vectors, followed by transfer of the injected oocytes into the oviduct of pseudopregnant female (recipient foster mothers) mice, successfully resulted in 67 newborns. Genotyping of the target regions of the *fviii* gene in the 67 newborns led to the detection of 7 mutant offspring. The mice bearing frameshift mutations were subjected to further analyses. The mating of two female founder mice with wild-type males resulted in mutant offspring. The results from genome analysis revealed a 22-bp deletion in the *fviii* gene in the first founder mouse and a 23-bp insertion in the other one. A coagulation test performed on the sera of the male newborn mice in the F1 generation of both founder mice showed a significant difference in the coagulation activity of FVIII compared to that in normal mice. Furthermore, our genotyping analyses revealed that the developed mice carry $fviii_{ko}$ genes and are capable of transferring the defective gene to the next generation. The stability of hemophilia A pathology has been consistently established in the consecutive generations of the two mouse models, considering both genotypic and phenotypic traits. The data achieved from the current study represents that the production of mouse models of hemophilia A using CRISPR/Cas technology is a more efficient, cost-effective, and time-saving method compared to conventional techniques. The development of hemophilia A mice in this work have provided valuable resources as non-human hemophilia A models to conduct *in vivo* studies with different therapeutic approaches, to develop new potential treatments for patients with hemophilia A.

Acknowledgments

This work was financially supported by a grant from the Stem Cell Development Headquarters under the

supervision of the Vice President of Science and Technology of Iran and grant number 419 from the National Institute of Genetic Engineering and Biotechnology-Iran. We are also grateful to our late colleague, Dr. Maryam Kabirsalmani, for her unwavering supports and encouragements. There is no conflict of interest in this study.

Authors' Contributions

A.Z., M.Sh., A.J.; Conceptualization, Methodology, and Software. A.Z, M.Sh., M.D.; Data curation, Data Analysis, and original draft preparation. A.R.-T., A.Z., M.D., F.M.; Imaging and Data collection. A.Z, M.Sh., M.D.; Writing- reviewing and Editing. All authors have read and approved the final manuscript.

References

1. De Brasi CD, Slavutsky IR, Larripa IB. Genética molecular de la hemofilia A [Molecular genetics of hemophilia A]. Medicina (B Aires). 1996; 56(5 Pt 1): 509-517.
2. Cafuir LA, Kempton CL. Current and emerging factor VIII replacement products for hemophilia A. Ther Adv Hematol. 2017; 8(10): 303-313.
3. Kaufman RJ, Dorner AJ, Fass DN. von Willebrand factor elevates plasma factor VIII without induction of factor VIII messenger RNA in the liver. Blood. 1999; 93(1): 193-197.
4. Batty P, Lillicrap D. Hemophilia gene therapy: approaching the first licensed product. Hemasphere. 2021; 5(3): e540.
5. Luo L, Zheng Q, Chen Z, Huang M, Fu L, Hu J, et al. Hemophilia a patients with inhibitors: Mechanistic insights and novel therapeutic implications. Front Immunol. 2022; 13: 1019275.
6. Booth CJ, Brooks MB, Rockwell S, Murphy JW, Rinder HM, Zelterman D, et al. WAG-F8(m1Ycb) rats harboring a factor VIII gene mutation provide a new animal model for hemophilia A. J Thromb Haemost. 2010; 8(11): 2472-2477.
7. Nielsen LN, Wiinberg B, Häger M, Holmberg HL, Hansen JJ, Roepstorff K, et al. A novel F8 -/- rat as a translational model of human hemophilia A. J Thromb Haemost. 2014; 12(8): 1274-1282.
8. Kashiwakura Y, Mimuro J, Onishi A, Iwamoto M, Madoiwa S, Fuchimoto D, et al. Porcine model of hemophilia A. PLoS One. 2012; 7(11): e49450.
9. Notley C, Killoran A, Cameron C, Wynd K, Hough C, Lillicrap D. The canine factor VIII 3'-untranslated region and a concatemeric hepatocyte nuclear factor 1 regulatory element enhance factor VIII transgene expression in vivo. Hum Gene Ther. 2002; 13(13): 1583-1593.
10. Porada CD, Sanada C, Long CR, Wood JA, Desai J, Frederick N, et al. Clinical and molecular characterization of a re-established line of sheep exhibiting hemophilia A. J Thromb Haemost. 2010; 8(2): 276-285.
11. Bi L, Lawler AM, Antonarakis SE, High KA, Gearhart JD, Kazazian HH Jr. Targeted disruption of the mouse factor VIII gene produces a model of haemophilia A. Nat Genet. 1995; 10(1): 119-121.
12. Healy PJ, Sewell CA, Exner T, Morton AG, Adams BS. Haemophilia in hereford cattle: factor VIII deficiency. Aust Vet J. 1984; 61(4): 132-133.
13. Turecek PL, Gritsch H, Richter G, Auer W, Pichler L, Schwarz HP. Assessment of bleeding for the evaluation of therapeutic preparations in small animal models of antibody-induced hemophilia and von Willebrand disease. Thromb Haemost. 1997; 77(3): 591-599.
14. Øvlisen K, Kristensen AT, Tranholm M. In vivo models of haemophilia - status on current knowledge of clinical phenotypes and therapeutic interventions. Haemophilia. 2008; 14(2): 248-259.
15. Bi L, Sarkar R, Naas T, Lawler AM, Pain J, Shumaker SL, et al. Further characterization of factor VIII-deficient mice created by gene targeting: RNA and protein studies. Blood. 1996; 88(9): 3446-3450.
16. Sarkar R, Gao GP, Chirmule N, Tazelaar J, Kazazian HH Jr. Partial correction of murine hemophilia A with neo-antigenic murine factor VIII. Hum Gene Ther. 2000; 11(6): 881-894.
17. Sabatino DE, Nichols TC, Merricks E, Bellinger DA, Herzog RW, Monahan PE. Animal models of hemophilia. Prog Mol Biol Transl Sci. 2012; 105: 151-209.
18. Austin CP, Battey JF, Bradley A, Bucan M, Capecchi M, Collins FS, et al. The knockout mouse project. Nat Genet. 2004; 36(9): 921-924.
19. Gama Sosa MA, De Gasperi R, Elder GA. Animal transgenesis: an overview. Brain Struct Funct. 2010; 214(2-3): 91-109.
20. Dow LE. Modeling disease in vivo with CRISPR/Cas9. Trends Mol Med. 2015; 21(10): 609-621.
21. Ge XA, Hunter CP. Efficient homologous recombination in mice using long single stranded DNA and CRISPR Cas9 nickase. G3 (Bethesda). 2019; 9(1): 281-286.
22. Chao BN, Baldwin WH, Healey JF, Parker ET, Shafer-Weaver K, Cox C, et al. Characterization of a genetically engineered mouse model of hemophilia A with complete deletion of the F8 gene. J Thromb Haemost. 2016; 14(2): 346-355.
23. Yen CT, Fan MN, Yang YL, Chou SC, Yu IS, Lin SW. Current animal models of hemophilia: the state of the art. Thromb J. 2016; 14 Suppl 1: 22.
24. Chao BN, Baldwin WH, Healey JF, Parker ET, Shafer-Weaver K, Cox C, et al. Characterization of a genetically engineered mouse model of hemophilia A with complete deletion of the F8 gene. J Thromb Haemost. 2016; 14(2): 346-355.
25. Hall B, Limaye A, Kulkarni AB. Overview: generation of gene knockout mice. Curr Protoc Cell Biol. 2009; Chapter 19: Unit 19.12 19.12.1-17.
26. Santacroce R, Acquila M, Belvini D, Castaldo G, Garagiola I, Giacomelli SH, et al. Identification of 217 unreported mutations in the F8 gene in a group of 1,410 unselected Italian patients with hemophilia A. J Hum Genet. 2008; 53(3): 275-284.
27. Ran FA, Hsu PD, Lin CY, Gootenberg JS, Konermann S, Trevino AE, et al. Double nicking by RNA-guided CRISPR Cas9 for enhanced genome editing specificity. Cell. 2013; 154(6): 1380-1389.

Cell J
Cell Journal (Yakhteh)
Homepage: https://www.celljournal.org/
Short Communication
Vol 25, No 9, September 2023, Pages: 660-664

Age-Related Skin Inflammation in A 2,4-Dintrochlorobenzene-Induced Atopic Dermatitis Mouse Model

Kyung-Ah Cho, Ph.D., Jiyun Kwon, M.S., Hyeon Ju Kim, M.S., So-Youn Woo, Ph.D.*

Department of Microbiology, College of Medicine, Ewha Womans University, Seoul, Republic of Korea

Abstract

One of the most affected aspects of the aging process is immunity, with age-related immune system decline being responsible for an increase in susceptibility to infectious diseases and cancer risk. On the other hand, the aging process is accompanied with low-grade pro-inflammatory status. This condition involves a persistent rise in cytokine levels that can activate both innate and adaptive immune systems. Finally, despite the fact that immunological responses to antigenic stimulations decrease with age, the incidence and prevalence of many common autoimmune diseases increase in the elderly population. Overall, the co-existence of a prolonged, low-grade inflammatory status and declining immune activity appears to be a paradoxical phenomenon. This study characterized skin inflammation in mouse dermatitis model of various ages to monitor possible changes of inflammatory responses during aging.

Keywords: Aging, Dermatitis, Immune System, Inflammation

Citation: Cho KA, Kwon JY, Kim HJ, Woo SY. Age-related skin inflammation in a 2,4-dintrochlorobenzene-induced atopic dermatitis mouse model. Cell J. 2023; 25(9): 660-664. doi: 10.22074/CELLJ.2023.2001403.1301

The aging process is accompanied with low-grade pro-inflammatory status (1). Inflammation is essential to health, helping organisms fight with the invasion of pathogens and playing essential roles in organ repair and maintenance (2, 3). Transient inflammation that increases when needed and decreases when no longer necessary is not associated with long-term adverse consequences. However, prolonged inflammation due to the intrinsic immune system dysregulation or the presence of a persistent inflammatory reaction trigger can result in accumulated damage that eventually manifests as pathology (3). Inflammation is accompanied by elevated levels of cytokines that are capable of activating both the innate and adaptive immune systems. On the other hand, aging of the immune system is termed immunosenescence (4). This phenomenon results in the remodeling of lymphoid organs, leading to immune dysfunction among elderly (5). Moreover, this age-related immune system decline affects both innate and adaptive arms of the immune system (6) and increases susceptibility to infections as well as the risk of cancer (7). In addition, the incidence and prevalence of many common autoimmune diseases such as rheumatoid arthritis and systemic lupus erythematosus increase among older population, despite declining immunologic responses to antigenic stimuli (8). This might be due to prolonged low grade inflammation that is a common characterization of aging. This state of chronic inflammation that correlates with aging is sometimes referred to as "inflamm-aging" and is a strong risk factor for the occurrence, progression, and complications of many chronic diseases (9). Overall, the co-existence of a prolonged, low-grade inflammation and weak immune activity appears to be a paradoxical phenomenon in elderly (10).

Our study is one of the first studies aimed to analyze immune characteristics associated with aging in a mouse model of dermatitis. We used antigenic stimulation to induce skin inflammation, mimicking atopic dermatitis (AD), and expanded our immunological analysis to the adaptive immunity. AD, a chronic and persistent inflammatory disease of the skin, which is characterized by eczema lesions and itching, has become a serious health problem (11-13).

To induce an AD-like condition in mice, we used the cutaneous application of 2,4-dinitrochlorobenzene (DNCB). DNCB is a chemical substance that causes chronic contact dermatitis and is widely used in human studies of AD (14-17). Mechanistically, it is generally thought that upon topical application, DNCB can complex with various skin proteins to form covalent conjugates and thereby function as immunogen(s) that activate local APCs, such as skin Langerhans cells, dermal dendritic cells, macrophages, and T cells (18-20). Approximately twenty-four hours after subsequent exposures to DNCB (often referred to as "challenges"), the visible inflammatory symptoms begin to appear (21). Thus, DNCB is a useful chemical to simply mimic AD-

Received: 02/May/2023, Revised: 01/July/2023, Accepted: 01/August/2023
*Corresponding Address: Department of Microbiology, College of Medicine, Ewha Womans University, Seoul, Republic of Korea
Email: soyounwoo@ewha.ac.kr
Royan Institute
Cell Journal (Yakhteh)

like skin dermatitis.

Specifically, 7-, 25-, and 39-week-old C57BL/6 mice (n=5/each group) were sensitized by topical application of 1% DNCB dissolved in an acetone: olive oil mixture (4:1 vol/vol) on the shaved back skin for 3 consecutive days. After 5 days, 1% DNCB dissolved in a PBS :olive oil mixture (9:1 vol/vol) was applied to the back skin for 2 consecutive days. Normal control mice were treated with the vehicle. A variety of mouse ages were adopted to compare the responses based on aging. All procedures were approved by the Ewha Womans University College of Medicine Animal Care and Use Committee (EWHA MEDIACUC 22-008-t). The day after the last application of DNCB or vehicle, the mice were sacrificed and their skin and spleen tissues were collected. On day 9, the dorsal skin of the mice sensitized with DNCB showed prominent erythema, edema, excoriation, and scaling/dryness compared with the dorsal skin of the mice treated with vehicle, indicating that DNCB efficiently induced an AD-like phenotype (Fig.1A). Although the visible extent of skin inflammation appeared similar across the different age groups, the oldest DNCB-treated mice had a higher mortality rate than the younger DNCB-treated mice, 7 weeks old DNCB-treated mice and 25 weeks old NDCB-treated mice, which was correlated with the extent and duration of weight loss, as shown in Figure 1B, C. The oldest DNCB-treated group (n=5) experienced greater than 20% weight loss, whereas the other DNCB-treated mice (7 and 25 weeks of age, n=5/each group) experienced less than 10% weight loss. Differences in body weight recovery were also noted across age groups. The 7 weeks old DNCB-treated mice regained their previous body weight more rapidly than the 25 weeks old DNCB-treated mice and 39 weeks old DNCB-treated mice. 25 weeks old DNCB-treated mice and 39 weeks old DNCB-treated mice revealed similar rate of regaining their basal weights (Fig.1C).

Histological examination of hematoxylin and eosin (H&E)-stained sections from the AD-like skin lesions obtained from DNCB-treated mice revealed epidermal and dermal hyperplasia, reflecting a hyper proliferative state compared with skin sections obtained from vehicle-treated mice. Also, hyperkeratosis and parakeratosis were observed in skin sections from DNCB-treated mice regardless of their age (Fig.2A). We observed the dermal accumulation of mast cells via toluidine blue stain in DNCB-treated mice at all ages and compared them to the vehicle-treated control mice, with the oldest mice showing the highest level of accumulation (Fig.2B, C). We further observed $CD3^+$ T cell infiltration in AD-like skin lesions by immunohistochemistry using anti-mouse CD3 antibody (Santa Cruz Biotechnology Inc., USA).

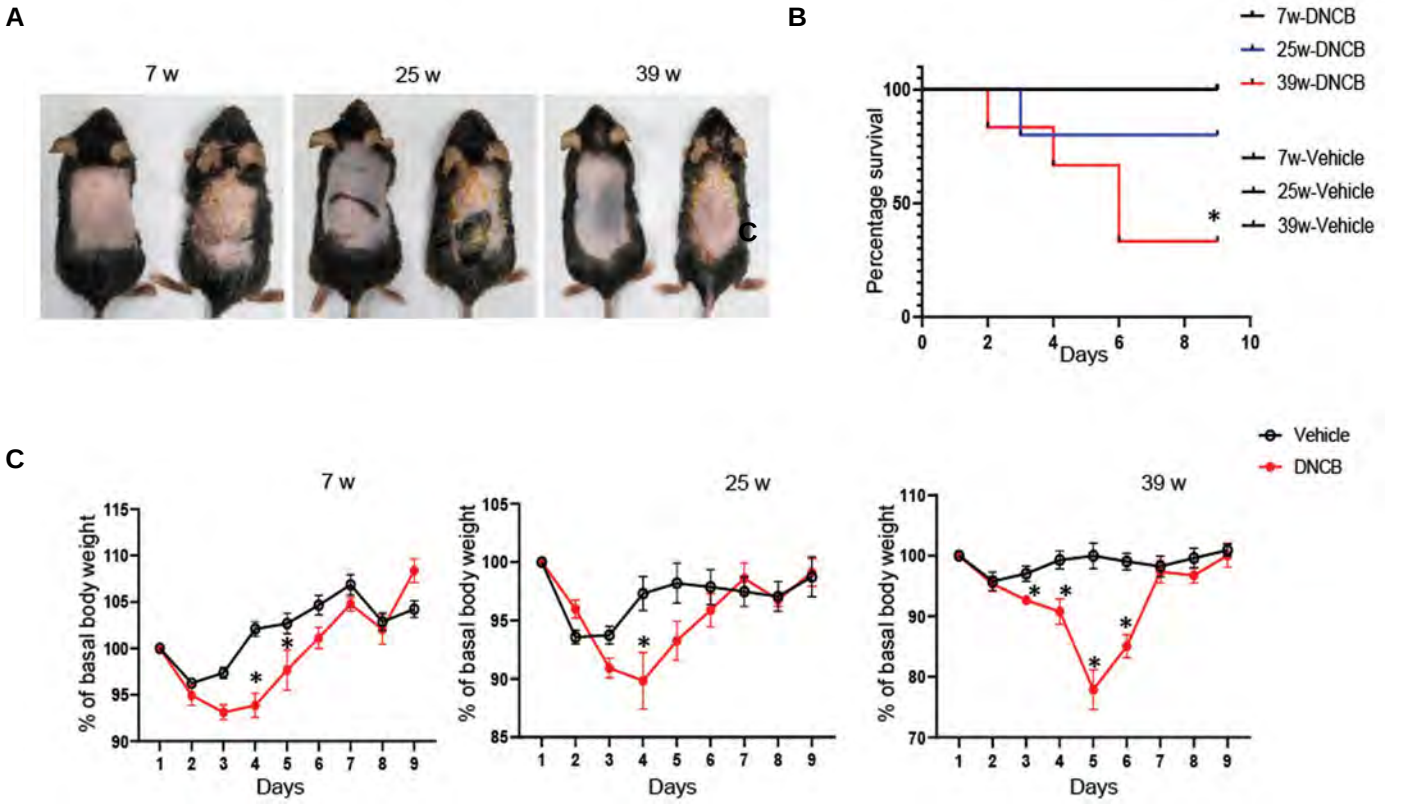

Fig.1: Survival course and weight change in DNCB-induced AD mice model at different ages. **A.** The back skins of vehicle-treated control mouse (left) and DNCB-treated mouse (right) at each age group are shown. Photographs were taken on the 10th day following drug administration from mice in each age group. **B.** Survival course of the experimental groups was measured using the Kaplan-Meier estimator and compared using log-rank test (*; P<0.05). The survival rate of 39wk-DNCB group was significantly low in comparison with 7wk-DNCB group. **C.** Total body weight of the experimental mice was monitored over the study duration. Basal body weight was determined as weight at the beginning of the experiments. Statistical analysis was performed by two-way ANOVA and data are presented as the mean ± SEM. DNCB; 2,4-dinitrochlorobenzene, AD; Atopic dermatitis, *; P<0.05 was considered significant, and w; Week.

Interestingly, the oldest DNCB-treated mice displayed the highest amount of accumulated $CD3^+$ T cells in inflammatory skin lesions across all ages, particularly in areas characterized by hyperkeratosis and parakeratosis (Fig.3A, B). Next, we measured the splenic expression of CD3 in each experimental mouse via quantitative reverse transcription-polymerase chain reaction using a StepOnePlus instrument (Applied Biosystems, USA) to investigate whether the increased expression of CD3 in the skin tissue is associated with an expression in CD3 in the spleen.

As shown in Figure 4, DNCB treatment led to decreased CD3 expression at all ages compared with that in the vehicle treatment group. Our results proposed age-dependent dynamics of immune cells, including T cells and mast cells, under certain inflammatory conditions. It is thought that the pathogenesis of DNCB-induced AD-like skin inflammation is predominantly the result of T cell-mediated immune responses (18). In our study, we also observed accumulation of T cells in the skin of mice treated with DNCB, and this phenomenon was particularly prominent in the oldest mice. Specifically, the decreased expression of CD3 in the spleen suggests that T cells may have migrated to the skin. These results suggest that DNCB treatment induces activation and migration of T cells, particularly eliciting a stronger response in the immune system of aged mice. Characterizing T cell infiltration in skin lesions and their effects on inflammatory processes may contribute toward identifying specific immune networks that are altered during aging. Although immunosenescence is thought to accompany aging, our results showed an active immune response in aged mice, which might be associated with mortality. If we can understand immune cell dynamics during aging, we may be able to support appropriate immune responses.

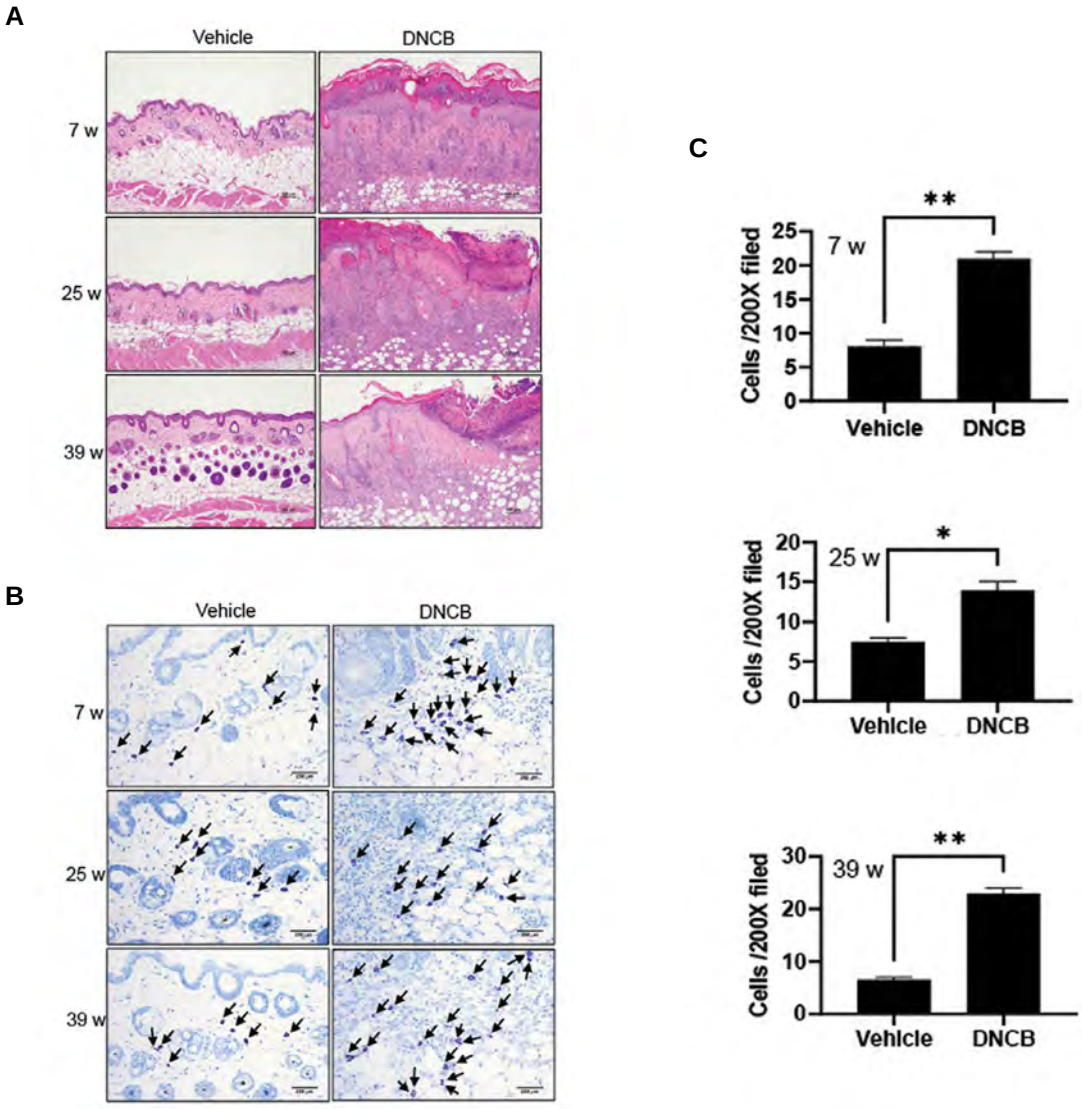

Fig.2: Histological characteristics of DNCB-induced AD mice model at different ages. **A.** H&E-stained sections of the back skin from vehicle- or DNCB-treated mice at each age. **B.** Toluidine blue-stained sections of the back skin sections from vehicle- or DNCB-treated mice at each age showed different amounts of mast cells in the dermis, as indicated by the arrowheads. Fields were taken using the Olympus DP71 and the DP controller software (Tokyo, Japan). **C.** Dermal mast cells from each experimental mouse were counted in toluidine blue-stained sections. Statistical significance was determined by t test and data are presented as the mean ± SEM. DNCB; 2,4-dinitrochlorobenzene, AD; Atopic dermatitis, w; Week, *; P<0.05, and **; P<0.01.

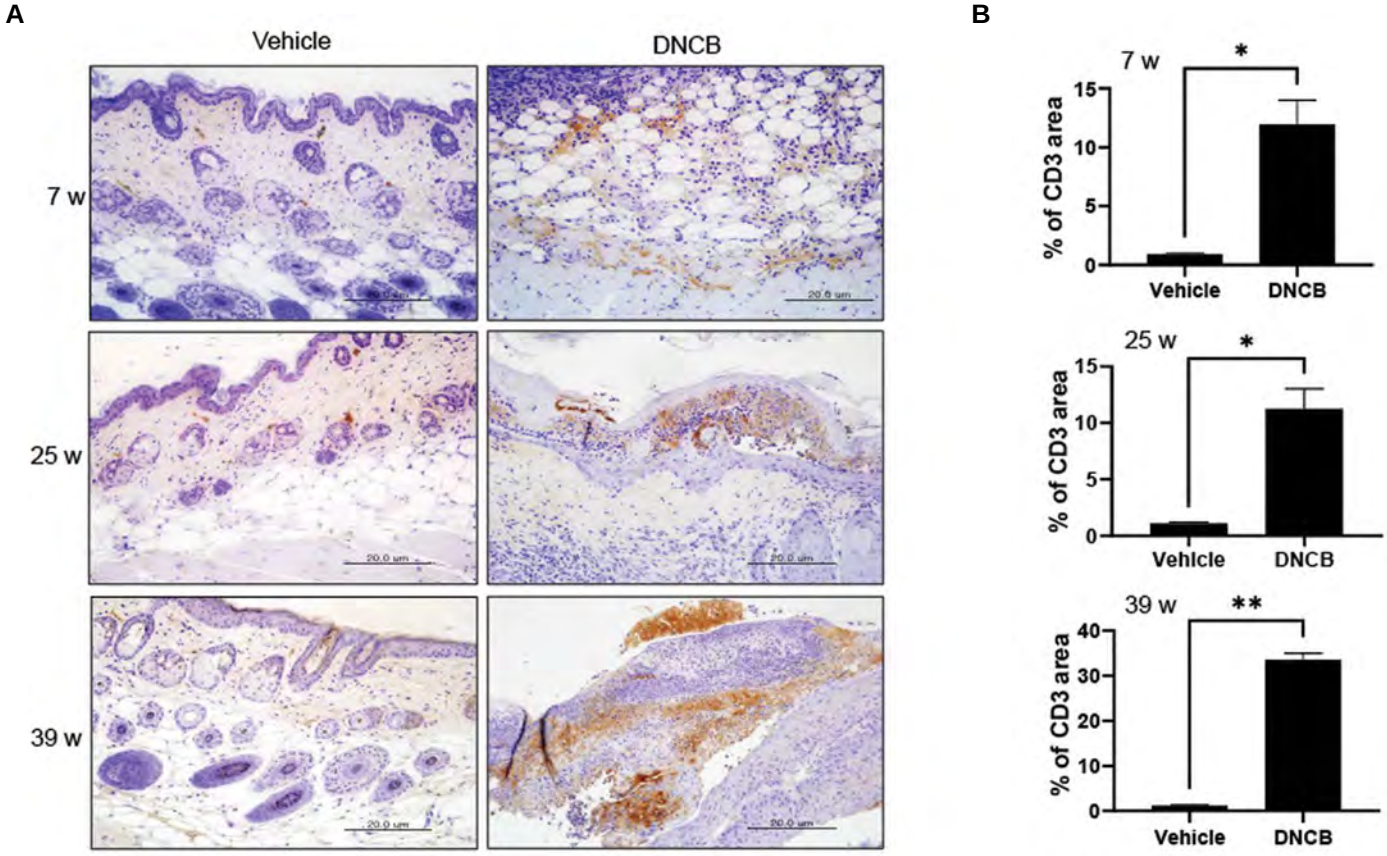

Fig.3: The skin expression of CD3 in DNCB-induced AD mice model at different ages. **A.** Immuno-histochemical staining for CD3 was performed on the posterior skin of control vehicle- and DNCB-treated mice (n=5/each group) to compare the accumulation of T cells (scale bar: 200 µm). **B.** The quantitative analysis of CD3 staining was performed using ImageJ program and statistical significance was determined by t test. DNCB; 2,4-dinitrochlorobenzene, AD; Atopic dermatitis, w; Week, *; P<0.05, and **; P<0.01.

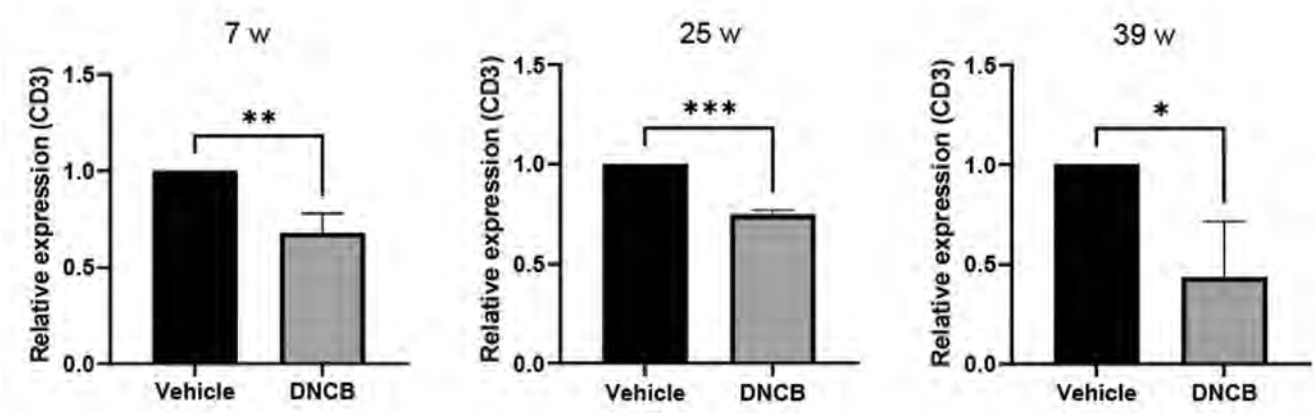

Fig.4: The spleen tissue from each experimental mouse was collected and mRNA expression of CD3 was analyzed by real time-quantitative polymerase chain reaction (RT-PCR). Statistical significance was determined by t test and data are presented as the mean ± SEM. DNCB; 2,4-dinitrochlorobenzene, w; Week, *; P<0.05, **; P<0.01, and ***; P<0.001.

Acknowledgments

This research was supported by Basic Science Research Program through the National Research Foundation of Korea (NRF), funded by the Ministry of Education (grant numbers NRF-2022R1I1A1A01066175 and NRF-2021R1A2C1012551). There is no conflict of interest in this study.

Authors' Contributions

K.-A.C.; Performed the experiments and wrote the

manuscript. J.Y.K., H.J.K.; Performed the experiments and analyzed data. S.-Y.W.; Designed the experiments and wrote the manuscript. All authors have read and agreed to the published version of the manuscript.

References

1. Neves J, Sousa-Victor P. Regulation of inflammation as an anti-aging intervention. FEBS J. 2020; 287(1): 43-52.
2. Medzhitov R. Inflammation 2010: new adventures of an old flame. Cell. 2010; 140(6): 771-776.
3. Chen L, Deng H, Cui H, Fang J, Zuo Z, Deng J, et al. Inflammatory responses and inflammation-associated diseases in organs. Oncotarget. 2017; 9(6): 7204-7218.
4. Lee KA, Flores RR, Jang IH, Saathoff A, Robbins PD. Immune senescence, immunosenescence and aging. Front Aging. 2022; 3: 900028.
5. Yousefzadeh MJ, Flores RR, Zhu Y, Schmiechen ZC, Brooks RW, Trussoni CE, et al. An aged immune system drives senescence and ageing of solid organs. Nature. 2021; 594(7861): 100-105.
6. Ponnappan S, Ponnappan U. Aging and immune function: molecular mechanisms to interventions. Antioxid Redox Signal. 2011; 14(8): 1551-1585.
7. Lian J, Yue Y, Yu W, Zhang Y. Immunosenescence: a key player in cancer development. J Hematol Oncol. 2020; 13(1): 151.
8. Ray D, Yung R. Immune senescence, epigenetics and autoimmunity. Clin Immunol. 2018; 196: 59-63.
9. Bektas A, Schurman SH, Sen R, Ferrucci L. Aging, inflammation and the environment. Exp Gerontol. 2018; 105: 10-18.
10. Fulop T, Larbi A, Dupuis G, Le Page A, Frost EH, Cohen AA, et al. Immunosenescence and inflamm-aging as two sides of the same coin: friends or foes? Front Immunol. 2018; 8: 1960.
11. Legat FJ. Itch in atopic dermatitis - What is new? Front Med (Lausanne). 2021; 8: 644760
12. Kapur S, Watson W, Carr S. Atopic dermatitis. Allergy Asthma Clin Immunol. 2018; 14(Suppl 2): 52.
13. Nomura T, Wu J, Kabashima K, Guttman-Yassky E. Endophenotypic variations of atopic dermatitis by age, race, and ethnicity. J Allergy Clin Immunol Pract. 2020; 8(6): 1840-1852.
14. Jang S, Ohn J, Kim JW, Kang SM, Jeon D, Heo CY, et al. Caffeoyl-pro-his amide relieve DNCB-induced atopic dermatitis-like phenotypes in BALB/c mice. Sci Rep. 2020; 10(1): 8417.
15. Hong S, Lee B, Kim JH, Kim EY, Kim M, Kwon B, et al. Solanum nigrum Linne improves DNCBinduced atopic dermatitislike skin disease in BALB/c mice. Mol Med Rep. 2020; 22(4): 2878-2886.
16. Min GY, Kim EY, Hong S, Kim JH, Kim M, Kim EJ, et al. Lycopus lucidus Turcz ameliorates DNCBinduced atopic dermatitis in BALB/c mice. Mol Med Rep. 2021; 24(6): 827.
17. Choi J, Sutaria N, Roh YS, Bordeaux Z, Alphonse MP, Kwatra SG, et al. Translational relevance of mouse models of atopic dermatitis. J Clin Med. 2021; 10(4): 613.
18. Zhang EY, Chen AY, Zhu BT. Mechanism of dinitrochlorobenzene-induced dermatitis in mice: role of specific antibodies in pathogenesis. PLoS One. 2009; 4(11): e7703.
19. Grabbe S, Schwarz T. Immunoregulatory mechanisms involved in elicitation of allergic contact hypersensitivity. Immunol Today. 1998; 19(1): 37-44.
20. Watanabe H, Unger M, Tuvel B, Wang B, Sauder DN. Contact hypersensitivity: the mechanism of immune responses and T cell balance. J Interferon Cytokine Res. 2002; 22(4): 407-412.
21. Tuckermann JP, Kleiman A, Moriggl R, Spanbroek R, Neumann A, Illing A, et al. Macrophages and neutrophils are the targets for immune suppression by glucocorticoids in contact allergy. J Clin Invest. 2007; 117(5): 1381-1390.